Zhao, Weizhong (2011). Optical fibre high temperature sensors and their applications. (Unpublished Doctoral thesis, City University London)

CITY UNIVERSITY LONDON
EST 1894

Optical fibre high temperature sensors and their applications

By

Weizhong Zhao

Thesis submitted for the degree of

Doctor of Philosophy

City University London

School of Engineering and Mathematical Sciences

Northampton Square, London EC1V 0HB

July 2011

Acknowledgements

It would be definitely impossible to finish the work presented in this thesis without the enormous help and support from many individuals and institutions.

In particular, I'd like to express my deepest gratitude toward Professor Kenneth T.V. Grattan, the chief supervisor of my thesis, and professor Tong Sun, the co-supervisor. Their valuable suggestions and constant observations helped me to move forward to the direction of research and to achieve this goal. They also supported financially to my research by permitting me materials and equipment. I thank them for their efforts.

Many thanks should be given to Dr. Zhiyi Zhang. His comprehensive investigation in the field of fluorescence-based fibre thermometry has set a solid foundation to the continued work.

Many thanks to Professor Yonghang Shen, Zhejiang University, China, for his supporting and cooperating in many of this work, particularly in preparing the special fibres for high temperature gratings.

Many thanks to, Dr. Suchanda Pal, Dr. Jahnal Mandal, Dr. Jackson Yeo, Dr. T. Venugupalan, Miss Shuying Chen and all the guys in Measurement and Instrumentation Centre of City University, London. Their kind assistance let me spend smoothly the years of study at City University.

Finally, I should thank my parents and in-laws, my wife and my daughters. Without their self-giving contributions, it would be impossible for me to complete this thesis. I do owe them a lot.

II

Declaration

I declare that the work presented in this thesis, except those specifically declared, is all my own work carried out and finished at The City University London

Copyright declaration

Abstract

Fibre-optic sensors based on different schemes, have grown rapidly since its concept was first discussed decades ago. In this thesis, two major types of optical fibre temperature sensors are built and comprehensively investigated. They are the fluorescence lifetime based fibre thermometer based and the fibre optic sensors based on the wavelength interrogation scheme of fibre Bragg gratings.

These two types of optical fibre temperature sensors are, normally, suitable for comparatively low or medium temperature range. One object of this thesis is to extend for their operation temperature range to an elevated temperature region, by exploring some novel fluorescent materials and the probe assembly technique for the fluorescence lifetime based thermometer, and developing a novel photosensitive optical fibre for strong FBG fabrication. Further to the exploring the material and principle of the optical fibre temperature sensors, great efforts have been also focused on the research and development of cost effective sensor systems, including hardware and interface software.

In the aspect of fluorescence based fibre thermometer, a modulated fluorescence lifetime optic fibre sensor system based on the PLD (phase locked detection) method, together with probes using Tm:YAG crystal as sensing element, was built and evaluated. This temperature sensor system has been tested in the laboratory and successfully used in some applications in industries..

In the aspect of FBG based temperature sensor, a novel fibre, Bi and Ge co-doped fibre, was developed for strong FBG fabrication, and an FBG wavelength interrogation system based on tunable fibre F-P filter was developed The interrogation system and probes using the written into the Bi/Ge fibre , have been tested and used for varies applications.

Results of obtained from this work were reported, and showed the great prospect of using these optical fibre temperature sensor systems in various industrial application

Table of contents

List of illustrations

List of tables

Symbols and abbreviations

$^4A_2$	Ground electronic state of transition metal ions in crystal fields
ac	alternating current
AOTF	Acousto-optic tunable filter
ASE	Amplified spontaneous emission
B	Boron
Bi	Bismuth
c	Velocity of light *in vacuo*, 2.9979¼ ´ 108 m/s
°C	Degrees Celsius
CCD	Charge coupled device
CDM	Coherence division multiplexing
CDMA	Code Division Multiple Access
Cr3+	Trivalent chromium ion
CW	Continuous wave
DAQ	Data acquisition
DSP	Digital signal processor
dc	Direct current
E, ΔE	Energy and energy splitting between two different energy States
^2E	One of the low-lying electronic states of transition metal ions in crystal fields, from which the sharp *R*-line emissions initiate
EDFA	Erbium doped fibre amplifiers
EMI	Electromagnetic interference
Er	Erbium
f	Frequency of a periodic signal
FBG	Fibre Bragg grating
FDM	Frequency division multiplexing
FEL	Free electron laser
FID	Fluorescence inducing and detecting device
FP	Fabry-Pérot

G	giga, 10^9
Ge	Germanium
GSM	Global System for Mobile Communication
GPRS	General Packet Radio Service
HWFM	Full width at half maximum
I	Luminous intensity
In	Indium
k	kilo, 10^3
K	Kelvin
LD	Laser diode
LED	Light emitting diode
LM, LMA	Levenberg-Marquardt algorithm
LPF	Low-pass electrical filter
m	meter, or milli, 10^{-3}
M	mega, 10^6
ME	Mobile engine for GSM communication
MSB	Most significant bit
MT	Mobile terminal for GSM communication
n	nano, 10^{-9}
NA	Numerical aperture
n_{eff}	Effective refractive index of the fibre core
Nd^{3+}	Trivalent neodymium ion
OSA	Optical spectrum analyser
PDU	Protocol Data Unit mode for GSM short message
PLD	Phase-locked detection of fluorescence lifetime
PLD-AMSR	Phase-locked detection with analog modulation of excitation source and single reference signal
PLD-PMSR	Phase-locked detection with pulse modulation of excitation source and single reference signal

PLD-PMTR	Phase-locked detection with pulse modulation of excitation source and two reference signals
PSD	Phase sensitive detector
PTFE	Polytetrafluoroethylene
PZT	Piezoelectric
RF	Radio frequency
s	Second
Sb	Antimony
SLED	superluminescent diode
Sn	Tin
t	Time
T	Temperature, or time
$\tilde{T}$	Period of a periodic signal
TE	Terminal engine for GSM communication
TEC	Thermo-Electric Cooler
TDM	Spatial division multiplexing
Tm^{3+}	Trivalent thulium ion
TTL	Transistor–transistor logic
UV	Ultraviolet
V	The amplitude of a voltage signal
VCO	Voltage-controlled oscillator
W	Power
WDM	wavelength division multiplexing
WLAN	Wireless Local Area Network
WMAN	Wireless Metro Area Network
WPAN	Wireless personal area network
WWAN	Wireless wide area network
Y_2O_3	yttria
YAG	Yttrium aluminium garnet ,$Y_3Al_5O_{12}$

λ	Wavelength
λ_B	Wavelength of fibre Bragg grating
Λ	The periodicity of the modulation in fibre core of an fibre Bragg grating
τ	The fluorescence lifetime

Chapter 1. Introduction

1.1 A brief review of optical fibre temperature sensors

1.1.1 Optical fibre sensor - a historical view

The first concept of the use of optical fibre techniques for sensor applications was discussed nearly four decades ago, indeed, the first patent of using optical fibres as a sensor goes back to the mid-1960s. Since then the research and development of fibre sensors have been intensively carried out in laboratories worldwide, under the initial drive for potential military and aerospace applications, where the cost factor in relation to the use of such optical fibre sensor technologies was less an issue, but the working environment is often more hostile than that experienced in some other areas. Such requirements are well met by the intrinsic characteristics of optical fibre sensors as they are lightweight, small, easily multiplexable, immune to electromagnetic interference (EMI), and require no electrical power at the sensing point, etc.

It was predicted, in the early 1980s, that the optic fibre sensors would rival other solid-state sensor technologies in market shares[1]. However, this prediction has not been fully realized in spite of their much-heralded advantages. The main hindrances of the application of optical fibre sensors are that, when compared to their conventional sensor counterparts, fibre sensors perform equally well but, due to the limited and low markets which have developed, the technology being usually more costly. Consequently, fibre sensors realise their value when the application has specialized needs, for example, a non-electrically active sensor head, or the need for a very lightweight/small volume device. In some applications, the ability to efficiently multiplex fibre sensors is the main criterion used to select fibre sensors over other technologies. This creates niche markets for fibre sensors, holding back the potential cost benefits which may be realized from high-volume production.

Thanks to the rapid technological advancement of optical communications and their related component fabrications in 1990s, there has been a significant change in terms

of the cost of optical devices and this has led to more cost-effective optical fibre sensor system development. A typical example of which fibre sensors may provide new capabilities over other sensors is the wide use of fibre Bragg gratings in structural health monitoring, taking advantage of the multiplexing characteristics of gratings over conventional strain gauges.

Although optical fibre sensors have not yet experienced the same dramatic commercial success as that of optical fibre communications, they have shown their own advantages in terms of small size, light weight, immunity to EM interference, resistance to chemical attacks and multiplexing capability, therefore they are continuously being researched and developed for different niche industrial applications. These include pressure, strain and flow measurement, temperature measurement, electric and magnetic sensing, nuclear and plasma diagnostics and chemical sensing, etc. There have been a number of reported successes using optical fibre sensing technologies, for underwater acoustic sensing [2], strain monitoring [3], rotation sensing (gyroscopes)[4], certain chemical/biomedical sensors (pH, CO_2, etc.) [5,6], and temperature sensing [7]. The detailed technologies, sensor devices and their respective applications have been discussed and reviewed in many literature [7-9].

1.1.2 Schemes of optic fibre thermometer

Temperature is one of the most importance parameters to be measured in industrial process control, in scientific activities and in daily life. A wide range of exsiting instruments is available for temperature measurement either in industries or in laboratories. Due to the unique advantages of the fibre-optics, optic fibre thermometers have become a active research and development areas in seeking of alternative means of temperature sensing.

In addition to the sensors based upon bulky optics, a wide variety of temperature sensors using fibre optics have been developed [10]. The fibre optic thermometer has been one type of modern instruments that can be used for temperature measurement accurately in a variety of environments. An optical thermometry can build upon several

different sensing mechanisms therefore there are a number of different optical thermometers, which include blackbody radiation thermometers (or remote pyrometers), thermal expansion thermometers, fluorescence thermometers, and thermometers based on optical scatterings including Raman scattering and Raleigh scattering, and fibre Bragg grating based thermometers.

1.1.2.1 Blackbody radiation thermometers

All materials with temperatures above absolute zero degree emit electromagnetic radiation (thermal radiation) and the amount of thermal radiation emitted increases with temperature [11]. Hence, the amount of thermal radiation emitted by a material can therefore be used as an indicator of its temperature. The basic operating principle of the radiation thermometers is to measure part of the thermal radiation emitted by an object and relate it to the temperature of the object using a calibration curve that has been pre-determined either experimentally or theoretically (from Planck's law) [11]. Typical radiation thermometers measure temperatures above 600 ^{o}C and this type of instrument dominates the instrument market for high temperature (>2000°C) measurement [12,13].

1.1.2.2 Thermometers based on thermal expansion

These are sensors that use the temperature dependence of the optical path length within a small optical resonance cavity, e.g. a Fabry-Pérot (FP), built in an optical fibre [14]. These temperature sensors measure the change in optical path length of a short piece of material whose thermal expansion coefficient and refractive index as a function of temperature are known. The temperature measurement range is dependent on the fabrication materials. Silica fibre based FP temperature sensor has been demonstrated for temperature measurement up to 800 ^{o}C, while single crystal sapphire fibre based FP temperature sensor has been demonstrated for temperature measurement up to 1500 ^{o}C [15].

1.1.2.3 Fluorescence-based temperature sensors

This type of sensor measures temperature by detecting the decay time or intensity of fluorescence signal generated from a sensor material as they are both temperature

dependent. In optical fluorescence-based fibre sensors, light from an excitation light source is guided through an optical fibre to illuminate a small sample of luminescent material either attached at the end of the fibre or incorporated into the guiding fibre. The decay time or intensity of the fluorescence signal can be captured for temperature measurements. Some of the most commonly used fluorescent materials involve rare-earth ions, such as Gadolinium or Europium, doped into a ceramic crystal, such as yttria (Y_2O_3) [16-18]. The fluorescence of these materials demonstrates strong temperature dependence and therefore enabling temperature measurement with good accuracy [19]. Such sensors have found applications in the measurement of temperatures within microwave ovens, or in very high-magnetic field regions where the conventional sensors fail to perform due to the EM interference.

1.1.2.4 Thermometers based on optical scattering

Another class of optical thermometers employs the temperature dependence of scattered light [20]. Rayleigh scattering, resulting from scattering of light by particles smaller than the wavelength of light, depends on both the size and number of scatters present.   It is the temperature-dependence of the scattering that enables the effect to be used in a thermometer [21-22]. Raman scattering [23], however, resulting from the scattering of light from phonons, or vibrational modes of the crystal, induces two wavelength-shifted scattered light signals. One is called "Stokes scattering", at a longer wavelength than that of the incident light, resulting from phonon emission, and the other, at a shorter wavelength, resulting from phonon absorption, is called "anti-Stokes scattering". The intensity of the anti-Stokes scattering depends strongly on the number of sufficiently energetic optical phonons in the crystal, which is a strong function of temperature. The ratio of the anti-Stokes to Stokes scattering is thus a sensitive indicator of temperature.

1.1.2.5 Fibre Bragg grating-based temperature sensor

A fibre Bragg grating is a section of fibre which includes a periodic modulation of the refractive index of the fibre core in the longitudinal direction. For a conventional fibre

Bragg grating, it reflects a very narrow band selective wavelength (typically less than 0.3 nm), termed Bragg wavelength value (λ_B), which is depending on geometrical and physical properties of both grating and optical fibre, and can be represented by [24]:

$$\lambda_B = 2n_{eff}\Lambda \tag{1.1}$$

where n_{eff} is the effective refractive index of the fibre core and Λ the periodicity of the modulation.

The Bragg wavelength of a fibre grating changes with external perturbations, such as temperature and strain perturbations, hence makes the gratings ideal for strain or temperature measurements, as the fundamental parameter being modulated is the wavelength of the reflected portion of the light from the grating, and thus intensity independent.   In recent years, fibre Bragg gratings (FBGs) have been identified as very reliable and cheap sensing elements, especially, for strain and temperature measurements in smart structures [25-27].

1.1.3   Advantages of fibre optic thermometer

The fibre optic thermometers, as one class of fibre optic sensors, encompass the major advantages of all types of fibre optic sensors, as summarized below.

- **Electrical, magnetic and electromagnetic immunity**

This is the main advantage of the optic fibre sensors over conventional sensors, when used in electrically or magnetically hostile environment. The materials used for optical fibre sensing and for signal transfer are mainly silica based material. They do not conduct electricity or absorb electromagnetic radiation, therefore they have demonstrated a high level of immunity to external electromagnetic interference (EMI).

- **Small sensor size**

The typical size of an optical fibre sensor can be, in principle, as small as the diameter of the fibre itself. This allows the sensors to be used in space critical applications, such as medicine and microelectronics, where size matters. The small size

of optical fibre sensors also offer the additional benefit of small thermal mass and hence have a very rapid thermal response.

- **Safety**

Another main feature of optical fibre sensors is their safety. Most optical fibre sensors require no electrical power at the sensor end. The signal is normally transferred "optically" in the form of low power light energy, therefore introducing little or no danger of electrical sparking in hazardous environments. The fibre itself, in general, is able to carry up to hundreds of milliwatts power. The fibre poses no hazard with any accidental fracture of cable, even in some chemical plants, where highly explosive gases or gas mixtures are used. Generally speaking, the optical fibre sensor system can be considered as intrinsically safe.

- **Ease of multiplexing**

The promise of multiplexing was a major attractive feature of fibre optic sensors, promoted as a major benefit over conventional single point devices. Many fibre optic thermometer systems also offer such an advantage. Multiplexing of sensors can reduce the individual sensor cost by using of a common source and detection system. In most of fibre optic thermometer schemes, the multiplexing can be achieved in a relatively straight forward way. The major multiplexing schemes used include wavelength division multiplexing (WDM), time division multiplexing (TDM), frequency division multiplexing (FDM), spatial division multiplexing (SDM) and coherence division multiplexing (CDM). Various combinations of these multiplexing techniques are possible to extend the numbers of the sensors multiplexed onto one single length of an optical fibre.

1.2   *Aims and objectives of this work*

As discussed above, the optic fibre thermometers have been, and are still, a highly active area for research and development as they have shown promise for a variety of industrial applications due to their advantageous characteristics.   The aims of this work are to design, develop and evaluate several important practical temperature sensor systems to meet industrial needs.   Building upon the success of previous research in

6

the field, two different types of optical fibre temperature sensor systems have been successfully developed. They are based on fluorescence decay and fibre grating techniques respectively, and have been designed specifically for elevated temperature measurements over 500° The sensor systems created have been successfully tested both in laboratory and on industrial sites and the details of which are discussed in the following chapters.

The basic research on temperature measurement based on fluorescence decay has already been extensively carried out both by the research group in the School of Engineering and Mathematical Science at City University London and by the other groups worldwide[28-29]. This work is aimed to take it further to create a new and cost-effective, reliable, and compact fluorescence-based thermometer, rather than theoretical research, specifically for industrial applications.

In addition to the above point fluorescence thermometer, a quasi-distributed fluorescence based fire alarm system, simultaneously measuring two different temperature-dependent decay lifetimes through the analysis of the double exponential decay signals obtained when the sensor is subjected to two different temperature zones has also been investigated. The aim of this work is to explore an alternative method using optical fibre and simple optical sources and detectors with low cost detection electronics.

The second part of this work is designed to investigate the temperature sustainability of fibre Bragg gratings (FBGs) written into some specialist photosensitive fibres for high temperature measurements and to develop a robust and cost-effective FBG sensor interrogation system.. In doing so a novel photosensitive fibre, Bi/Ge co-doped fibre, was designed and fabricated. FBGs written into this fibre were also evaluated.

To create an effective FBG sensor system, it is essential to have a proper FBG wavelength interrogation system, indicating clearly the relationship between the Bragg wavelength shift as a function of temperature variation. In this work, a robust

interrogation system with a user friendly interface was successfully created and evaluated for potential commercial applications.

In light of the above, the major objectives and deliverables of the work and the contributions made in terms of the new techniques explored and new applications applied are summarized and discussed below:

- Development of a cost-effective, reliable and compact fluorescence-based fibre thermometer for industrial applications, especially in the high temperature range over 500°C, up to 900°C

- Evaluation and testing of the fluorescence-based thermometer under several laboratorial and industrial conditions

- Development and evaluation of a novel fluorescence-based fire alarm system, in close cooperation with *Kidde Plc*., UK

- Fabrication of 'strong' FBGs into a specially developed bismuth doped germanium fibre for high temperature sensor applications.

- Systematic tests and evaluation of temperature sustainability of the FBGs written into the Bi/Ge co-doped fibre.

- Development of a FBG sensor system for temperature/strain measurement, using a self-developed FBG interrogation system

- Development of a quasi-distributed FBG-based fire alarm system, capable of identifying hot spot zones again background temperature.

- Development of a remote sensor system using GSM short message technique.

1.3 Outline of this thesis

The thesis describes the extensive research work has been designed and carried out to fulfil the above aims and objectives, in the field of fluorescence-based temperature sensors and FBG-based sensor systems. The work is present and discussed in detail in the following chapters, the contents of which can be summarized

as below:

Chapter 1 provides a short review of optical fibre thermometry and a brief introduction of the thesis and its aims, objectives and structure.

Chapter 2 begins with a brief induction of the operational principle of fluorescence thermometry and of signal interrogation schemes used for fluorescence lifetime measurement. This is followed by discussions about the design and setup of the fluorescence based thermometer and the test results obtained from both laboratory and field tests.

Chapter 3 briefly describes the application background of fluorescence-based fire alarm system, showing both the technical specifications required and several key issues in relation to the practical application and their impact on the sensor design.

Chapter 4 investigates the design and fabrication of novel Bi/Ge co-doped photosensitive fibre and its characteristics at elevated temperatures following an overview of fibre Bragg gratings and their applications.

Chapter 5 discusses the technique used in this work for FBG wavelength interrogation and presents the system setup of the FBG sensor system. This is followed by discussions of the test and evaluation results obtained by using the interrogation system developed

Chapter 6 introduces a FBG-based fire alarm system, showing it a better alternative compared to the fluorescence base-base fire alarm system, discussed in Chapter 3

Chapter 7 extends the FBG-based sensor into a remote sensor system by integrating the FBG sensor with a GSM technique.

Chapter 8 concludes the thesis with a summary of the work, highlighting the contributions made and some suggestions for future work.

References

[1]. A.L. Harmer, "*Optical fibre sensor markets*", First International Conference on Optical Fibre Sensors (OFS-01), London, UK, 1983, pp. 53-56

[2]. J. A. Bucaro, et al., "*Fibe r optic hydrophone*", Journal Acoustics Social American, vol. 62, 1977, pp.1302.

[3]. W. K. Burns (Ed.), "*Optical Fiber Rotation Sensing*", Academic Press, San Diego, 1994.

[4]. D. Butter, and Hocker, G. E. "*Fiber optics strain gauge*" , Apply Optics, vol. 17, 1978, pp.2867.

[5]. M. Brenci and F. Baldini, "*Fiber optic optrodes for chemical sensing*" , in Proceeding of Optic fiber sensor conference OFS-8, 1992, pp. 313.

[6]. G. Mignami and F. Baldini, "*In-vivo biomedical monitoring by fiber optic systems*", IEEE Journal Lightwave Technology, vol. 13, 1995, pp.1396.

[7]. K. T. V. Grattan, "*Fiber optic techniques for temperature sensing*", In: *Fiber Optic Chemical Sensors and Biosensors*, Vol. II, Edited by Wolfbeis, O. S. (London CRC press): pp. 151-192

[8]. K. A. Wickersheim, "*Fiberoptic thermometry: an overview*", In: Temperature – Its measurement and control in Science and Industry, Vol. 6, part 2 (New York: The American Institute of Physics), 1992, pp711-714.

[9]. B. H. Lee, "*Review of the present status of optical fiber sensors*", Optical Fiber Technology, Vol. 9(2), 2003, pp57-79.

[10]. S. M. Vaezi-Nejad, "*Selected topics in advanced solid state and fiber optic sensors*" , Published by the Institute of Electrical Engineers, London, United Kingdom. 2000, IEE circuits, devices and systems series 11,

[11]. D. P. Dewitt and G. D. Nutter, "*Theory and practice of radiation thermometry*", John Wiley&Sons, Inc. New York, 1988.

[12]. R. R. Dils, "*High-temperature optical fiber thermometer*", Journal of Applied Physics, vol. 54(3), 1983, pp.1198-1201.

[13]. B. E. Adams, "*Optical fiber thermometry for use at high temperatures*", In: Temperature: its measurement and control in science and industry, vol. 6, American Institute of Physics, New York, 1992, pp.739-743.

[14]. R. O. Claus, M. F. Gunther, A. Wang, K. A. Murphy, "*Extrinsic Fabry-Perot sensor for strain and crack opening displacement measurement from –200 to 900°C*", Smart Materials and Structures, vol. 1(3), 1992, pp.237.

[15]. H. Xiao, J. Deng, R. May, and A. Wang, "*Single crystal sapphire fiber-based sensors for high-temperature applications*", Proc. SPIE 3201, Bonston, MA, September 19, 1999.

[16]. M. Sun, "*Fiberoptic thermometry based on photoluminescent decay times,*" In: Temperature: its measurement and control in science and industry, vol. 6, American Institute of Physics, New York, 1992, pp.715-719.

[17]. Z. Zhang, K.T.V. Grattan, and A.W. Palmer, "*Fiber-optic high temperature sensor based on the fluorescence lifetime of alexandrite,*" Review of Scientific. Instruments, vol. 63, 1992, pp.3869-73.

[18]. B. W. Noel, etc., "*Phosphor thermometry on turbine-engine blades and vanes*", In: Temperature: its measurement and control in science and industry, vol. 6, American Institute of Physics,, New York, 1992, pp.1249-54.

[19]. K. A. Wickersheim, and M. H. Sun, "*Fiberoptic thermometry and its applications*", Journal of Microwave Power, vol. 22(2), 1987, pp.85-94.

[20]. O. Iida, T. Iwamura, K. hashiba, and Y. Kurosawa, "*A fiber optic distributed temperature sensor for high-temperature measurements*", In: Temperature: its measurement and control in science and industry, vol. 6, American Institute of Physics, New York, 1992, pp.745-749.

[21]. A. B. Murphy and A. J. D. Farmer, "*Temperature measurement in thermal plasma by Rayleigh scattering*", Journal of Physics D: Applied Physics, vol. 25, 1992, pp.634-643.

[22]. A. B. Murphy, "*Laser-scattering temperature measurements of a free burning arc in nitrogen*", Journal of Physics D: Applied Physics, vol. 27, 1994, pp. 1492-1498.

[23]. J. P. Dakin, etc., "*Distributed optical fiber Raman temperature sensor using a semiconductor light source and detector*", Electronics Letter, vol. 21, 1985, pp.569-570.

[24]. A. Othonos and K. Kalli, "*Fiber Bragg Gratings: Fundamnetals and Applications in Telecommunication and sensing*", Artech House, 1999

[25]. A. Othonos, "*Fibre Bragg Gratings*", Review of Scientific Instruments, vol. 68, 1997, pp. 4309-4341.

[26]. A. D. Kersey, M.A. Davis, H.J. Patrick, et al., "*Fiber grating sensors*", IEEE Journal of Lightwave Technology, Vol. 15, 1997, pp.1442-1463

[27]. Y. J. Rao, "*In-fibre Bragg grating sensors*", Measurement Science and Technology, Vol. 8, 1997, pp.355-375

[28]. Maurice E, Monnom G, Dussardier B, Saıssy A, Ostrowsky DB, Baxter GW. "Erbium doped silica fibers for intrinsic fiber optic temperature sensors". Applied Optics Vol.34, 1995, pp. 8019–25

Wade SA, Collins SF, Baxter GW, Monnom G. "Effect of strain on temperature measurements using the fluorescence intensity ratio technique (with Nd^{3+} and Yb^{3+}-doped silica fibers)". Review of Scientific Instruments, Vol. 72, 2000, pp.3180-5.

Chapter 2. Fluorescence-based high temperature sensor system

2.1   *Principle of the fluorescence based thermometry*

2.1.1   Photoluminescence

Photoluminescence is a light or radiation emission from a material excited by electromagnetic radiation, e.g. laser. The incident excitation radiation sources used are usually in the ultraviolet, visible or infrared regions of the spectrum. The resulting emission, which may be either in the form of fluorescence or phosphorescence, or both, is the release of the energy gained from the absorption of the incident photon energy. Following the removal of the excitation, the continued fluorescence emission of the fluorescent materials depends on the lifetime of the excited energy state(s) involved in the emission. Usually, the emission decays in an exponential form with a time-constant, often termed *fluorescence lifetime* or *fluorescence decay lifetime*, which may be used as a measure of the lifetime of the excited state(s). This fluorescence emission process is illustrated in Figure 2.1.

Energy absorption and emission   Fluorescence decay
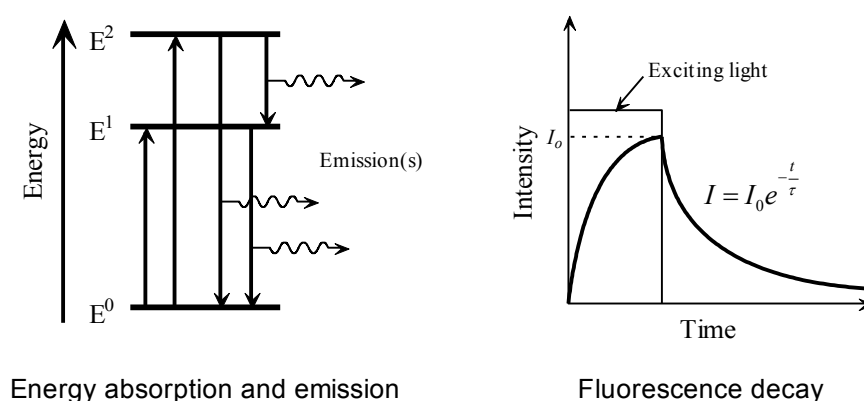
Figure 2.1 Illustration of fluorescence decay

The fluorescence emission normally has an intrinsic temperature dependant nature, such as temperature dependant lifetime or/and temperature dependant intensity, etc.

13

There are several fibre optical thermometry systems utilizing the fluorescence technique and the details of which have been discussed and widely reported over the past two decades [1,2].

2.1.2 Fluorescence decay lifetime-based thermometry

Most of the earlier systems were based on the temperature-dependent fluorescence intensity of appropriate fluorescence materials. Prime examples of these are the two commercial fluorescence thermometers, i.e. the Luxtron Model 1000, which used the europium-activated lanthanum and gadolinium oxysulphide as sensor materials [3], and the ASEA 1010 system, in which a small crystal of gallium arsenide sandwiched between gallium aluminium arsenide layers is used as the active fluorescence material [4]. These fluorescence-based systems have certain limitations in terms of performance and cost. As these systems rely purely on the intensity modification, the limitations stem from the need for an additional "referencing channel", for the separation of the thermally induced effects from other non-thermal sources of intensity changes, such as fibre bending, light source fluctuation and detector degradation, etc.

As a result, an alternative technique based on the measurement of fluorescence decay lifetime was developed [5-7]. It is intensity-independent and has been widely used in the development of state-of-art commercial fluorescence-based thermometers.

In a fluorescence lifetime-based optical thermometry, the temperature dependant lifetime of the fluorescence emitted from an appropriate material is utilized. There is a great range of fluorescence materials that can potentially be used for the temperature sensing. In this kind of fluorescence thermometry, most fluorescence materials used have a relatively long lifetime ($>10^{-6}$ s), compared to some laser materials, which normally have a lifetime of less than 10^{-7}s. This allows simple, accurate, and low-cost measurement systems to be built, as high speed photo detection devices and electronic components are not needed and the design of the lifetime detection electronics can be easily created for long lifetime measurement.

2.1.3   Fluorescence materials used for optical fibre thermometry

There are several classes of potentially useful fluorescent materials now available for fluorescence lifetime-based temperature sensing. They include rare-earth doped silica fibres, fluorescence oxide powers and a variety of rare-earth ion and transition metal ion doped crystal of high optical grade quality. Clearly, the choice of sensor materials determines the performance of a fluorescence-based thermometer, in term of temperature range, sensitivity, and stability, to a great extent. To achieve stable operation, the sensor material should be chosen to be stable over a specified temperature range for a long operation lifetime. As the selection of fluorescence materials is not a main topic of this work, hereby the fluorescence materials used for temperature sensors are only briefly listed below according to their material classification. Further information can be found in the text book by Grattsn and Zhang [8] and other related literatures [9,10].

Table 2-1 Typical fluorescence materials for optical fibre thermometry

Fluorescence material		Temperature range	Examples of work
Glass fibre	Nd-doped optical fibres	-190oC to 900oC	Zhang et al. [11]
	Er - doped silica	room temperature to 1100 oC	Zhang et al. [12]
Fluorescence Crystal	alexandrite	room temperature to 900 oC	Zhang et al. [13]
	Cr3+:YAG	room temperature to 550K	Zhang et al. [15],
	Nd: YAG	room temperature to 1100K	Zhang et al. [16],
	Er doped YAG	room temperature to below 1000 oC	Grattan et al. [17]
	Tm:YAG	room temperature to below 1200 oC	Zhang et al. [18,19]
Crystal fibre	Tm-doped YAG crystal fibre	room temperature to below 1400 oC	Shen et al. [20,21]
	Sapphire crystal fibre	cryogenic temperature to 1900-2000 oC	Shen et al. [22,23]

2.1.3.1 Silica Glass fibres for fluorescence lifetime thermometry

Silica optical fibres are clearly constitute a significan material, which has been widely used in optical communications and fibre-optic sensing systems, for example, the specific silica fibres doped with rare-earth ions, have been used as the gain media, in applications of erbium doped fibre amplifiers (EDFA) and fibre lasers. As a result, a wide range of doped glass fibres has been developed over the past twenty years, particularly for laser studies. Some of these doped fibres, particularly rare earth doped fibres, have been used for fluorescence thermometers. Among them, Nd^{3+} doped and Er^{3+} doped silica-based fibres the most commonly used.

Zhang et al. [11]   reported on the Nd-doped optical fibres for temperature sensing. The lifetime characteristics over the temperature range from -190°C to 900°C were evaluated, and it was shown that the probe made from this Nd-doped silica fibre is suitable for temperature measurement over the wide temperature range below 700°C.

Erbium (Er) doped silica is another widely used and familiar fibre material among the doped fibres that are widely commercially available. The characteristics of such fibre are very well known because of its wide applications as erbium doped fibre amplifier (EDFA). The fluorescence characteristics of the Er-doped silica fibre at elevated temperatures have been extensively studied, e.g. by Zhang et al. [12]. The thermal characteristics of the fluorescence decay of Er-doped fibres of different active dopant concentration under similar conditions were observed. The results of the tests on the fluorescence characteristics of the erbium doped fibres shown above seemed to indicate that the fibres are good candidates for thermometry within the temperature region from room temperature to below 1000 ^{o}C.

2.1.3.2 Fluorescence crystals used for fluorescence lifetime thermometry

Unfortunately, due to the difficulties in preventing the fibre material from crystallization at high temperatures, silica glass fibres are not suitable for long-term operation under elevated temperatures. Under these circumstances, the fluorescence ion doped crystals may be a better candidate in terms of the performance stability at

high temperatures. Probes fabricated from crystal materials are normally preferred for long-term high temperature applications, as the crystal materials are physically and chemically stable without any tendency to becoming opaque after long-term operation at high temperatures as long as the melting point of these crystal are substantially higher than the working temperature concerned, These crystals can be transition metal ion (for example, Cr^{3+}) doped crystals or rear earth ion (for example Tm^{3+}, and Nd^{3+}) doped crystals.

Cr^{3+} ion activated materials have shown wide optical absorption spectra, and a significant variety of the temperature dependence of fluorescence lifetime, which makes these materials a suitable candidate for a wide range of temperature measurement. A range of Cr^{3+} doped crystals have been investigated as sensor elements in fluorescence lifetime-based fibre thermometers. These crystals include alexandrite [13], emerald [14], Cr^{3+}:YAG [15], for example.

In addition to transition-metal ion doped crystals, rare-earth ion doped oxides or crystals are good sensing materials for fluorescence lifetime-based thermometry. Several types of rare-earth doped oxides and crystal garnets have been investigated intensively, e.g., Grattan at al investigated the fluorescence characteristics of Nd:YAG at elevated temperature up to 1100K [16].

Along with Nd: YAG, Er doped YAG also shows a strong fluorescence even at temperatures up to 1100K. In the work reported by Zhang et al [17], a monolithic crystalline fibre optic temperature sensor, with a tip of Er^{3+} doped YAG, was used as the sensing material. The fluorescence lifetime versus temperature was determined over the temperature range from room temperature to 1100K.

Zhang et al [18,19], investigated another type of fluorescence crystal of YAG crystal, Tm:YAG, as a temperature sensing material, after some early work on thermal florescence characteristics of Tm:Y_2O_3 power [20]. The fluorescence characteristics of Tm-doped fibre were investigated up to the temperature of $1200^{o}C$. The results had proved that these materials with a dopant of Tm^{3+} are good candidates for high

temperature measurement.

2.1.3.3 Crystal fibre-based fluorescence thermometry

Known as functional fibres, optical crystal fibres offer a combination of material properties and waveguide geometry unavailable in either glass optical fibres or bulk crystals. Compared to silica glass fibres, they usually appear as single-crystal fibres with relatively large diameters and short length, and in most cases without cladding.

Crystal optical fibres were first introduced as a promising fluorescent sensing candidate by Shen et al in 1996 [21]. The construction of the crystalline fibre probe, with a certain length of sapphire (less than a millimetre) as temperature-sensing element on the tip of a YAG crystal fibre, offers great advantage in performance. Firstly, the thermometer probe is compact. Secondly, the probe can be used in severe conditions where a normal fibre bundle cannot sustain or survive, as the YAG fibre is used as part of the guiding fibre. Such a crystal fibre based thermometer can be operated in the temperature range from cryogenic to very high temperature near the melting point of the crystal fibre (1900-2000 $^{\circ}$C) [22,23].

Among the fluorescence materials listed above and many other materials, Tm:YAG crystal was selected in particular in this work as a sensing medium for a high temperature sensor system due to its long fluorescence lifetime and stability at elevated temperatures, while Nd doped fibre was used for a fluorescence-based fire alarm system, which will be discussed in Chapter 3.

2.2 Fluorescence decay lifetime measurement schemes

In addition to the selection of appropriate fluorescence materials to meet the requirements of the applications, the design of an effective, simple and economic electronic system for the detection of the fluorescence decay lifetime is also a vital issue in the development of a practical temperature sensor system with potential for commercialization. Several signal processing techniques for the measurement of fluorescence lifetime have been used and reported in fluorescence lifetime-based temperature sensor systems and these can be categorized into three main approaches

according to the signal processing techniques used. The outlines of some of these typical schemes are discussed in the following sub-sections.

2.2.1 Pulse measurement of fluorescence lifetime

In this approach, the excitation light applied to the fluorescence material is in the form of a delta function or a rectangular pulse, and the measurement is carried out from the observation of the fluorescence decay following the removal of the excitation light. The following are some methods used to derive the lifetime from the decay signal which have been used in some fluorescence lifetime-based thermometer systems

2.2.1.1 Two-point constant measurement method

This is a relatively straightforward method used by several research groups at the early stage of the development of fluorescence-based sensor systems [7,24-25]. The simple principle of this method is illustrated in Figure 2.2. The approach is to compare the fluorescence intensity at two points along the exponential decay curve after the termination of the excitation light. The electronics deployed for this measurement detect the first value, I_o of the decay signal at a fixed time, t_1, after the removal of the excitation light. When the decaying signal falls to the second intensity level, of the value I_o/e, at the time t_2, when a "crossover" occurs is noted. The interval of between t_2 and t_1 is the time constant, τ, of the exponentially decaying signal, and the time constant, τ, may be used as the value of the fluorescence lifetime.

This type of approach is simple and inexpensive in relation to the electronic components used. However, a significant disadvantage of this technique is that the signal is only measured at two specific points, and as a result, the accuracy of it is greatly limited.
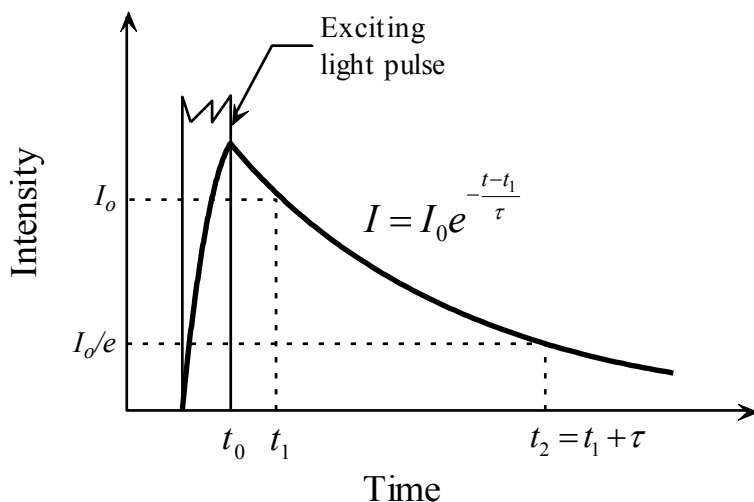
Figure 2.2 Principle of the two-point time constant measurement approach

2.2.1.2 Integration method

To achieve a higher accuracy from the pulse measurement approach, several techniques have been developed which are based on the integration of the decaying signal over different periods of time.

One example of this is the signal processing scheme introduced by Sholes and Small [5]. As shown in Figure 2.3, when the decaying signal falls below a pre-set level, the start measurement is triggered. The signal integration is performed over two fixed time intervals, t_1 and t_2, and the integration values, A and B of this two periods are sampled. When the time derivative of the signal has reached zero, the integrator is reset and restarted, and the integrated noise and dc offset levels are then captured, and given by the values of C and D, which are equivalent to the noise and dc offset components in A and B respectively. Therefore, the fluorescence lifetime, τ, can be derived from the following relation [5]:

$$\frac{A-C}{B-D} = \frac{1-e^{-t_1/\tau}}{1-e^{-t_2/\tau}} \tag{2.1}$$
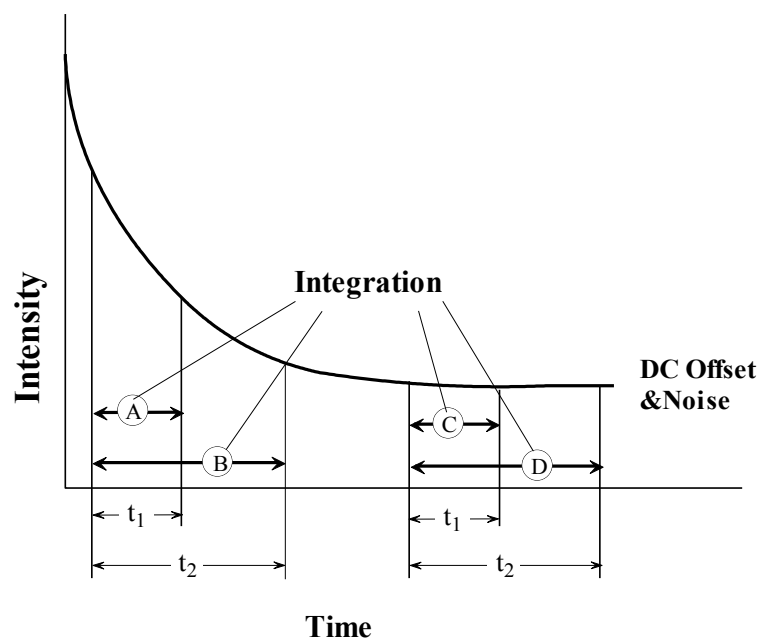
Figure 2.3 Schematic illustration of Integration method

2.2.1.3 Digital curve fit method

Since high speed digital signal processors (DSPs) or data acquisition (DAQ) cards are commercially available at relatively low cost, some fluorescence thermometry systems utilizing digital data acquisition and signal processing have been developed [26]. This kind of digital regression approach is termed as "digital curve fit method", which was described in detail by Sun [27].

In such a system, the fluorescence material is excited by sequential light pulses, modulated by a TTL rectangular waveform, and as a result a periodic fluorescence decay signal can be captured and processed.   In doing so, a selected portion of the decaying curve is digitally sampled. The digitalized samples, after a correction of any dc offset, shown in Figure 2.4, are processed by the DSP or a PC to provide the best fitted exponential curve, using a numerical algorithm, such as the *least-squares* curve fit and *single Prony* method. Then the lifetime, τ, can be derived from the exponential curve.
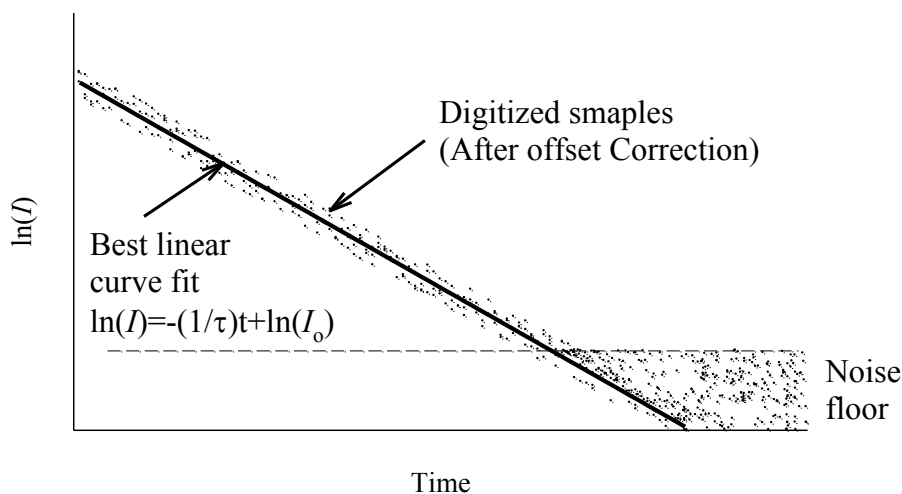
Figure 2.4 Illustration of digital curve fit technique

An investigation into the errors caused by the *dc* baseline offset and noise in the *least-squares* estimation of the exponential lifetime has been carried out by Dowell and Gillies [28], It showed that such two-parameter estimation approach only estimates I_o and τ, and assumes zero baseline offset, therefore is rather sensitive to the small, residual baseline offset. Thus a three parameter estimation, which includes the estimation of the baseline offset, was proposed as a better solution. However, this results in increasing the complexity of programme and prolonging the signal processing time, though this is not a significant issue as the processing speed of PC is increasing continuously every year.

2.2.2   Phase and modulation measurement

The technique of phase and modulation measurement of fluorescence lifetime is schematically illustrated in Figure 2.5. The intensity of the excitation is sinusoidally modulated, so that the fluorescence signal from the sensor material follows the same sinusoidal pattern, but has a phase shift of φ behind the excitation light. The phase, φ, can be expressed as [29]:

$$\tan\varphi = 2\pi f \tau \qquad\qquad (2.2)$$

where tanφ=2πfτ and φ=phase difference
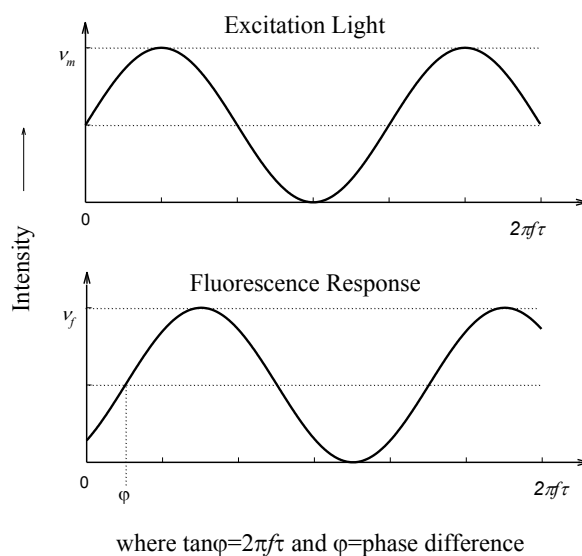
Figure 2.5 Phase and modulation measurement of fluorescence lifetime

Thus, the lifetime, τ, can be derived from the measurement of the phase shift, φ.

As inherently insensitive to *dc* offset and the *ac* noise in the sinusoidal signal, this approach is of high accuracy and is mainly meant to be used in precision instrumentation. Grattan *et al*. [29] have demonstrated the use of this technique in a ruby fluorescence-decay thermometer, where a high-power green LED was used as the excitation light source. Over the range from room temperature to 170 °C, a quite satisfactory measurement deviation was achieved under a poor signal-to-noise ratio condition. A similar system, reported by Augousti, et al., used alexandrite as the sensor material and was capable of measuring temperature over a range 20 - 150 °C with an accuracy of ±1°C and a response time of 1 sec [30].

However, since the system requires the measurement of fluorescence during the excitation period, it is highly sensitive to the excitation light leakage to the detector and the optics required to prevent such leakage can make the system very costly

2.2.3   Phase locked detection (PLD) scheme

This phase-locked detection of fluorescence lifetime is a signal processing

approach, used to develop a simple, inexpensive and versatile interrogation electronics system for the detection of fluorescence lifetime. As illustrated schematically in **Error! eference source not found.** [31], the excitation light source is modulated by a signal from a voltage-controlled oscillator (VCO), either of a sine-wave or square-wave form. The response fluorescence signal from the sensor material has the same pattern of the intensity of the excitation light source, but lags behind it by a phase shift, φ, as described in Equation 2.2. The fluorescence signal is fed back to a lock-in amplifier to mix with a reference signal derived from the VCO unit output with a phase delay of a fixed portion, α, of the period. Then the mixed signal is filtered by a low-pass filter (LPF) and further integrated. The resultant voltage is fed back to control the output frequency of the VCO. The final frequency of the VCO will be the value at which the integration of the mixed signal is zero. The period of this final frequency is directly proportional to the phase and hence fluorescence lifetime.
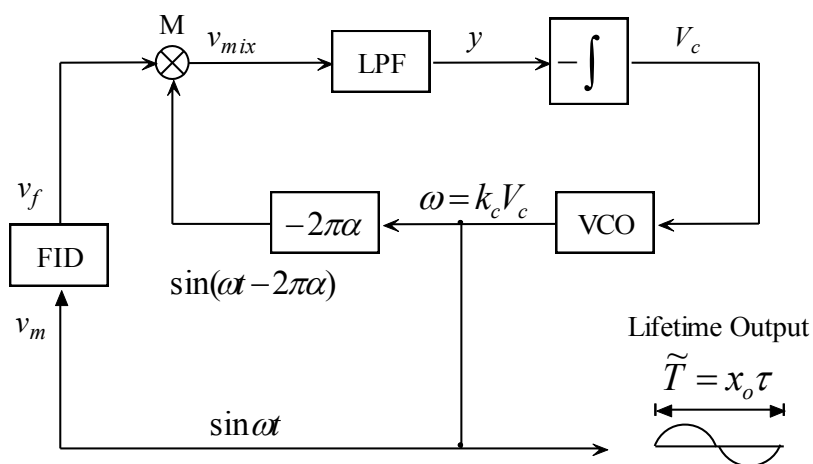
Figure 2.6: phase-locked detection scheme using single reference signal.
FID: fluorescence inducing and detecting devices, v_m: signal to modulate the output intensity of the excitation light source; v_f: the fluorescence signal; LPF: low-pass filter; VCO: voltage-controlled oscillator.

This technique offers a high resolution of the sensor system to be achieved over a wide range of lifetime measurement. In such a system, the locked frequency varies with the fluorescence lifetime, and the phase shift between the excitation light source and the fluorescence signal is always kept at a constant value, which is determined by the

reference signal delay ratio, α. Therefore this category of techniques has been termed the "phase-locked detection" by Zhang et al [31].

2.2.3.1 Simple Oscillator Method

Bosselmann reported the earliest scheme which is closely related to the phase-locked detection technique [32]. In this scheme, a positive feedback is formed by sending the fluorescence response signal back to control the output intensity of the excitation light source, via a timing circuit which amplifies the signal with an added phase shift, so that the system will oscillate at a frequency determined by the combination of the time-constant of the timing circuit and the fluorescence lifetime. The measurement of the lifetime is then derived from the oscillating frequency, which is subject to the parameter drifts of the timing circuit. The sensitivity of the frequency to the lifetime is also limited by the fact that is given by the combination of the lifetime and the time-constant of the timing circuit.

2.2.3.2 Phase-locked detection using single reference signal

A primitive form of the phase-locked detection scheme was reported by Bosselmann *et al* [6], as a revision of the simple oscillator method, and it was termed as *phase-locked detection using single reference signal* later by Zhang *et al* [31] .The operational principle of the scheme is similar to that illustrated in Figure 2.6, except that a square-wave type of VCO unit is used, thus excitation light is square-wave modulated.

Bosselmann pointed out that the measurement sensitivity of using square-wave modulation had been enhanced by a factor of 2 than that of using sinusoidal modulation, after a comparison was made between this primitive phase-locked detection scheme and the simple oscillator scheme mentioned above. This difference arises from the electrical system configurations rather than the modulation schemes used. In the simple oscillator system, the fluorescent material is directly used as a timing component in the oscillator by means of optoelectronic coupling. The oscillating frequency is determined by the combination of the fluorescence lifetime and the time-constant of an additional electronic timing circuit, which limits the sensitivity of the oscillating frequency to the

lifetime. However, in the phase-locked detection system, the oscillation is generated by a VCO with the oscillating frequency only controlled by the fluorescence lifetime, and thereby the sensitivity of the frequency to the lifetime is higher than that in the former case.

Several groups have demonstrated the success of utilizing this scheme [6,33-34] for fluorescence thermometers, confirming that this interrogation scheme is highly suited to high precision, wide range applications. However, as the system requires the measurement of fluorescence during the excitation period, even a tiny fraction of excitation light leaking into the photodetector will seriously degrade the performance of the system. An excess of such leakage can even cause the system to fail [31]. Therefore, high quality filter optics are needed to prevent such leakage and this could make the system costly and bulky.

2.2.3.3 Phase-locked detection using two reference signals

This version of phase-locked detection has been introduced by Zhang *et al* [35] to overcome the problem of excitation light leakage in a high-temperature measurement fluorescence based system using phase-locked detection with one reference. In this approach, two reference signals derived from the VCO output are used to mix successively with the fluorescence signal to delete the excitation leakage component from the signal. The integration of the mixed signal is then used to control the oscillating frequency of the VCO.

This technique, which has been proved both theoretically and experimentally, is intrinsically immune to the impact of the excitation leakage. Therefore, it is no longer necessary to use expensive and complex optical arrangements.

In this work, a fluorescence lifetime-based thermometry system is developed based on the phase-locked detection using two reference signals approach and the details of which will be discussed in Section 2.3. The details about the fluorescence lifetime measurement schemes and the techniques used are summarized by Zhang et al [8,9].

2.3   *Design of the fluorescence-based temperature sensor system*

A robust fluorescence lifetime based temperature sensor system has been successfully developed and evaluated in this work, based upon the phase-locked detection scheme with two reference signals as discussed above in section 2.2.3.3, and the use of Tm:YAG as sensing element, to address the challenges arising from a range of temperature measurements needs.   The details of the sensor system design are discussed in this section.

2.3.1   Sensor probe configuration

A typical configuration of Tm:YAG crystal fluorescence temperature probe, for low temperature applications, is shown in **Error! Reference source not found.**. A piece of m:YAG crystal polished to a small rod with a diameter of around 330μm is used as sensing tip.   Subsequently the Tm:YAG rod and a 300/330 μm silica fibre are inserted into a 570/700 μm silica glass capillary. Both are fixed in the capillary using epoxy resin at the tips for good optical coupling, which is vital for obtaining strong fluorescence signal from the sensing material. Then the capillary with the fibre and the Tm:YAG rod is inserted into a stainless steel tubing for protection. If the probe is used to measure temperature in some environment, such as in microwave environment, where steel itself is heated by the microwave energy, a ceramic tubing may be used to replace the stainless steel tubing.   As epoxy resin, which cannot sustain temperatures higher than 300°C~400°C (even with special high temperature epoxy), is used, this type of probes can only be used for some low temperature measurement applications (less than 400°C).

For the high temperature (over 400°C) applications, there is no high temperature sustainable epoxy commercially available. In addition, the sensing materials may also react with the epoxy at high temperatures, which can degrade the fluorescence signal, and hence degrade the temperature measurement ability of the system. In order to achieve good optical coupling under elevated temperatures, a special approach has to

be used for assembling the probe. Instead of using epoxy resin to fix the Tm:YAG rod and the fibre, as for the low temperature probes, fusing and shrinking of the silica capillary can be used to fix the core components. After the crystal rod and the fibre being inserted into the capillary, the capillary is fused using a high temperature miniature torch at several points along the fibre, one of which is used to fix the Tm:YAG rod with the capillary. While the capillary is cooling down immediately after the torch having been removed, it shrinks to fix the position of the Tm:YAG rod and the fibre within the capillary. Careful handling is required to avoid breaking the delicate capillary and melting the silica fibre and this can be achieved by carefully controlling the flame of the torch and the distance between the torch and the capillary. The configuration of this type of probes is illustrated in Figure 2.8**Error! Reference source not found.**. As there is no epoxy involved at the tip of senor material, the probe can be used for high temperature measurements and the sensing range is only limited by the measurement range of fluorescence lifetime, which can be up to 1000°C, or higher than 1100°C if
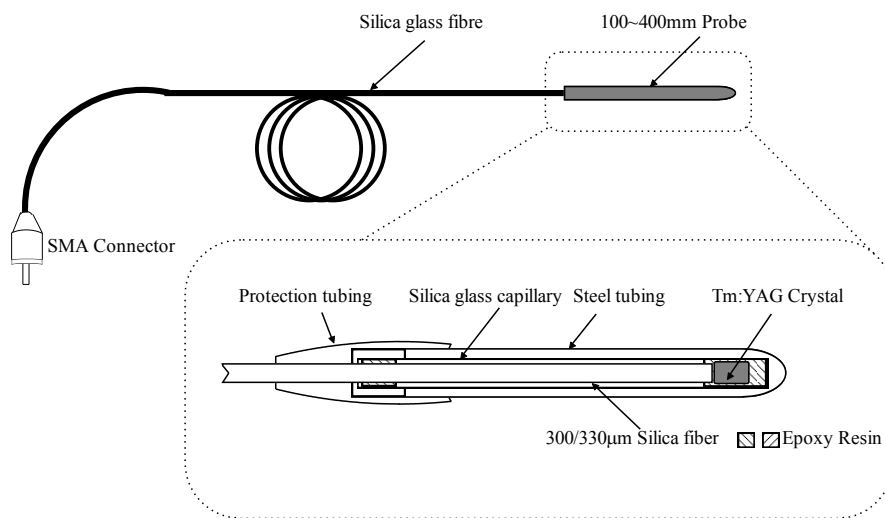
Figure 2.7 Configuration of Tm:YAG probe for low temperature applications
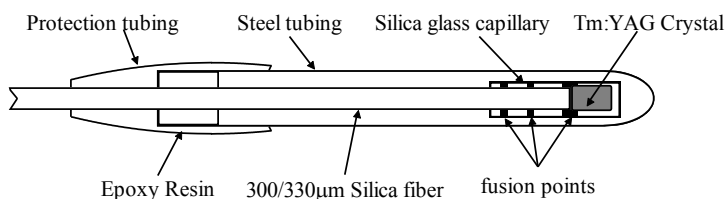
Figure 2.8: Configuration of Tm:YAG probe for high temperature applications

radiation compensation is introduced [36].

2.3.2   Interrogation system design and the PLD approach

An enhanced model of a sensor interrogation system was built in this work on the basis of phase-locked fluorescence detection using two reference signals, which was first introduced by Zhang et al [35]. The sensor system, connected to a PC via a user-friendly interface as shown in Figure 2.9, is illustrated in Figure 2.10.   A 785 nm Laser, modulated by the TTL signal from the PLD unit, is used as the pump light source, and its light is launched to the sensor probe through a Y-coupler to excite the Tm:YAG crystal.   The fluorescence signal generated is collected and coupled back to a PIN photo-detector. This signal is processed by the PLD unit to lock the modulation frequency in respect to the fluorescence signal. The modulation frequency is then measured by a microchip unit, which performs the frequency measurement, and passed to a PC for lifetime calculation.   Thus its corresponding temperature value can be obtained based on the calibration data obtained prior to the tests.
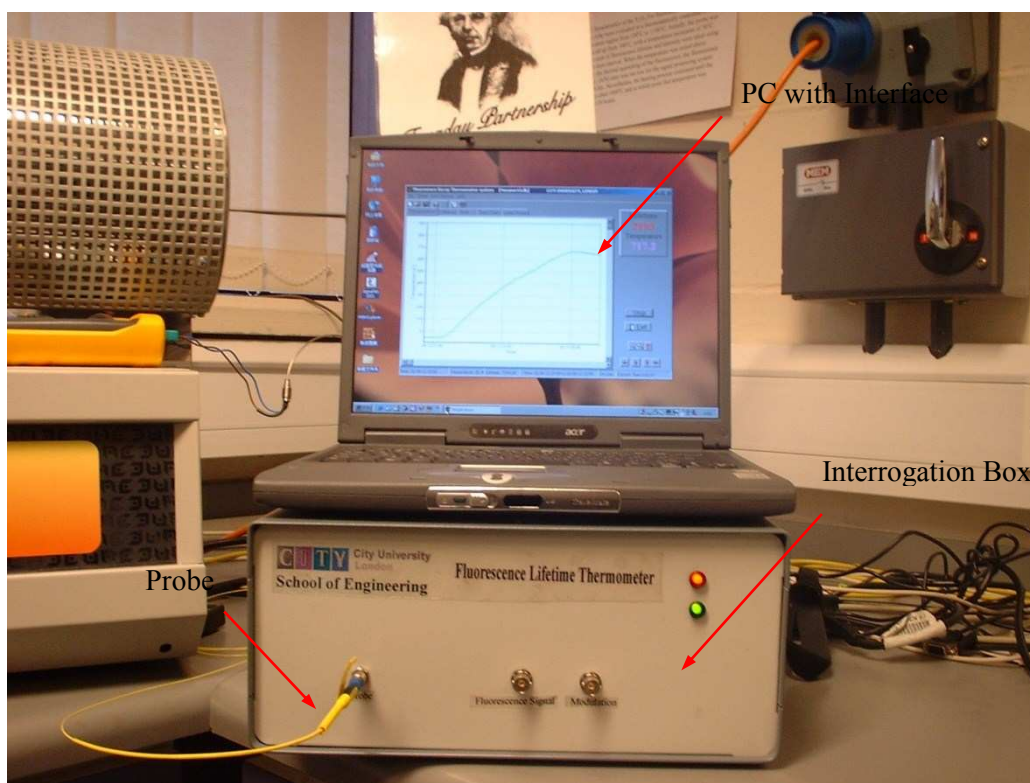
Figure 2.9: Fluorescence lifetime-based thermometer connected with a PC
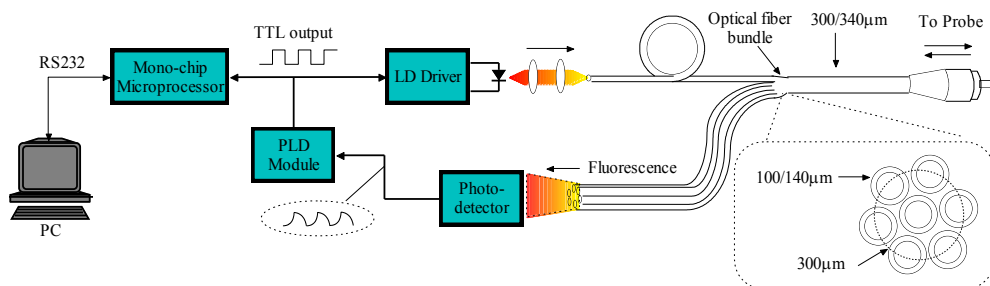
Figure 2.10: System setup of enhanced fluorescence lifetime-based thermometer

As shown in Figure 2.10, an AT80C51 microprocessor was specifically designed to be included in the signal processing system to detect the laser modulation frequency (or period), which is proportional to the fluorescence lifetime of the fluorescence-based temperature sensor probe. The microprocessor unit is connected to the PC via a RS-232 serial port for data transmission. As a result there is no need for a timer card and any standard computer, including laptop, can be readily used for the temperature measurement. This makes experiments carried out outside the laboratory much easier to perform as a dedicated computer with timer card added-on is not needed.

Due to the multi-functionality of the mono-chip microprocessor used, the developed fibre thermometer system has the potential for a multi-channel temperature measurement, for example, for the measurement of heat flux which requires simultaneous multi-point temperature measurements.

2.3.2.1 Design of the phase locked detection system for fluorescence lifetime measurement

The pulse modulated phase locked detection (PLD) with two references (PLD-PMTR) method used for this system is illustrated schematically in Figure 2.11[35]. This approach is created to eliminate the excitation leakage, which is caused by the excess radiation from the light source reaching photo-detector along with the fluorescence signal. The waveforms of the signals designed are illustrated in Figure 2.12.
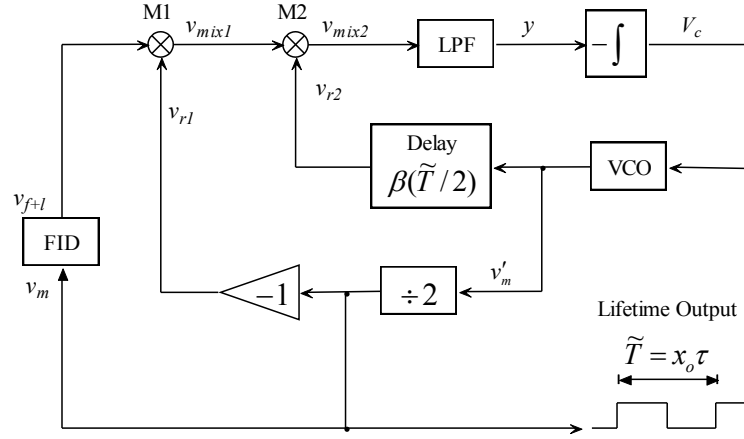
Figure 2.11: phase-locked detection of fluorescence lifetime using two reference signals
(components as Figure 2.6)

With the presence of the excitation leakage, the output from the fluorescence inducing and detecting device (FID) is given by [35]

$$v_{f+l} = v_f(t) + v_l(t) \tag{2.3}$$

where $v_f(t)$ is the actual fluorescence response, and $v_l(t)$ is the excitation leakage. Therefore the output of mixer M1 and M2 in Figure 2.11, v_{mix1} and v_{mix2}, could also be expressed as the sum of their fluorescence and excitation leakage components respectively, as depicted in Figure 2.12, where the upper traces show the components corresponding to the fluorescence signal, and the lower traces corresponding to the excitation leakage. As the leakage signal is in the phase of the modulation signal v_m and is rectangularly profiled, thus v_{f+l} is given by[35]:

$$v_{f+l} = v_f(t) + v_l(t) = \begin{cases} v_f(t) + V_{lo}, & 0 \le t \le \widetilde{T}/2 \\ v_f(t) - V_{lo}, & \widetilde{T}/2 \le t \le \widetilde{T} \end{cases} \tag{2.4}$$

where V_{lo} is the amplitude of the excitation leakage

As illustrated in Figure 2.12, the output of the first mixer, M1, is given as follows[35]:

$$v_{mix1} = -v_f(t) - V_{lo}, \quad 0 \le t \le \widetilde{T}/2 \tag{2.5}$$

and

31
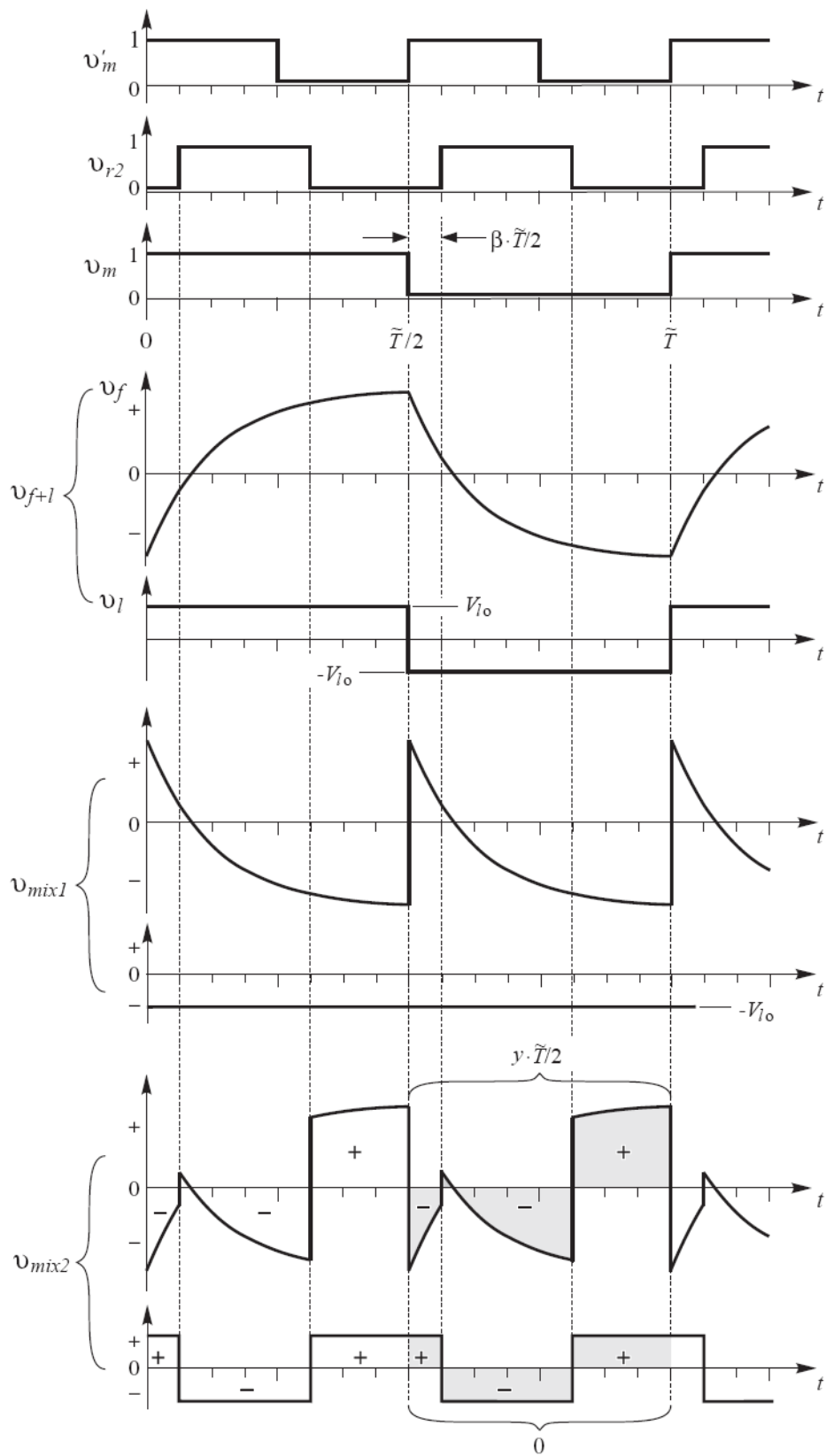
Figure 2.12: Output waveforms of PLD

$$v_{mix1}(t + \widetilde{T}/2) = v_{mix1}(t) \tag{2.6}$$

Thus the output of phase sensitive detector (PSD), y, is given as[35]:

$$
\begin{aligned}
y &= \frac{1}{\widetilde{T}} \int_0^{\widetilde{T}} v_{mix2}(t)dt = \frac{2}{\widetilde{T}} \int_0^{\widetilde{T}/2} v_{mix2}(t)dt \\
&= \frac{2}{\widetilde{T}} \left[\int_0^{\beta \widetilde{T}/2} v_f(t)dt - \int_{\beta \widetilde{T}/2}^{(\beta+1/2)\widetilde{T}/2} v_f(t)dt + \int_{(\beta+1/2)\widetilde{T}/2}^{\widetilde{T}/2} v_f(t)dt \right] \\
&+ \frac{2}{\widetilde{T}} \left[\int_0^{\beta \widetilde{T}/2} v_{lo}(t)dt - \int_{\beta \widetilde{T}/2}^{(\beta+1/2)\widetilde{T}/2} v_{lo}(t)dt + \int_{(\beta+1/2)\widetilde{T}/2}^{\widetilde{T}/2} v_{lo}(t)dt \right]
\end{aligned}
\tag{2.7}
$$

where the last part of the above equation is zero. y is determined only by the actual true fluorescence response as depicted in Figure 2.12. It can be shown that [35]:

$$y = f(x, \beta) = \frac{4kV_{lo}(1 - e^{-x/4})(1 - 2e^{-\beta x/2} + e^{-x/4})}{x(1 + e^{-x/2})} \tag{2.8}$$

where k is the gain of the phase delay unit, β is the phase delay, and x is the ratio of the period of the modulation signal $\widetilde{T}$, to the lifetime, τ, given by Equation 2.9 [35].

$$x = \widetilde{T}/\tau \tag{2.9}$$

The integrated value y is independent to the excitation leakage. Thus the system is theoretically immune to the effect of excitation leakage.

When $y=0$, it is a "locked" state for the phase-locked detection system, which means keeping the modulation period to the lifetime ratio at the value given by [35]:

$$x_o = x|_{f(x,\beta)=0} \tag{2.10}$$

Thereby, the measurement of the fluorescence lifetime can be made from the measurement of the modulation frequency using the following formula [35]:

$$\widetilde{T} = x_o \tau \tag{2.11}$$

2.3.2.2 Electronic design of fluorescence sensor interrogation system

A modular configuration of the hardware design was introduced to ensure the

robustness of the sensor system. The electronic system of the fluorescence lifetime-based temperature sensor system can be divided into three main modules:

- *PLD module: Florescence lifetime measurement (to a period proportional to lifetime)*

- *Photo detector module:* Weak fluorescence signal detection and amplification

- *Micro-processor module:* period measurement and data transfer.

Each module is laid on one standard DIN card and linked with other cards via the interface board. This configuration makes the system much more flexible and easy to be debugged, as the modular cards are interchangeable. Figure 2.13 shows the sensor interrogation system with three modular DIN cards inside. The design of the electronic circuits of these modules is discussed below.
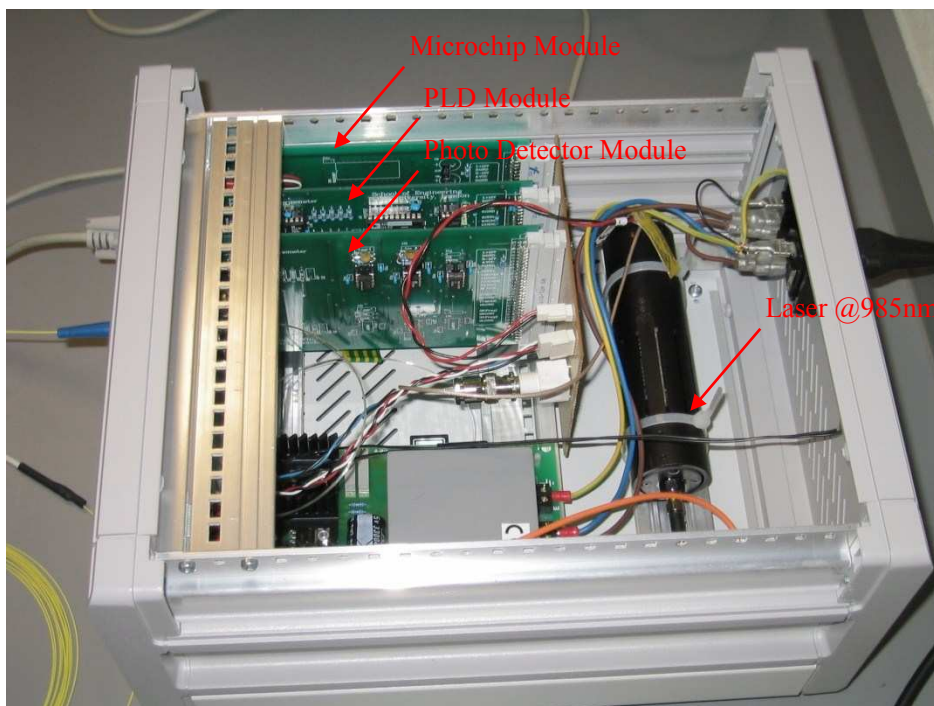
Figure 2.13: Fluorescence lifetime-based temperature sensor interrogation system

● **PLD module**

The operational principle of the PLD has been discussed in the previous sections.

The electronic system to perform this PLD function is illustrated in Figure 2.14. The corresponding output and waveform are shown in Figures 2.11 and 2.12 respectively, as described previously.
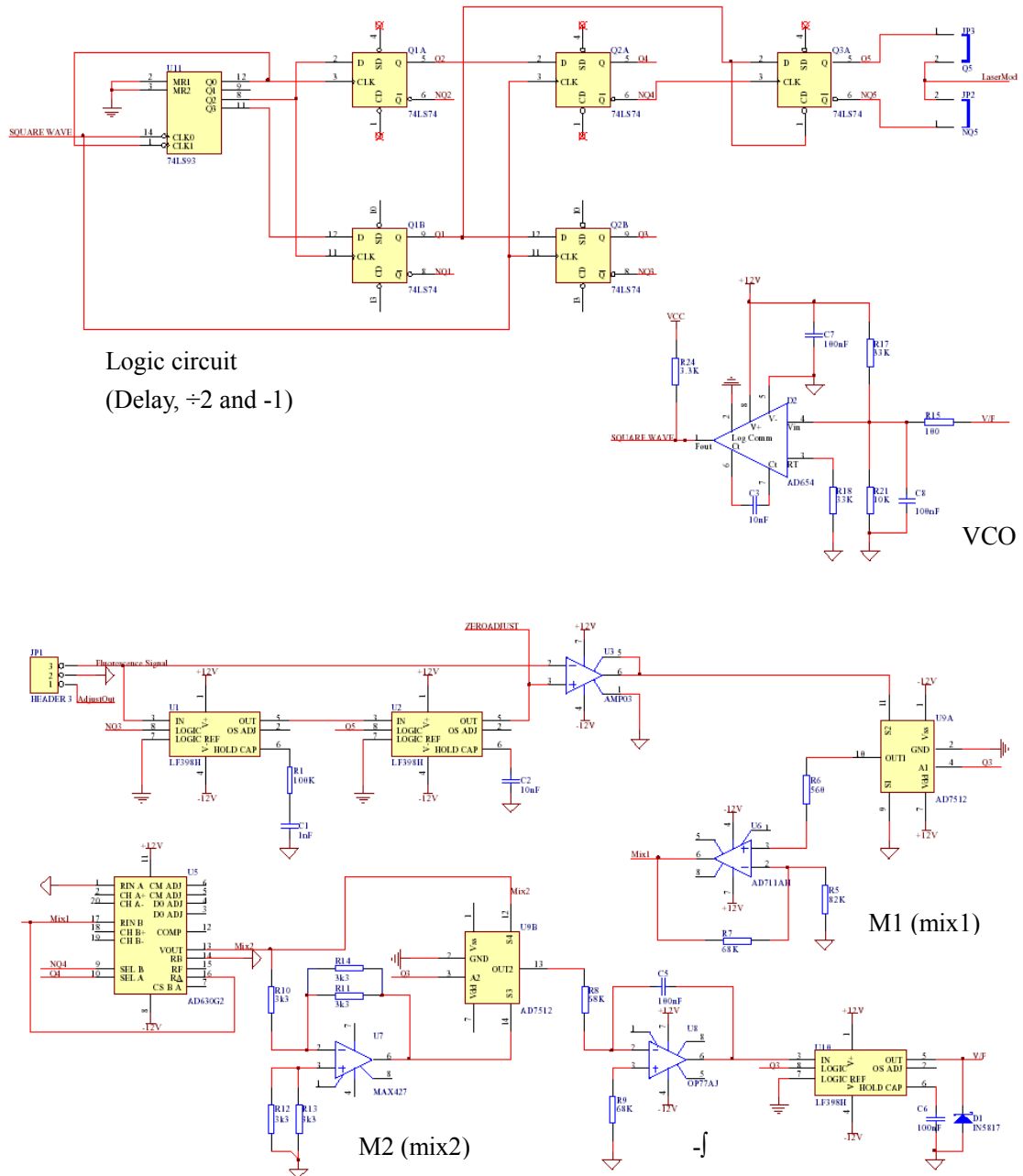
Figure 2.14: Electronic circuit of PLD module

- **Photo detector module**

An extended InGaSn PIN photo detector was used to convert the optical

fluorescence signal from the excited sensor material into a voltage signal. A I-V converter and a two-stage amplifier, as illustrated in Figure 2.15, were used to amplify the weak fluorescence signal to enable it to be processed by the PLD module.

FID
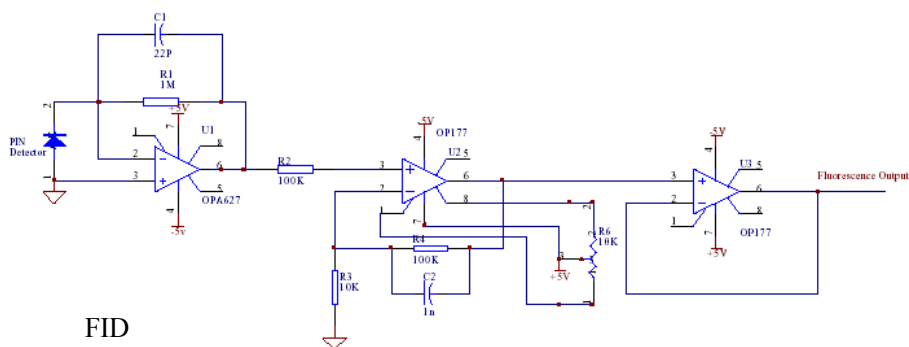
Figure 2.15: Photo detector module of the fluorescence lifetime-based thermometer

● **Micro-chip processor module**

The main electronic circuit of the micro-chip processor module is shown in Figure 2.16. This is used to perform the period measurement and send the measurement data to a connected PC via RS232 serial port. The details of the design will be discussed in the following sections.
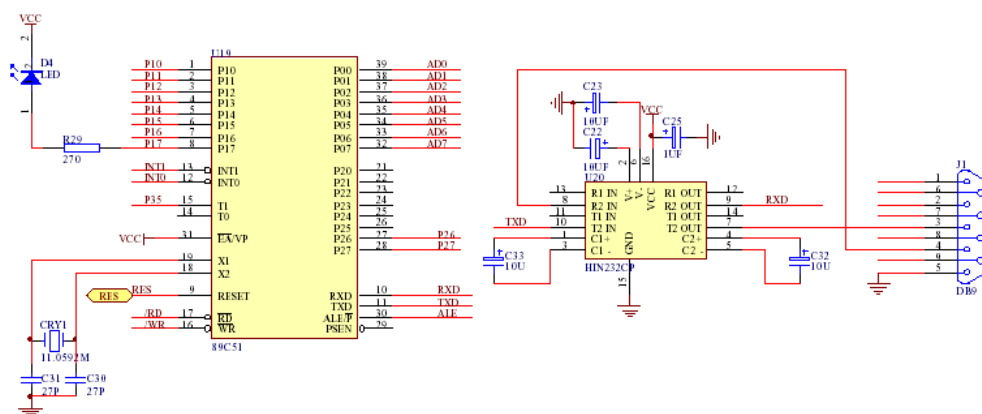
Figure 2.16: Circuit of micro-chip processor for period measurement

2.3.2.3 Microchip system for the optical thermometer

● **Measurement of the modulation period**

The modulation period, $\widetilde{T}$, proportional to the fluorescence lifetime, τ, normally is a rectangular TTL signal, and it can be measured using a timer card, as   used by Zhang *et al* [35]. In such an approach, a dedicated PC with a timer card added-on has to be used, which hinders field applications of the system. Therefore, another method using AT89C51 microchip to measure the modulation period, $\widetilde{T}$, was developed in this work.

The schematic of the system is illustrated in Figure 2.17. In the system, the modulation TTL signal from the PLD module is connected to the timer/counter, T1, of the AT89C51. The internal pulse number, n_p, is counted between two consequent rising edges of the TTL signal using the T1 counting function. Then the period of the signal, $\widetilde{T}$, can be derived using the given formula as:

$$\widetilde{T} = n_p \times T_p \tag{2.12}$$

where T_p is the internal pulse period, which is related to the oscillator frequency of the microchip system.
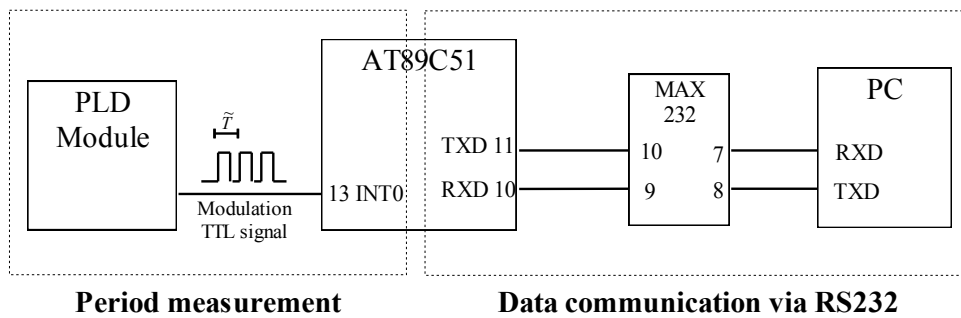
Figure 2.17: Schematic setup of the AT89C51 module for period measurement

AT89C51 microchip has two timers/counters, T0 and T1, and they can all work at four different modes.

1) Mode 0

In mode 0, the timers are an 8-bit counter with a divide-by-32 prescaler, and the

timer registers (TL, TH) are configured as 13-bit registers.

2) Mode 1

Mode 1 is as same as mode 0, except the registers are configured as 16- bit ones

3) Mode 2

Mode 2 configures the timer register as an 8-bit Counter (TL1) with automatic reload.

4) Mode 3

Timer 1 in Mode 3 simply holds its count. The effect is the same as setting TR1 = 0. Timer 0 in Mode 3 establishes TL0 and TH0 as two separate counters.

In the fluorescence-based system, mode 1 of timer/counter T1 is used for measurement of the period of the modulation signal. The flow chart, depicted in Figure 2.18, shows the procedure of the period measurement using mode 1 of timer T1. As a
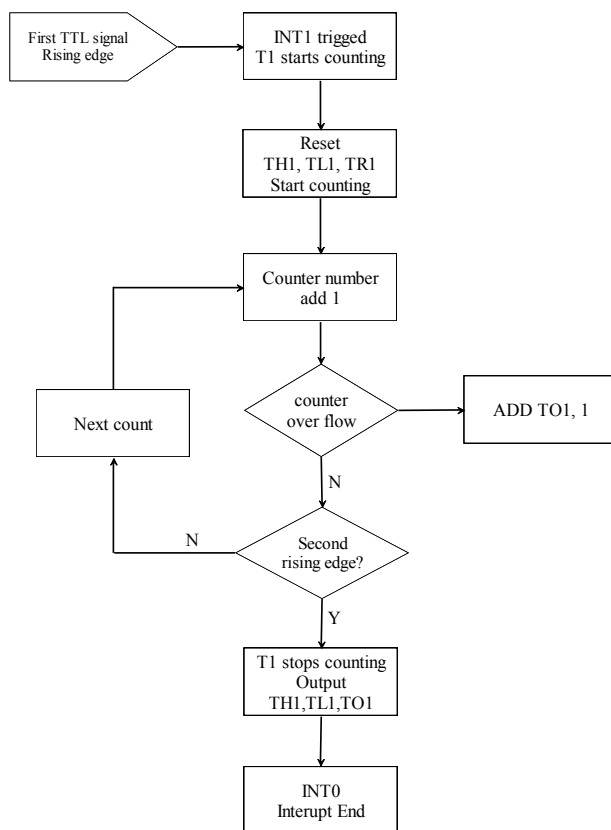
Figure 2.18: Flow chart of period measurement using timer/counter of AT89C51

16 bit counter it is not enough to hold the pulse counts of the period, another 8 bit

register, TO_1, was assigned to hold the overflow of the counter registers (TL_1 and TH_1). Hence the pulse count number is given by:

$$n_p = 256 \times TL_1 + 256^2 \times TH_1 + 256^3 \times TO_1 \qquad (2.13)$$

● **Data communication between PC and the sensor interrogation system**

The data communication of the sensor interrogation system is linked to the PC via the RS-232 serial port. The hardware connection is illustrated in Figure 2.16, with the protocol being described in Figure 2.19, showing how the connection and the communications between the PC and the interrogation system are established.
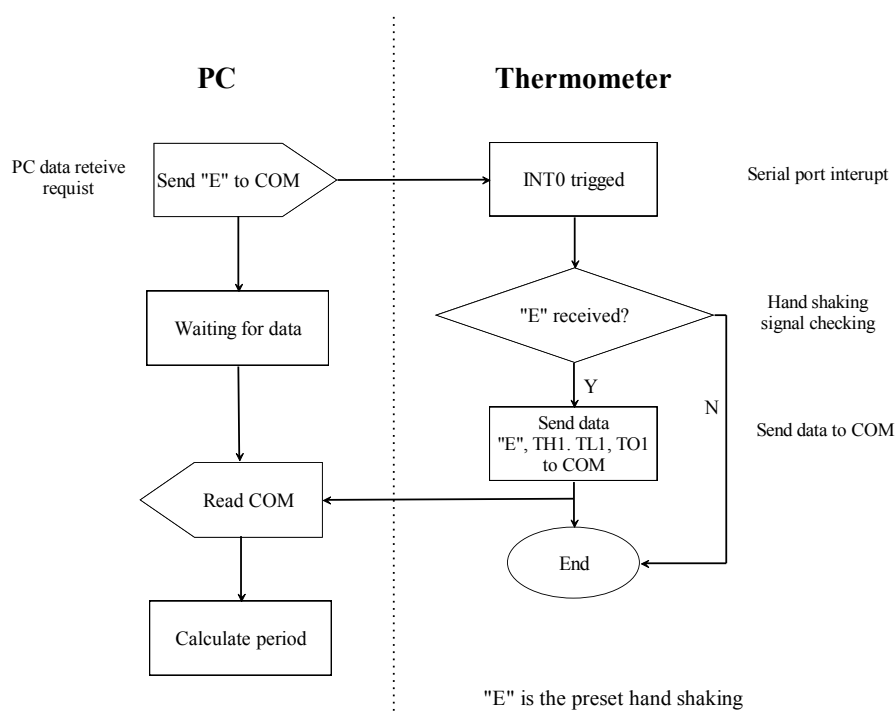
Figure 2.19: data communication between fluorescence thermometer and PC

2.3.3   Interface software

A user-friendly interface, written in *Delphi* language, has been developed for the fibre thermometer. The main functions of the interface software include the remote control of the microprocessor, thus the sensor system, from the host PC, data retrieve,

data processing and display of experimental results, etc.

The function of remote control and data transmission between the microprocessor of the sensor unit and the computer are realized via a RS232 serial port. The computer sets the sample request rate of the fluorescence lifetime and data transmission is made upon request from the computer. The fluorescence lifetime data received from the sensor unit are then processed and converted to the measured temperature value based on the stored calibration data.

The measurement results of fluorescence lifetime thus temperature variation
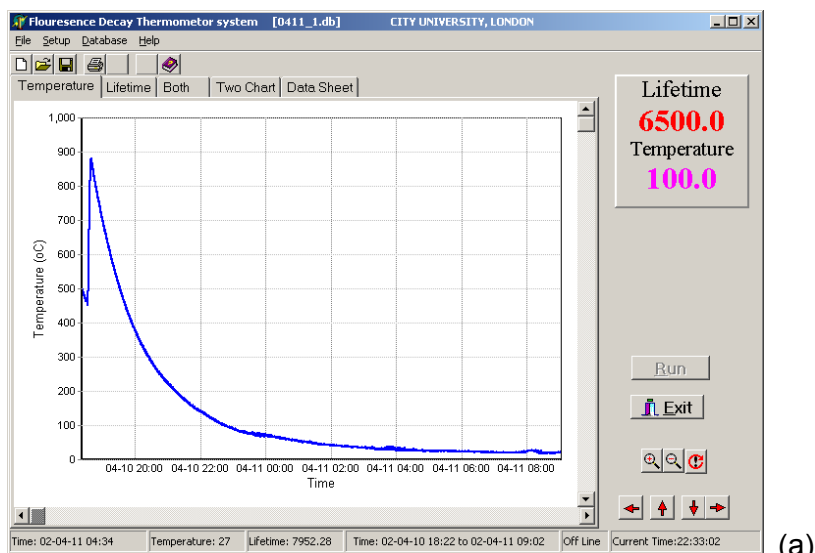
(a)
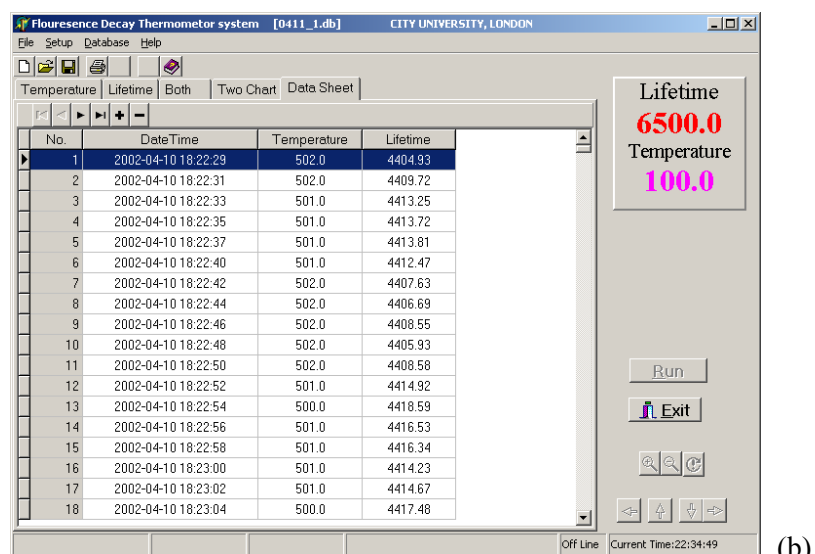
(b)

Figure 2.20: Screen print out of the fluorescence thermometer
(a) Graphic (b) Data sheet presentation of results

40

against time are clearly displayed either in graphic format (Figure 2.20a) or in datasheet (Figure 2.20b). The measured temperature/fluorescence lifetime recorded can also be traced to any time when the measurement was performed.

As experienced in the laboratory calibration of the fluorescence lifetime based thermometer, the temperature dependence of the fluorescence lifetime of different probe materials will likely be different. Therefore, the calibration curve of each probe would then be different, and appropriate calibration parameters should be pre-determined in relation to the specific sensing material chosen for some specific applications. A standard calibration procedure, illustrated in Figure 2.21, was introduced to enhance the software compatibility so that it could be used for different probing materials and thus for a wide range of temperature measurements. The temperature is thus derived from the lifetime τ using the following 6th polynomial equation using pre-calibrated parameters. Normally, only a few parameters are needed.

$$T = P_0 + P_1\tau + P_2\tau^2 + P_3\tau^3 + P_4\tau^4 + P_5\tau^5 + P_6\tau^6 \qquad (2.14)$$
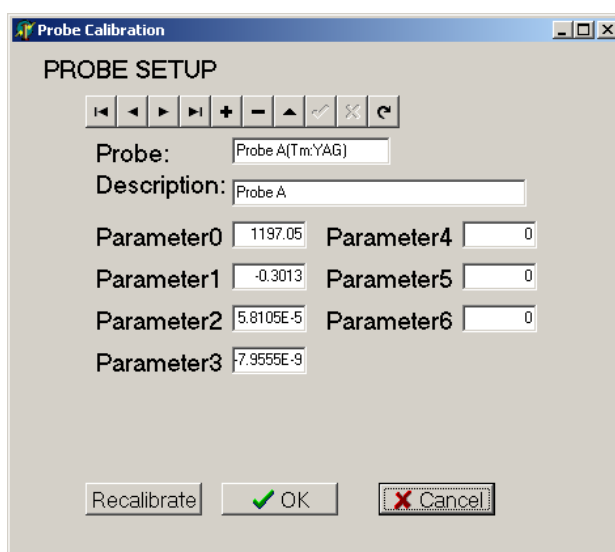
Figure 2.21: Calibration data selection of the interface program

2.4 Laboratory tests and evaluation of the fluorescence-based temperature sensor system

2.4.1 Calibration

Prior to any tests, a sensor calibration needs to be carried out to establish the

relationship between the fluorescence decay lifetime and the measured temperature. Before the calibration, the sensor probes are required to be annealed at a temperature higher than the maximum temperature to be measured to enable the stability and repeatability of the sensor. In this specific work the probe was annealed at 800°C for 48 hours before the calibration. The typical procedure of calibration and results obtained are presented below.

The fluorescent lifetime was monitored using the PLD fluorescence lifetime measurement system developed above. No observable lifetime change was observed during the annealing process when the probe was placed at 800°C. Subsequently when the annealing temperature was raised to 900 $^{\circ}$C, a significant lifetime change was observed within one hour. The annealing process at 900 $^{\circ}$C was then stopped after one hour, but restarted as temperature dropped to 800°C again. No lifetime change was observed again as expected under the temperature of 800 $^{\circ}$C.

Following the annealing, the probe was then calibrated using the readout system developed along with a K-type thermometer. The calibration curve of the fluorescence lifetime against temperature is presented in Figure 2.22., The calibration curves of different probes have a slight difference from each other, due to the different annealing process and small the material differences. However, each single probe does demonstrate a high repeatability (deviation less than 0.1%) when experiencing cycles of temperature going up and down (ranging from room temperature to 750 $^{\circ}$C) after annealing.
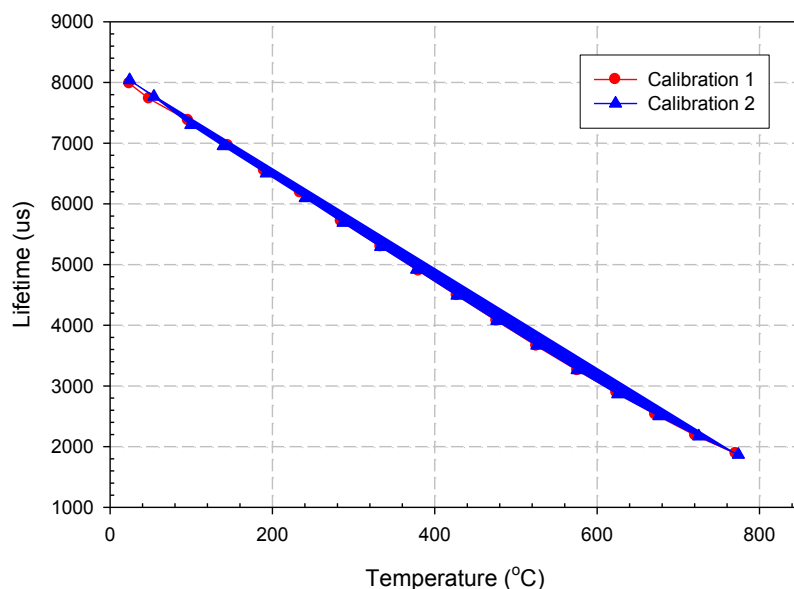
Figure 2.22: Lifetime versus temperature characteristics of Tm:YAG

2.4.2 System performance

2.4.2.1 Temperature measurement – cross comparison with K-type thermocouple at laboratory

A cross-comparison between the fibre thermometer developed and a K-type thermocouple was made when both probes were placed intimately at the same centre position of a Carbolite tube oven, which can reach a maximum temperature of $1200^{\circ}C$. Considering different dynamic responses of the probes, measurements were taken at each temperature after 30 minutes with an increment of 50 ^{0}C from the room temperature to nearly $800^{\circ}C$. Then the power supply of the oven was shut off, and the temperature fell naturally to the room temperature. In Figure 2.23, the readings of the thermocouple thermometer and the optical fibre thermometer are shown. A good agreement between the fibre fluorescence thermometer and the thermocouple could be found, the differences between them was less than $\pm1^{\circ}C$, as shown in Figure 2.24. Further tests have shown that with this fluorescence lifetime measurement system, using the above calibration data, a temperature resolution of 1 ^{o}C was realized over the

temperature range from room temperature to 800°C.

2.4.2.2 Long term stability
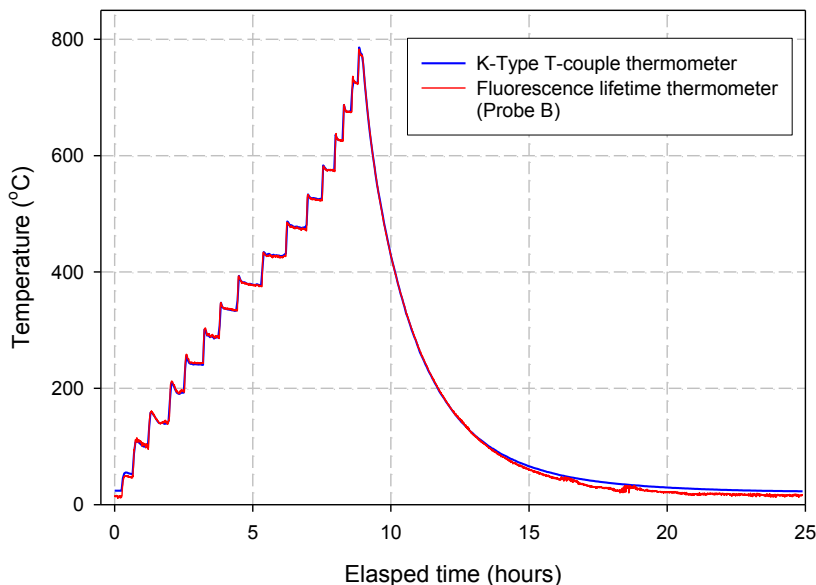
Figure 2.23: Thermal cycling of Carbolite tube containing an optical fibre thermometer and a
K-type thermocouple
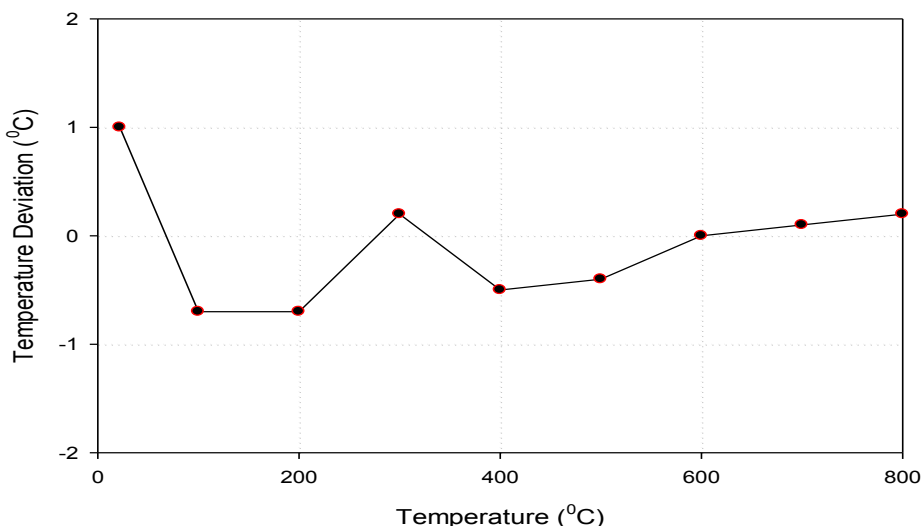
Figure 2.24: Temperature difference between the optical fibre thermometer and a K-type
thermocouple during thermal cycling

The long term stability of this fluorescence-based sensor system was investigated

when the probe was placed in the tube oven at different temperatures for a few days.

The measured temperature stability at different temperatures over this period (several

hours at each temperature) is shown in Figure 2.25. A standard deviation of the measurement ranging from 0.97 ^{o}C to 0.13 ^{o}C was estimated over the temperature region from room temperature to nearly 800 ^{o}C and the results are shown in Figure 2.26.
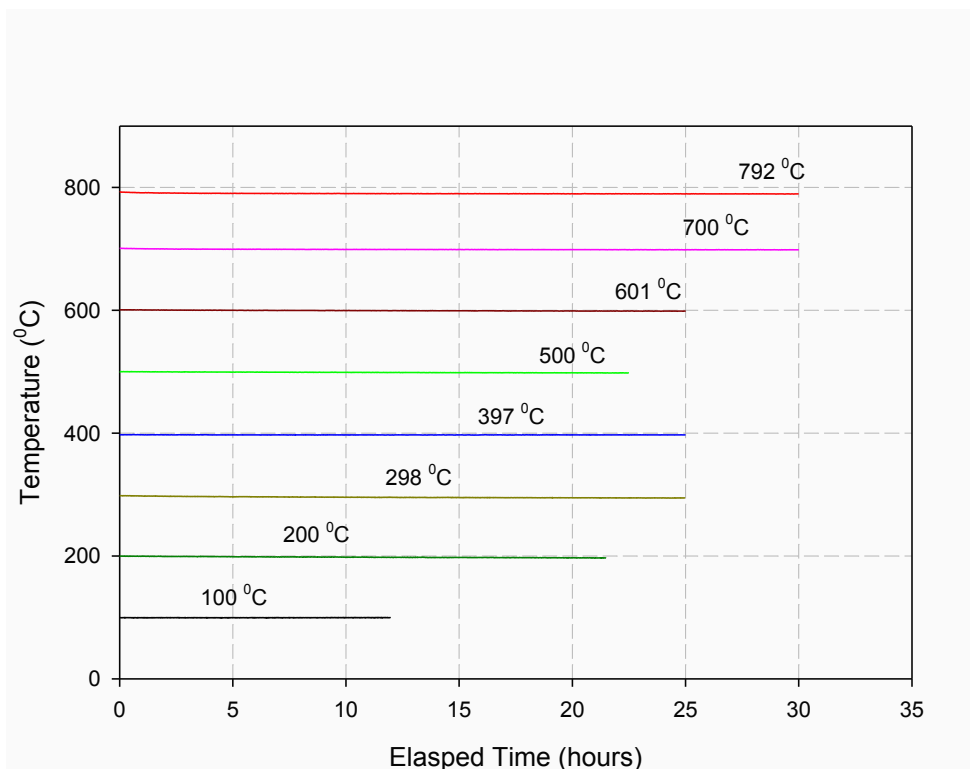
Figure 2.25: Long term stability of the fluorescence thermometer
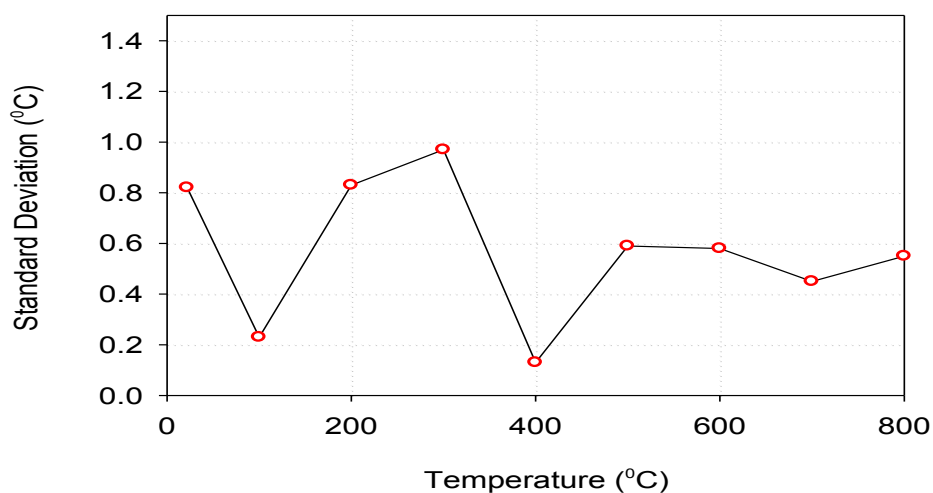
Figure 2.26: Standard deviation of the fluorescence thermometer at different temperatures

2.4.3　Main specifications of the fluorescence thermometer

As a summary of the laboratory test, the main specifications of the fluorescence decay lifetime thermometry system using the PLD approach are listed in table 2.1

Table 2-2 Main specifications of the fluorescence thermometer

Sensor Material	Tm:YAG crystal
Operation temperature range	Rroom temperature to 900°C
Temperature resolution	1°C
Maximum measurement error	$\pm$2°C
Stability (fluctuation)	$\pm$1°C (1 hour) $\pm$2°C (5 hours) $\pm$2.5^{o}C (5 hours)
Response time	~1 second

2.5　Applications of the fluorescence-based temperature sensor

Along with the series tests and evaluation of the fluorescence lifetime-based temperature sensor system developed in the laboratory environment, the system has been used and tested in some industrial contexts with the help from industrial partners for some industrial process controlling and monitoring applications, and some typical applications are presented in the following sections.

2.5.1　High temperature measurement at Corus, UK

The fluorescence lifetime-based thermometer system, tested and evaluated at the laboratory environment, clearly shows that the system can operate at temperatures up to 900°C over a long period, and therefore shows potential for monitoring the refractory furnace linings in the steel industry, where a real-time and reliable monitoring and control of the temperature of furnaces is required.

An evaluation of this fibre thermometer in the practical industrial field was carried out at Corus, Teeside Technology Centre, Middlesborough, UK. The performance of the fibre thermometer was compared with that of a K-type thermocouple when they were

both inserted into the inside of a refractory brick, which was the same type used currently in steel furnace as lining. The experimental setup of the test is shown in Figure 2.27.
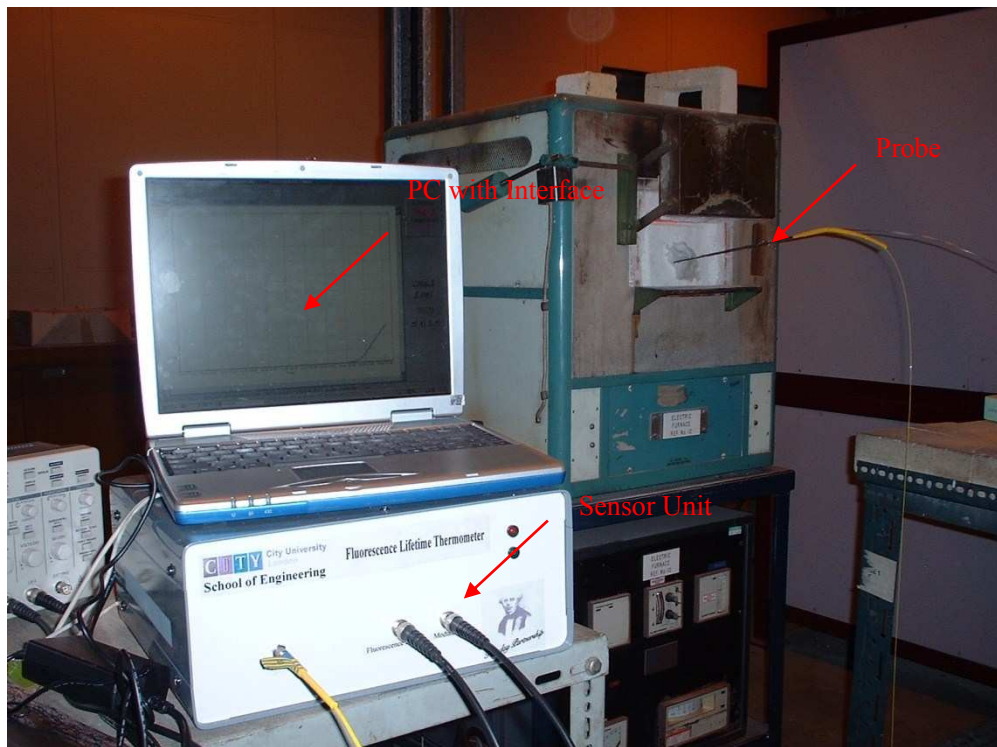
Figure 2.27: Experimental setup of the test carried out at Corus

The refractory brick, which was placed in an oven, was heated up gradually by the high surrounding ambient temperature. The temperature inside the brick, where the probes were located, would gradually rise until reaching the equilibrium state, if sufficient time was given. After having reached the thermal equilibrium state, the power of the oven was then switched off, and the surrounding ambient temperature of the oven dropped quickly and the temperature inside the brick would fall following the ambient temperature. As a refractory brick in the furnace was of high quality, both the process of heat flowing in or out from the brick took a long time. For evaluating the dynamic performance of the system, both the probes of the fibre thermometer and of the thermo-couple were taken out from the brick and then put into the brick again quickly on two separate occasions during the whole process. Two separate cycles of tests were performed, and the results of the temperature measured from the fibre thermometer and the thermo-couple against time are illustrated in Figure 2.28, showing a good

agreement between of the two independent temperature measurement devices in responding to the temperature changes.
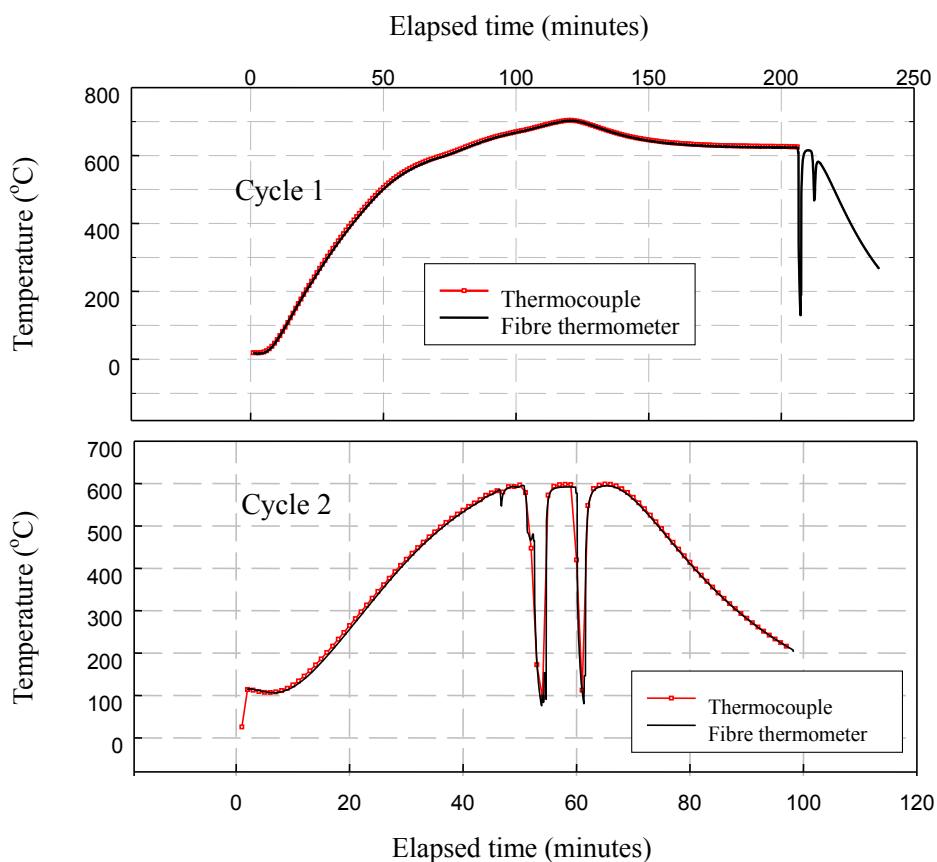
Figure 2.28: Test results of the fluorescence based thermometer and of the thermocouple at Corus

2.5.2 Temperature monitoring of a precision free electron laser heating process

This is a novel application of the fibre fluorescence temperature sensor system in the establishment and monitoring of stable temperature conditions for precision adhesion of small components in the semiconductor industry. The specific application is to heat and thus prepare a small globule of adhesive on the back of a precision integrated circuit which is to be used to adhere it to a credit card - the process of the manufacture of "smart cards" widely used by consumers. The temperature must be carefully monitored and thus controlled to prevent damage to the delicate, thin chip and to ensure the optimum conditions for adhesion to the credit card.

To achieve efficient, precision heating, a microwave free electron laser (FEL) is used

to deliver a precise amount of power onto the glue sample, taking full advantage of the highly directional properties of the laser beam [37]., As shown by this work, thermocouples and other electrically-based thermometer systems suffer from self-heating due to "pick up" from the microwave fields and thus cannot be used for precision temperature measurement. They always read "higher" than the actual temperature under such circumstances in which microwave energy is present. Thus optical technology, here the fluorescence lifetime-based thermometry, with the inherent immunity to electromagnetic interference (EMI), offers a satisfactory alternative to the electrical based thermometry. The benefits of the use of an accurate optical fibre temperature sensor of this type are clearly demonstrated in this application, opening up the possibility of the use of the same monitoring technique for other cases where microwave radiation is used

Figure 2.29 shows a group of integrated circuits for smart cards with a small coin (a one penny piece) for comparison of size. In order to fix these circuits to the plastic card, a small globule of adhesive was applied on the back of a chip before it was heated by the FEL microwave. The system setup for focused adhesive heating was shown in Figure 2.30, where the power from the laser is delivered by the microwave waveguide and two temperature probes, one an optical probe and the other a K-type thermocouple, were mounted in such a way that they touched the surface of the glue. The temperature change was monitored at the same spot on the surface.
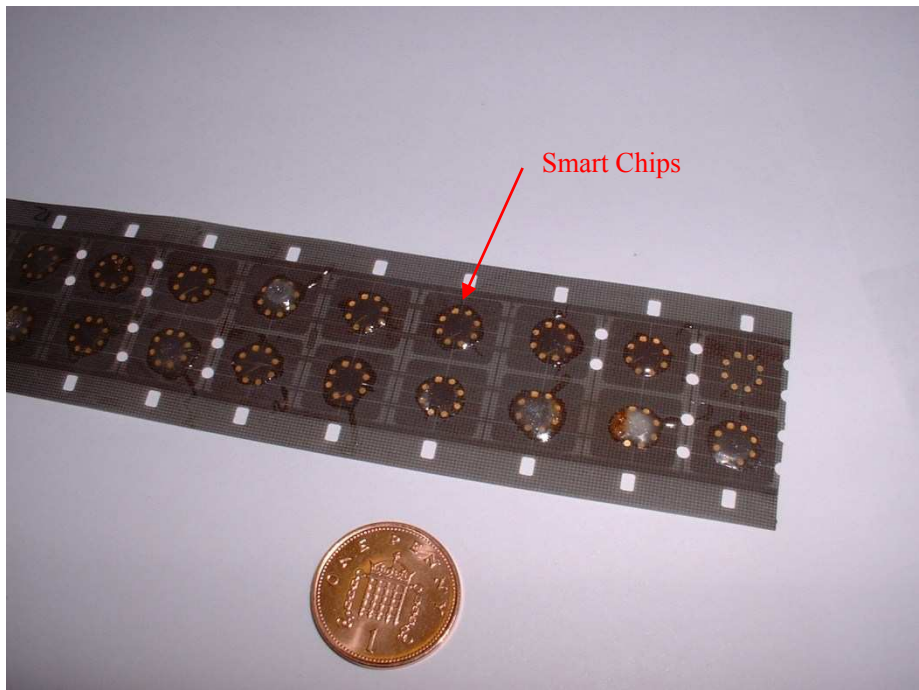
Figure 2.29: Integrated circuits for smart cards
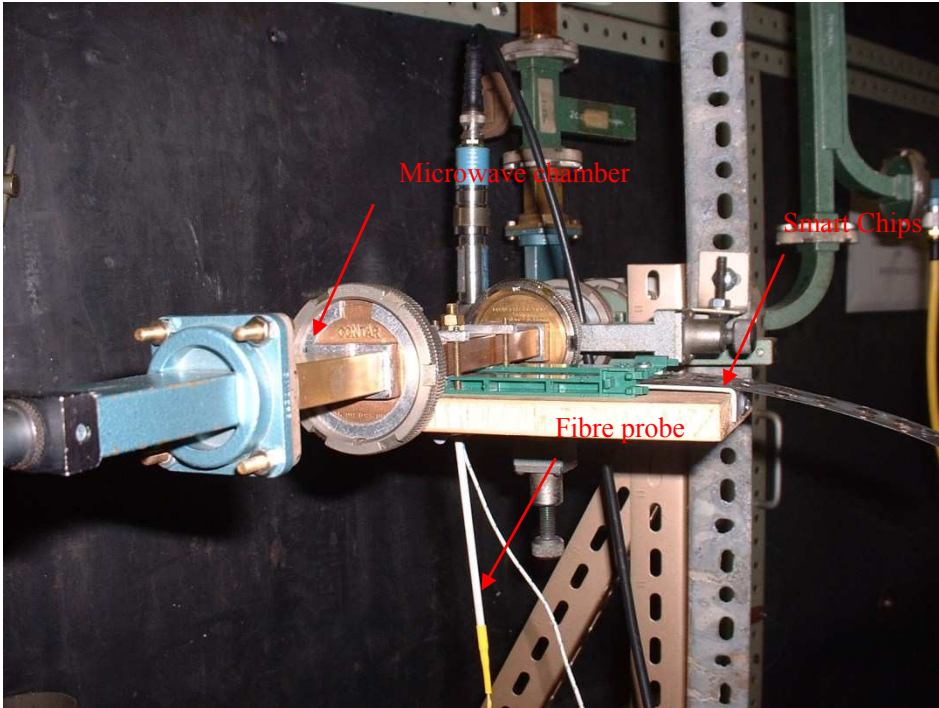
Figure 2.30: Setup for adhesive curing using Microwave FEL

Several samples were tested when the microwave FEL was switched on and off over the period of the fast heating of the glue. A typical result of such a test is shown in Figure 2.31, where the data from both thermometers are illustrated. The temperatures read from both thermometers were consistent before the FEL was switched on, showing

that both techniques used were applicable under normal conditions. However, once the FEL was switched on, the adhesive was immediately subjected to the focused heating of the microwave beam and the data obtained from the two sensors demonstrated a dramatic difference due to the fact that the thermocouple itself was experiencing 'self-heating'. As a result, it was no longer able to show the 'true' temperature of the glue surface in this microwave environment. By contrast, the optical fibre sensor was immune to the microwave interference and performed in a satisfactory way to give a accuracy temperature measurement. After the FEL was switched off, the thermocouple gradually cooled down and the temperature monitored was approximately the same as to that read by the optical fibre sensor.
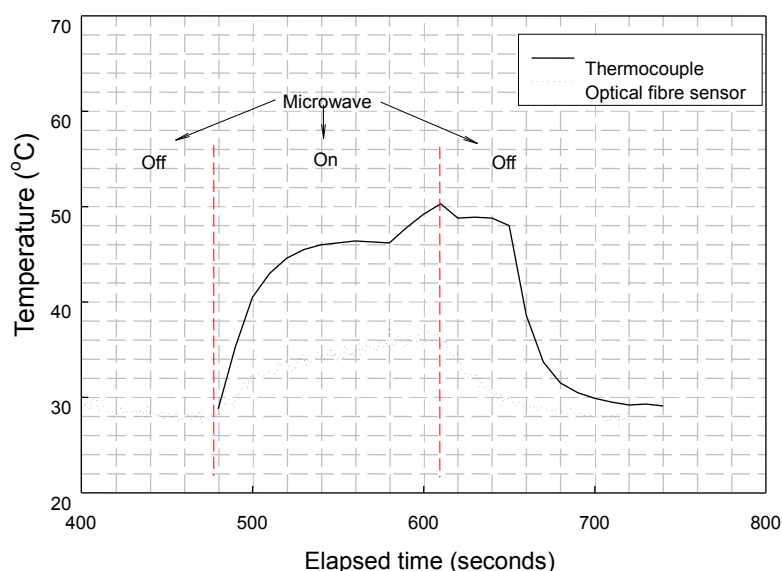
Figure 2.31: Adhesive temperature monitoring using the thermocouple and the optical fibre sensor

In most practical cases of adhesive temperature monitoring, it is preferable that the inner temperature rather than the surface temperature of the adhesive is to be monitored. In such cases, care is needed to be taken to ensure that the probe could be removed easily from the adhesive after the measurement is finished. Polytetrafluoroethylene (PTFE) material proved to be satisfactory for protecting the probe from the glue without degrading the sensor performance. The experimental results under a similar procedure of switch on and off of the microwave FEL, obtained

using a PTFE coating around the probe, are shown in Figure 2.32.
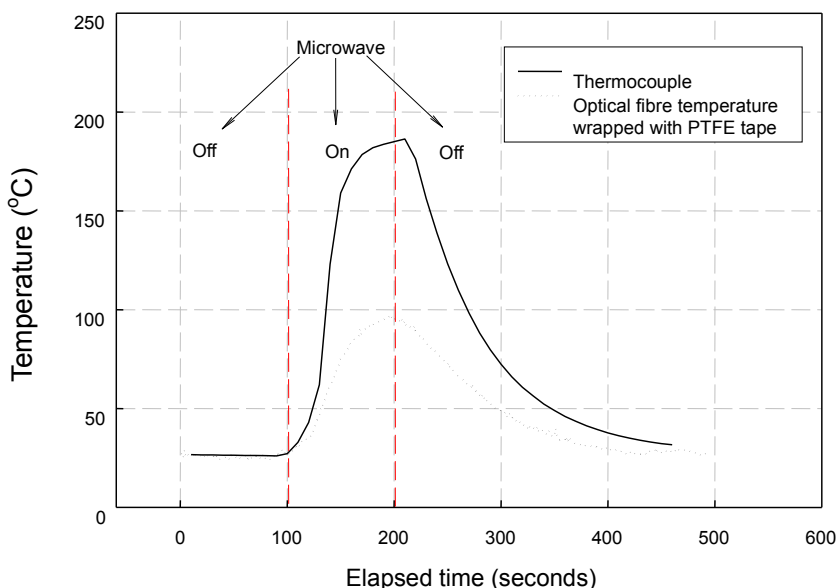
Figure 2.32: Adhesive temperature monitoring using the thermocouple and the optical fibre sensor (wrapped with PTFE tape) during the on-off process of the microwave FEL

To verify that it was the thermocouple over-reading the temperature rather than the fibre fluorescence base system under-reading the temperature, a test was carried out for measuring the water heated with FEL. The output power was varied to change of the water temperature. As shown in Figure 2.33, thermocouple read a temperature >100°C while the fluorescent thermometer shows a value below 100°C, when the water was not boiling. This result clearly indicates that the thermocouple was over-reading when the FEL was on, and thus the optical fibre thermometer is a better suited candidate in such environment where microwave energy is present.
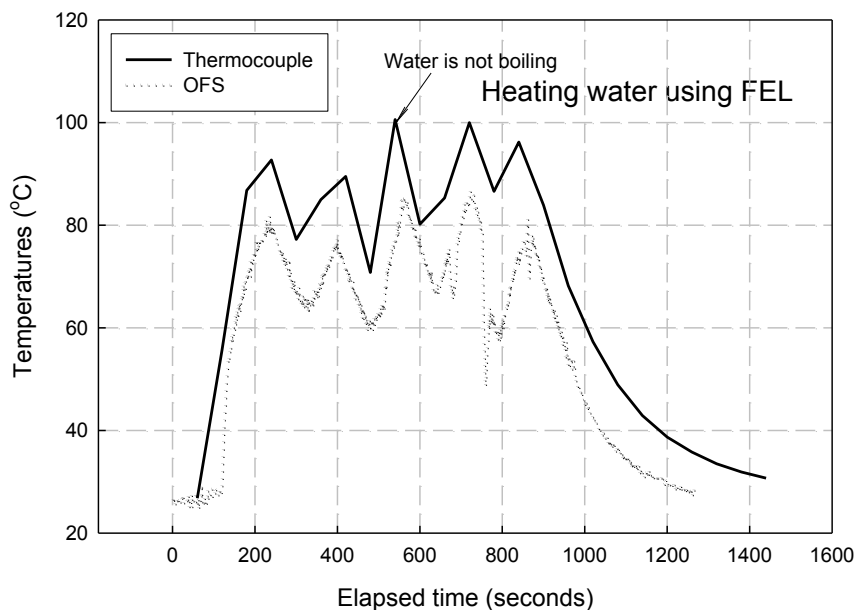
Figure 2.33: Cross comparison of the temperature monitoring of water heated by FEL microwave

2.6   Summary

A fluorescence based thermometry system developed in this investigation has shown promise for high temperature measurement applications when comapred against other optical fibre temperature sensors,.   In this work a fluorescence lifetime-based optical fibre temperature sensor system, including interface software and hardware using phase locked detection (PLD) scheme has been successfully developed, tested and evaluated both in the laboratory and in industrial context. The results showed that the fibre fluorescence thermometer, which can measure the temperature up to $900^{\circ}C$ with an accuracy of around $2^{\circ}C$ when using Tm:YAG crystal as the sensing material, could potentially be implemented for high temperature applications, especially under some circumstances when traditional methods have shown limitations.

References

[1].   K. T. V. Grattan, "*Fiber optic techniques for temperature sensing*", In: *Fiber Optic Chemical Sensors and Biosensors*, Vol. II, Edited by Wolfbeis, O. S. (London CRC press): pp. 151-192

[2].   K. A. Wickersheim, "*Fiberoptic thermometry: an overview*", In: Temperature – Its measurement and control in Science and Industry, Vol. 6(2), New York: The American Institute of Physics, 1992, pp711-714.

[3].   K. A. Wickersheim and R. V. Alves, "*Fluoroptic thermometry: a new RF-immune*

technology", Biomedical Thermology, Alan Liss, New York, 1982, pp.547-554,

[4]. C. Ovren, M. Adoleson and B. Hök, "*Fibre optic systems for temperature and vibration measurements in industrial applications*", Optics and Lasers in Engineering, Vol. 5(3), 1984, pp. 155-172

[5]. R. R. Sholes and J. G. Small, "*Fluorescent decay thermometer with biological applications*", Review of Scientific Instruments, vol. 51(7), 1980, pp.882-884.

[6]. Th. Bosselmann, A. Reule and J. Schröder, "*Fibre-optic temperature sensor using fluorescence decay time*", Proc. of 2nd Conf. on Optical Fibre Sensors (OFS '84), SPIE Proceedings, vol. 514, 1984, pp.151 -154.

[7]. K. T. V. Grattan and A. W. Palmer, "*A fibre optic temperature sensor using fluorescence decay*", SPIE Proceedings, Vol. 492, 1984, pp. 535.

[8]. K. T. V. Grattan and Z. Y. Zhang, "*Fibre optic fluorescence thermometry*", Chapman & Hall, London, 1995.

[9]. Z. Y. Zhang, "*Fibre Optic Fluorescence Thermometry*", Ph. D thesis, City University, London, 1993

[10]. Y. H. Shen, "*Charaterization of optical fibre senso systems for applications at high temperatures*", Ph. D thesis, City University, London,2005

[11]. Z.Y. Zhang, K.T.V. Grattan, A.W. Palmer, and B.T. Meggitt, "*Spectral characteristics and effects of heat treatment on intrinsic Nd-doped fibre thermometer probes*", Review of Scientific Instruments, vol. 69, 1998, pp.139-145

[12]. Z.Y Zhang, K.T.V. Grattan, A. W. Palmer, B. T. Meggitt, and T. Sun "*Characterization of erbium-doped intrinsic optical fibre sensor probes at high temperatures*", Review of Scientific Instruments vol. 69, 1998, pp.2924-2929

[13]. Z.Y. Zhang, K.T.V. Grattan, A.W. Palmer, "*Fibre-optic high-temperature sensor based on the fluorescence lifetime of alexandrite*", Review of Scientific Instruments, vol. 63, 1992, pp.3869-3873

[14]. W.H. Fonger and C.W. Struck, "*Temperature dependences of Cr3+ radiative and nonradiative transitions in ruby and emerald*", Physical Review B, vol. 11, 1975, pp.3251-3260

[15]. Z.Y. Zhang, K.T.V. Grattan, "*Temperature dependence of YAG:Cr3+ fluorescence lifetime up to 550 K*", Journal of Luminescence, vol. 62, 1994, pp.263-269

[16]. K.T.V. Grattan, J.D. Manwell, S.M.L. Sim, C.A. Willson, "*Lifetime investigation of fluorescence from neodymium-yttrium-aluminum garnet at elevated temperature*". Optics Communications, vol. 62, 1987, pp.104-107

[17]. Z. Zhang, J.H. Herringer and N. Djeu, "*Monolithic crystalline fibre optic temperature sensor*", Review of Scientific Instrument, vol. 68, 1997, pp.2068-2070

[18]. Y. Shen, W.Z. Zhao, T. Sun and K.T.V. Grattan, "*Characterization of an optical fibre thermometer using Tm3+:YAG crystal, based on the fluorescence lifetime approach*", Sensors and Actuators: A. Physical，vol. 109(1-2), 2003, pp.53-59

[19]. Y. Shen, W.Z. Zhao, J. He, et al, "*Fluorescence decay characteristic of Tm-doped YAG crystal fibre for sensor applications, investigated from room temperature to 1400 ᵒC*", IEEE Sensors Journal, 3(4), 2003, pp.507-512

[20]. Z.Y. Zhang, T. Sun, K.T.V. Grattan, A.W. Palmer, "*Optical Fiber Temperature Sensor Scheme Using Tm:Doped Yttrium Oxide Powder-Based Probe*", paper #P2-4, in

Proceedings of OFS'13, Kyongju, Korea, 13-16 April 1999

[21]. Y. Shen, R. Xu, "*Development of a compact sapphire fibre thermometer probe using fluorescent decay*", SPIE Proceedings,vol. 2895, 1996, pp.144-153

[22]. Y. Shen, Y. Wang, L. Tong and L. Ye. "*A novel sapphire fibre thermometer using fluorescent decay*", Sensors & Actuators A, vol. 71, 1998, pp70-73

[23]. Y. Shen, L. Tong, Y. Wang, L. Ye, "*Sapphire fibre thermometer ranging from 20 to 1800 ^{o}C*", applied Optics, vol. 38, 1999, pp.1139-1143

[24]. K. A. Wickersheim and M. H. Sun, "*Fiberoptic thermometry and its applications*", Journal of Microwave Power, vol. 22(2), 1987, pp.85-94

[25]. K. A. James, W. H. Quick and V. H. Strahan, "*Fiber optics: the way to true digital sensors?*" Control Engineering, vol. 26(2), 1979, pp.30-33

[26]. K. A. Wickersheim, "*Application of fibre optic thermometry to the monitoring of winding temperatures in medium and large power transformers*", SPIE Proceedings, vol. 1584, 1991, pp.3-14

[27]. M. Sun, "*Fiberoptic thermometry based on photoluminescent decay times*", In: Temperature - Its Measurement and Control in Science and Industry, American Institute of Physics, New York, Vol.6, Part 2, 1992, pp.715-719

[28]. L. J. Dowell and G. T. Gillies, "*Errors caused by baseline offset and noise in the estimation of exponential lifetimes*", Review of Scientific Instruments, vol. 62(1), 1990, 242-243

[29]. K. T. V. Grattan, R. K. Selli and A. W. Palmer, "*Ruby decay-time fluorescence thermometer in a fiber-optic configuration*", Review of Scientific Instruments, vol. 59(8), 1988, pp.1328-1335

[30]. A. T. Augousti, K. T. V. Grattan and A. W. Palmer, "*Visible-LED pumped fiber-optic temperature sensor*", IEEE Transaction of Instruments & Measurement, vol. 37(3), 1988, pp.470-472

[31]. Z. Y. Zhang, K. T. V. Grattan and A. W. Palmer, "Phase-locked detection of fluorescence lifetime and its thermometric applications, In: International Conference of Biomedical Optics '93, Los Angeles, January 1993. SPIE Proceedings, vol. 1885, 1993, pp.228-239

[32]. Th. Bosselmann, UK Patent Application GB 2,113,837A , 1983

[33]. Z. Y. Zhang, K. T. V. Grattan and A. W. Palmer, "*A novel signal processing scheme for a fluorescence based fibre-optic temperature sensor*", Review of Scientific Instruments, vol. 62(7), 1991, pp.1735-1742

[34]. V. Fernicola and L. Crovini, "*Two fluorescent decay-time thermometers*". In: 7th International Symposia Temperature, Toronto, Canada, April 30, American Institute of Physics, 1992.

[35]. Z. Y. Zhang, K. T. V. Grattan and A. W. Palmer, "*Phase-locked detection of fluorescence lifetime and its thermometric applications*", In: International Conference of Biomedical Optics '93, Los Angeles, January 1993. SPIE Proceedings, vol. 1885, 1993, pp.228-239.

[36]. Y. Shen, W. Zhao, J. He, T. Sun, K.T.V. Grattan，"*Fibre thermometer based on the cross detection of the fluorescent decay of Tm:YAG crystal fibre and background radiation*", SPIE Proceedings, Vol. 4920, 2002, pp.16-24

[37]. C.C Wright, R.A Stuart, J Lucas, A Al-Shamma'a,"*Low cost undulator magnets for industrial free electron lasers",* Optics Communications, Vol. 185,2000, 387-391

Chapter 3. Fluorescence-based optical fire alarm system

3.1   Application background

Optical fibre temperature sensors, compared to conventional fire alarm systems, such as electrical sensors using coaxial cables, are light weight and small size, therefore show potential for energy saving through lower fuel consumption when they are used for aircraft engine temperature excursion detection.   This chapter shows the development and evaluation of a fluorescence-based optical fibre fire alarm system, designed specifically for aerospace applications through collaboration with an industrial partner, Kidde plc.   The sensing concept discussed, however, is generic and can be extended to other sensing applications.

3.1.1   The requirements of fire alarm system for application

As required by the industrial partner, Kidde plc, the optical fire alarm system developed is required to meet the following specifications

- **Lightness**

This is a key requirement as the light weight of the sensor system will result in less fuel consumption therefore energy saving.   This is in line with the trend of the development in the modern aerospace industry, where more and more light and strong new materials are needed.

- **High accuracy**

Any error in measurement and monitoring in the aerospace application will potentially result in catastrophe. Therefore high accuracy of the sensor system is vital.

- **Rapid response**

It is also essential to have a rapid response of the appearance of any type of temperature excursion or hot spot before it causes a fatal damage to the aeroplane.

● **Wide temperature operational range**

The fire alarm system employed in aerospace applications should allow a wide temperature operational range (from -40°C to 600°C) for aero-engine condition monitoring, with an ability to detect any hot spot with excursion temperatures of 50°C above the background operational temperature.

● **Safety**

While the system is used to detect the existence of a hot spot for safety protection, the sensor itself should not create any potential hazards, such as short circuit, burst, etc.

3.1.2   Why fluorescence-based optical fibre sensor system?

As discussed in previous chapters, the fluorescence-based temperature systems have shown advantages in temperature measurement applications, such as of small size, light weight, safety, immunity to electromagnetic interference, and also sustainability in high temperature environments.   Fire detection using optical fibres, on the basis of fluorescence, has been discussed extensively by Sun [1-3] in consideration of the viability of an optical alternative to the current "industrial standard" system, which is based on the resistance and capacitance change of a co-axial cable, widely used for aircraft engine fire detection [4].

While the system discussed and developed in Chapter 2 was designed for single point temperature measurement, it is possible to extend it to be a multiplexed temperature sensor system. In the following sections, an Nd-doped fibre fluorescence lifetime-based fire alarm system is described and evaluated.

3.2   Principle of fluorescence-based fire alarm system

3.2.1   Two fluorescence decay lifetimes measurement

The sensing principle is based on the assumption that a single exponential decay of fluorescence lifetime is observed when a fluorescence material is exposed to a uniform temperature environment.   Therefore when a 'hotspot' occurs along the full length of

the fibre which is used as a sensor element, the temperature change against the uniform background temperature will result in a fluorescence signal showing two decay lifetimes, with each representing different temperature zones.   As there is no specific requirement for the fire alarm system to be location-sensitive, the more expensive and complex time domain reflectometry approach is not needed, instead the fluorescence based-system has been proved to be well suited to this application.

The fluorescence of the fibre, Nd-doped fibre in this case, is induced by the light from a laser diode (LD) at a wavelength where the rare earth ion absorbs. The fluorescence signal which contains both the decay lifetimes of fluorescence from the 'hotspot' and from the dominate background is detected and processed.   Therefore the temperatures of both hotspot and background can be derived through the deconvolution of the two corresponding fluorescence lifetimes using the methods discussed in detail below.

The fire alarm system developed in this work uses the light from a square wave modulated LD source at a wavelength of 785nm. Following the termination of the excitation light, a temperature-dependent fluorescence decay signal is emitted from the Nd-doped fibre. In the case of the Nd-doped fibre is exposed to a uniform temperature background, the fluorescence decay signal may be described as a single-exponential by:

$$f(t) = A\exp(-t/\tau) \tag{3.1}$$

where A is the initial fluorescence amplitude and τ is the corresponding fluorescence decay lifetime, which is related to the background temperature.

When a hotspot occurs along the fibre, a double-exponential decay is expected to be obtained and the resulting signal can thus be expressed as

$$f(t) = A_1 \exp(-t/\tau_1) + A_2 \exp(-t/\tau_2) \tag{3.2}$$

where A_1 and A_2 are the initial amplitudes, τ_1 and τ_2 are the lifetimes corresponding to the background temperature T_1 and the hotspot temperature T_2 respectively. Thus the temperatures of the background and the hotspot can be derived from the fluorescence

signal, which contains both of the lifetimes of the τ_1 and τ_2, through Equation 3.3.

$$T_1 = f_1(\tau_1), \;\; T_2 = f_2(\tau_2) \tag{3.3}$$

In practice, the actual fluorescence signal obtained is not exactly an ideal exponential decay, as described in Equation 3.2, either due to a non-single exponential decay signal obtained from the Nd-fibre or the nonlinear response of the signal transfer and data acquisition system, or a combination of them. The complexity of the signal obtained makes the determination of the hotspot temperature more difficult, as the signal which contains the hotspot temperature only represents a very small portion of the fluorescence signal from the fibre, under the dominating background signal. Hence some measures of the solution have to be introduced into the sensor system design to enhance the accuracy and performance of the system, which will be discussed in the following sections.

3.2.2 Digital regress of double exponential signal

As discussed above, the PLD method is used in the point fluorescence based temperature sensor discussed in the previous chapter, however this is not a suitable method for the application of fluorescence based fire alarm system. This is due to the fact that the signals obtained from the system usually demonstrate to be two or more exponential decay. To overcome the limitation of the PLD method discussed above, a digital processing procedure is then introduced for regressing the double exponential decay. Below shows the discussions about the two algorithms which are commonly used for double exponential regression.

3.2.2.1 Double Prony approach

For a general exponential process, a function can be expressed as follows [4]

$$f(x) = A_1 \exp(a_1 x) + A_2 \exp(a_2 x) + \cdots + A_n \exp(a_n x) \tag{3.4}$$

where equation (3.4) can also be approximately expressed in the following generalized form [5]:

$$f(x) = A_1 u_1^x + A_2 u_2^x + \cdots + A_n u_n^x \qquad (3.5)$$

To solve this kind of approximation, a Prony's method will be used where the values of $f(x)$ are specified as a set of N equally spaced points, f_i. A linear change of variables has been introduced in advance in such a way that the data points, $x = 1, 2, \cdots, (N-1)$ form a set of linear equations:

$$f_{j+n\Delta N} + f_{j+(n-1)\Delta N}\alpha_1 + f_{j+(n-2)\Delta N}\alpha_2 + \cdots + f_j\alpha_n = 0$$
$$j = 0, 1, 2, \cdots, (N - n\Delta N - 1) \qquad (3.6)$$

where the sample spacing index, ΔN, in each equation is an integer which satisfies $(N - n\Delta N) \geq n$, and $\alpha_i (i = 1, 2, \cdots, n)$ are the unknown coefficients. After the values of $\alpha_i (i = 1, 2, \cdots, n)$ are determined, the ΔN^{th} powers of u_i in Equation 3.5, $u_i^{\Delta N} (i = 1, 2, \cdots, n)$ can be derived as they are the roots of the following algebraic equation [5]:

$$y^n + \alpha_1 y^{n-1} + \alpha_2 y^{n-2} + \cdots + \alpha_{n-1}y + \alpha_n = 0 \qquad (3.7)$$

In the case of the fluorescence based fire alarm system, the observed double exponential fluorescence decay signal is described in Equation 3.2. The Prony's method discussed above can be directly applied to obtain the corresponding lifetimes through a four-parameter model. According to Equation 3.6, $(N - 2\Delta N)$ linear equations can be directly formed from the N samples, $f_j (j = 1, 2, \cdots, N)$ given as

$$f_{j+2\Delta N} + f_{j+\Delta N}\alpha_1 + f_j\alpha_2 = 0$$
$$j = 0, 1, 2, \cdots, (N - 2\Delta N - 1) \qquad (3.8)$$

or by the following matrix form [5]:

$$\mathbf{Y} = \mathbf{XA} \qquad (3.9)$$

61

where $\mathbf{Y} = \begin{bmatrix} f_{2\Delta N} \\ f_{2\Delta N+1} \\ \vdots \\ f_{N-1} \end{bmatrix}$, $\mathbf{X} = \begin{bmatrix} f_{\Delta N} & f_0 \\ f_{\Delta N+1} & f_1 \\ \vdots & \vdots \\ f_{N-\Delta N-1} & f_{N-2\Delta N-1} \end{bmatrix}$ and $\mathbf{A} = \begin{bmatrix} -\alpha_1 \\ -\alpha_2 \end{bmatrix}$.

By means of the least squares method, matrix $\mathbf{A}$ in Equation 3.9 can be calculated by the use of the following matrix algorithm:

$$\mathbf{A} = \begin{bmatrix} \mathbf{X}^T\mathbf{X} \end{bmatrix}^{-1} \mathbf{X}^T\mathbf{Y} \tag{3.10}$$

and $\begin{bmatrix} \mathbf{X}^T\mathbf{X} \end{bmatrix} = \begin{bmatrix} \sum\limits_{j=0}^{N-2\Delta N-1} f_{j+\Delta N}^2 & \sum\limits_{j=0}^{N-2\Delta N-1} f_j f_{j+\Delta N} \\ \sum\limits_{j=0}^{N-2\Delta N-1} f_j f_{j+\Delta N} & \sum\limits_{j=0}^{N-2\Delta N-1} f_j^2 \end{bmatrix}$

As a result of the noise present in the samples, the matrix $\mathbf{A}$ determined by Equation 3.10 cannot be used as a consistent estimate of Equation 3.9. To solve the resulting problem, an auxiliary matrix $\mathbf{Z}$ is introduced, and Equation 3.9 is rewritten as follows [5],

$$\begin{aligned} \mathbf{Z}^T\mathbf{Y} &= \mathbf{Z}^T\mathbf{X}\mathbf{A} \\ \mathbf{A} &= \begin{bmatrix} \mathbf{Z}^T\mathbf{X} \end{bmatrix}^{-1} \begin{bmatrix} \mathbf{Z}^T\mathbf{Y} \end{bmatrix} \end{aligned} \tag{3.11}$$

where $\mathbf{Z} = \begin{bmatrix} f_{\Delta N+k} & f_k \\ f_{\Delta N+k+1} & f_{k+1} \\ \vdots & \vdots \\ f_{N+k-\Delta N-1} & f_{N+k-2\Delta N-1} \end{bmatrix}$, $0 \le k \le \Delta N$

and $\begin{bmatrix} \mathbf{Z}^T\mathbf{X} \end{bmatrix} = \begin{bmatrix} \sum\limits_{j=0}^{N-2\Delta N-1} f_{j+\Delta N} f_{j+\Delta N+k} & \sum\limits_{j=0}^{N-2\Delta N-1} f_{j+\Delta N+k} f_j \\ \sum\limits_{j=0}^{N-2\Delta N-1} f_{j+k} f_{j+\Delta N} & \sum\limits_{j=0}^{N-2\Delta N-1} f_{j+k} f_j \end{bmatrix}$, $\begin{bmatrix} \mathbf{Z}^T\mathbf{Y} \end{bmatrix} = \begin{bmatrix} \sum\limits_{j=0}^{N-2\Delta N-1} f_{j+2\Delta N} f_{j+\Delta N+k} \\ \sum\limits_{j=0}^{N-2\Delta N-1} f_{j+2\Delta N} f_{j+k} \end{bmatrix}$.

After α_1, α_2 are determined by Equation 3.11, $u_1^{\Delta N}$ and $u_2^{\Delta N}$ are the roots of algebraic equation:

$$y^2 + \alpha_1 y + \alpha_2 = 0 \tag{3.12}$$

thus
$$\begin{cases} u_1^{\Delta N} = \dfrac{-\alpha_1 + \sqrt{\alpha_1^2 - 4\alpha_2}}{2} \\ u_2^{\Delta N} = \dfrac{-\alpha_1 - \sqrt{\alpha_1^2 - 4\alpha_2}}{2} \end{cases}$$

Then the two estimations of lifetime will be given by

$$\begin{cases} \tau_1 = -\Delta / \ln(u_1) \\ \tau_2 = -\Delta / \ln(u_2) \end{cases} \tag{3.13}$$

where Δ is the sampling time interval.

3.2.2.2 Levenberg-Marquardt Algorithm

The Levenberg-Marquardt (LM) algorithm is an iterative technique that locates the minimum of a multivariate function which is expressed as the sum of squares of non-linear real-valued functions [6-7]. The LM algorithm is the most popular curve-fitting algorithm; it is used in almost of the software packages that provides a generic curve-fitting tool. A short description of the LM is given below. Detailed analysis of the LMA is beyond the scope of this thesis but is available in literatures [8-9].

To solve a problem of curve fitting of a double exponential decay signal expressed in Equation 3.2, or of a general non-linear function of:

$$\mathbf{X} = f(\mathbf{P}) \tag{3.14}$$

where $\mathbf{P}$ is a parameter vector.   The curve fitting process is to find the $\mathbf{P}^+$ that best satisfies the measured vector $\hat{\mathbf{X}}$ to enable the squared distance between $\hat{\mathbf{X}}$ and the estimated vector $\mathbf{X}$, i.e. $\varepsilon = \hat{\mathbf{X}} - \mathbf{X}$ to be minimum.   The basis of the LM is to find a linear approximation to f in the neighbourhood of $\mathbf{P}$. For a small $\delta_\mathbf{P}$, a Taylor series expansion leads to the approximation of [6]

$$f(\mathbf{P} + \delta_\mathbf{P}) \approx f(\mathbf{P}) + \mathbf{J}\delta_\mathbf{P} \tag{3.15}$$

where $\mathbf{J}$ is the Jacobian matrix $\dfrac{\partial f(\mathbf{P})}{\partial \mathbf{P}}$.

Similar to all the other non-linear optimization methods, LM algorithm is iterative.

Initiated at the starting point $\mathbf{P}_0$, the method produces a series of $\mathbf{P}_1, \mathbf{P}_2 \ldots$ that converges towards a local minimizer for f. At each iteration step, it is required to find a $\delta_\mathbf{P}$ that can minimize the square of $\hat{\mathbf{X}} - f(\mathbf{P} + \delta_\mathbf{P}) \approx \hat{\mathbf{X}} - f(\mathbf{P}) - \mathbf{J}\delta_\mathbf{P} = \mathbf{\varepsilon} - \mathbf{J}\delta_\mathbf{P}$. The sought $\delta_\mathbf{P}$ is thus the solution: the minimum is attained when it is orthogonal to the column space of $\mathbf{J}$. Thus this leads to $\mathbf{J}^T(\mathbf{J}\delta_\mathbf{P} - \mathbf{\varepsilon}) = 0$, where $\mathbf{J}^\mathrm{T}$ is the transposition of $\mathbf{J}$, which yields $\delta_\mathbf{P}$ as the solution of the so-called *normal equations* [6]:

$$\mathbf{J}^T \mathbf{J} \delta_\mathbf{P} = \mathbf{J}^T \mathbf{\varepsilon} \tag{3.16}$$

The matrix $\mathbf{J}^T\mathbf{J}$ in the left hand side of Equation 3.16 is the approximate Hessian, i.e. an approximation to the matrix of second order derivatives.

The LM algorithm actually solves the equation by a 'damped version' of Equation 3.16, known as the *augmented normal equations*

$$\mathbf{N}\delta_\mathbf{P} = \mathbf{J}\mathbf{\varepsilon} \tag{3.17}$$

where the off-diagonal elements of $\mathbf{N}$ are identical to the corresponding elements of $\mathbf{J}^T\mathbf{J}$ and the diagonal elements are given by

$$\mathbf{N}_{ii} = u + (\mathbf{J}^T\mathbf{J})_{ii} \tag{3.18}$$

This strategy of altering the diagonal elements of $\mathbf{J}^T\mathbf{J}$ is called *damping* and u is referred as the *damping term* (or *damping factor*).

In each iteration step of LM algorithm method, the parameter vector $\mathbf{P}$ is replaced by a new estimate $\mathbf{P} + \delta_\mathbf{P}$, if the updated parameter vector $\mathbf{P} + \delta_\mathbf{P}$ with $\delta_\mathbf{P}$ calculated from Equation 3.17 leads to a reduction in the error of $\mathbf{\varepsilon} = \hat{\mathbf{X}} - \mathbf{X}$, the update is accepted and the process repeats with a decreased damping term. Otherwise, the damping factor is increased, the augmented normal equations are required to be solved again and the process iterates until a value of $\delta_\mathbf{P}$ that decreases $\mathbf{\varepsilon} = \hat{\mathbf{X}} - \mathbf{X}$ is found. The process of repeatedly solving Equation 3.17 for different values of the damping

term continues until an acceptable update to the parameter vector is found that leads to one iteration of the LM algorithm. The LM algorithm terminates when at least one of the following conditions is met, and the last parameter vector $\mathbf{P}$ is considered to be the solution [6]:

- The magnitude of the gradient of $\varepsilon^T\varepsilon$, i.e. $\mathbf{J}^T\varepsilon$ in the right hand side of Equation 3.16 drops below a threshold.

- The relative change in the magnitude of $\delta_\mathbf{P}$ drops below a threshold.

- The error $\varepsilon^T\varepsilon$ drops below a threshold.

- A maximum number of iterations is completed

For the fire alarm system, a four parameter Vector $\mathbf{P}=(A_1,B_1,\ A_2,B_2)$ can be used to represent the following measured double exponential decay using LM algorithm:

$$f(t) = A_1 \exp(B_1 t) + A_2 \exp(B_2 t) \qquad (3.19)$$

where $B_1 = -\dfrac{1}{\tau_1}$ and $B_2 = -\dfrac{1}{\tau_2}$.

For a double-exponential regression, the *Double-Prony method* offers a fast solution, however the *Levenberg-Marquardt Method* gives higher accuracy, but at a cost of longer computing time due to its algorithm complexity. In this work, the latter method was used for high accuracy measurement after a preliminary comparison of this two algorithms using a commercial simulation software package of Matlab. The detailed procedure of the LM algorithm is programmed in the interface software using *Delphi* Ver. 6.0, though its detail is not present in this thesis due to the complex nature of the program, which is part of the whole Delphi project of the system, and the limitation of the space of the thesis.

3.2.3   Solutions to the fire alarm system signal processing

The determination of the hotspot temperature, and thus the decay time associated

with that requires the de-convolution of that signal from the background. With the added problem of non-linearity of the observed signal, it is difficult to obtain the temperatures corresponding to the background and to the hotspot directly from the original signal using Equation 3.2, and a modified signal processing approach is required. In this work, two different methods, termed as the *correction method* and the *lifetime adjustment method*, were introduced and implemented to solve the problem and obtain comparative data.

3.2.3.1 Correction method

The *correction method* aims to transform the obtained complex signals into near ideal ones, which can then be further processed by the use of equations 3.1-3.3.

When the Nd-fibre experiences a uniform temperature, the observed signal, $f(\tau,t)$, can be adjusted to be an ideal single exponential through the following modification

$$f'(\tau,t) = f(\tau,t)/h(\tau,t) \tag{3.20}$$

where τ is the lifetime obtained by fitting the actual signal with single exponential, $f'(\tau,t)$ is the corresponding ideal single exponential signal, and $h(\tau,t)$ is the experimental correction factor given by

$$h(\tau,t) = f(\tau,t)/f'(\tau,t) \tag{3.21}$$

which can be derived from a curve fitting of the observed signal $f(\tau,t)$ and the ideal signal $f'(\tau,t)$ when the entire fibre is exposed to an uniform temperature. Once the correction factor is obtained, the same correction factor is then used for the rest of measurement, either with or without the presence of a hotspot.

When there is a hotspot, the received signal is adjusted by the correction factor to achieve a double exponential signal.

$$f'(\tau_1,\tau_2,t) = f(\tau_1,\tau_2,t)/h(\tau,t) \tag{3.22}$$

where $f(\tau_1, \tau_2, t)$ is the actual received signal, and $f'(\tau_1, \tau_2, t)$ is the corrected signal. τ is the lifetime of single exponential fitting of the signal $f(\tau_1, \tau_2, t)$, and $h(\tau, t)$ is the corresponding correction factor of τ.

After correction, $f'(\tau_1, \tau_2, t)$ can be processed using Equation 3.2 to obtain two values of the lifetimes (τ_1, τ_2), which are related to the corresponding temperatures (T_1, T_2) by Equation 3.3.

However, the correction method has demonstrated certain limitations and they are listed below

- The best suited correction factor $h(\tau, t)$ is difficult to be obtained under the wide range of conditions of this experiment (temperature ranges of both the hotspot and the background)

- The accuracy of the calibration obtained is poor

3.2.3.2 Lifetime Adjustment Method

In view of the difficulty of obtaining a suitable correction factor $h(\tau, t)$ and other problems in the system using the above approach, such as the sensitivity to the fluctuations of LD light intensity, a second approach, i.e. *lifetime adjustment method*, was introduced and discussed in this section.

In this method, no correction factor is involved, and instead all the decay signals were treated as double exponentials, no matter whether a hot spot is present or not. Thus two lifetimes (τ_1, τ_2) are obtained, and two temperatures are derived. The temperatures are calculated using Equation 3.3 directly from lifetime (τ_1, τ_2). Then they are adjusted according to a predefined initial lifetime set of (τ_1^0, τ_2^0), and this approach is thus termed as *Lifetime Adjustment Method* and described as follows.

As an initial condition, in the absence of a hotspot, the initial values, τ^0 from a single exponential fitting and τ_1^0, τ_2^0 from a double-exponential fitting are obtained

respectively from the fluorescence signal.   Thus the initial temperature T_0 was obtained from lifetime τ^0, and, as there is no hot spot present at the initial condition, the lifetimes τ_1^0, τ_2^0 obtained from the same fluorescence signal using double-exponential fitting, should respond to the same temperature value of T_0.   Given a uniform temperature background, the following conditions are satisfied

$$
\begin{aligned}
T_0 &= f(\tau^0) \\
g(\tau_1^0) &= T_0, \qquad h(\tau_2^0) = T_0
\end{aligned}
\tag{3.23}
$$

where the functions, $f(\tau), g(\tau_1), h(\tau_2)$ are predefined through an initial calibration of the experimental data.

At any other temperature, weather a hot spot is present or not, the lifetimes τ_1 and τ_2 interpreted from the double-exponential signal fitting, may be transformed to represent their corresponding temperatures T_1 and T_2, after the adjustment using the initial values of T_0, τ_1^0, τ_2^0

$$
\begin{aligned}
T_1 &= F_1(\tau_1, \tau_1^0) = g(\tau_1^0) + F_1'(\tau_1, \tau_1^0) = T_0 + F_1'(\tau_1, \tau_1^0) \\
&= T_0 + \left[A_0 + A_1(\tau_1 - \tau_1^0) + A_2(\tau_1 - \tau_1^0)^2 \right]
\end{aligned}
\tag{3.24}
$$

$$
\begin{aligned}
T_2 &= F_2(\tau_2, \tau_2^0) = h(\tau_2^0) + F_2'(\tau_2, \tau_2^0) = T_0 + F_2'(\tau_2, \tau_2^0) \\
&= T_0 + \left[B_0 + B_1(\tau_2 - \tau_2^0) + B_2(\tau_2 - \tau_2^0)^2 \right]
\end{aligned}
\tag{3.25}
$$

where A_0, A_1, A_2, and B_0, B_1, B_2 are the calibration parameters from experiments.

A series of more complex calibration functions, shown in Equation 3.26 and 3.27, may be required to achieve a higher accuracy, especially under the circumstances with a varying background.

$$
T_1 = T_0 + [A_0 + A_1(\tau_1 - \tau_1^0) + A_2(\tau_1 - \tau_1^0)^2] + G(\tau_1, \tau_2)
\tag{3.26}
$$

$$
T_2 = T_0 + [B_0 + B_1(\tau_2 - \tau_2^0) + B_2(\tau_2 - \tau_2^0)^2] + H(\tau_1, \tau_2)
\tag{3.27}
$$

The correlation functions, termed as $G(\tau_1, \tau_2)$ and $H(\tau_1, \tau_2)$, are added to take into account of the effect caused by the varying background.

If the LD intensity fluctuation is taken into consideration, the above equations should be modified as follows

$$T_1 = H(I) \cdot \{T_0 + [A_0 + A_1(\tau_1 - \tau_1^0) + A_2(\tau_1 - \tau_1^0)^2] + F(\tau_1, \tau_2)\} \qquad (3.28)$$

$$T_2 = H(I) \cdot \{T_0 + [B_0 + B_1(\tau_2 - \tau_2^0) + B_2(\tau_2 - \tau_2^0)^2] + G(\tau_1, \tau_2)\} \qquad (3.29)$$

where $H(I)$ is the correction factor in relation to the fluctuation of the light source intensity.

To implement this Lifetime Adjustment method requires the availability of a set of predefined parameters and this can only be achieved through a series of pre-defined experiments.

3.2.3.3 Flowcharts for the two methods

For comparison, the flowcharts of the data processing procedures for the two methods are illustrated in Figure 3.1.

These two approaches used to provide a better signal processing and thus enhance the performance of the fire alarm system. With preliminary tests and evaluations, the lifetime adjustment method was observed to offer better performance, in terms of accuracy, which is believed to be benefited from more experimental calibration parameters being used. More details of the experimental tests will be discussed in the following sections.

Correction method   *Lifetime Adjustment*
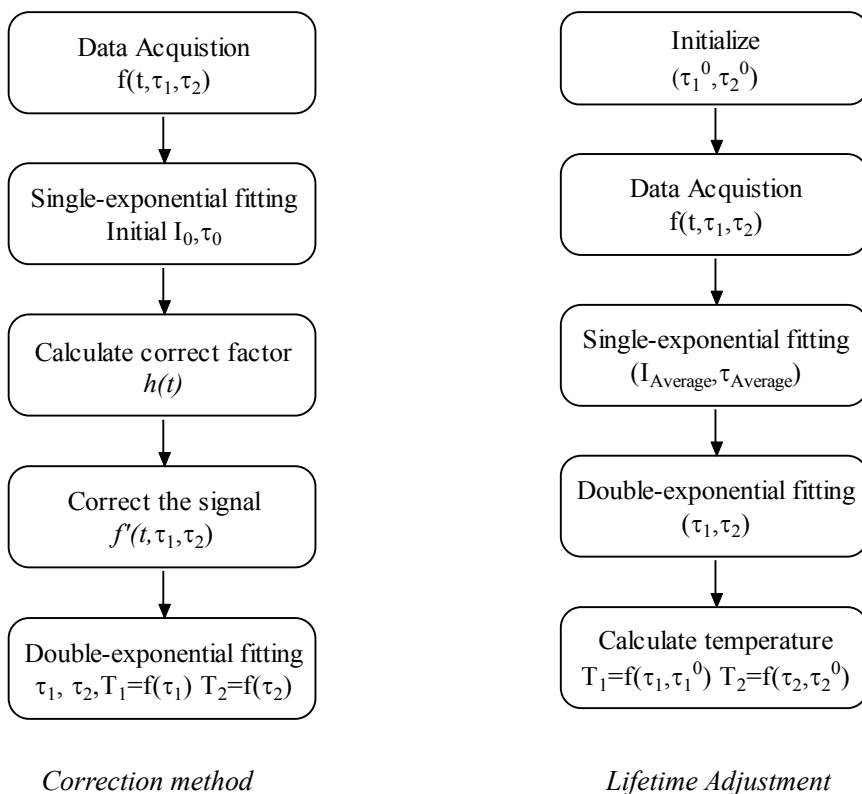
Figure 3.1: Flowcharts of the two signal processing methods

3.3 *Experimental setup of the fluorescence-based fire alarm system*

3.3.1 Probe configuration

A one meter probe was prepared for the fire alarm system, as shown in Figure 3.2. The probe consisted of one piece of Nd-doped fibre of 80 cm length, with the tips connected to two pieces of plain glass fibres. The maximum length of the sensor fibre, 3-4 meters estimated, will be limited by the absorption of the fibre and the fluorescence signal ration of that of hotspot to that of background. The Nd-fibre was placed in a one meter steel tube for protection. Before being placed into the protective tube, the Nd-fibre was annealed at 600°C for about 24 hours, as this had previously been seen as important for stabilizing the performance of the fibre. The probe thus assembled can endure temperatures up to 550°C (for continuous exposure) and 700~800°C (for a pulsed temperature excursion), based on the test results of the fluorescence characteristics of Nd doped fibres carried out by Zhang et al [10].
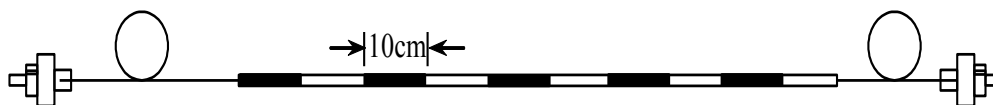
Figure 3.2: Assembly of a sensing probe

3.3.2 System setup

A schematic diagram of an optical fibre fluorescence-based fire alarm system, using the 1m Nd-doped fibre probe described above as a sensing element, is illustrated in Figure 3.3.   Figure 3.4 shows the experimental setup of the fire alarm system prototype in the laboratory.   A 785 nm laser diode, whose output is modulated by a TTL square wave, is used to pump the doped fibre at both ends through a 2×2 coupler. Following the termination of the stimulation light, the fluorescence signal generated is captured by an InGaAs PIN photo-detector from the other arm of the coupler. Subsequently the captured fluorescence decay signal is digitalized and passed to a computer via a *PowerDAQ* data acquisition card.   An interface software program was written and used to regress the digitalized fluorescence signal, and hence to obtain the lifetimes and their corresponding temperatures, both of the background and of the hotspot.
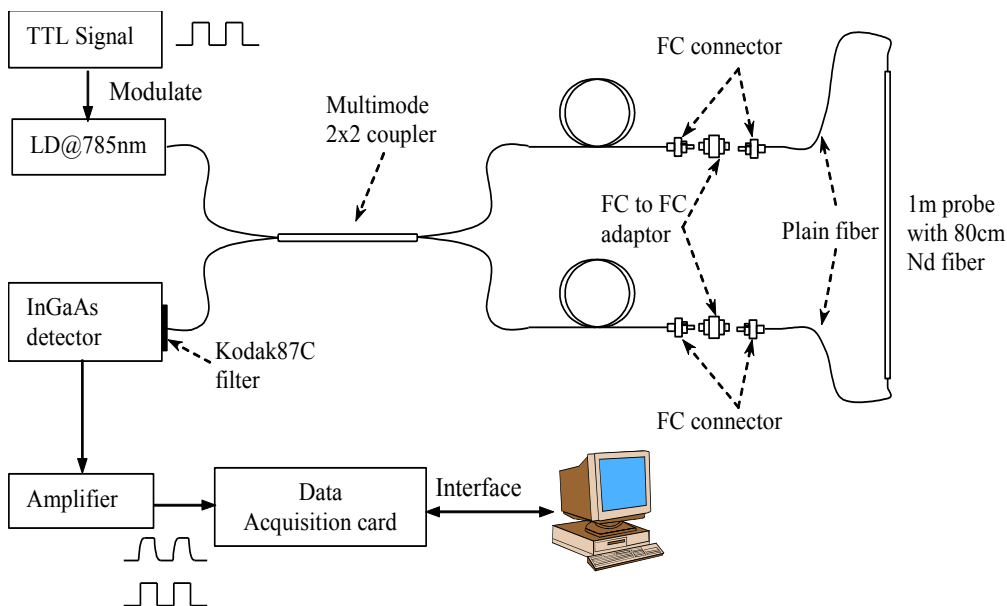
Figure 3.3: Schematic of the fluorescence fire alarm system
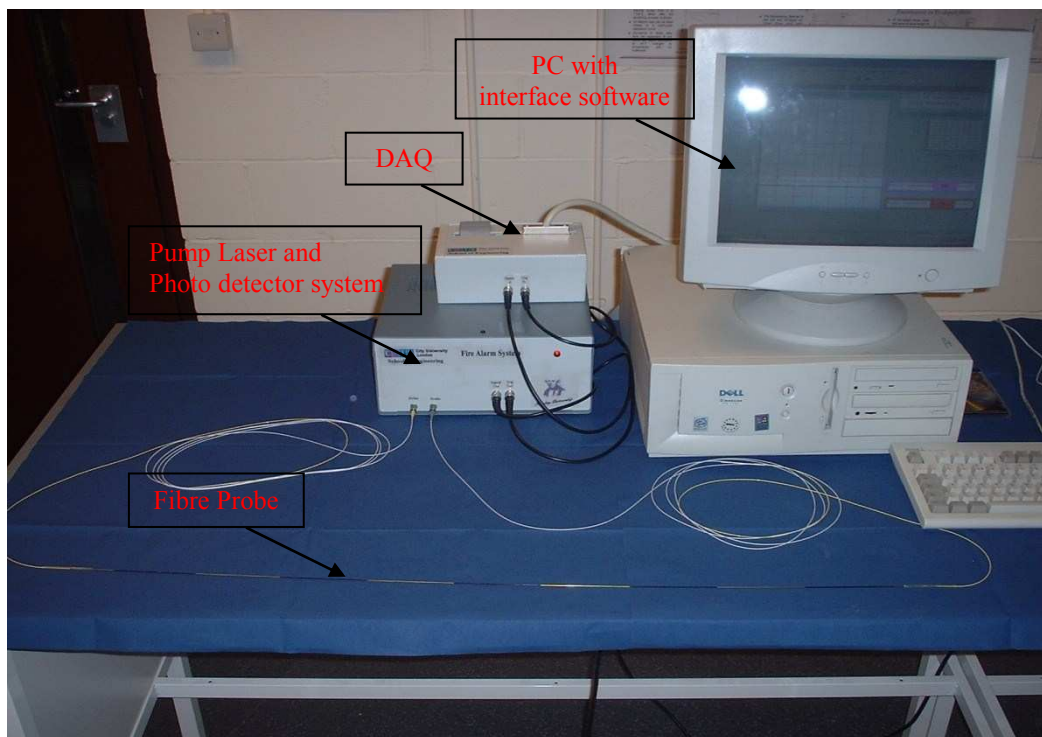
Figure 3.4: Fluorescence Fire Alarm System, showing 1m length of test fibre and the processing electronics

3.3.3 Interface software

The user interface software of the fire alarm system was developed using the platform of *Delphi Ver. 6.0*. Figure 3.5 shows a printout of the user-friendly interface designed specifically to reflect both the background and hot-spot temperature variations.

The software was designed to control and access the data acquisition card, read data from the card. It was programmed to calculate the lifetimes using Levenberg-Marquardt Algorithm for double exponential data fitting from the digitalized fluorescence signal (after being adjusted by a correction factor, or after the resulted lifetimes having been adjusted), and derive and display the corresponding temperatures, of the background and of the hotspot.
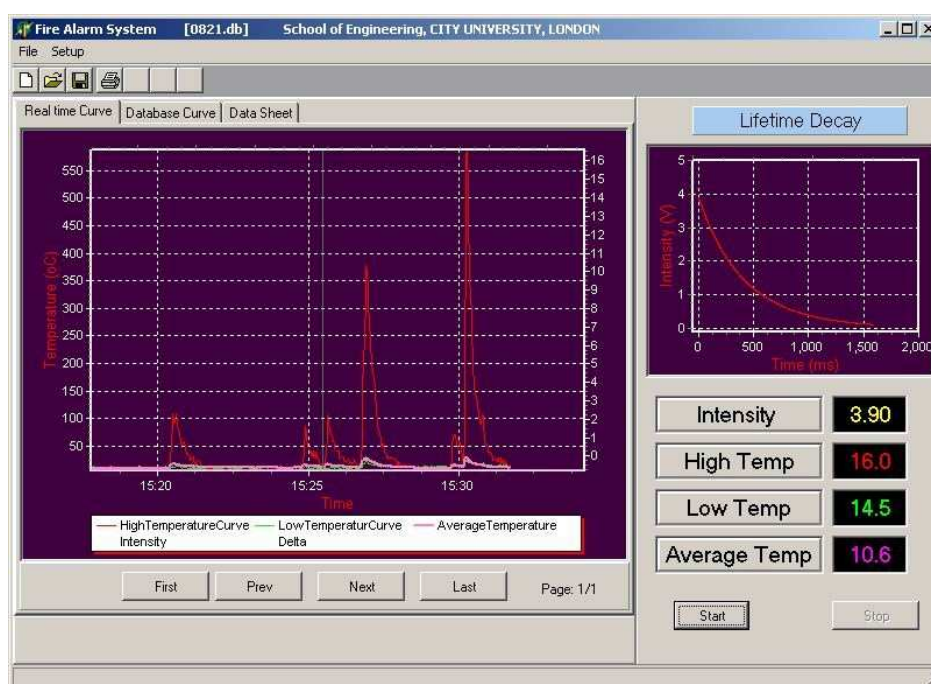
Figure 3.5: Printout from the interface software – fluorescence-based fire alarm system

The program was built with a function of self-calibration, which is carried out automatically under certain pre-set conditions using the experimental data obtained during the evaluation. This is essential to minimize the influence of the signal intensity variation and several other potential system errors.

The interface software also provides some additional functions, such as data management, providing a user-friendly graphic and datasheet presentation of the measurement, etc.

3.4   *Tests and evaluations of the fluorescence-based fire alarm system*

The fluorescence-based fire alarm system developed has undergone some tests

and evaluations in the laboratory. The results are presented below, some of which were obtained during the system development period.

3.4.1 Simulated experimental results

A simulated experimental system, as illustrated in Figure 3.6, was established to test the signal processing method, under different temperatures generated in the laboratory. Two ovens were used to simulate the hotspot and the background individually and separately. A tube oven, which operates up to 1200°C, provides the hotspot, while a large cube oven, which operates up to 300°C, simulates the various background circumstances.
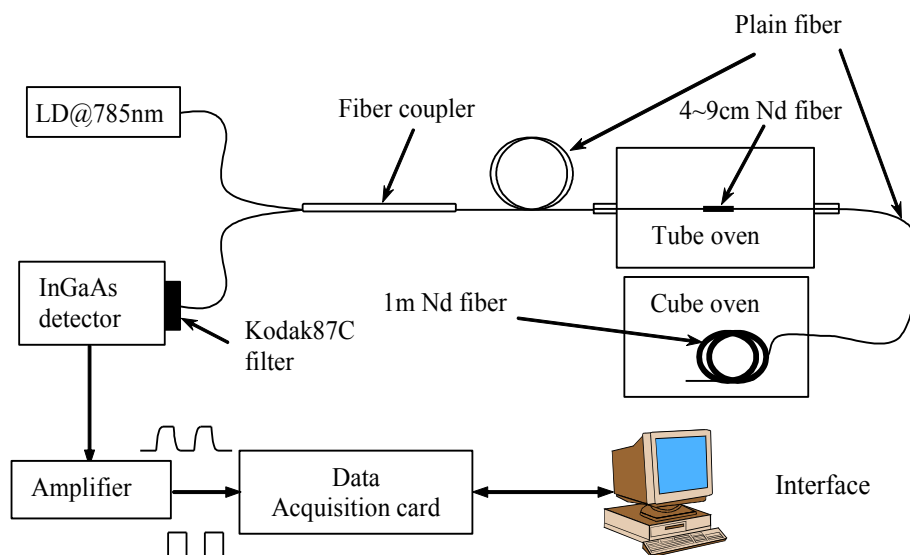
Figure 3.6: Experimental arrangement for simulation

As the 1m straight probe is protected by a stainless steel tube, it is difficult to vary the background temperature with different hotspot temperatures. To offer some flexibility, the simulated experimental setup described above is to use the 1 meter Nd fibre for background temperature measurement and one piece of Nd-doped fibre around 8 cm length for the hot spot temperature measurement. In doing so the simulated fire alarm system was able to test both the data acquisition system and the signal processing method by varying background and hotspot temperatures. After a certain correction factor was determined and applied (correction method), the fluorescence decay data were fitted to obtain two lifetimes corresponding to both the background and

the hotspot. The results are illustrated in Figure 3.7, which shows that an obvious difference between the two lifetimes is observed when the difference of temperatures between the background and the hotspot is larger than 100°C. But when the temperature difference of them is less than 100°C, the lifetime difference of the background and the hotspot is difficult to be distinguished.
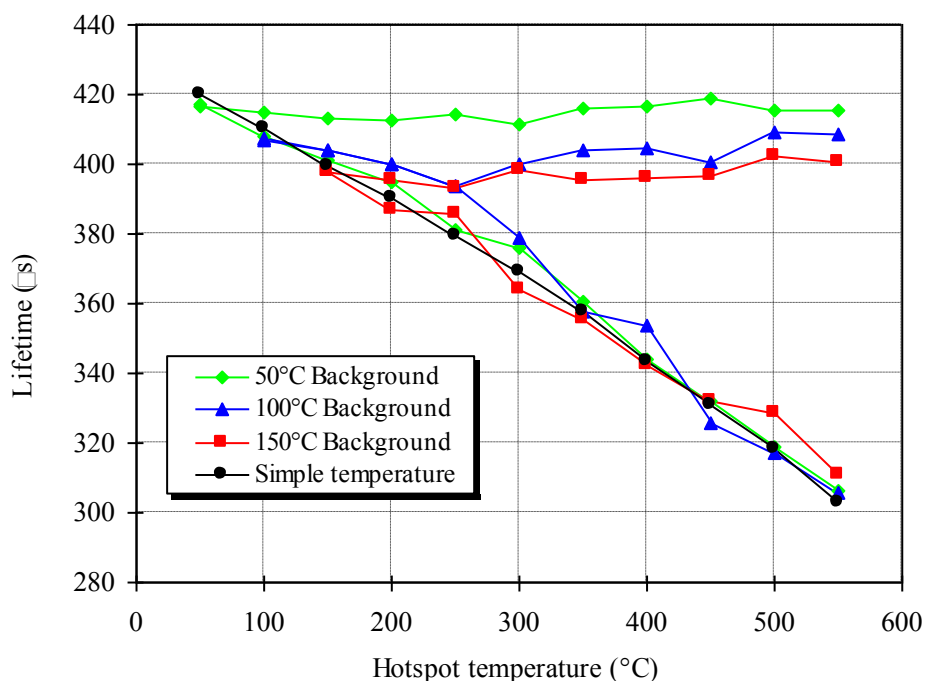
Figure 3.7: Lifetimes obtained of simulative experiment vs. hotspot temperature at vary background

3.4.2 System performance at a room temperature background

Following the above simulation tests, the fire alarm system with the 1 meter probe was tested at room temperature. A heat-gun or a gas burner was used to provide the hotspot over a spatial region of less than 100mm. The maximum operational temperature of the heat-gun is about 350°C, and that of the gas burner is around 1100°C. The system was tested when the hotspot temperature varied from room temperature up to a maximum continuous temperature of 550°C, with some short peak temperatures of about 700~750°C. Both the correction method and the lifetime adjustment method had been used in the test.

For the *correction method*, the typical response time was about 5 seconds (using HPVV as interface software program platform, and may vary with different computers). A hotspot could be determined when it lasted for more than 2~3 s (heated for 2~3 s with a heat-gun or gas burner). In the tests, it was noticed that the system missed some "transient" hotspots (heated for less than 1 second by passing through the heat gun over the probe). The method also had the problem with the measured values of the background and the hotspot temperatures. When there was a hotspot along the probe, the background temperature dropped dramatically while the hotspot temperature rises, as shown in Figure 3.8.
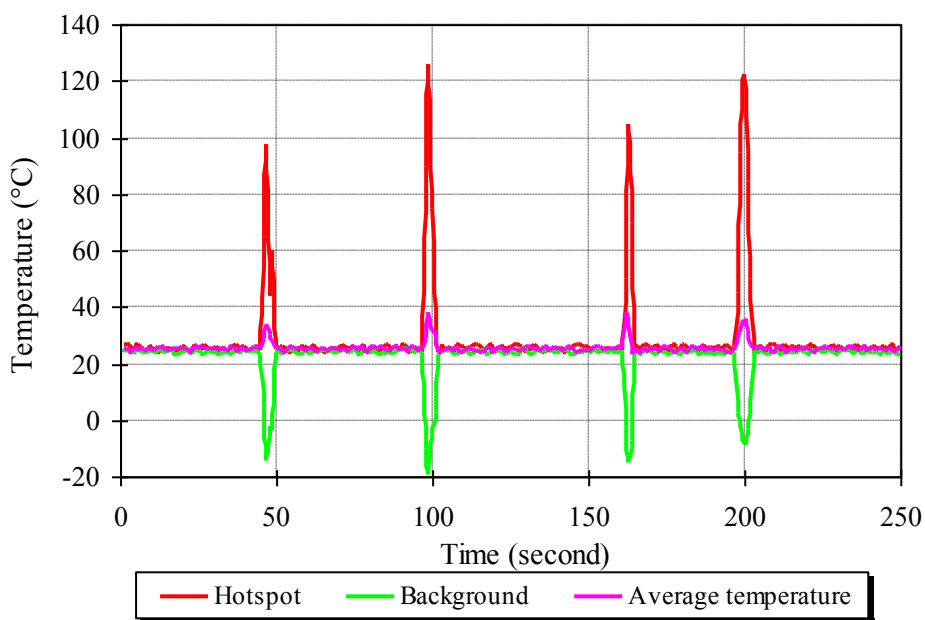
Figure 3.8: Response of hotspot at room temperature background-- *Correction method*

Given the problems arising with the *correction method*, the *lifetime adjustment method* is found to be more suitable for the application to improve the performance of the system, as discussed below.

When using *lifetime adjustment method*, almost every rapidly appearing hotspot, e.g. from a sweeping of the heat gun or the burner behind the probe, could be picked up. The typical response time is about 2 seconds (with the same computer), as shown in Figure 3.9. After the system being calibrated using Equation 3.24 and Equation 3.25, it was observed that , at room temperature with the hotspot temperature varying from

100°C to 450°C, the system error of determining the hotspot temperature was estimated to be about ±20°C.

The lifetimes and the corresponding measured temperatures using the *lifetime adjustment method* are shown Figure 3.10, in which the average temperature is derived from the lifetime obtained from a single exponential regression of the fluorescence signal. The results obtained have confirmed that the *lifetime adjustment method* offers
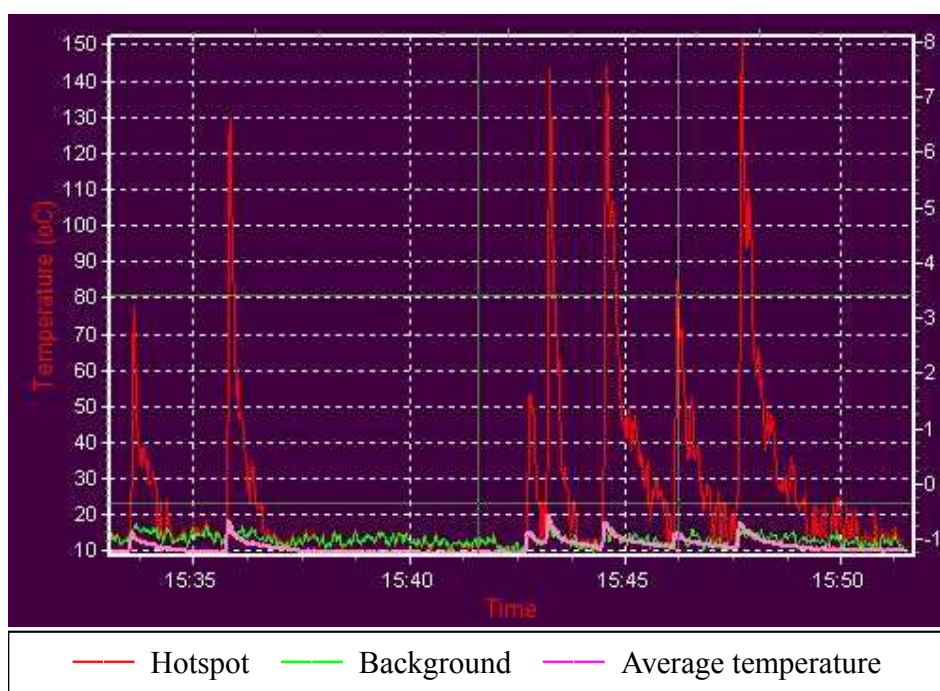
Figure 3.9: Response of hotspot at room temperature background
-- lifetime adjustment method (print-out from interface software)

a better option.

3.4.3   Hotspot location and the influence of LD light Intensity

Based on the experimental results obtained, it was noticed that two major issues, i.e. the hot spot location and the intensity of the light source, affected the lifetime measurement of the fluorescence-based fire alarm system.
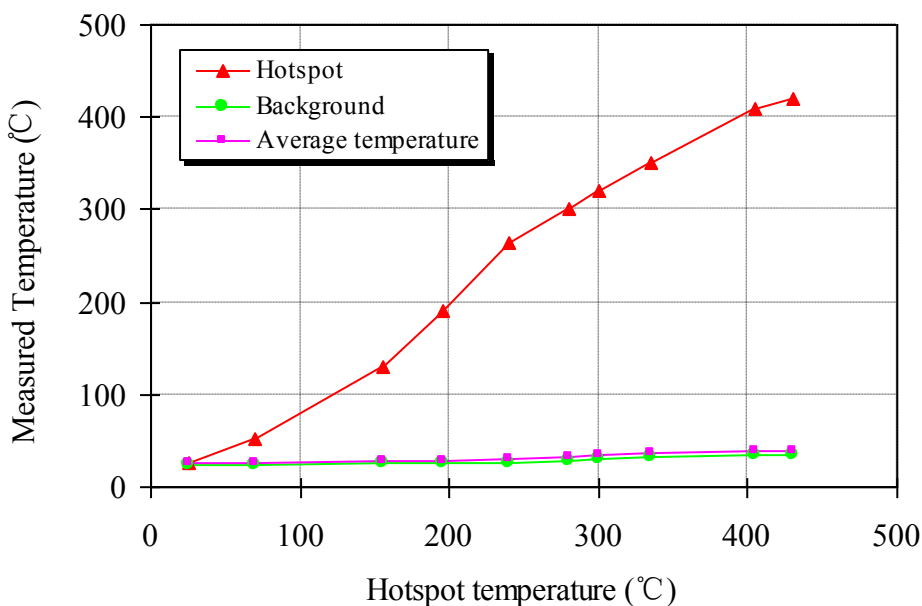
Figure 3.10: Measured temperatures vs. hotspot temperature at room temperature background

- **Hotspot location influence**

The influence of the hot spot location has been investigated. When the probe was heated by the heat-gun, which was set at a constant temperature but at different positions along the probe length, different responses were observed, as shown in Figure 3.11. Firstly, the two ends of the probe were more sensitive to the hotspot temperature change than the middle of it, the derived hot spot temperature readings at the ends and at the middle of the fibre have shown a difference of some $70^{\circ}C$, when the actual hot spot temperatures are almost the same. This is because the signal change is more significant when the fibre ends are heated up compared to that in the middle. Secondly, as the 2×2 coupler is not absolutely 50:50 in its intensity division, therefore the sensitivities at both ends are slightly different.
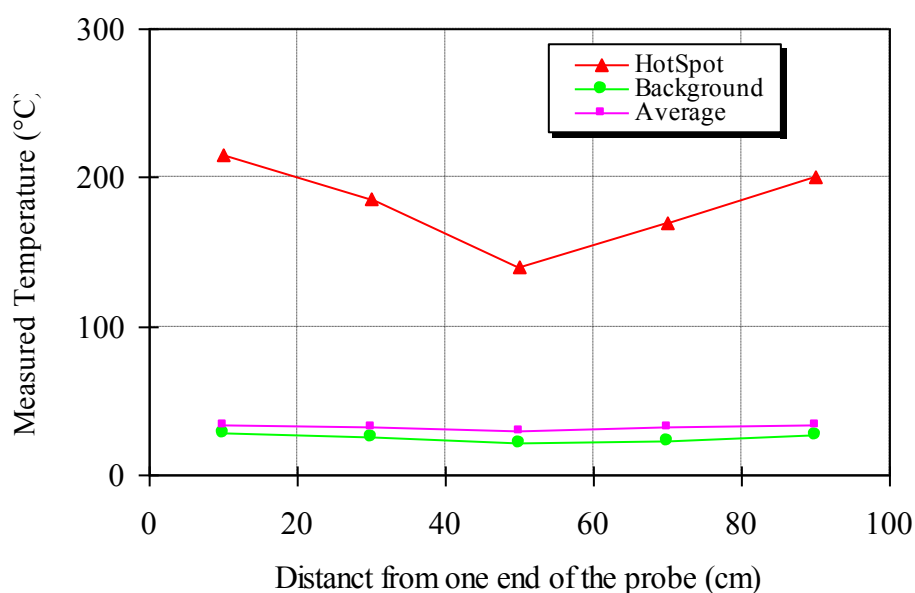
Figure 3.11: Position sensitivity of the fire alarm system (At room temperature background and 200°C hotspot)

- **LD light intensity influence**

Another issue is the fluctuation of the LD light intensity which induces the initial intensity variation of the fluorescence decay signal generated.   It has shown a substantial effect on the temperature (fluorescence lifetime) measured.   While keeping the 1 meter probe under a constant ambient temperature, the fluorescence intensity was changed by an optical adjustable attenuator, and the corresponding temperature readings at different intensity were recorded. The results are shown in Figure 3.12. The measured temperature had a maximum fluctuation of 8°C when the fluorescence intensity is changed from 4.3 to 4.9 voltage. This suggests the importance of adding an intensity factor in the calibration function, and thus using Equation 3.26 and Equation 3.27 for the lifetime adjustment.
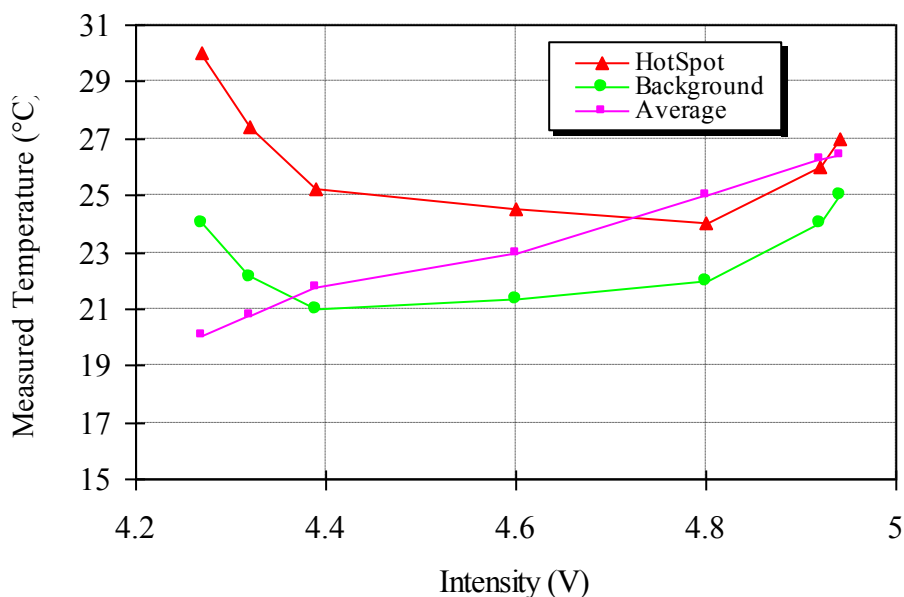
Figure 3.12: Intensity sensitivity of the fire alarm system (At room temperature background in absence of hotspot)

3.5 Summary and Conclusions

The fire alarm system, based on fluorescence lifetime measurement using data fitting method, has demonstrated the potential of their applications in aero industry. In summary, the fire alarm system developed has shown acceptable performance, with the main specifications of system highlighted below having been met by using the *lifetime adjustment method* approach.

Table 3-1: Specification of the fluorescence based fire alarm system

Typical response time	~2 seconds
Precision of measurement	Background: ±5~10 °C Hotspot: ±10~20 °C
Temperature Range	Background: room temperature up to 350°C Hotspot: room temperature up to 500°C

However the system has also demonstrated some limitations which are required to be overcome and these include the dependence of the signal processing on the laser power stability and the sensitivity to the location of hot spots. If the sensing length is required to be extended from 1m to 3m, it involves a series of changes being made,

mainly as followings:

- Higher power LD pumping source

- A pumping source with a central wavelength which is not matching with the absorption peak wavelength of Nd-doped fibres to avoid absorption saturation

- Neodymium fibres with lower doping concentrations.

In light of the above issues and the challenges arising, a more practical sensing system, using arrays of fibre Bragg gratings, has been developed and will be discussed in detail in Chapter 5.

References

[1]. T. Sun, K. T. V. Grattan, W. M. Sun, et. Al., "*Rare-earth doped optical fiber approach to an alarm system for fire and heat detection*", Review of Scientific Instruments, vol. 74, 2003, pp. 250-255

[2]. T. Sun, Z. Y. Zhang, K. T. V. Grattan, "*Frequency-domain fluorescence based fiber optic fire alarm system*", Review of Scientific Instruments, vol. 72, 2001, 2191-2196

[3]. T. Sun, Z. Y. Zhang, K. T. V. Grattan, and A. W. Palmer, "*Determination of local high temperature excursion in an intrinsic doped fiber fluorescence-based sensor*", Review of Scientific Instruments, vol. 69, 1998, 2930-2934()

[4]. Fire Fighting, Extinguishing, Protection and Detection Products, http://www.kidde.com

[5]. T. Sun, Z. Y. Zhang, et al., "*Analysis of double exponential fluorescence decay behavior for optical temperature sensing*", Review of Scientific Instruments, vol. 68, 1997, pp.58-65;

[6]. K. Levenberg, "*A Method for the Solution of Certain Non-linear Problems in Least Squares*", Quarterly of Applied Mathematics, vol. 2(2), 1944, pp.164–168

[7]. D.W. Marquardt, "*An Algorithm for the Least-Squares Estimation of Nonlinear Parameters*", SIAM Journal of Applied Mathematics, vol. 11(2), 1963, pp.431–441

[8]. O. Nelles, "*Nonlinear system identification*", §4.5, Springer, 2001.

[9]. W. T. Vetterling, "Numerical recipes example book (C)", §15.5, Cambridge University Press, 1992

[10]. Z. Y. Zhang, K. T. V. Grattan, A. W. Palmer, and B. T. Meggitt, "Spectral characteristics and effects of heat treatment on intrinsic Nd-doped fibre thermometer probes", Review of Scientific Instruments 69, 1998, pp.139-145

Chapter 4. Strong Fibre Bragg gratings for high temperature sensor applications

4.1 Introduction of Fibre Bragg grating

A fibre Bragg grating (FBG) is a type of distributed Bragg reflector constructed in a short segment of optical fibre that reflects a particular wavelength of light and transmits all others. This is achieved by creating a periodic variation in the refractive index of the fibre core, as shown in Figure 4.1 [1].
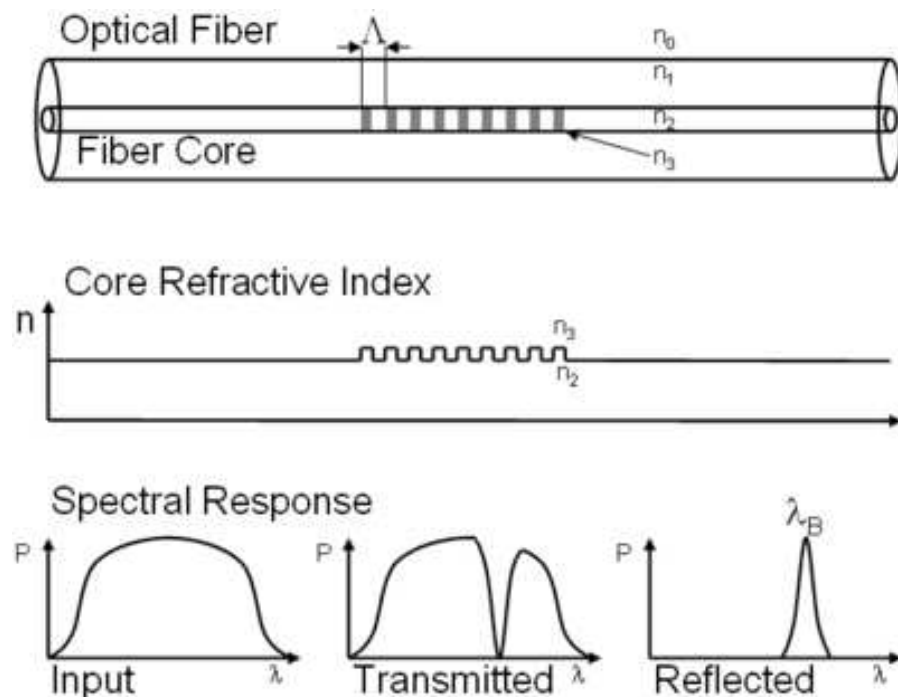
Figure 4.1: Structure of a fibre Bragg grating

For a conventional FBG, the periodicity of the index modulation has a physical spacing and when light is launched into the grating and the Bragg reflection condition [1] between the grating planes and incident light is satisfied, a narrow band spectrum, centred at Bragg wavelength, λ_B, of the incident light is reflected back. The Bragg wavelength of the grating, can be represented by:

$$\lambda_B = 2n_{eff}\Lambda \tag{4.1}$$

83

where n_{eff} is the effective refractive index of the fibre core, and Λ is the grating spacing of the refractive index modulation.

The fibre Bragg grating can work as a wavelength specific dielectric mirror. Therefore, a fibre Bragg grating can be used as an inline optical filter to block certain wavelengths, or as a wavelength-specific reflector. The wavelength of the reflected narrow bandwidth of light responds also to changes in temperature and strain, thus the FBG can be used as a sensing element. Up to a few thousands of FBG sensors can be recorded into a single optical fibre and interrogated simultaneously with a single instrument [1] - the effect offers a very low-cost option for distributed monitoring of strain and/or temperature within large structures. The suitability of FBGs for structural health monitoring has been widely reported [2,3]. Since the first discovery of the FBG, the invention of it has revolutionized the fields of telecommunication and sensing, and has led to numerous applications in these fields[4,5]..

4.1.1 Short History of fibre Bragg gratings

The first observations of photosensitivity and index of refraction changes in germanosilica fibres were reported by Hill and co-workers at the Communication Research Centre (CRC), Canada, in 1978 [6,7]. During an experiment carried out to study the nonlinear effects in a specially designed optical fibre with heavy germanium dopant, the visible light from an argon ion laser ($\lambda = 488$ nm) was launched into the core of the fibre, under a prolonged exposure, an increase in the attenuation of the fibre was observed, and it was noticed that the intensity of the back reflected light from the fibre increased significantly with exposure time. This increase in reflectivity was recognized as a result of a permanent refractive-index grating, thought to be very weak in an order approximately of 10^{-6}, being photo-induced in the fibre, which resulted in a narrow-band reflection at the writing wavelength.

In their experiment, the refractive-index perturbation of the fibre was formed as a result of a standing wave intensity pattern being formed by the 4% Fresnel back reflection at the far end and the forward-propagating light. This refractive-index grating

acted as a distributed reflector that coupled the forward propagating light to the counter propagating light beams. This coupling of the beams provided positive feedback, which enhanced the strength of the back-reflected light, and thereby increased the intensity of the interference pattern, which in turn increased the index of refraction at the high intensity points. This process was continued until eventually the reflectivity of the grating reached a saturation level. These gratings were, thus, called *self-organized* or *self-induced* gratings since they formed spontaneously without human intervention. The periodic refractive index perturbation in a meter or so of fibre formed a Bragg grating with a bandwidth being around 200 MHz.

This new nonlinear photorefractive effect in optical fibres was called photosensitivity. The importance of this discovery in potential applications was recognized even at that time. However, the discovery did not bring a significant technical breakthrough for nearly a decade. The main reason for this is believed to be the difficulty in repeating the set-up of the original experiments, and it was thought the observations were confined only to the "magic fibre" at CRC.

Although the discovery of the photosensitivity played a key role in the advancements of optical fibre technology, devices such as the self-induced gratings, demonstrated by Hill et al [7], were not practical, primarily due to the Bragg resonance wavelength being limited by the argon ion laser writing wavelength (488nm). The major breakthrough came with the report on the side writing technique using single-photon absorption at 244 nm by Meltz et al [8] almost a decade later. They demonstrated reflection gratings in the visible part of the spectrum (571-600 nm) using two interfering beams external to the fibre. The wavelength of Bragg condition can be altered by changing the angle between the interfering beams. This side writing technique provides the much-needed degree of freedom to shift the Bragg resonance to longer and useful, almost any, wavelength, such as 1530 nm, permitting their use in modern communications and many other applications.

In the last two decades, groups worldwide achieved breakthroughs in direct optical inscription of high-quality gratings into the core of optical fibres using various techniques

such as the interferometric, phase mask, and point-by-point exposure to ultraviolet laser light. Gratings with a wide range of bandwidths and reflectivity can be formed on time scales ranging from a few nanoseconds (duration of the laser pulse) to a few minutes, depending on the characteristics required. These gratings are low-loss in-line fibre devices that can be written into the core non-invasively when and where desired, offering narrow-band wavelength selection to precise specifications.

4.1.2 Types of Fibre Bragg gratings

4.1.2.1 Uniform Fibre Bragg gratings

Fibre Bragg gratings can be classified into three distinct formation regimes according to the fabrication procedure and conditions, and they are type I, type IIA, and type II gratings respectively.

- **Type I**

Type I gratings are generally formed into most photosensitive fibres when exposed to continuous wave (CW) or low frequency pulse UV radiation at a relatively low energy. As seen in the transmission and reflection spectra of a type I grating exposed under a broadband light source, a fundamental characteristic of this type of grating is that the reflection spectrum of the guide mode is complementary to the transmission signal, implying that there is negligible loss due to the absorption or reflection into the cladding. Type I gratings, written into some photosensitive fibres, normal highly germanium doped silica fibre, can be erased at a relatively low temperature (~300 ^{o}C) due to this photosensitivity type of the grating. However, type I gratings writing into some other photosensitive fibres may have higher sustainable temperature. Nevertheless, the type I gratings are the most used gratings, and operate effectively in the temperature regime from -40 ^{o}C to 80 ^{o}C, a temperature that satisfactorily covers most telecommunication and sensor applications.

- **Type II**

While gratings formed at low energy intensity are referred as type I gratings, another

type of grating is formed when the energy intensity of the writing light beam exceeds over approximately 30 mJ [9]. This type of grating is termed as type II grating, which is a damage grating physically caused in the fibre core on the side of the writing beams under a single pulse exposure. Type II gratings usually have an irregular reflection spectrum due to the non-uniformities of the excimer laser beam profile. By spatially filtering the beams, type II gratings with better reflection profile, but with reduced reflectivity, can be created. One main characteristic of this type of gratings is their extreme stability at elevated temperatures [9]. No degradation in the grating reflectivity was observed at $800^{o}C$ over a period of 24 hours. This extreme temperature stability can be utilized for sensing applications in some harsh environments. Another attractive feature of the type II gratings is that the highly reflective gratings can be formed in a few nanoseconds (the duration of a single laser pulse), suitable for large-scale mass production of strong gratings. They can also be inscribed during the drawing process before application of the protective coating.

- **Type IIA**

Type IIA grating represents another type of grating formed in non-hydrogen-loaded photosensitive fibres. Type IIA gratings are inscribed at low power densities through a long exposure of approximately 30 minutes (depending on the fibre type and the exposure beams), following type I grating inscription[10,11].It was found that the type IIA gratings had dramatically improved temperature stability over the type I gratings. Type IIA grating is able to withstand a higher temperature than the original Type I gratings, a noticeable grating erasure by high temperature is observed only at the temperatures over $500^{o}C$[10]. Clearly, the type IIA gratings are not very practical in terms of fabrication. However, the improved temperature stability is very useful if the system is exposed to high ambient temperatures in some applications.

All the above three different types of gratings are uniform in structure as illustrated in Figure 4.2, where the grating planes along the whole grating are equally spaced and identical to each other. There are other types of non-uniformly structured fibre gratings, such as tilting gratings, chirped gratings, etc.

Figure 4.2: Structure of a uniform fibre Bragg grating

4.1.2.2 Tilted grating

Tilted (blazed) grating is a grating formed by tilting (or blazing) the grating plane at an angle to the fibre axis, as illustrated in Figure 4.3. This results in the light being coupled into loosely bound, guided-cladding or radiation. The coupling efficiency and bandwidth of the light that is tapped out is determined by the tilt of the grating plane and the strength of the modulation.
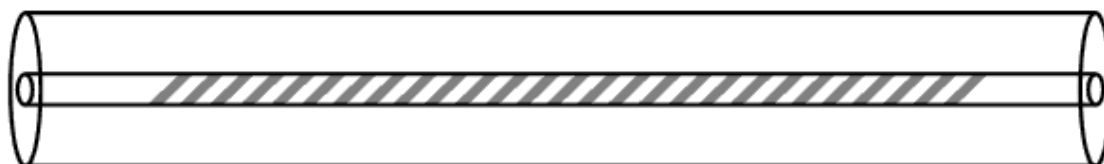
Figure 4.3:   Structure of a tilted grating

The main applications of the tilted grating are spectrometer and mode discriminator[12], and in flattening the gain of EDFAs (Erbium doper fibre amplifiers) [13].

4.1.2.3 Chirped grating

Another type of Bragg grating structure with most interesting applications in telecommunication is the chirped grating. This type of grating has a monotonically varying period, as illustrated schematically in Figure 4.4.
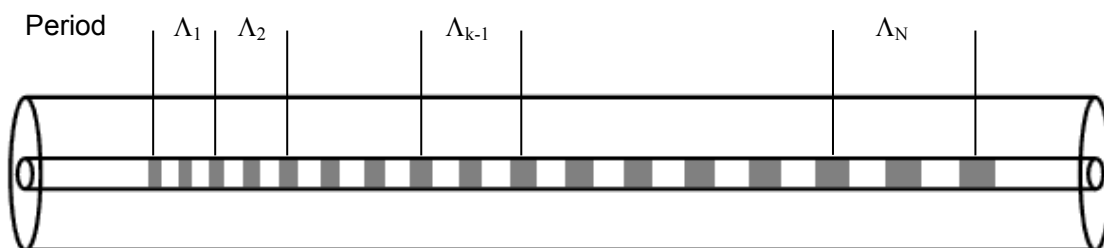
Figure 4.4: Structure of a chirped grating

For a varied period grating, from Equation 4.1 we have:

$$\lambda_B(z) = 2n_{eff}(z)\Lambda(z) \qquad\qquad (4.2)$$

The simplest type of the chirped grating structures is the one in which the variation in the grating period is linear:

$$\Lambda(z) = \Lambda_0 + \Lambda_i z \qquad\qquad (4.3)$$

where Λ_0 is the starting period, and Λ_i is the linear change of the period along the length of the grating. This type of chirped grating structures can be considered as it is made up of a series of smaller lengths of uniform Bragg gratings with increased period. If properly designed, this type of structure can be used as a broadband reflector, which is useful in both telecommunication and sensor applications.

4.2   Applications of fibre Bragg Gratings

Since the innovation of the fibre Bragg gratings, they have been extensively used in telecommunications due to their unique filtering properties and versatility as in-fibre devices. Bragg gratings have also been widely utilized as in-fibre sensors for many applications as the Bragg wavelength of gratings responses directly to the temperature or/and stain perturbations. In this section, the applications of FBGs in communication and sensor systems are briefly summarized.

4.2.1   Applications in communication

Fibre Bragg gratings have emerged as important components in various lightwave applications in telecommunication. Many in-fibre devices deploying fibre Bragg gratings, such as fibre lasers, wavelength division multiplexers and demultiplexers, Raman amplifiers, remote pumping amplifiers, dispersion compensators, and gain equalisers, have been demonstrated and developed for the applications in communication [14-24]. As these device arising from these applications in telecommunications are also widely used as sensor system components, the following section will briefly describe some of these applications

4.2.1.1 Fibre laser

Fibre lasers have been widely used in the telecommunication systems to meet the

increasing demand of high speed and high capacity transmission, as they offer great advantages of being easily integration into the basic fibre communication systems. The development of fibre Bragg gratings has further enhanced the functionality of fibre lasers.

An example of a simple erbium-doped fibre laser configuration is schematically illustrated in Figure 4.5 [14]. In this fibre laser, the laser cavity consists of a 2-meter long erbium-doped fibre with Bragg gratings at each end for providing feedback. The output coupler has a narrow band grating of around 80% reflectivity with 0.12nm linewidth. The broadband mirror was formed by a series of narrowband gratings, which nowadays can be easily replaced by a single broadband grating, such as a chirped grating. The fibre laser output is at the wavelength of the narrowband output coupler Bragg grating, when pumped at 3.0 mW, while the lasing threshold of the laser was 0.5 mW.
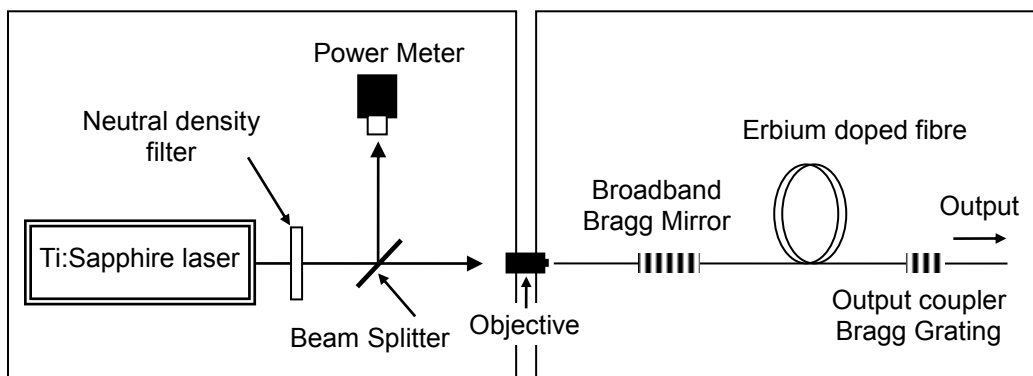
Figure 4.5: Schematic of an erbium-doped fibre laser with Bragg gratings at each end providing feedback to the laser cavity

Other fibre lasers utilising fibre Bragg gratings, such as with multi-wavelength operation lasers [15], single-mode/single frequency fibre lasers [16,17], mode-locked fibre lasers [18], and fibre Raman laser [19] have also been reported for telecommunication applications.

4.2.1.2 Fibre amplifiers

Erbium doped fibre amplifiers (EDFAs) are a device which has received the most attention in the modern lightwave communication systems. They have significantly changed the future of optical communications. Fibre Bragg gratings have been wide

deployed in the EDFAs as a selective reflector for the signal and pump light. Over the last several years, fibre Bragg gratings have been designed and optimized to dramatically improve the performance of EDFAs, for example for pump laser wavelength stabilisation, pump reflectors, and gain wavelength flattening. Fibre Bragg gratings have therefore become an important integral part of EDFA for tailoring its performance.

Figure 4.6 shows several configurations that have been proposed for fibre amplifiers utilising fibre Bragg grating reflectors to improve performance [20]. For instance, by placing a fibre Bragg grating as a broadband reflector at the output of EDFA, it can increase the small-signal gain and efficiency by recycling the remnant pump light. The fibre grating can also act as a wavelength selective reflector that discriminates between the signal and the pump light, thus increasing the saturated output power.
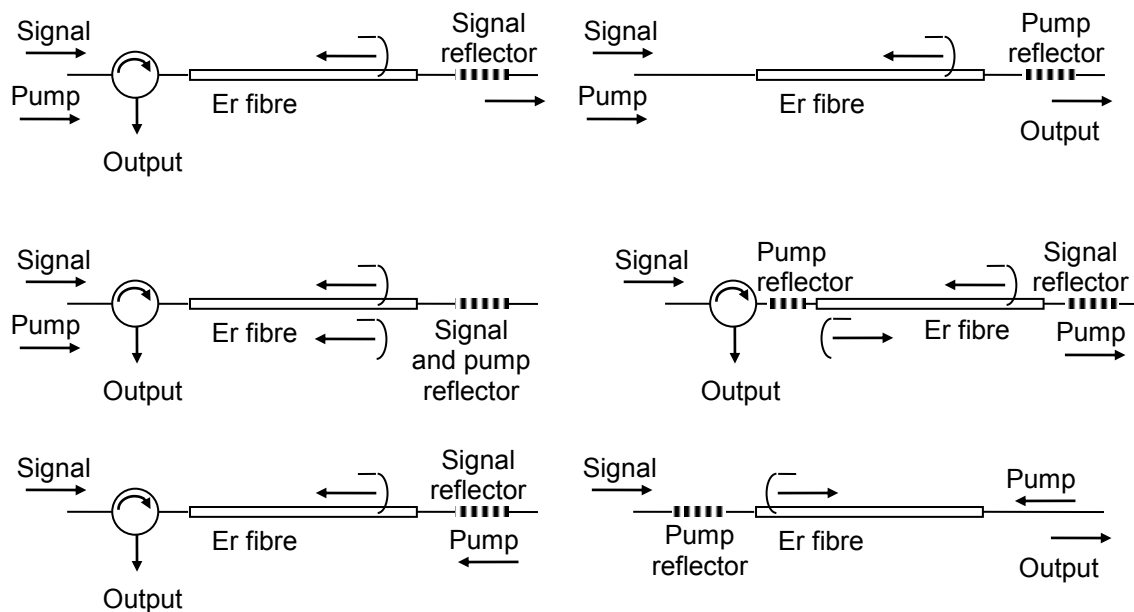
Figure 4.6: Configurations of reflected pump and signal in EDFA.
Reflection by gratings nearly doubles the small signal gain and increases saturated output power (after [20])

4.2.1.3 Wavelength Division Multiplexers/Demultiplexers

The rapid growth in the use of phones, internet, etc, has increased the volume of telecommunication traffic enormously. The capacity of long-distance telecommunication

links had to increase to keep the pace with it. Wavelength division multiplexer (WDM), which allows multiple wavelengths to carry multiple optical signals in a single fibre simultaneously, is a promising and widely used device to enhance the capacity of modern optical fibre communication links.

WDMs utilising fibre Bragg gratings have been studied and developed by many researchers. One of the earliest demonstrations of this technique is reported by Mizrahi [21]. The operational principle of this WDM is illustrated in Figure 4.7a. It consisted of a 1x4 fused fibre splitter in conjunction with a fibre grating transmission filter in each of the output ports. The filters were designed to pass the signal wavelength of each port while rejecting the other three channels. The fibre transmission filter was formed by pairing two gratings that do not have any overlap in wavelengths, which makes it possible to create a simple band-pass filter, in which the two gratings reject a broad range of wavelengths, but the desired wavelengths pass through unaffected between the grating stopbands. The test result of this device of a high-resolution measurement is shown in Figure 4.7b. The signal wavelength space of the channels of the WDM was around 200 GHz (~1.6 nm intervals). The peak attenuation of the filter was measured to be over 80 dB, which resulted in excellent crosstalk performance.

(a)   (b)
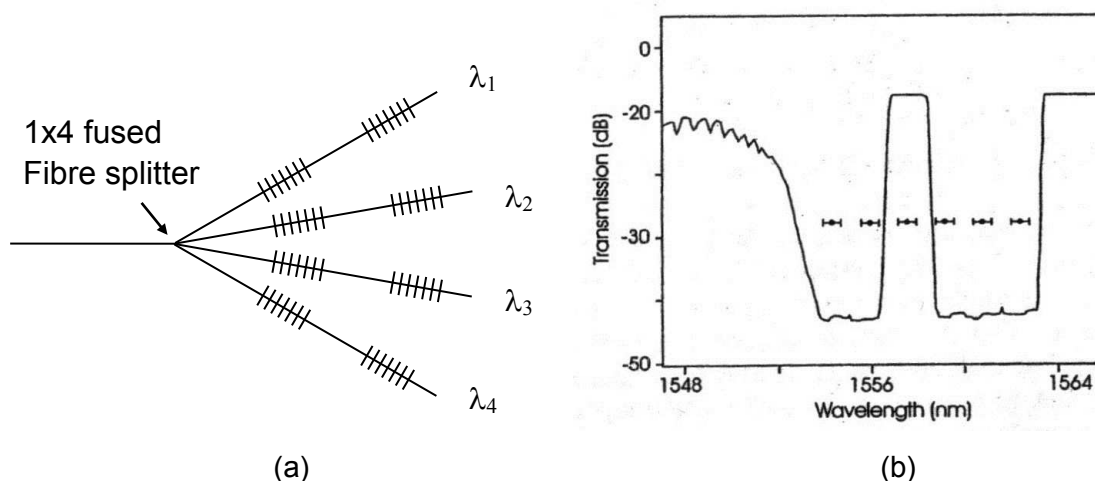
Figure 4.7: Schematic illustration of a four channel fibre grating WDM. The plot (b) shows a high resolution measurement of a complete demultiplexers system for one of the channels (after [21])

There are many other devices used in communications, such as dense wavelength division multiplexers (DWDM) [22], dispersion compensation devices[23], optical fibre

phase conjugators[24], in which the fibre Bragg gratings are employed. They will not be discussed here as they are beyond the research of this thesis. Readers are referred to text books, e.g. by Othonos [3], for more detailed information.

4.2.2   Applications in optical fibre sensors

As the Bragg wavelength of fibre Bragg gratings is changed with the perturbation applied on the grating, fibre gratings have been considered as excellent sensing media since the earliest stage of their development. Sensor systems based on fibre Bragg gratings have been reported to measure static and dynamic measurands, such as temperature, strain, pressure, and some chemicals [5,26-34]. One of the major advantages of such FBG-based sensor systems is the transmitted signal is the wavelength-encoded which makes the sensor independent of signal intensity variations, e.g. due to the fluctuating light source power level and connector insertion losses etc. Moreover, FBG based sensors can be easily multiplexed, making a promising sensor network for large structure measurement. Since the innovation of fibre Bragg gratings, FBG-based sensors have been widely applied in the field of civil structure monitoring, aerospace industries, off-shore engineering, process control, and medical applications.

4.2.2.1   Optical sensing mechanism of fibre Bragg gratings

A fibre Bragg grating has an inherenet sensitivity to strain and temperature, as its resonance wavelngth is dependent on the effective refractive index of the fibre core and the grating period.   Therefore gratings can be used for measurement of strain, temperature, or some other measurands, by monitoring the Bragg wavelength shift.

By differentiating Equation 4.1, the wavelength shift of the Bragg wavelength ($\Delta\lambda_B$) is given by:

$$\Delta\lambda_B = 2n_{eff}\Delta\Lambda + 2\Lambda\Delta n_{eff} \qquad\qquad (4.4)$$

Hence, the wavelength shift ($\Delta\lambda_B$) due to strain and temperature changes can be given by:

$$\Delta\lambda_B = 2\left(\Lambda\frac{\partial n_{eff}}{\partial l} + n_{eff}\frac{\partial\Lambda}{\partial l}\right)\Delta l + 2\left(\Lambda\frac{\partial n_{eff}}{\partial T} + n_{eff}\frac{\partial\Lambda}{\partial T}\right)\Delta T \qquad (4.5)$$

where l is the length of the grating, and T is the temperature applied on it.

The first term in Equation 4.5 represents the strain effect on the Bragg wavelength. This corresponds to the physical deformation experienced by the fibre which changes the grating period ($n_{eff}\frac{\partial\Lambda}{\partial l}$), and strain-optic induced change in the effective refractive index ($\Lambda\frac{\partial n_{eff}}{\partial l}$). This strain induced term is commonly expressed as [5]:

$$\Delta\lambda_B(\varepsilon) = \lambda_B(1 - P_e)\varepsilon_z \qquad (4.6)$$

where P_e is the strain-optic coefficient and is defined by:

$$P_e = \frac{n_{eff}^2}{2}\left[P_{12} - v(P_{11} + P_{12})\right] \qquad (4.7)$$

where P_{11} and P_{12} are the Pockel's coefficients (typical values for a garmanosilicate optical fibre P_{11}: 0.131, and P_{12}: 0.252), and v is the Poisson's ratio (typical value: 0.16)[5]. P_e is usually treated as a constant coefficient which can be calculated using the fibre parameters and has a typical value of ~0.22 [5]. For sensors operating at the 1550 nm wavelength region and at a constant temperature, the typical strain sensitivity of a FBG is of the order of ~1.2 pm/$\mu\varepsilon$ [5].

Similarly, the second term in equation 4.5 represents the effect of temperature on the fibre Bragg grating. This is linked to a wavelength shift in the Bragg wavelength due to the thermal expansion changes the grating spacing ($n_{eff}\frac{\partial\Lambda}{\partial T}$), and the effective refractive index ($\Lambda\frac{\partial n_{eff}}{\partial T}$). This fractional wavelength shift due to temperature change may be expressed as [3].

$$\Delta\lambda_B(T) = \lambda_B(\alpha_\Lambda - \alpha_n)\Delta T \qquad (4.8)$$

where $\alpha_{\Lambda} = \dfrac{1}{\Lambda}\left(\dfrac{\partial \Lambda}{\partial T}\right)$ is the thermal expansion for the fibre (typically 0.55 x 10^{-6} for

silica fibre), and $\alpha_{n} = \dfrac{1}{n_{eff}}\left(\dfrac{\partial n_{eff}}{\partial T}\right)$ represents the thermo-opto coefficient

(approximately 8.6 for germania-doped, silica core fibre). It is clearly shown that the thermo-optic induced index change is the dominant effect. From equation 4.8, the temperature sensitivity of a Bragg grating operating in 1550 nm region is expected to be around 13 pm/^{o}C [5], which may vary between different materials.

As shown in equation 4.5, the wavelength shift in the Bragg wavelength due to an external perturbation to the grating, is the sum of the strain and temperature effect terms. A crosstalk between these two effects is possible. Therefore, in many sensing applications where only one measurand is of interest, it is necessary to deconvolute the strain and temperature perturbations. In some cases, a simultaneous measurement of strain and temperature is required.

4.2.2.2 Fibre Bragg grating sensor applications

Fibre Bragg grating based sensors have been continuously and rapidly developed since they were first demonstrated for strain and temperature measurement about two decades ago. In this section, a brief summary of the applications of FBG based-sensors is addressed.

● **Applications in aerospace**

The aerospace industry is very conservative where new development are concerned, and all new sensors must undergo a long and rigorous testing period before being accepted. However, Bragg grating sensor systems have shown potential for aerospace applications as they cab be made into compact and lightweight temperature, strain and pressure sensors compared to existing sensors already in use. Dunphy et al. [26] presented a smart Bragg grating fibre sensor for monitoring of reinforced carbon fibre composites (RCFCs) for curing and impact detection. Dunphy identified a number of benefits arising from the combination of optical fibres and composites.

Interests of applications of Bragg grating sensors to space bound craft, where all structures are subject to high acoustic and vibration loads to simulate the launch conditions, have also been demonstrated. The Photonics Group at the NASA Ames Research Centre designed specialized fibre Bragg sensor that could monitor the condition of the cryogenic tanks aboard a Reusable Launch Vehicle [27]. The fibre sensor was identified as an ideal candidate of embedded sensors for measuring strain load on the cryogenic tanks (range 2500 $\mu\varepsilon$, resolution 10 $\mu\varepsilon$), since fibre sensors provided accurate data and being of a small size and lightweight, presenting no spark hazard. Sensors are required to operate over a wide temperature range from -250 ^{o}C to 380 ^{o}C, in the application of space bound craft.

● **Applications in marine industry**

Bragg grating sensors have great potential to be included in marine down-hole instrumentation for exploring the natural oil resources, where conventional electronic sensors cannot be used because of the extremely harsh marine environments.

In the late 1990s, Hjelme first used the fibre Bragg sensor for the characterization of scaled marine vehicle models [28]. The system was designed to measure the slamming forces between the wet deck and sea waves by locking the wavelength of the light from a laser diode to the peak wavelength of a Bragg grating sensor mounted on the wet deck of the vehicle model. The sensor had a dynamic range of 27 dB in a 1 kHz range. Later on, a 16-channel system was developed for composite panel slamming test to stimulate transient loading forces [29]. In the system, the grating sensors were attached to the wet and dry side of the composite panel, which was mounted on a mechanical rig loaded with weights exceeding 100 kg. The measurement results provided the information of the survival characteristics of the grating sensors. The system demonstrated a sub-10 $\mu\varepsilon/Hz^{1/2}$ resolution and a bandwidth of over 5 kHz for the maximum ±1000 $\mu\varepsilon$ strain levels.

● **Applications in civil engineering**

Structural health monitoring in civil and structural engineering has undergone

continuous growth over the last few decades. Exploring new sensing technologies in these applications has led to many innovations and development in sensor systems. Due to the harsh environments in the civil engineering industry, fibre Bragg grating sensors offer a viable approach with a number of advantages over traditional sensors. Novel FBG sensors have been developed and deployed on highway bridges to measure dynamic strain, static strain [30-32], and for various engineering structural monitoring [33-34]. Results of these studies indicate that, if properly packaged, FBG sensors can survive the severe conditions associated with the construction environments of civil infrastructure.

- **Medical applications of fibre Bragg sensors**

Optical fibre sensors, as well as Bragg grating based sensors, have been used in medical applications. FBG-based temperature sensors are particularly suitable for medical applications, where conventional electrical thermometers are inappropriate. Rao et al. [35,36]presented a novel temperature sensor system in early years of FBG sensor research and development, utilising Bragg gratings for remote temperature measurements in an NMR machine. The system achieved an measured resolution of ±0.2 ^{o}C with an accuracy of ±0.8^{o}C, limited by the quality of the flitter PZT element. Samset et al. [37] demonstrated a FBG based temperature sensor for soft tissue measurement. The system was calibrated to the temperature range of –195.8°C to 100°C for temperature measurement during the process of freezing (cryoablation) porcine liver in vivo. The system yielded a temperature profile with 6.5 mm spatial resolution and 5 second temporal resolution.

Fisher et al [38] demostrated that the fibre Bragg sensor could be used in principle to detect the high frquency ultasonic field, in line with the requirement of improved safety of ultrasound for medical applicaions. Cowie and his co-workers[39], presented fibre Bragg sensor used for tactile sensing for biomedical applications. A two-dimensional sensing surface using the system was demonstrated, with potential applications in human balance and gait analysis, capable of detecting simultaneously the position and shape of an object placed upon it.

● **Other applications of fibre Bragg sensors**

In addition to the above mentioned areas, Bragg grating sensors have also been employed for nuclear environment monitoring[40], current measuremnent of power transmission line [41,42], off-shore wind turbine strain monitoring[43], etc. The FBG-based system developed by the author in this project, has been employed in several field tests, such as bridge strain structural monitoring, high temperature monitoring, automotive exhaust temperature measurement, etc. and further details are presented in Chapter 5.

4.2.2.3 Advantages of fibre Bragg grating based sensors

Compared with other fibre-optic sensors developed and reported, fibre Bragg grating sensors have shown a number of distinct advantages, such as:

● The signal obtained from an FBG sensor is encoded directly in wavelength which is, in general, an advantage over other sensing schemes as it is intensity-independent and also facilitates wavelength division multiplexing (WDM);

● FBGs can be directly written into the fibre without changing the fibre diameter, therefore making them suitable for conditions where small diameter probes are required, for example, embedding sensors in advanced composite materials for strain mapping or attaching to the human body for temperature profile.

● The FBG sensor devices are simple, intrinsic sensing elements and have all the advantages normally attributed to fibre sensors, such as electrically passive operation, EMI immunity, high sensitivity, and potential low cost.

● Another significant benefit that FBG sensors offer for remote monitoring is their stability over time. Being a passive sensor, a FBG has zero drift and can be used for many years with no need for recalibration. Indeed, it is practical to attach sensors to bridges for instance and return with an instrument to interrogate the sensors every few years to obtain a true picture of any structural movement

since the last reading. This further increases the economic advantage of the technology since only one interrogation unit can service hundreds of structures

These advantages emphasize the important characteristics of FBGs, however, FBGs are sensitive to both strain and temperature, therefore it is essential to address this cross-sensitivity effect when they are used for specific applications. One key problem for a practical system is the demodulation technique used to interrogate a small Bragg wavelength shift as a function of the strain/temperature variation. Conventional spectrometers or monochromators are not suitable for the measurement of Bragg wavelength shifts as they are bulky, expensive and not robust enough for field applications. In this work a practical FBG wavelength interrogation system together with interface software for sensor applications has been developed, and the detail of it is discussed further in Chapter 5.

4.3   Fabrication techniques of fibre Bragg gratings

Fibre Bragg gratings are created by "inscribing" or "writing" a periodic variation of refractive index into the core of an optical fibre using an intense ultraviolet (UV) source, such as a UV laser. While the very first grating, which was *self-organized* or *self-induced,* formed spontaneously inside the fibre core without human intervention, many techniques for the inscription of Bragg gratings externally in photosensitive fibres have been reported[8]. The later developed external inscription processes proposed and widely used by various researches and institutes, for example, interferometric [8], point by point [44] and phase mask [45] methods, have been developed for FBG fabrication.

This section gives a brief summary of the common external writing methods reported. More comprehensive information and details on these various FBG inscription techniques to create regular uniform grating or complex grating structures can be found in the textbooks about fibre Bragg gratings, e.g. by Othonos [3], or by Kashyap [46].

4.3.1   Interferometric FBG inscription techniques

The first interferometric technique for FBG inscription was demonstrated by Meltz *et*

al [8] in 1989. The method, specifically used for uniform gratings, is based on an amplitude splitting interferometer which consists of a beam splitter and a set of mirrors, as illustrated in Figure 4.8. In such a set-up, the incoming inscription UV laser is split into two beams and subsequently recombined together to generate an interference pattern thus creating a periodic intensity distribution along the axis of the fibre. The refractive index of the photosensitive fibre changes according to the intensity of light that it is exposed to. This method allows for quick and easy changes to the Bragg wavelength, which is directly related to the interference period as it is identical to the period of the Bragg grating, and is give by Equation 4.9 [3].

$$\Lambda = \frac{\lambda_w}{2\sin\theta} \tag{4.9}$$

where λ_w is the wavelength of the writing laser and θ is the half angle of the intersection
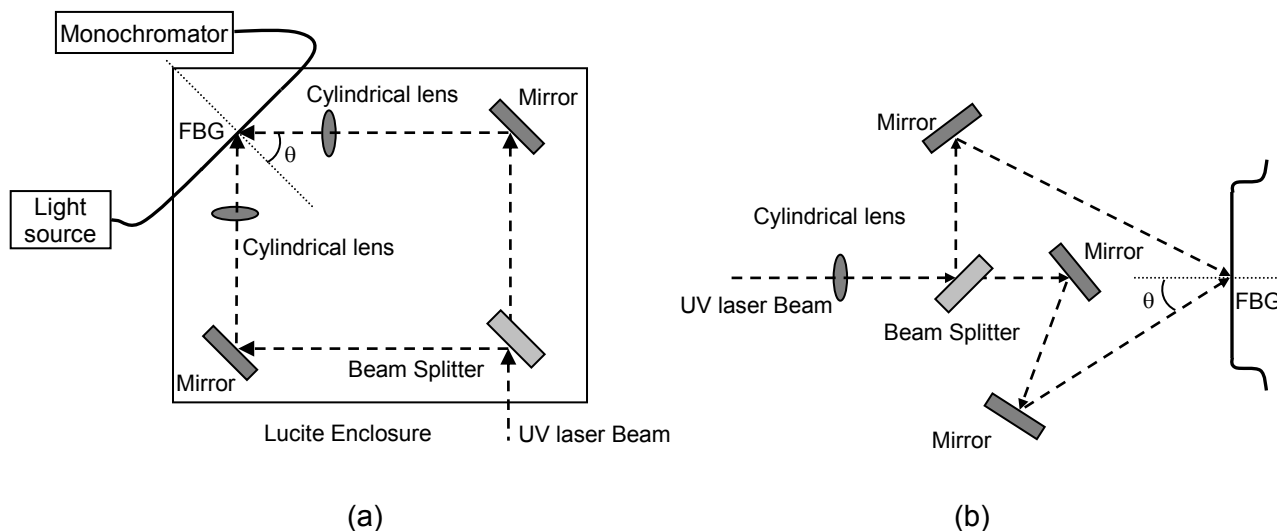
Figure 4.8: Schematic illustration of amplitude interferometric FBG inscription technique.
(a) Setup used by Meltz et al. (after ref[8]) for the first demonstration of side written gratings

(b) An alternative configuration with additional mirror to compensate for the imbalanced beam path in setup (a) due to the number of reflections.

beams. Thus the wavelength of the Bragg grating can be given as:

$$\lambda_B = \frac{n_{eff}\lambda_w}{\sin\theta} \tag{4.10}$$

The amplitude splitting interferometric technique offers flexibility in terms of the Bragg wavelength selection. However, the fabrication system setup is susceptible to mechanical vibration and requires precise alignment of the optical components. The interference pattern fringe also tends to drift over a period of time due to the long optical path length.

Another type of interferometric techniques for FBG fabrication using wavefront splitting interferometer has also been reported and demonstrated. Lloyd mirror interferometer [45] and prism interferometer [46] are examples of wavefront splitting interferometric methods, shown in Figure 4.9.
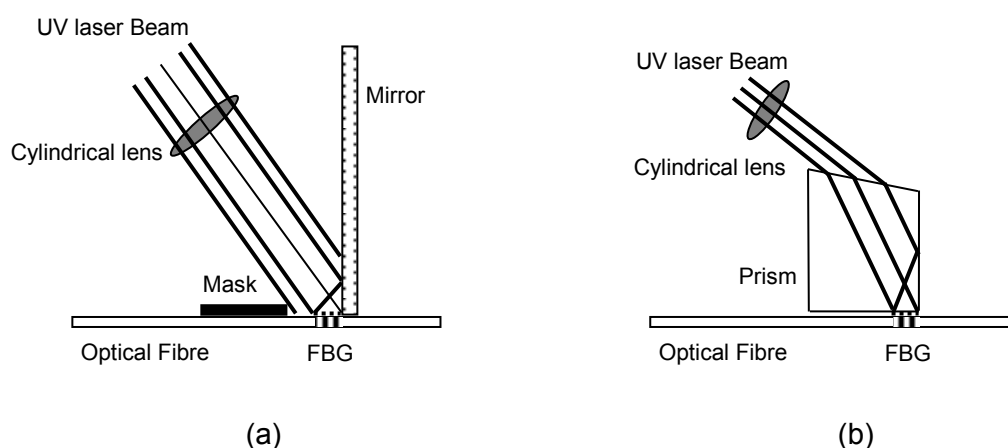
Figure 4.9: Schematic illustration of wavefront splitting interferometric FBG inscription technique. (a) Lloyd mirror interferometer. (b) Prism interferometer

The experimental setup of the Lloyd interferometer consists of a dielectric mirror, which splits half of the UV laser beam intensity to a fibre placed perpendicularly to the mirror. The overlap of the direct and deviated portions of the beam creates interference fringe along the fibre axis, which forms the refractive index modulation in the fibre core.

In the prism interferometric approach, the mirror is replaced by a prism. The UV beam is spatially bisected by the prism edge, and half of the beam intensity is reversed by the total internal reflection from its face. The two halved beams then recombine at the output face of the prism, giving an interference fringe parallel to the fibre core. This type of interferometer is intrinsically stable as the path difference is generated within the prism and remains unaffected by vibrations.

A key advantage of the wavefront splitting interferometric method is the requirement for only one optical component, which greatly reduces its sensitivity to mechanical vibrations. In addition, the distance propagated by the UV beam is also shortened with reducing of optical components. This reduces the wavefront distortion induced by air currents and temperature differences between the two interfering beams. Furthermore, these types of assembly can be easily rotated to vary the angle of the intersection of the two beams for easy wavelength tuning. However, a major drawback of this technique is the limitation of the length of the grating it can write, which is restricted to half of the beam width.

4.3.2   Point-by-point fabrication of fibre Bragg gratings

The point-to-point FBG fabrication technique is accomplished by illuminating the fibre by a highly focused single UV laser beam, which induces a refractive index change in the fibre core one step a time. The periodic modulation of the refractive index is formed by repeatedly exposing a single spot while the fibre is translated through a distance Λ, corresponding to the grating period, along the grating plane. This technique was first demonstrated by Malo *et al*. [44], using pulses of 248nm UV laser beam. They reported a third order FBG containing 225 index perturbations with a period (Λ) of 1.59μm. The system setup they used is shown in Figure 4.10.

One main advantage of this technique is its flexibility to alter the Bragg grating parameters. As the grating is formed one point a time, variations in grating length, spatial pitch, and spectral response can be easily realized. Chirped gratings can be accurately produced using this technique by increasing the amount of the precisely controlled fibre translation each time the fibre is illuminated. This method is also specifically applicable to the fabrication of long period fibre gratings. The major disadvantage of the writing technique is that the fabrication process is time consuming.
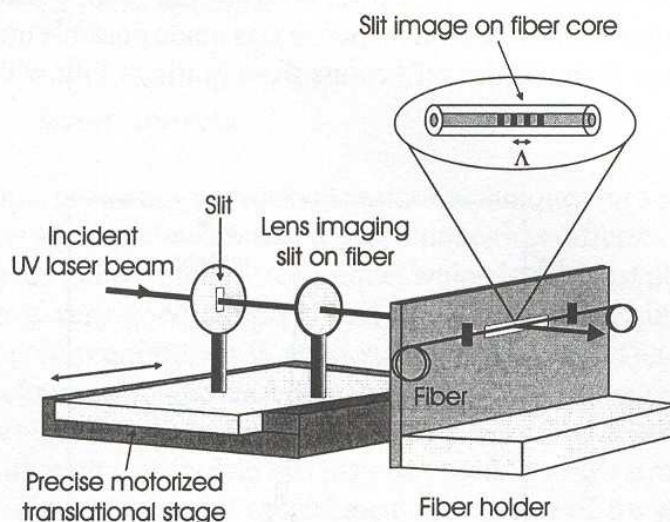
Figure 4.10: Point-by-point technique for the fabrication of fibre Bragg gratings.

4.3.3 The phase mask technique for fibre Bragg grating fabrication

The phase mask technique for fibre Bragg grating fabrication was first reported by Hill *et al*. [45]. In their experiment, a KrF excimer UV laser with pulse duration of 12 ns was used as writing light source. The period of the phase mask used was around 1060 nm. In the report, a peak reflectivity of 16% was achieved for a grating of approximately 0.9 mm in length.

This technique is one of the most commonly currently used methods for FBG fabrication. This approach employs a phase-mask, a diffractive optical component formed by using either holographic or electron-beam lithography technique, to create a spatial modulation of the UV inscribing laser beam. The interferometric fringe pattern of the diffracted beams of the phase mask then determines the grating structure based on the transmitted intensity of light striking the fibre. The phase-mask technique for the fabrication provides an effective and straightforward way of FBG fabrication, with high tolerance against mechanical vibration and the laser beam coherence quality.

The system set-up of the phase mask technique FBG inscription is schematically illustrated in Figure 4.11. In this method, the UV laser beam at normal incidence is passed through the phase mask to create an interference fringe pattern (Bragg grating pitch) in the photosensitive fibre core placed behind, and in close proximity, parallel to

the phase mask used. The interference of the plus and the minus first-order diffracted beams photo-imprints a refractive index modulation in the optical fibre core and thus results in the formation of the gratings. The period of the grating fringe (Λ) is one-half of the period of the phase mask ($\Lambda_{pm}/2$) used. Hence the Bragg wavelength of the fibre gratings written can be given by:

$$\lambda_B = 2n_{eff}\Lambda = n_{eff}\Lambda_{pm} \qquad (4.11)$$

UV laser beam

Cylindrical lens

Phase mask

Optical Fibre

Fringe Pattern

FBG

Diffracted beams

-1st order

1st order

Zero order
(<3% of throughout)
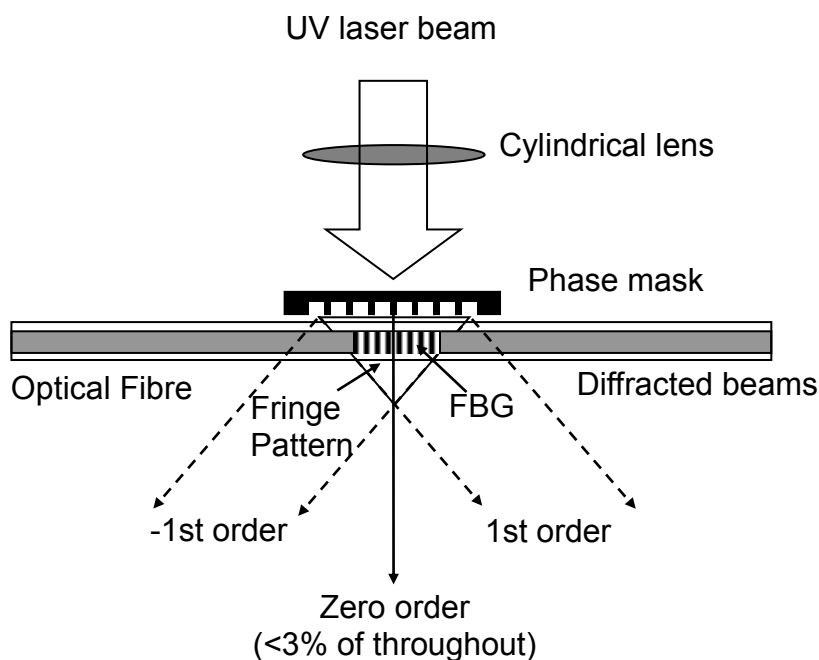
Figure 4.11: Schematic illustration of a phase mask FBG fabrication technique.

One major advantage of the phase mask technique over the two-beam interferometer technique is that the wavelength of Bragg gratings, as given in Equation 4.11, is independent of the writing laser wavelength. Thus the Bragg wavelength of the gratings can be easily tailored by using different periods of phase masks. Additionally, since the photosensitive fibre is placed directly behind the phase-mask in the near field of the diffractive (plus and minus first-order) beams, the sensitivity to mechanical vibrations (optical beam path length is reduced) is minimised. The use of one optical diffractive element reduces the complexity of the fabrication system and thus makes the device inherently more stable for reproducing identical samples.

In the work described in this thesis, this phase mask fabrication approach has been used for all Bragg grating fabrication. The experimental setup used at City University for the fabrication of fibre Bragg gratings is shown in Figure 4.12 schematically and Figure 4.13 photo graphically. A plano-cylindrical lens (focal length of 20 mm) is deployed to converge the UV laser beam into a line (rectangular shape, beam length of around 6.5 mm) along the core of the photosensitive fibre. The KrF excimer laser beam is passed through a uniform phase mask at normal incidence to create an interference pattern in the photosensitive fibre core. The photosensitive fibre is placed just behind and in close proximity, parallel to the phase mask and photo-imprinting a refractive index modulation
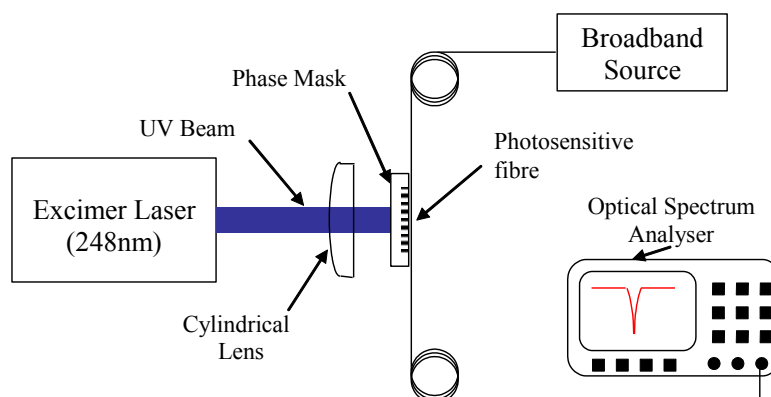
Figure 4.12: Schematic of the experimental set-up for fabrication of fibre Bragg gratings using the phase-mask technique at City University London.
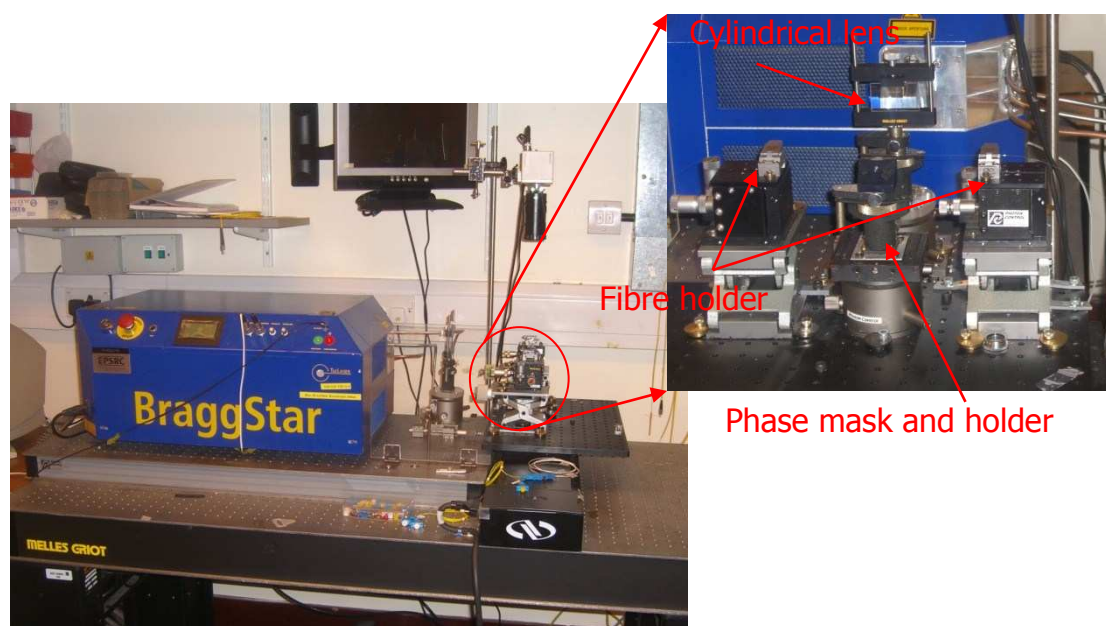
Figure 4.13: FBG fabrication system at City University

in the fibre core forms a Bragg grating. The fibre is connected to a broadband light source and to an optical spectrum analyser (OSA) to monitor the spectral profile of the grating formed during fabrication.

4.4   Strong Fibre Bragg gratings for high temperature applications

4.4.1   Commercial photosensitive fibres

As mentioned in the previous sections, the gratings written into a silica fibre are mainly inscribed by exposing the fibre to interference pattern fringes created by a UV laser beam from a KrF excimer laser working at 248 nm or a double frequency Argon ion laser working at 244 nm, through a phase mask. With most of fibres, such as silica fibres used for telecommunications, the photo-induced refractive index change is negligible. While with some special fibres, the refractive index change is significantly observable, and may result in a strong peak wavelength reflection, Bragg reflection. This characteristics of the photo-induced reflective index change (permanently) in fibres, when they are exposed to UV laser emission, is normally termed as photosensitivity, and the fibres with high photosensitivity are termed as photosensitive fibres.

Since the discovery of the photosensitivity phenomena in silicas fibre in 1978 [6,7] and the invention of external side-writing FBG fabrication technique in 1989 [8], intensive research on photosensitive fibre has been undertaken. It was reported that heavily germanium doped silica fibres are generally of highly photosensitive, and the common telecommunication silica fibres, which of lower Ge concentration (namely less than 4 mol%), are normally not photosensitive. The highly germanium doped silicate fibre is the first fibre in which the photosensitivity phenomenon was observed [6]. Nowadays, widely commercially available high Ge doped fibres, such as those fabricated by FibreCore limited, USA, normally have a germanium concentration of about 20 mol%. These types of fibres are highly photosensitive when exposed to the UV laser emission such as of 244 nm, 248nm and 193 nm. A value of 2.5×10^{-4} in the refractive index change can be easily achieved when the fibre is exposed to UV laser beam irradiative.

In additional to the highly Ge doped fibres, another commonly available commercial photosensitive fibre is boron (B) doped germannosilicate fibre. Compared to the high Ge fibres, the B/Ge co-doped fibre has shown a higher photosensitivity and a relatively lower value of numerical aperture (NA), which means it is possible to keep a large core diameter while retaining single mode characteristics. Since this type of B/Ge co-doped fibres has very high photosensitivity, a large refractive index change of about 7.5×10^{-4} can be easily obtained after the fibre is exposed to a modest power of 1 W/cm^2 from a double frequency argon ion laser for several minutes [49]. The B/Ge co-doped fibre is the "standard" type of photosensitive fibres used in this work.

4.4.2   Photosensitive fibres for high temperature FBG writing

The weak point of the fibre sensors based on FBGs written into conventional photosensitive fibres, such as the commercially available Ge doped fibre and B/Ge co-doped fibre, is their comparatively low temperature resistance. Normally, FBGs written into B/Ge co-doped fibres decay rapidly at elevated temperatures and can be completely washed out at temperatures over 350°C within a few hours [50].   Because of this irreversible degradation at high temperatures, the sensors based on FBGs written into B/Ge co-doped fibre have their limitation in some applications, especially in high temperature operation, although the silica fibre itself can survive temperatures over 1000°C for long term operations. The low temperature sustainability of these gratings is mainly due to the decay of the photo induced refractive index change formed in the fibre core during inscribing of the grating by the UV radiation.

Compared to FBGs written into B/Ge co-doped fibres, the performance of FBGs inscribed into highly Ge doped fibre silica fibres is more stable at elevated temperatures. Normally, type I gratings written into these Ge doped fibres can survive at temperatures below 650°C for many hours. For type IIA gratings, the temperature sustainability is even higher [10]. Almost no degradation of gratings is observed when they are annealed at temperature below 650°C. However, further annealing test on the gratings written into the high Ge doped fibres has shown that the gratings (both type I and type IIA) decay very quickly at temperatures over 700°C and eventually disappear completely after

being annealed at 750°C for a few hours [49]. However the FBGs inscribed into high Ge doped fibres are generally suitable for sensing applications in the moderate temperature region. In order to expand the FBG applications to higher temperature, novels fibres with higher temperature sustainability are desired.

Improving the high temperature sustainability of gratings is one of the main topics of optical sensor research, with an aim to widen the sensing range of FBG-based fibre sensors. If the operational temperature of FBG-based sensors can be increased to over 1000°C, FBG sensors will be suitable for a number of applications, such as aero-engine heat leakage measurement and combustion temperature studies, temperature monitoring in the oil and gas industries, and furnace lining temperature measurement, temperature monitoring of high-power microwave set-ups, etc.

In light of the above, a detailed investigation has been conducted by the research group at City University London and it was found that the host fibre materials play an important role in determining the FBG thermal sustainability. In this work a brief summary is given below in terms of the thermal sustainability of FBGs written in a number of host fibres, including tin doped fibre [52-53] and erbium co-doped fibre [51,54], antimony doped fibre [55] and Indium doped fibre [56].

4.4.2.1 Sn doped photosensitive fibres

Tin (Sn) doped photosensitive fibre was first developed by Dong et al [52], at Southampton University, UK, by co-doping Sn into the fibre core of phosphosilicate fibre to increase its photosensitivity. It was found that with the presence of a small amount of Sn in the core of the phosphosilicate fibre or germanosilicate fibre, an enhanced photosensitivity of the fibre can be realized and strong gratings can be inscribed into these fibres [53]. Further research by the City group reported that FBGs written into the Sn doped fibre could survive at very high temperatures, over 800°C, and a considerable value of reflectivity remained after annealing at such an elevated temperature for several hours [52]. However the photosensitivity of this specialist fibre is not as good as that of B/Ge fibres. To fabricate a FBG with a reflectivity of over 95% into

the Sn doped fibre normally takes around half an hour with a 248nm laser emission of 12 mJ at a frequency of 100Hz, while FBGs written into B/Ge fibre with a reflectivity greater than 99% only takes less than one minute under the same fabrication condition. This will be a limitation for a volume production of high reflectivity FBGs using the Sn doped fibre.

4.4.2.2 Er doped silica photosensitive fibres

Three different types of Erbium (Er) doped photosensitive fibres, i.e. erbium/germanium (Er/Ge) fibre, erbium/tin/germanium (Er/Sn/Ge) fibre, erbium/antimony/germanium (Er/Sb/Ge) fibre have been manufactured and studied for high temperature FBG evaluations and the details have been reported by Shen et al [49,54]. These fibres have demonstrated an enhanced photosensitivity while remaining high temperature sustainability.

The photosensitivity of these fibres was observed and compared by writing FBGs into these fibres under same condition with the laser emission of a KrF excimer laser at energy of 12 mJ per pulse at a repetition rate of 100 Hz using phase mask technique. The laser exposure time was controlled for each FBG sample fabrication until it reached a high level of reflectivity (typically > 95%). For the Er/Ge fibre, it took less than 2 minutes of exposure time for the FBG to reach its reflectivity over 99% before it became saturated and the reflectivity decreased (a type IIA grating could be formed with this fibre when a longer exposure time was applied). For the Er/Sn/Ge fibre, it took an exposure of around 11 minutes to reach its maximum reflectivity of 96%. And for the Er/Sb/Ge fibre, it was exposed for around 12 minutes to achieve a reflectivity of 99.6%. No decrease in the reflectivity of FBGs in the Er/Sn/Ge fibre and the Er/Sb/Ge fibre was observed when a prolonged writing time was implemented after the gratings had reached their saturated state. The corresponding refractive index modulation of 2.85×10^{-4} and 1.82×10^{-4} for the Er/Sb/Ge fibre and the Er/Sn/Ge fibre respectively was achieved.

Subsequently, the thermal characteristics of these gratings were investigated by

testing in a tube oven. The temperature of the oven was raised from room temperature to around 900°C with steps of 100°C or 50°C each time, and at each temperature the FBGs were annealed for 24 hours. The results obtained clearly indicated that the grating written in the Er/Ge fibre was erased at 700°C, and those written in the Er/Sb/Ge and Er/Sn/Ge fibres still retained a considerable level of reflectivity after being annealed at 850°C for 24 hours and 900°C for 4 hours respectively. The results obtained are of great importance for high temperature applications.

4.4.2.3 Sb/Ge co-doped fibre and In/Ge co-doped fibre

Based on the results obtained, Shen et al. have designed and fabricated more photosensitive fibres in order to meet requirements for even higher temperature applications. A novel Sb/Ge co-doped fibre has been specially designed and developed for the fabrication of "strong" gratings with very high temperature sustainability. The fibre is of high photosensitivity with FBGs inscribed into it can reach a high refractive index modulation of greater than 2.7 x 10^{-4}. The FBG written into the Sb/Ge co-doped fibre, with initial reflectivity over 99%, could sustain an elevated temperature of 900°C over a period of 24 hours and yet retained a considerable level of reflectivity of over 18%. It remained a reflectivity of 3.4% after having been annealed at extreme high temperature of 950°C over a period of 8 hours, with an observable reflection peak after 20 hours. These results were much better than those obtained from Sn doped fibre [56] and Sb/Er/Ge [57] co-doped fibres reported earlier.

In addition to the Sb doped fibre, Shen et al. also developed a Indium (In) co-doped germanosilicate fibre for high temperature FBG inscribing with high photosensitivity[58]. The gratings can reach high reflectivity of 99.0% and 99.8% using the excimer laser of 12 mJ per pulse with repetition rates of 200 Hz and 300 Hz respectively, representing refractive index modulation of 2.4 x 10^{-4} and 3.2 x 10^{-4}. After having being annealed at 900°C for 24 hours, the gratings retained a considerable level of reflectivity of 11% (200 Hz repetition rate) and 21% (300 Hz repetition rate). After being annealed at 950 ^{o}C for hours and 1000 ^{o}C for 2 hours before the annealing temperature was cooled down to the room temperature step by step. The retained reflective spectrum showed that the

reflectivity of the grating could still be interrogated by instrumentation.

4.4.3   Strong FBGs written into Bi/Ge co-doped fibres

Further to the study of Sb doped and In doped fibre, which has shown that these fibres had good photosensitivity and a strong temperature sustainability of the gratings written into them, another type of high photosensitive fibre was specially developed, with partners at Zhejiang University, China and the China Building Materials Academy, for systematic evaluations of the gratings at high temperatures. The temperature sustainability and thermal decay of the FBGs written into this fibre were observed and evaluated.

4.4.3.1   Fabrication of Bi/Ge co-doped fibre

In an attempt to investigate a novel and highly photosensitive fibre for extreme high temperature FBG applications, the bismuth doped germanosilicate fibre (Bi/Ge fibre), was developed. The choice of the element bismuth was mainly made on the basis of the electron charge effect of the outer shell electrons in the atom, similar to the situation in In-doped fibre, with the large cation Bi^{3+} ion size (130 pm, greater than that of 76 pm of Sb^{3+} and 80 pm of In^{3+}) in its atomic construction [59]. It is believed that this larger size of the doping ion may effectively stabilize the performance of the material concerned, as in the situation of the fluorescence performance of Tm-doped Yttrium Aluminium Garnet (YAG), where the doping of the Tm ion composition has created a garnet with a very stable fluorescence intensity and decay lifetime when experiencing annealing temperatures as high as 1200 $^{\circ}$C [60]. The choice of doping another element, Ge, in the fibre is aimed both to enhance the photosensitivity of the fibre and to increase the refractive index of the fibre core.

The fibre was fabricated at the China Building Materials Academy, Beijing, China as a joint research venture. The fibre preform, with a composition of GeO_2 ~15 wt%, Bi^{3+}:5000 ppm, was fabricated by the method of Modified Chemical Vapour Deposition (MCVD. A long length of fibre with a core diameter of about 8 μm and a cladding diameter of 125 μm was then drawn from the preform at 2100 $^{\circ}$C, using the normal fibre

drawing approach.

4.4.3.2 FBGs written into the Bi/Ge co-doped fibre

A number of strong FBG samples were fabricated into the specially developed Bi/Ge fibre through phase mask technique, using ultra-violet (UV) exposure at a wavelength of 248nm from a KrF excimer Laser with an energy of 10-12mJ per pulse at a repetition frequency of 100Hz or 200hz. An optical spectrum analyzer (OSA) was used to monitor the reflectivity of the grating during fabrication. The total exposure time was from 5 minutes to 15 minutes for these FBGs. The increasing reflectivity of some of these gratings with exposure time is illustrated in Figure 4.14. It is clearly shown that the grating can easily reach a high reflectivity (greater than 99% for the samples used here) in 5 to 15 minutes, varying with the writing condition. It takes a much longer time for writing high reflective gratings compared to Ge doped fibre and B/Ge co-doped fibre, which require around 1 minute laser exposure to reach the reflectivity over 99%.

4.4.4 Thermal characteristics of strong FBGs written into Bi/Ge fibre

The thermal characteristics of the strong FBGs written into the special photosensitive fibre were tested at the laboratory of City University by annealing the gratings in a tube oven at different temperatures. The experimental setup is illustrated in Figure 4.15. The gratings were put into a tube oven and loosely placed at the centre of it. The transmission spectrum of the FBG was monitored by an OSA (HP86140A), when the grating was illuminated by light from an ASE broadband light source. The Bragg wavelength and the reflectivity of the grating were recorded and analysed. Several different annealing procedures were carried out, which are detailed as follows.
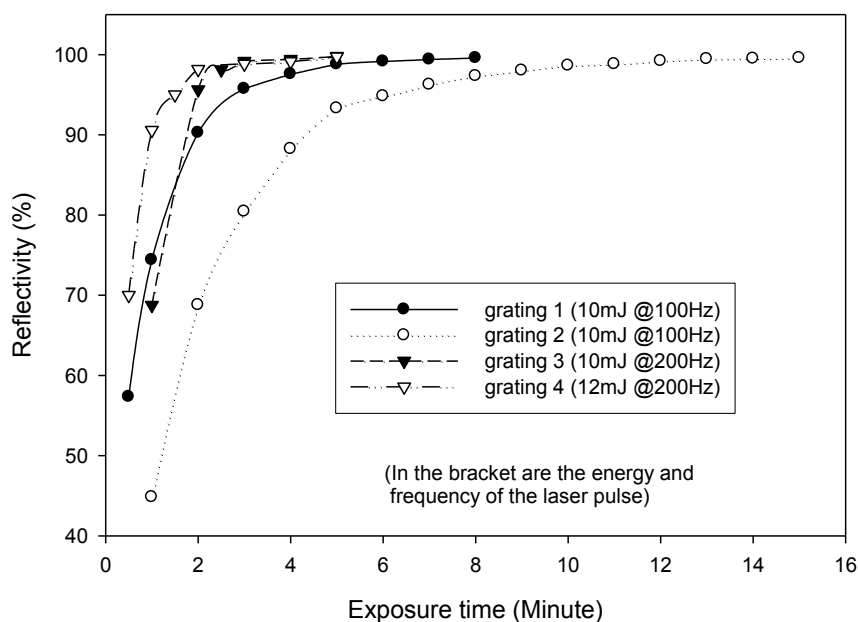
Figure 4.14: Reflectivity change of FBGs vs. exposure time during fabrication
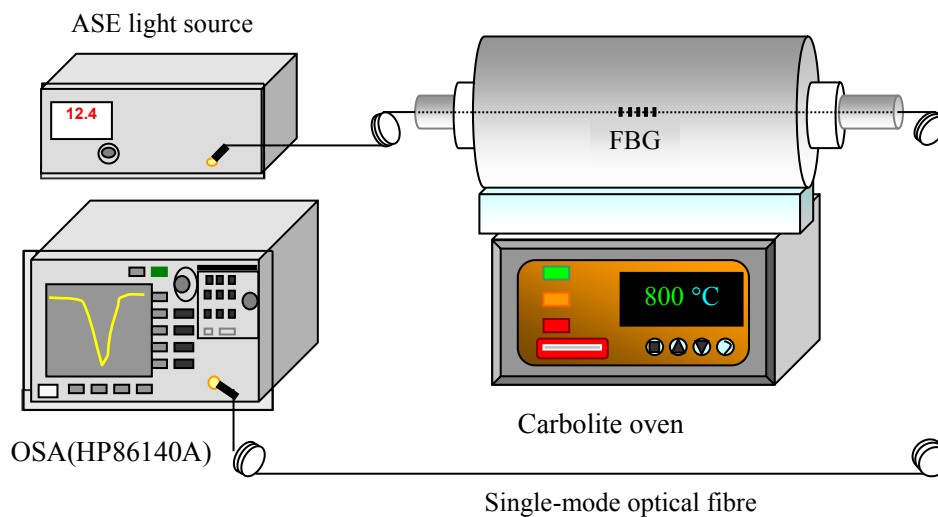
Figure 4.15: Experimental set-up for testing the temperature characteristics
of the strong FBGs written into a Bi/Ge fibre

4.4.4.1 Thermal decay test of the FBGs

The thermal decay characteristics of FBG sample 1 were observed over the temperature range from 300°C to 900°C, in increments of 100°C. The FBG was

annealed at each isothermal temperature for about 24 hours. The Bragg wavelength shift and the reflectivity change of these FBGs are shown in Figure 4.16. It is clearly shown that the FBGs, could sustain a high temperature of 900°C for 24 hours, and yet still remained a considerable reflectivity of about 20%. The Bragg wavelength, as expected, increased with any increase of temperature. Whereas, at each isothermal temperature, a small wavelength shift towards a shorter wavelength was observed along with the elapsed time, taking about 8-10 hours to reach an relative stable value of $\lambda_B(T)$ at each temperature. This shift of λ_B at each temperature of these FBGs is similar to that of the FBGs written into some Ge doped and B/Ge co-doped fibres, which has been discussed by Pal et al [61].
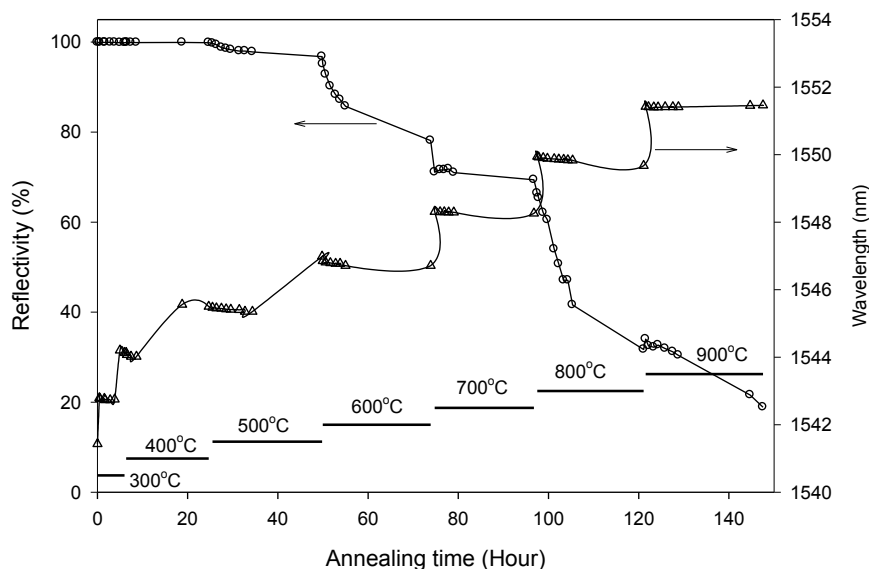
Figure 4.16: The Bragg wavelength shift and reflectivity change of FBG, annealed at temperatures from 300°C to 900°C.

4.4.4.2 High temperature sustainability tests

A further annealing procedure was applied to three other FBG samples, gratings 2, 3 and 4, created in a similar way to grating 1. They were first annealed at 550°C for over 650 hours, then at 650°C for 190 hours and finally at 850°C for 55 hours. The decay of the reflectivity and the wavelength shift of these gratings with the annealing time are illustrated in Figure 4.17. The reflectivity of gratings 3, 4 and 5, after being annealed at 550°C for 650 hours, were 57%, 67% and 70% respectively, reduced to 37%, 46% and

48% after being annealed at 650°C for 190 hours, and finally reduced to 16%, 22% and 29% after being annealed at 850 $^{\circ}$C for 55 hours. These results show that the FBGs write into this novel Bi/Ge co-doped fibre can be used in high temperature applications for a prolonged period.
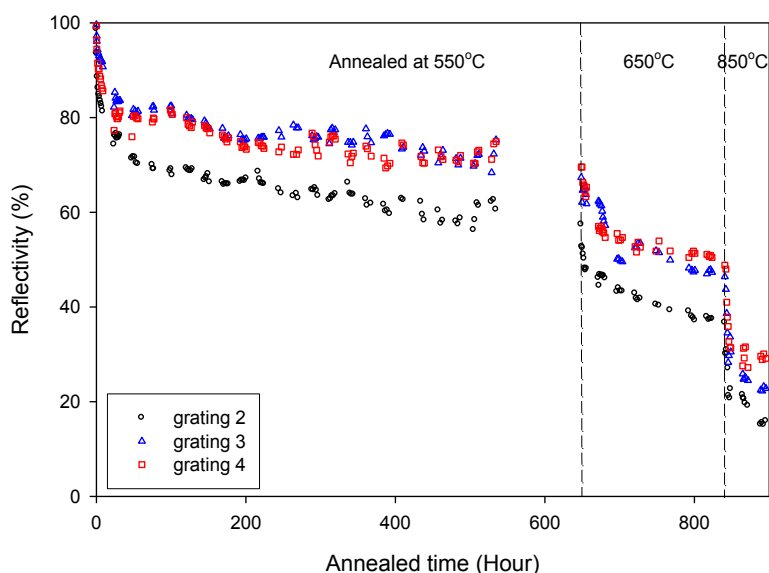
Figure 4.17: The reflectivity of the FBGs, annealed at 500°C, 650°C and 800°C, for 650, 190 and 55 hours respectively.

4.4.4.3 Wavelength shift of the FBGs with temperature

Following annealing using the above mentioned procedures, the Bragg wavelength shift was observed, as a function of temperature, over the range from room temperature to 1100°C, in increments of 50°C. An exposure of about 30 minutes at each temperature (except at 1050°C or 1100°C where the gratings were totally erased in about 5-20 minutes) was used. The Bragg wavelengths of these gratings at these different temperatures, measured in the reflection mode with the OSA, are illustrated in Figure 4.18. The results show that the temperature resolution of these gratings is ~14pm/$^{\circ}$C and good linearity (~1%) over the full temperature range has been demonstrated.
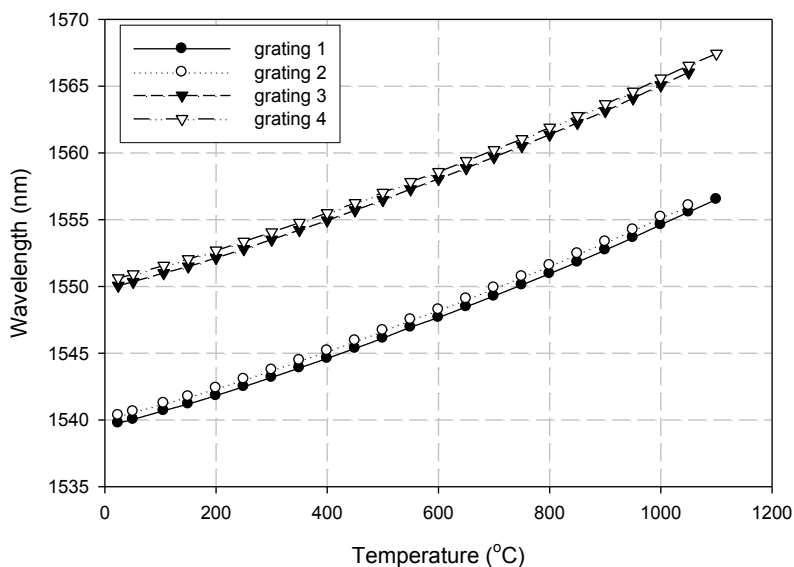
Figure 4.18: The temperature dependent Bragg wavelengths of the FBGs, from room temperature to 1100°C.

4.4.4.4 High temperature measurement – "shock test"

Some of the FBGs created with an initial reflectivity of >99%, without being pre-annealed, were exposed to a high temperature for "shock" test. The FBGs, placed loosely into a 1mm diameter stainless steel tube, were quickly inserted into the high temperature zone in the oven, which was pre-set to a high temperature, typically 1000°C or 1100°C. A K-type thermocouple is intimately attached to the steel tube with the FBG inside. The wavelength and reflected light intensity were recorded, using a MicronOptics sm125 Optical Sensing Interrogator, until the FBGs were totally erased.

The results obtained, together with one set of data obtained from a FBG written into B/Ge co-doped fibre for comparison, are shown in Figure 4.19. The tests show that the FBGs written into the Bi/Ge fibre survived for ~15 seconds after being inserted in the oven at 1100°C, and ~300 seconds at 1000°C. By contrast, the FBG written into B/Ge fibre, when inserted into the oven at 1000°C, only lasted a few seconds before it was completely erased as the temperature rose beyond 800°C. The results again clearly indicate that the Bi/Ge FBG had much higher temperature sustainability, even when it was exposed to a sudden high temperature change. However, these FBGs, which were

not pre-annealed, tended to last for a shorter time at high temperatures than those which had been annealed, as the thermal pre-treatment is known to stabilise the index modulation of the fibres [62].
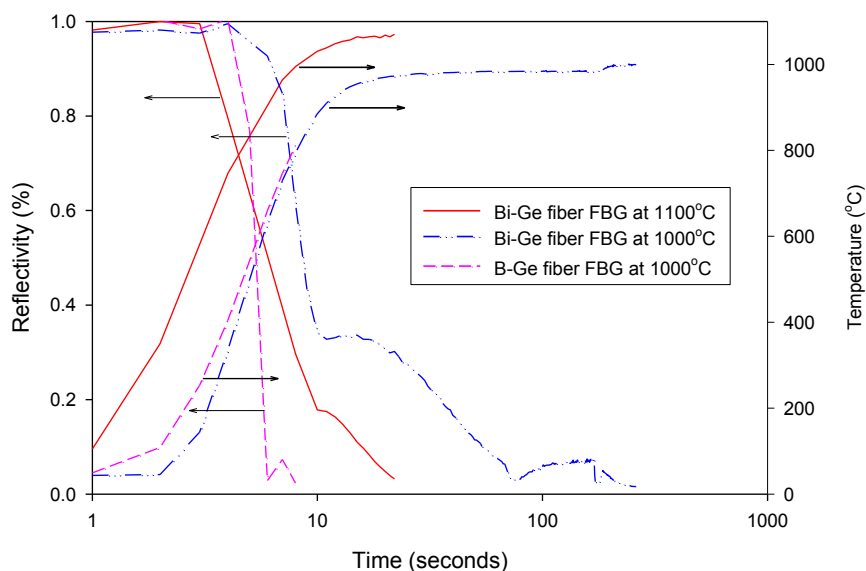
Figure 4.19: 'Shock' test of FBGs at 1000°C and 1100°C

The experimental results from the tests on high temperature exposure and annealing of the specialized FBGs created have clearly indicated that gratings inscribed in the Bi/Ge fibre had much high temperature sustainability than those written into conventional fibres. The results of this work give clear evidence that such gratings are well suited to those sensing applications where high temperature sustainability is essential.

In addition, the temperature sustainability of the FBGs created in the Bi/Ge fibre was observed to be related to the initial reflectivity arising from the initial UV exposure of the fibre during the grating writing. This observation suggests that an initial reflectivity of >99% is preferred for high temperature applications.

4.5   Summary

After giving a brief review and introduction of fibre Bragg gratings and their applications in telecommunications and sensors, the focus of the study has been on the

evaluation and cross-comparison of a number of gratings written into different host fibre materials for their thermal sustainability for potential high temperature applications. The photosensitivity and thermal characteristics of fibre Bragg gratings inscribed in a newly developed Bi/Ge co-doped fibre have been systematically tested and evaluated. The results show that the strong gratings written into the Bi/Ge fibre can retain high reflectivity after being annealed at elevated temperatures over 900 $^{\circ}$C, therefore are well suitable for high temperature applications.

Reference

[1]. B. A. Childers, M. E. Froggatt, S. G. Allison, T. C. Moore, D. A. Hare, C. F. Batten and D C. Jegley, "*Use of 3000 Bragg grating strain sensors distributed on four 8-m optical fibers during static load tests of a composite structure*", Proc. SPIE Vol. 4332, Smart Structures and Materials, 2001, pp.133-142

[2]. A. Othonos, "*Fibre Bragg gratings*", Review of Scientific Instrument, Vol. 68, 1997, pp.4309-4341.

[3]. A. Othonos and K. Kalli, "*Fiber Bragg Gratings: Fundamnetals and Applications in Telecommunication and sensing*", Artech House, 1999

[4]. Y. J. Rao, "*Recent Progress in Applications of In-Fibre Bragg Grating Sensors*", Optics and Engineering, 31, (1999), pp.297-324.

[5]. A. D. Kersey, M.A. Davis, H.J. Patrick, M. LeBlanc, K.P. Koo, C.G. Askins, M.A. Putnam, E.J. Friebele, "*Fiber grating sensors*", Journal of lightwave technology, Vol. 15, 1997, pp.1442-1463

[6]. K.O. Hill, Y. Fujii, D. C. Johnson, B. S. Kawasaki, "*Photosensitivity in optical fibre waveguides: application to reflection fibre fabrication*", Applied Physics Letters, Vol. 32, 1978, pp.647-649.

[7]. B. S. Kawasaki, K. O. Hill, D. C. Johnson, and Y. Fujii, "*Narrow-band Bragg reflectors in optical fibres*", Optics Letters, Vol.3, 1978, pp.66-68.

[8]. G. Meltz, W. W. Morey and W. H. Gkenn. "*Formation of Bragg gratings in optical fibres by a transverse holographic method*". Optics Letters, Vol.14, 1989, pp. 823-825

[9]. J. L. Archanbault, L. Reekie, and P. J Rusell, "*100% reflectivity Bragg reflector produced in optical fibers by single excimer laser pulse*", Electronics Letters, Vol. 29, 1993, pp. 453-455

[10]. W.X. Xie, W.X. Xie, P. Niay, P. Bernage, M. Douay, J.F. Bayon, T. Georges, M. Monerie, B. Poumellec, "*Experimental evidence of two types of photorefractive effects occurring during photo inscriptions of Bragg gratings written within Germanosilicate fibres*", Optical communications, Vol. 104, 1993, pp. 185-195

[11]. L. Riant, and F. Haller, "*Study of the photosensitivity at 193nm and comparison with photosensitivity at 240nm influence of fibre tension: Type IIA aging*", IEEE Journal of Lightwave Technology, Vol. 15, 1997, pp.185-195

[12]. K.O. Hill, F. Bilodeau, B. Malo, D.C. Johnson, "*Birefringent photosensitivity in*

monomode optical fiber: Application to external writing or rocking filters", Electronics Letters, Vol. 27, 1991, pp. 1548-1550

[13]. R. Kashyap, R. Wyatt, and P. F. McKee, "*Wavelength flatten saturated erbium amplifier using multiple side-tap Bragg gratings*", Electronics Letters, Vol. 29, 1993, pp. 1025-1026

[14]. A. Othonos, X. Lee and D. P. Tsai, "*Spectrally broadband Bragg grating mirror for and erbium doped fibre laser*", Optical Engineering, Vol. 35, 1996, pp1088-1092

[15]. J. Chow, G.Town, B. Eggleton, M. Ibsen, K. Sugden, and I. Bennion, "*Multi-wavelength generation of an erbium doped fibre laser using in-fiber comb filters*", IEEE photonics Technology letters, 1996, pp.60-62.

[16]. G. A. Ball, W. W. Morrey, and W. H, Glenn, "*Study of monomode erbium fiber laser*", IEEE photonics Technology letters, Vol. 3, 1991, pp.613-615

[17]. J. L. Zyskind, V. Mizrahi, D.J. DiGiovanni, J.W Sulhoff,,"*Short single frequency erbium doped fiber laser", Electronics letters*", Vol. 28. 1992, pp.1385-1286

[18]. R. P. Davey, R.P.E. Fleming, K. Smith, R. Kashyap, J.R. Armitage, "*Mode-lock erbium fiber laser with wavelength selected by means of fiber Bragg grating reflector*", Electronics letters, Vol. 27. 1991, pp.2087-2088

[19]. S. G. Grubb, T. Strasser, W. Y. Cheung, W. A. Reed, V. Mizrahi, T. Erdogan, P. J. Lemaire, A. M. Vengsarkar, D. J. DiGiovanni, D. W. Peckham, and B. H. Rockney, "*High-power 1.48μm cascaded Raman laser u germanosilicate fibers*", Proc. Optical Amplifier and Their applications, Davow, Switzerland, Paper SaA4, 1994

[20]. C. R. Giles, "*Lightwave applications of fiber Bragg gratings*", IEEE photonics Technology letters, Vol 7, 1995, pp.980-982

[21]. V. Mizrahi, T. Erdogan, D.J. DiGiovanni, P.J. Lemaire, et al. "*Four channel fire grating demultiplexer*", Electronics letters, Vol. 30. 1994, pp.780-781

[22]. J. J. Pan and Y Shi, "Steep skirt fibre Bragg grating fabrication using a new apodised phase mask", Electronics letters, Vol. 33(22), 1997, pp. 1895-1896

[23]. H. G. Winful, "*Pulse compression in optical fiber filters*", Applied physics letters, Vol. 46, 1985, pp.527-529

[24]. C. R. Giles, V. Mizrahi, T. Erdogan, "*Polarization-independent phase conjugatin of lightwave signals*", IEEE photonics Technology letters, Vol. 7, 1995, pp.126-128

[25]. K. O. Hill and G. Meltz, "*Fiber Bragg grating technology*", Journal of lightwave technology, Vol. 15, 1997, pp. 1263-1276

[26]. J.R. Dunphy, G. Meltz, F. Lamm, and W. Morey, "*Multifunction, distributed optical fibre sensor for composite cure and response monitoring*", society of Photo-optical instrumentation Engineering, Fibre Optic Smart Structure and Skins III, Vol.1370, 1990, pp.116-118

[27]. Internet reference: ic.are.nasa.gov/ic/projects/photonics/os/healthsensors/health.html

[28]. D. R. Hjelme, "*applications of Bragg grating sensors in the characterization of scaled marine vehicle models*", Applied optics, Vol. 36 1997, pp. 328-336

[29]. S. T. Vobra, M. A Davis, A. Dandridge, et al, "*Sixteen channel WDM fibre Bragg grating dynamic strain sensing for composite panel slamming tests*", Proceedings of the optical fibre sensor conference (OFS12), Williansburg, VA, USA, 1997, pp. 328

[30]. E. J, Ferribele, "*Fiber Bragg grating strain sensor: Present and future applications in*

smart structures", Optics and Photonics, Vol. 9, 1998, pp33-37.

[31]. *E. Joseph Friebele, "Fiber Bragg Grating Strain Sensors: Present and Future Application in Smart Structures,"* Optics & Photonics News, Vol. *9(8), 1998, 33- ()*

[32]. Yung Bin Lin, Chih Liang Pan, Yuan Hung Kuo, Kuo Chun Chang and Jenn Chuan Chern, "*Online monitoring of highway bridge construction using fiber Bragg grating sensors*", Smart Material Structure, Vol. 14**,** 2005, pp.1075-1082

[33]. P. Moyo, "*Development of fiber Bragg grating sensors for monitoring civil infrastructure*", Engineering Structures Vol. 27, 2005, pp.1828-1834

[34]. Liang Ren, Hong-Nan Li, Jing Zhou, Dong-Sheng Li and Li Sun, "*Health monitoring system for offshore platform with fiber Bragg grating sensors*", Optical Engineering, Vol. 45, 2006, 084401;

[35]. Y.J. Rao, B. Hurle, D.J. Webb, D.A. Jackson, L. Zhang, and I. Bennion, "*In-situ temperature monitoring in NMR machines with a prototype in-fibre Bragg grating sensors system*", Proceedings of the optical fibre sensor conference (OFS12), Williansburg, VA, USA, 1997, pp. 646-649

[36]. YJ Rao, DJ Webb, DA Jackson, L. Zhang, and I. Ben- nion, "*In-fibre Bragg grating temperature sensor system for medical applications*", IEEE Journal of Lightwave Technology, Vol. 15, 1997, pp. 779-785

[37]. E. Samset, T. Mala, R. Ellingsen, I. Gladhaug, O. Søreide, E. Fosse, "Temperature measurement in soft tissue using a distributed fiber Bragg grating sensor system". Minimally Invasive Therapy and Allied Technologies, Vol. 10, 2001, pp. 89-93.

[38]. N E Fisher, J Surowiec, D J Webb, D A Jackson, L R Gavrilov, J W Hand, L Zhang and I Bennion., "*In-fibre Bragg gratings for ultrasonic medical applications", Measurement Science and Technology*", Vol. 8 ,1997, pp.1050-1054

[39]. B.M. Cowie, D.J. Webb, B. Tam, P. Slack, P.N. Brett, "*Distributive Tactile Sensing using Fibre Bragg Grating Sensors for Biomedical Applications*", The First International Conference on Biomedical Robotics and Biomechatronics (BioRob 2006), 2006, pp. 312 - 317

[40]. A. F. Fernandez, A Gusarov, B Brichard, M Decréton, F Berghmans, P Mégret, and A Delchambre, "*Long-term radiation effects on fibre Bragg grating temperature sensors in a low flux nuclear reactor*" Measurement Science and Technology, Vol. 15 ,2004, pp.1506-1511

[41]. P. M. Cavaleiro, F.M. Araujo, A.B.L. Ribeiro, "*Metal-coated fibre Bragg grating sensor for electric current metering*", Electronics Letters, Vol. 34, 1998, pp. 1133 -1135

[42]. Jianmin Gong, C. C. Chan, M. Zhang, W. Jin, J. M. K. MacAlpine, and Y. B. Liao "*Fiber Bragg grating current sensor using linear magnetic actuator*", Optical Engineering, Vol. 41, 2002, pp557;

[43]. K. Krebber, W. Habel, T. Gutmann and C. Schram, "*Fiber Bragg grating sensors for monitoring of wind turbine blades*", Proceedings of the optical fibre sensor conference (OFS17), 2005, pp. 1036-1039

[44]. B. Malo, K.O.Hill, F. Bilodeau, D.C. Johnson, J. Albert,. "*Point-by-point fabrication of micro-Bragg grating in photosensitive fibre using single excimer pulse refractive index modification techniques*", Electronics letters, Vol. 29, 1993, pp.1668-1669

[45]. K. O. Hill, B. Malo, F. Bilodeau, D.C. Johnson, J. Albert, "*Bragg grating fabrication in*

monomode photosensitive optical fibre by UV exposure through a phase mask", Applied Physics letters, Vol. 62, 1993, pp.1035-1037

[46]. R. kashyap, "*Fiber Bragg gratings*", Academic Press, New York, 1999

[47]. R. Kashyap, J.R. Armitage, R. Wyatt, S.T. Davey, D.L. Williams, "*All-fiber narrow band reflecting grating at 1500 nm*", Electronics Letters, Vol. 26, 1990, pp. 730-732

[48]. H. G. Limberger, P.Y. Fonjallaz, P. Lambelet, C. Zimmer,, "*Photosensitivity and self organization in optical fibers and waveguides*", SPIE, Vol.2044, 1993, pp.272

[49]. D. L. Williams, B.J. Ainslie, J.R. Armitage, R. Kashyap, R. Campbell, "*Enhanced UV photosensitivity in boron codoped germanosilicate fibres*", Electronics Letters, Vol. 29, 1993, pp.45-47

[50]. S. R. Baker, H.N. Rourke, V. Baker, D. Goodchild, "*Thermal decay of fibre Bragg gratings written in boron and germanium codoped silica fibre,*" IEEE Journal of Lightwave Technology, Vol.15, 1997, pp.1470-1477

[51]. Y. Shen, S. Pal, J. Mandal, et al, "*Investigation on the photosensitivity, temperature sustainability and fluorescence characteristics of several Er-doped photosensitive fibres*", Optics Communications, Vol. 237, 2004, pp.301-308

[52]. L. Dong, J.L. Cruz, J.A. Tucknott, L. Reekie, D.N. Payne, "*Strong photosensitivity gratings in tin-doped phosphosilicate optical fibres*", Optics Letters, Vol.20, 1995, pp.1982-1984

[53]. L. Dong, J.L. Cruz, L. Reekie, M.G. Xu. "*Enhanced photosensitivity in tin-codoped germanosilicate optical fibres*", IEEE Photonics Technology Letters, Vol. 7, 1995, pp.1048-1050

[54]. Y. Shen, T. Sun, K.T.V. Grattan and M. Sun, "*Highly photosensitive Sb/Er/Ge codoped silica fibre for fibre Bragg grating (FBG) writing with strong high-temperature sustainability*", Optics Letters, Vol.28, 2003, pp.2025-2027

[55]. Y. Shen, J. He, T. Sun, K.T.V. Grattan, "*High temperature sustainability of strong FBGs written into Sb/Ge co-doped photosensitive fibre - decay mechanisms involved during annealing*", Optics Letters, Vol.29, 2004, pp.554-556

[56]. Y. H. Shen, "*Charaterization of optical fibre sensor systems for applications at high temperatures*", Ph D thesis, City University, London, 2005

[57]. G. Brambilla, V. Pruneri and L. Reekie, "*Photorefractive index gratings in SnO_2:SiO_2 optical fibres*", Applied Physics Letters., Vol.76, 2000, pp. 807-809

[58]. Y. Shen, J. Xia, T. Sun and K.T.V. Grattan, "*Photosensitive Indium doped germano-silica fibre for strong FBGs with high temperature sustainability*", IEEE Photonic Techology Letters, vol. 16, 2004, pp. 1319-1321

[59]. A. M. James and M.P. Lord, Macmillan's Chemical and Physical Data, The MacMillan Press Ltd, 1992

[60]. Y. H. Shen, W. Zhao, T. Sun and K.T.V. Grattan, "*Characterization of optical fbre thermometer using Tm3+:YAG crystal, based on fluorescence lifetime approach*", Sensors and Actuators: A. Physical, Vol. 109, 2003, pp. 53-59

[61]. S. Pal, J. Mandal, T. Sun, and K.T.V. Grattan "*Anlysis of thermal decay and prediction of operational lifetime for a type I boron-germanium codoped fiber Bragg grating*", Apply Optics, Vol. 42(12), 2003, pp. 2188-2197

[62]. J. Rathje, et al. "*Continuous anneal method for characterizing the thermal stability of*

ultraviolet Bragg gratings", Journal of Applied Physics, Vol. 82(2), 2000, pp. 1050-1055

Chapter 5. Development *of fibre Bragg grating based sensor systems for different applications*

5.1   Wavelength interrogation schemes of FBG sensors

For the FBG sensor applications,, such as temperature and/or strain sensors, the accurate measurement of the Bragg grating wavelength shift is critical to achieve good sensor performance. The simplest and easiest method to measure the spectrum of an FBG(s) is using a commercially available Optical Spectrum Analyser (OSA). This method is very commonly used in laboratories for preliminary sensor tests and evaluations. But the spectrometers are very expensive. A normal OSA with a wavelength resolution of 0.01nm costs over £15K.   Particularly, in cases where a high wavelength resolution, e.g. a resolution of 1 pm, is required to resolve a small temperature change of 0.1°C, or stain change of 1 $\mu\varepsilon$, the price of such an OSA is even higher. In addition, conventional OSAs are very large and bulky, which limits their field applications, especially for in-situ measurements. The OSAs, though providing some functions for integration into user applications based on newly developed mathematical models, do not usually have the flexibility to be developed fully as a cost-effective interrogation system with a user-friendly interface for particular applications. Thus, it is a challenge to create a low cost and compact electro-optics unit to replace an OSA to accurately measure the Bragg grating wavelength (or its shift) and as a result a considerable amount of research has been on-going to find an effective solution to this.

The most common method for interrogation of wavelength shift of Bragg gratings is to use a broadband illumination, where the bandwidth of the broadband light source covers the grating wavelength shift range when it is exposed to a perturbation. The narrowband reflected light at the Bragg wavelength from the grating is then subsequently directed to the wavelength detection system. Although a wide variety of techniques have been demonstrated for monitoring Bragg wavelength shifts in many literatures for the last few decades since the grating sensor system has been developed,

only a limited number of schemes appear to have the potential for being realized as a practical, cost-effective instrumentation system for real-world applications. The schemes of the wavelength interrogation system, which might be suitable for practical applications, are listed in Table 5.1 [1], and discussed in the following sections.

Table 5-1: Summary of FBG wavelength interrogation schemes

	Edge filter	Tunable filter	Interferometric	Tunable laser	CCD-Spectrometer
Range to resolution	10^2-10^3	10^3-10^4	10^3-10^4	10^3-10^5	10^3-10^4
Measurement speed	High	high	High	high	high
Long term stability	Good	good	Good	good	good
WDM compatibility	Low	high	High	high	high
Potential cost	Low	medium	Low	high	medium

5.1.1   Edge filter wavelength interrogation scheme

One simple approach based upon opto-electronics is to measure the wavelength shift using the edge filter method. In this method, an edge filter, which has a linear relationship between wavelength shifts and the resulting output intensity changes, is utilized for Bragg wavelength shift interrogation when its cutoff is close to the signal wavelength,. As shown in Figure 5.1, the operational principle behind this method is that the Bragg wavelength shift induced by the measurand is obtained by measuring the intensity change from the output of the edge filter. The influences of the light source fluctuations and losses in the optical links can be removed by consideration of a reference signal. The wavelength shift $\Delta\lambda$ can be obtained by measuring the ratio of the signal intensity I_S and the reference intensity I_R, given by [2]:

$$\frac{I_S}{I_R} = A\left(\lambda_B - \lambda_o + \frac{\Delta\lambda}{\sqrt{\pi}} \right) \tag{5.1}$$

where A is the sensitivity of the filter.

A resolution of tens of $\mu\varepsilon$ had been achieved for strain measurement by this low cost system. This method offers several advantages over the OSA system in terms of low cost and ease of use. However, it also has some intrinsic disadvantages, such as the lack of multiplexing capability and limited resolution.
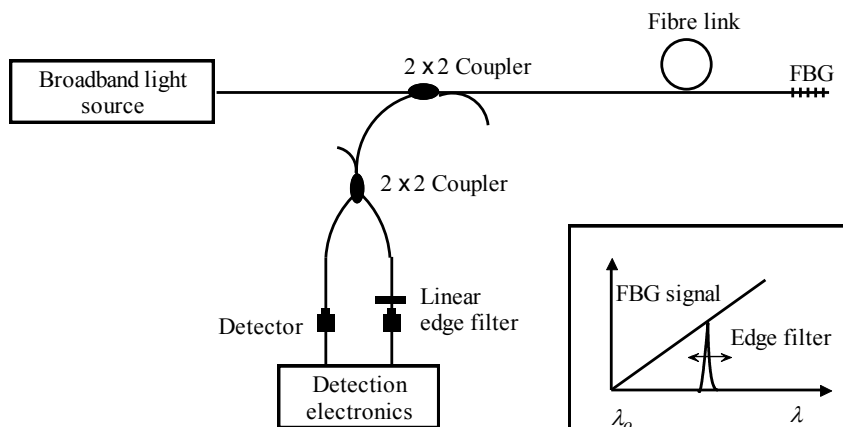
Figure 5.1: Example of bulk edge filter wavelength interrogation system

An improved all-fibre approach, exploiting a WDM fused-tapered fibre coupler, has been demonstrated to overcome the limitation and complexity of alignment of bulky optics components [3]. By taking the ratio between the difference and the sum of the two outputs, P_1 and P_2, from the two arms of the WDM coupler, as shown in Figure 5.2, the drift-compensated output can be obtained and used for the FBG wavelength-shift detection. This scheme offers the features of all-fibre approach, i.e. being very compact, very low power loss and low cost, making it an ideal interrogation approach for relatively low-accuracy measurements (typically ~1% of full measurement scale).
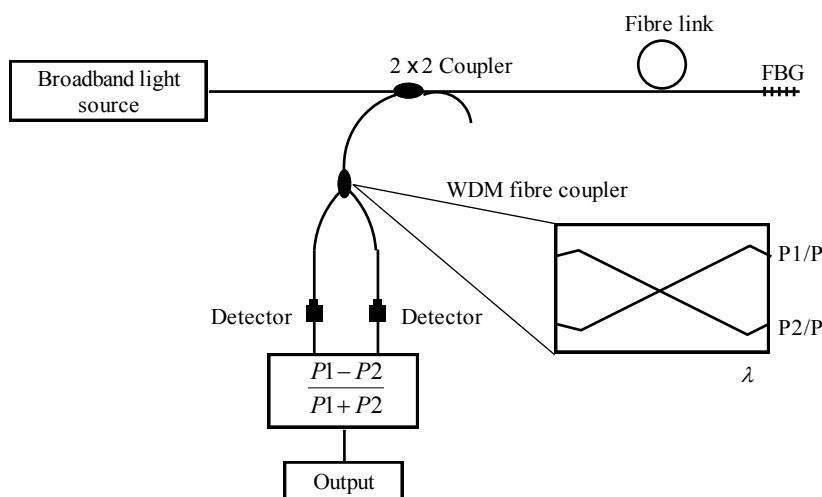
Figure 5.2: All fibre wavelength interrogation system based on a fibre fused-tapered WDM coupler

5.1.2   Tunable filter wavelength interrogation scheme

One of the most successful and attractive wavelength interrogation approaches is to use a scanning optical filter to retrieve the wavelength changes of the FBG(s). The principle of the approach is illustrated in Figure 5.3, a narrowband tunable filter is scanning through over the whole range of the wavelength spectrum of the grating (or gratings), which is luminated by a broadband light source, and the spectrum is given by the scanned signal intensity against the control signal of the tunable filter.
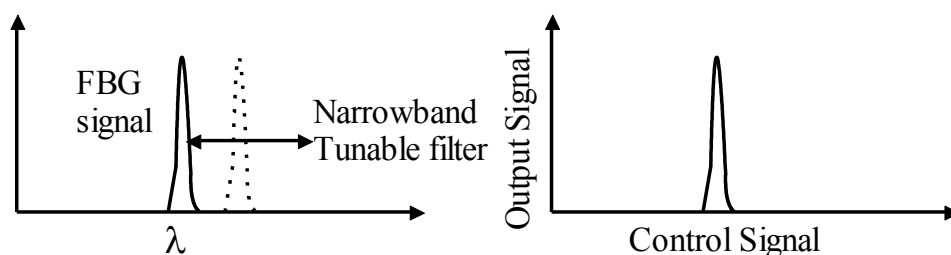
Figure 5.3: Optical scanning filter wavelength interrogation scheme

The optical filters include the fibre Fabry-Perot tunable filter [4], acoustic-optic filter [5] and tunable fibre Bragg grating based filter [6], etc. Sensor systems based on these filters have been demonstrated and deployed. Some specific examples of the above filters are briefly presented in the following sections.

5.1.2.1   Fibre Fabry-Perot tunable filter

The Fabry-Perot filter is an optical resonator discovered by Charles Fabry and Albert Perot in 1987[7]. This device has been used successfully in sensor and measurement applications. This type of filters transmit a narrow band of wavelengths and rejects wavelengths outside of that band. The interesting feature of these filters used for FBG sensor applications is their ability to "select" the peak wavelength of the grating when the filter is tuned, mainly by accurately displacing separation of the interference mirrors using a piezoelectric (PZT) element. The narrow and stable filtering band of FP filters makes them ideal for FBG wavelength interrogation and many FBG sensor systems utilizing the FP filters have been developed and deployed in various applications [4, 8-10]. F-P filters are characterised by Free Spectral Range (FSR), minimum resolvable

bandwidth and filter finesse. These figures of merit of a FP filter are the major parameters considered when selecting an appropriate filter for specific sensor applications. The scanning rate of a tunable FP filter should also be taken into account when dynamic measurement is required.

Figure 5.4 schematically illustrates how a tunable FP filter is employed to interrogate the wavelength shift of a single FBG, which can be set either in a tracking (close-loop) or scanning mode. In the scanning mode, which the F-P filter is scanned through the interested spectral range, and can be used to address more than one grating, while in close-loop mode, which is locked to the FBG wavelength by the feedback control system, it can only address one FBG wavelength. A resolution of ~ 1pm over an operation range of around 100 nm of such a system can be readily achieved.
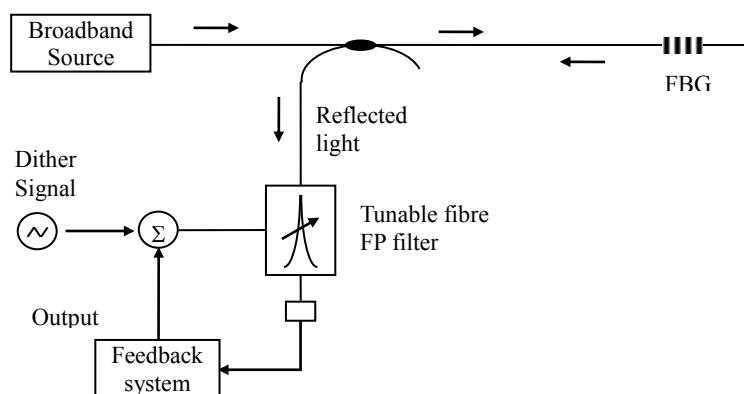
Figure 5.4: FBG wavelength shift demodulation system using tunable FP filter

A number of the sensors can be easily multiplexed by using optical switches, which is a notable advantage of tunable filter based wavelength interrogation system. Figure 5.5 demonstrates a FBG wavelength demodulation system based on a tunable filter, which allows for addressing several serial arrays with over 60 sensors [10]. The number of sensors can be further increased by increasing the number of switches or having a multi-input/output port tunable filter.
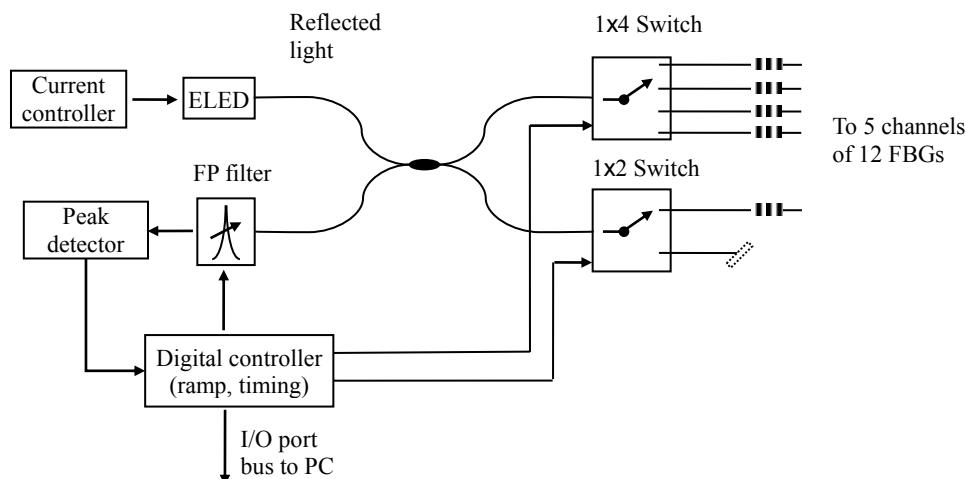
Figure 5.5: Schematic diagram of multiplexed FBG sensor electro-optic system with 60 sensors

5.1.2.2 Acousto-optic tunable filter

The acousto-optic tunable filter (AOTF) is all solid-state, compact, electronically tunable with no moving components, narrow band light filter. The main component of an AOTF is the birefringent acousto-optic crystal, where the interaction between the acoustic wave and optical radiation occurs. When a light wave travels in the anisotropic crystal, it is diffracted by the acoustic wave through the acousto-optic effect [11-12]. Changes in the acoustic frequency alter the diffraction properties of the crystal, enabling very rapid wavelength tuning in the order of microseconds, limited only by the acoustic transit time across the crystal. The AOTF has a very large wavelength tuning range being up to several micrometres. Thus this type of opto-electronic devices provides an attractive solution to wavelength multiplexing of a large number of FBG arrays [5,13-16].

Small changes in wavelength of the AOTF are linear to the changes of the applied RF frequency, which is a very convenient parameter to be measured allowing for accurate measurement and long term stability. There are two principal modes of operation contributing to the wavelength demodulation of the FBGs using the AOTF: scanning mode and lock-in mode. In scanning mode, as shown in Figure 5.6 (a) [17], the AOTF is tuned via a voltage controlled oscillator (VCO) over the whole wavelength range of interest. This mode is very useful for multi-FBG measurement. In lock-in mode, the system tracks the instantaneous wavelength change of a particular grating using a

feedback loop, as illustrated in Figure 5.6 (b) [18].
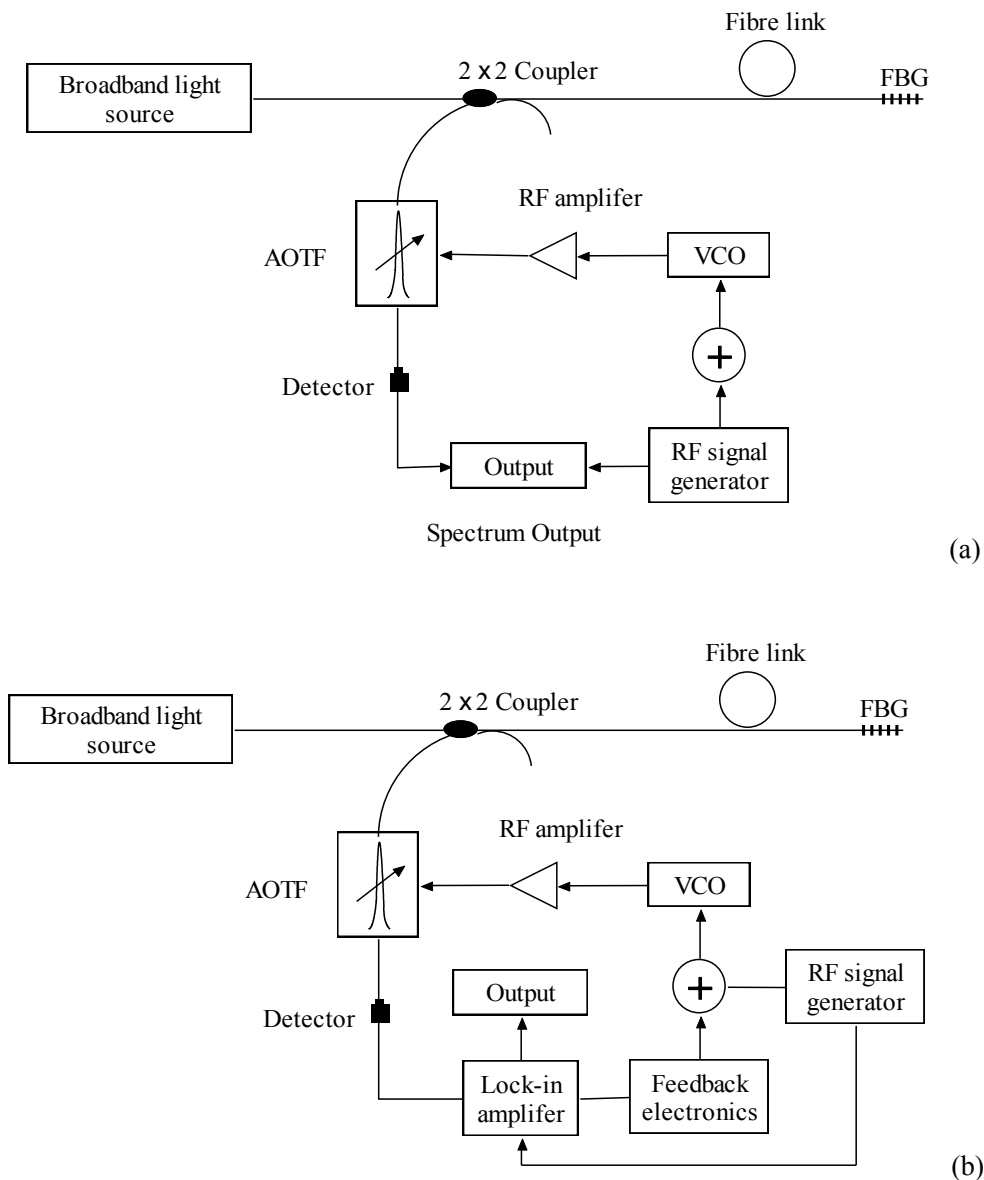
Figure 5.6: Schematic of AOTF Bragg grating demodulation scheme (a) Scanning mode (b) Lock-in mode

One of the most notable advantages of the AOTF over the other types of optical filters is the possibility of driving the device at multiple RF signals to allow for true parallel processing of multiple wavelength signals using a single device and detector. A practical system for simultaneous monitoring of two or more FBGs using a single AOTF has been successfully demonstrated [19].

5.1.2.3 Other tunable filters

Tunable fibre Bragg gating based filters have also been employed to track the wavelength shift from FBG sensors [20-23]. With such a system, the measurement range and resolution are mainly determined by the PZT element used in the system. The system demonstrated by Brady et al. had measured strain and temperature with resolutions of 2.8 $\mu\varepsilon$ and 0.2 ^oC, respectively. [20]

Coroy and Measures [24-25] have reported another type of wavelength measurement systems, using a semiconductor quantum well electro-absorption filtering detector (QWEFD). The system had a resolution of ±8 $\mu\varepsilon$ in strain and of ±9.7 pm in wavelength.

5.1.3 Tunable laser wavelength interrogation schemes

Calibrated, narrow-linewidth, single frequency, continuously wavelength-tunable fibre lasers have been used to interrogate the wavelength shift of fibre grating sensors. Different configurations of such fibre lasers have been employed for sensing applications. Ball G. A. et al. [26] demonstrated an Er doped fibre laser source for grating array interrogation. With an output power of 100mW in a 20 kHz linewidth, the system achieved a temperature resolution of 0.18 ^oC over a temperature range from room temperature to 180 ^oC. FBG sensor demodulation has also been implemented using a broadband and short pulse generated mode-locked fibre laser [27-29]. The system illustrated in Figure 5.7, has achieved a strain sensitivity of ±20 $\mu\varepsilon$ over a strain range over 3500 $\mu\varepsilon$, which is primarily limited by the total fibre dispersion.

In addition to the above mentioned tunable fibre laser source used for FBG wavelength interrogation, other lasers have also been reported for FBG sensing applications. Yun et al. have demonstrated a 0.1 nm linewidth, wavelength swept erbium doped fibre laser, scanned over a 28 nm range and used to demodulate a FBG array with a strain resolution of 0.47 $\mu\varepsilon$ at 250 Hz [30]. A supercontinuum light source with 140 nm bandwidth pumped by a mode locked semiconductor laser source has also been demonstrated for potential application in FBG sensors [31].

In general, FBG sensor systems interrogated using fibre lasers offer some advantages over the other interrogation schemes, such as high resolution, high signal noise ratio (SNR), and showing promise for long distance monitoring.
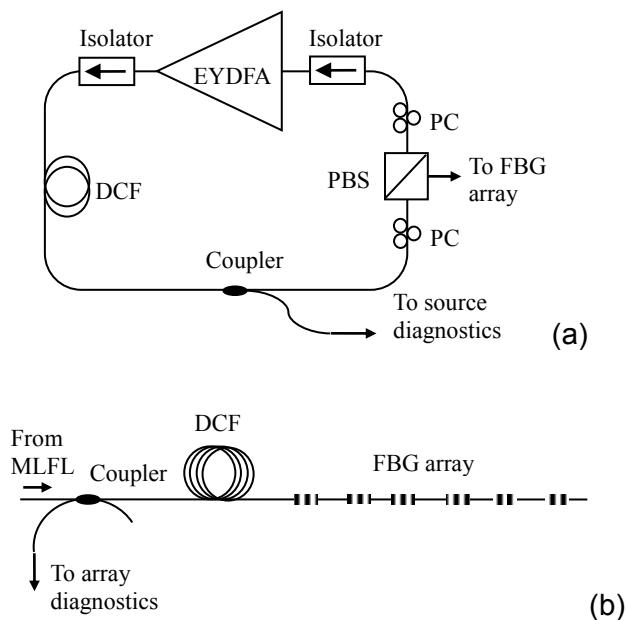
Figure 5.7: (a) Passively mode-locked fibre laser source, using Er/Yb co-doped fibre amplifier and dispersion compensating fibre. (b) Fibre Bragg grating array interrogation system.

5.1.4   CCD spectrometer wavelength interrogation scheme

A fibre Bragg grating wavelength Interrogation scheme using a charge coupled device (CCD) has also been implemented by some researchers for sensor applications [32-34]. This method, as shown in Figure 5.8, can overcome the drawback of scanning filters requiring sufficient overall optical power, but uses a parallel detection allowing all reflected light to be detected by a CCD array. Since it collects all the light reflected by the fibre gratings over the whole scanned range, $E_D = E_R$, and a grating even with 1% reflectivity can provide as much signal required through this parallel detection, as a 95% grating does via a scanned detection approach. The wavelength resolution of this approach is determined by the linear dispersion of the grating at the detector plane per pixel width, defined as nanometres per pixel (nm/pixel). The resolution can be further improved by the so-called centroid detection algorithm[35], as the spectrum from each

grating is spread across many adjacent pixels, and a weighted average of the centre wavelengths of the illuminated pixels scaled according to the incident signal level gives a computed central grating wavelength. This and some other software algorithms can dramatically improve the wavelength resolution and make it a very attractive approach for many applications.
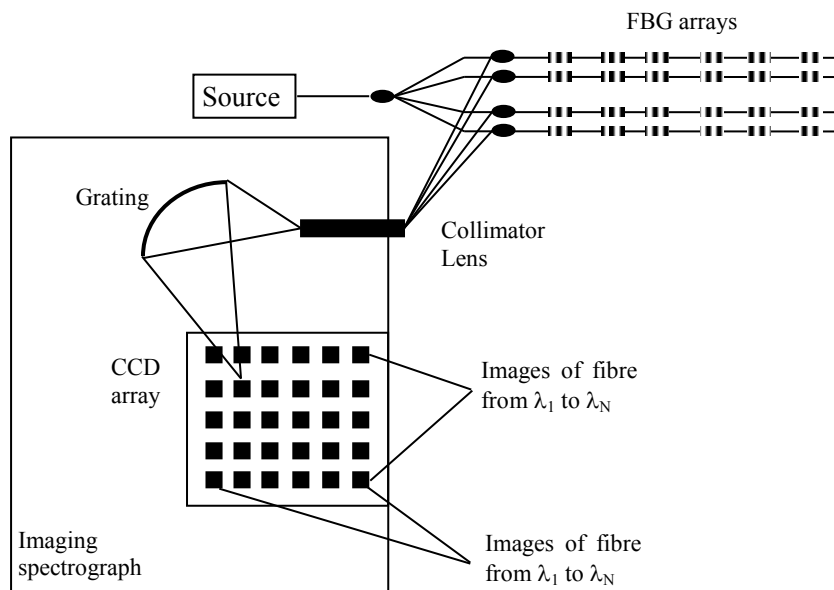
Figure 5.8: Schematic setup of fibre Bragg grating interrogation system employing a CCD-based spectrometer [32]

5.1.5   Other wavelength interrogation schemes

Other fibre Bragg grating wavelength interrogation schemes, such as Interferometric wavelength-shift detection [36-39] and Fourier transform spectroscopy [40-42], have also been reported and demonstrated for different applications.

5.2   FBG-based temperature sensor using fibre Fabry-Perot tunable filter

With an overall consideration in terms of system performance, cost and flexibility in multiplexing multiple FBG-based sensors is taken into account, a system using a tunable fibre Fabry-Perot (FP) filter for FBG wavelength interrogation, may be considered to be the most promising.   This approach has shown to be able to satisfy most of the application requirements and in this work such a system was specifically built, tested, evaluated and discussed.

5.2.1 System setup

Figure 5.9 illustrates the operational principle of a FBG-based sensor system based on Fabry-Perot tunable filter. The system mainly consists of four parts: (1) a broadband light source, which can normally be a SLED or ASE source; (2) a FBG probe for temperature and/or strain measurement, which contains one or more gratings; (3) a wavelength interrogation system using a tunable F-P filter; (4) Interface software for controlling, signal processing and data management.
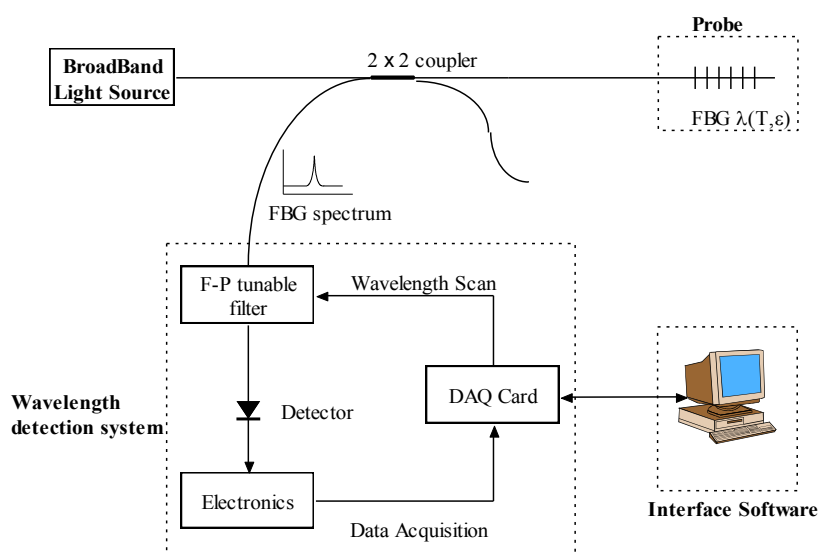
Figure 5.9: Schematic system setup of a F-P filter based FBG sensor system

In the system, light from the broadband source, a SLED (DL5037 from Denselight ltd, Singapore) with a central wavelength of 1550 nm and a bandwidth of 60 nm (HWFM) and 3 mW output power in this case, is launched to the FBG probe through a 2 x 2 coupler, the reflected narrowband light at the Bragg wavelength, λ_B, from the probe is then launched into the tunable F-P filter (FFP-TF2 1580-003G4000-40 from Micronoptics, USA), which scans through the wavelength range of interest under the control signal, V_{F-P}, from a DAQ card D/A output. The filtered optical signal through the F-P filter is detected by an InGaSn PIN photo-detector and then is digitalized through data acquisition with the DAQ card. The spectral profile, $\Lambda(\lambda)$, of the FBG probe can thus be obtained from the digitized optical signal, I_{FBG}, against the control scanning signal, V_{F-P}, following the equation below:

$$\Lambda(\lambda) = \Lambda(I_{FBG}, V_{F-P}) \qquad\qquad (5.2)$$

The Bragg wavelength, λ_b, can be derived from the peak position, V_{F-P}^{peak} of the spectrum, $\Lambda(\lambda)$, as:

$$\lambda_b = f\left(V_{F-P}^{peak}\right) = f\left(V_{F-P}\Bigg|_{\frac{\partial I_{FBG}}{\partial V_{F-P}}=0}\right) \qquad\qquad (5.3)$$

and the above function $f\left(V_{F-P}\right)$ can be pre-calibrated based on the data sheet of the F-P filter provided.

In practice, the calibration of the wavelength against the corresponding scanning signal is critical for the determination of the sensor system performance by using the F-P filter approach. Generally, the wavelength spectrum can be calculated by the following equation as a function of the control scanning signal, V_{F-P}:

$$\lambda = f(V_{F-P}) \qquad\qquad (5.5)$$

Normally, only a relative wavelength can be derived from equation 5.5. In order to obtain the absolute wavelength of the FBG of the probe under a perturbation, a known certain wavelength, λ_{ref}, should be introduced as a wavelength reference. Thus the wavelength can be obtained, based on the presumption that the performance of F-P is linear over the wavelength range of interest, as shown in equation 5.3.

$$\lambda = f(V_{F-P}) = \lambda_{ref} + A(V_{F-P} - V_{F-P}^{ref}) \qquad\qquad (5.6)$$

where V_{F-P}^{ref} is the corresponding scanning voltage of the F-P filter at a wavelength of λ_{ref}, and A is the scale of free spectrum range (FSR) and V_{F-P} is the scanning voltage over one FSR. If the non-linearity of F-P is taken into account, a more sophisticated calibration process should be included.

Obviously, FBGs, one or two, or even more FBGs, at certain wavelengths can serve as wavelength references for the F-P filter. This method offers a simple solution. To

achieve better performance with higher accuracy for wavelength measurement, some other wavelength reference methods, such as using a traceable gas cell absorption wavelength reference, might be used. The details of the FBG sensor systems based on these wavelength reference methods will be discussed in the following sections.

5.2.1.1 F-P filter interrogation system with two FBGs as wavelength references

As mentioned above, FBGs with certain known wavelengths offer a convenient solution to wavelength references for the F-P filter. If one FBG is used as a reference, the measured wavelength can be obtained from equation 5.6. In a preliminary test of a sensor system using one FBG as a reference, it was found that A in equation 5.6 would change slightly with the operational time, especially in the early hours after the system had started running. This resulted in a significant shift of the measured FBG wavelength although the FBG was actually kept at a constant wavelength. The drift of A is mainly caused by the intrinsic nature of the PZT used in the F-P filter to tune the distance of the two fibre reflectors to achieve the interference.

In order to overcome this limitation, a sensor system with two FBGs as references was then built. As illustrated in Figure 5.10, the light from a SLED is launched to a FBG probe and two reference FBGs, which are connected respectively to the two ends of a 2x2 coupler. The reflected light which contains spectra from both of the probe and the references is then passed through the coupler to the wavelength interrogation unit. A typical spectrum is shown in Figure 5.11 where the wavelengths of the reference FBGs with one being around 1528 nm and the other around 1570 nm, are located at the two ends of the wavelength range of interest to be measured.
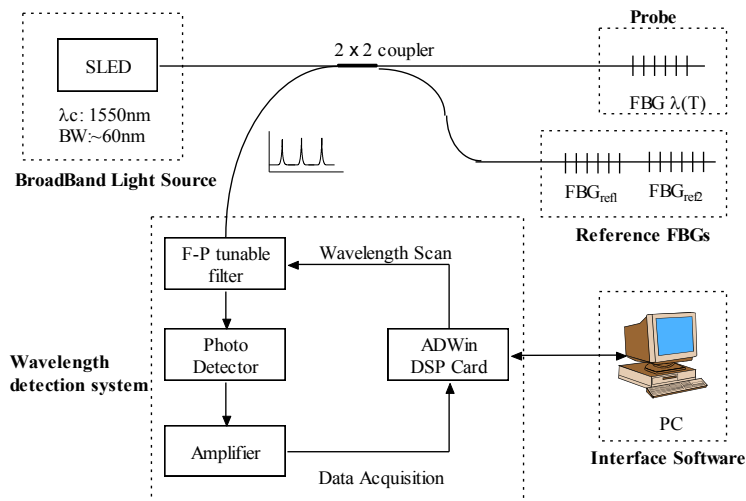
Figure 5.10: F-P filter interrogation system with two FBGs as wavelength reference
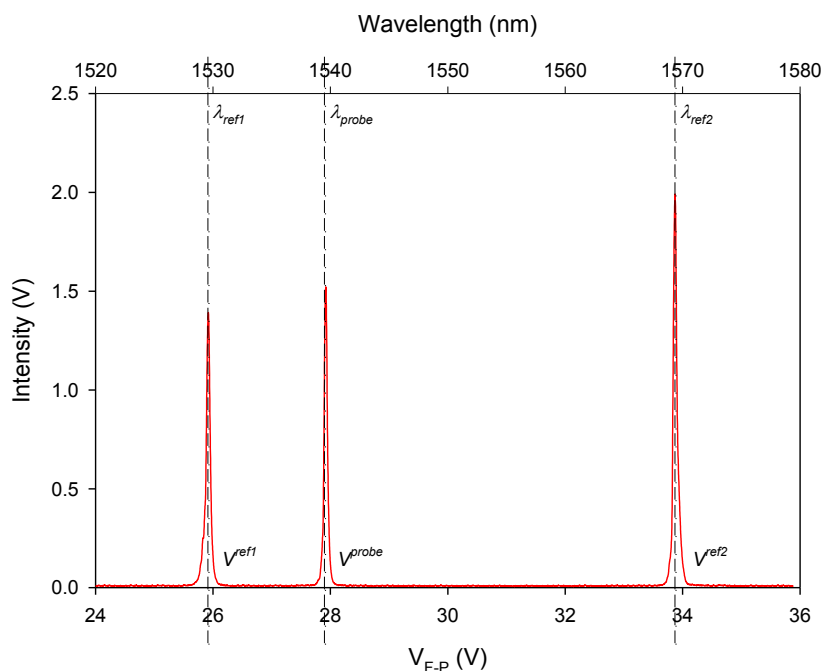
Figure 5.11: Spectrum obtained from both the FBG probe and two FBG references

As illustrated in Figure 5.11, the Bragg wavelength of the probe and the other reference wavelengths shown in the spectrum, can be derived from the following equation,

$$\lambda_{probe} = \lambda_{ref1} + \left(\frac{\lambda_{ref2} - \lambda_{ref1}}{V_{F-P}^{ref2} - V_{F-P}^{ref1}}\right) \cdot \left(V_{F-P}^{probe} - V_{F-P}^{ref1}\right) \qquad (5.7)$$

where λ_{probe}, λ_{ref1}, λ_{ref2} are the wavelengths of the probe, references 1 and 2.

V_{F-P}^{probe}, V_{F-P}^{ref1}, V_{F-P}^{ref2} represent their corresponding scanning voltages of the F-P filter.

Compare to equation 5.6, the scale A in equation 5.6 is replaced by the term

$\dfrac{\lambda_{ref2} - \lambda_{ref1}}{V_{F-P}^{ref2} - V_{F-P}^{ref1}}$ in equation 5.7, which can be dynamically calculated during operation, in

order to eliminate the drift problem arising from the scale A. Figure 5.12 shows the

measured wavelength drift of two FBGs reference system within 15 hours after the

system being switched on, for comparison with that from the one FBG reference system.

During the test, the probe was kept at a constant temperature of 25°C with no strain

variation and the wavelength of the grating was expected to be stabilized at a certain

value. However, the measured wavelengths show a drift of around 80pm for the 2

reference FBGs system and 180 pm for the 1 reference FBG system, which represents

equivalent temperature changes of ~8 °C and ~18 °C respectively.
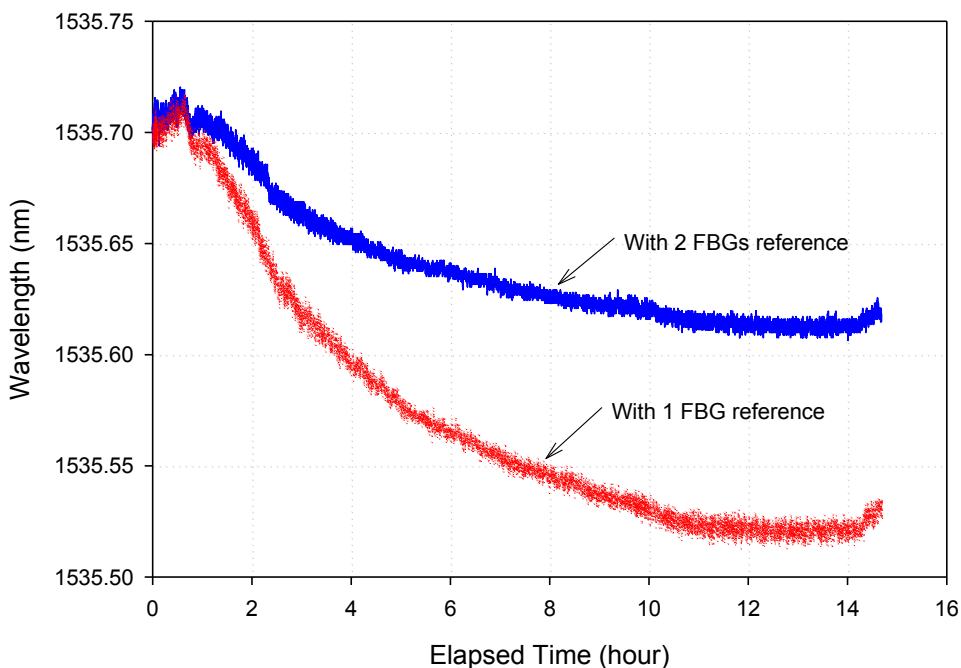
Figure 5.12: Measured wavelength drift within 15 hours of the F-P based sensor system with
FBGs as references

The above observed wavelength measurement drifts were mainly caused by two

effects. Firstly, the reference FBGs may have experienced a certain level of temperature

change during the measurement period. It has been observed that the temperature of

the system enclosure, where the reference grating was located, increased a few

degrees during the experiment. Secondly, the slight nonlinearity of the F-P filter

esulted in the wavelength calibration errors. This is especially evident for the one

reference FBG interrogation system, as shown in Figure 5.12.

With an implementation of temperature compensation through the measurement of the local temperature where the reference FBGs were located, the operating temperature effect on the system can be eliminated to a certain level. In such a system, the wavelengths of the reference FBGs in the calibration equation 5.7 are replaced by temperature dependent wavelengths, and the calibration equation can be rewritten as follows:

$$\lambda_{probe} = \lambda_{ref1}(T) + \left(\frac{\lambda_{ref2}(T) - \lambda_{ref1}(T)}{V_{F-P}^{ref2} - V_{F-P}^{ref1}} \right) \cdot \left(V_{F-P}^{probe} - V_{F-P}^{ref1} \right) \qquad (5.8)$$

where $\lambda_{ref1}(T)$, $\lambda_{ref2}(T)$ are the temperature dependent wavelengths, given by

$$\lambda_{ref_i}(T) = \lambda_{ref_i}(T_o) + A_i(T - T_o) \qquad (i = 1,2) \qquad (5.9)$$

where $\lambda_{ref_i}(T_o)$ is the wavelength at an initial temperature, T_o, and A_i is the temperature sensitivity coefficient of the reference FBGs.

A similar test for the measurement stability with temperature compensation was carried out when the probe was kept at a constant temperature of 25°C. As the results shown in Figure 5.13, the measured temperature drift was reduced to less than 1°C in two hours with the temperature compensation, thus the reference wavelengths were adjusted according to the temperature, compared to 3~4°C of that of the system without using the temperature compensation.

Another method can be utilized for eliminating the measured temperature drift is to stabilize the local temperature at the position of reference FBGs using some temperature controlling element, such as TEC (Thermo-Electric Cooler). In this case, the measurement stability is related to the stability of the control system.

Both of these approaches can be implemented to enhance the stability of the FBG sensor system by eliminating the negative temperature effect on the wavelengths of the reference FBGs. However, these methods have their limitations, in terms of resolution and accuracy etc.
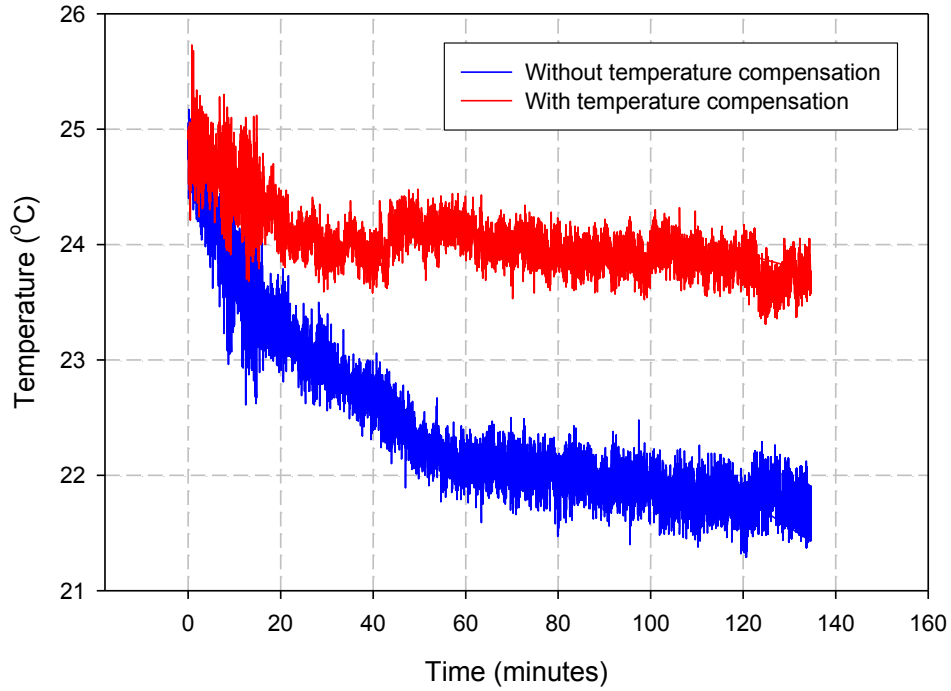
Figure 5.13: Temperature measurement drifts during operation of the FBG sensor system with two reference FBGs, with and without temperature compensation

For the temperature compensation method, the inclusion of extra temperature sensor(s), enables the resolution, accuracy and stability of that sensor to be carried forward to affect the overall performance of the FBG senor system and this would normally degrade the performance. The final temperature measurement accuracy of the sensor will be given by:

$$T_{Accuracy}^{System} = T_{Accuracy}^{\lambda_{FBG}} + T_{Accuracy}^{compensation} \tag{5.10}$$

where $T_{Accuracy}^{\lambda_{FBG}}$ is the temperature measurement accuracy according to the grating wavelength, and $T_{Accuracy}^{compensation}$ is the accuracy of the temperature sensor used for the temperature compensation.

To fully optimize the performance of the FBG-based sensor system, some types of operational temperature independent wavelength references (or wavelength calibration) must be included. Therefore, in this work a FBG interrogation system with traceable gas cell absorption as wavelength reference was built and evaluated, and will be discussed in detail in the following section.

5.2.1.2 F-P filter FBG interrogation system with traceable gas cell absorption reference

Traceable gas cells are able to use molecular absorption to provide standard NIST (National Institute of Standards & Technology, US) traceable wavelength references with unmatched stability over time irrespective of environmental disturbance. They are commonly used as a standard for calibrating output signals of optical spectrum analyzers. They have many other applications as well, for example as a wavelength calibrator in many optical instruments, as a local reference for chemical sensing system, for wavelength locking of lasers, spectroscopic research, and environmental and physical sensing.

An F-P filter-based FBG wavelength interrogation system using a traceable gas cell as a reference and a calibration standard for the wavelength correction is shown in Figure 5.14. The broadband light scanned after the F-P filter is split into two using a 3 dB coupler. One branch of the coupler is connected to a gas cell, allowing the output spectrum of the light to be measured based on the absorption lines of the gas cell. The results obtained from the gas cell measurement are used for wavelength calibration of the system. The other branch of the coupler is connected to FBG probes via a 2x2 fibre coupler. The reflected spectra of the probes can thus be obtained from the calibration data obtained from the gas cell.

● **The traceable gas cell**

The gas cell used in the system is hydrogen cyanide gas, HCN-13-C-100-FCPC, supplied by Wavelength References, ltd, USA. It provides an equivalent standard of the NIST SRM 2519, a standard wavelength calibration reference for 1530nm-1560nm. The absorption spectrum of the gas cell is shown in Figure 5.14 and its main specifications are listed in Table 5.2[43]. The gas cell provides very good wavelength
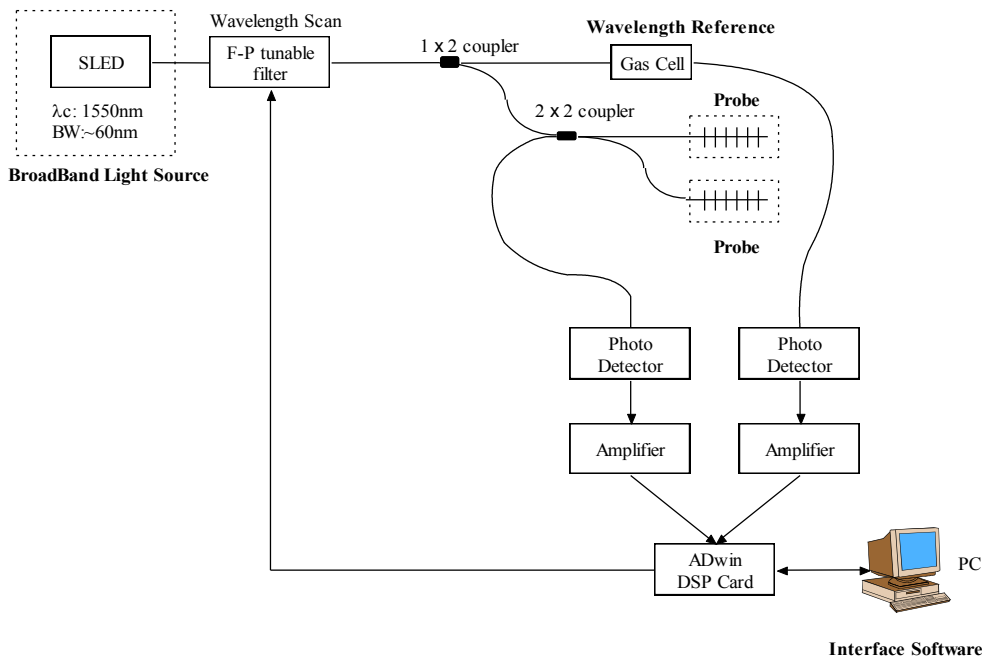
Figure 5.14: F-P filter based interrogation system with traceable gas cell reference

accuracy and temperature stability which is well suited for wavelength calibration in the FBG sensor system. The wavelength shift is around 0.2pm when the operational temperature changes 20°C.   If there is no temperature compensation, this small wavelength shift caused by the temperature variation can contribute to the system error of the FBG interrogation system, although in most applications, this drift is considered to be negligible.

Table 5-2: Specifications of the HCN gas cell

Wavelength Range	nm	1525nm to 1565nm
Wavelength Accuracy	pm	± 0.3 (1 sigma, 100 Torr)
Temperature dependence	pm	<0.01/$^\circ$ C
Linewidth (-3dB)	nm	0.070 typical (100Torr)

● **Wavelength calibration**

As shown in Figure 5.15, the gas cell has a series of 51 absorption lines at discrete wavelengths, λ_{Abs}^i (*i*= 1…51). The wavelength calibration of the system can thus be obtained through the correlation between the measured absorption spectrum of the gas cell and the F-P scanning voltage, which is related to the order of the data points taken

through the DSP card sampling. The F-P control voltages, V_{F-P}^i (i= 1...51), corresponding to the absorption lines, can be derived from the absorption spectrum of the gas cell, $i(V_{F-P})$, using some peak (dip) searching algorithms.   Then the wavelength calibration equation can be obtained by data regression from the data set obtained ($\lambda_{Abs}^i, V_{F-P}^i$) (($i$= 1...51). In practice, a 2nd order polynomial regression is used, and the wavelength calibration equation is given by:

$$\lambda = A_0 + A_1 \cdot V_{F-P} + A_2 \cdot (V_{F-P})^2 \qquad (5.11)$$

where A_0, A_1, A_2 are the calibrated parameters, and V_{F-P} is the control voltage of the F-P filter in relation to the sampling data points.
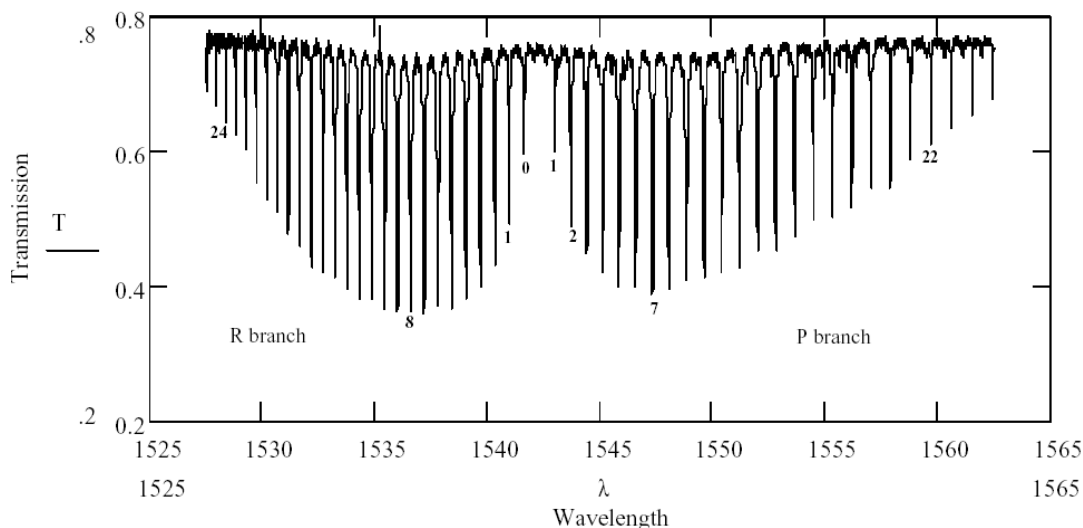
Figure 5.15: Absorption spectrum of HCN gas cell

In a practical system, the actual absorption spectrum obtained from the system, shown in Figure 5.16, which is a absorption spectrum superimposed with the SLED light source spectrum, may not be shown clearly to indicate the absorption lines as shown in Figure 5.15.   This is contributed by the use of a narrowband F-P filter, electronic noise of the photo-detection system etc.   As a result of this, some optimization techniques are required to improve the system performance.   The first step of such a technique is to normalize the spectrum according to the light intensity at different wavelengths, and

then reverse the signal to turn the absorption dips to numerical peaks for easy algorithmic calculations, and furthermore this procedure allows initial peaks to be selected (Figure 5.17a).   The second step is to eliminate any unwanted peaks appearing due to signal noises (Figure 5.17b).   Finally it is important to recover those peaks which were not detected as they were submerged in the noise (Figure 5.17c).
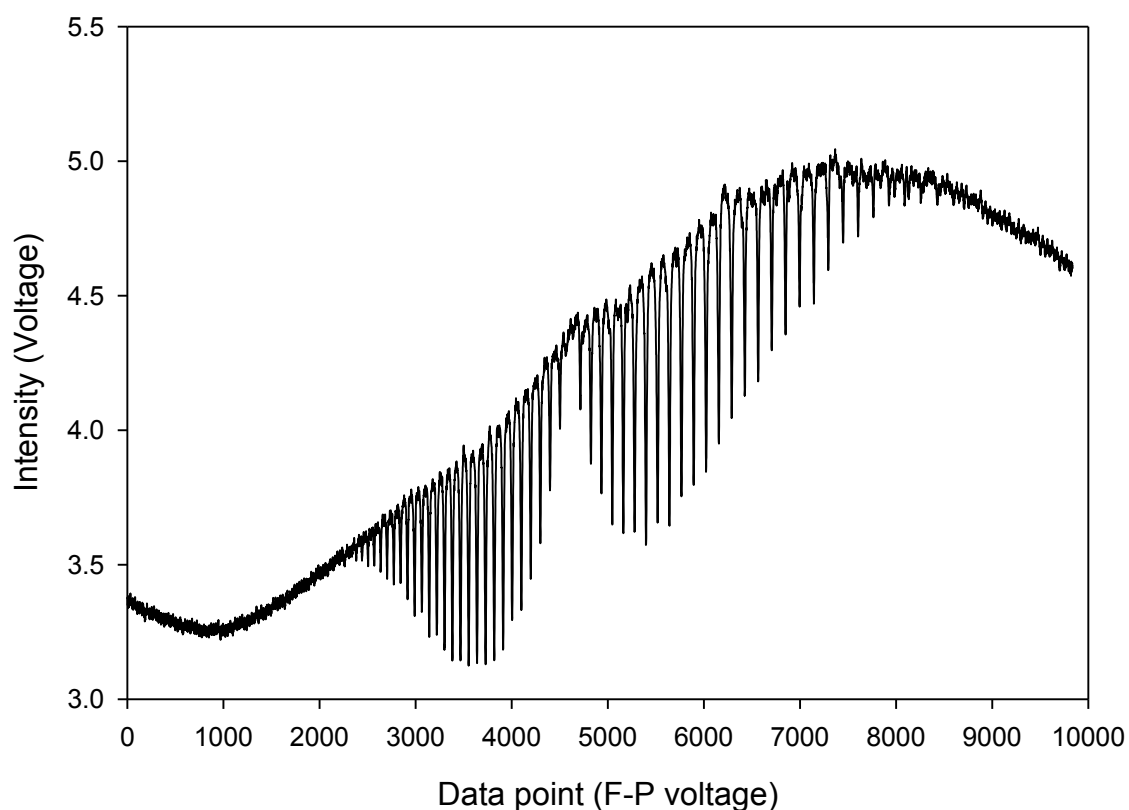
Figure 5.16: Actual gas cell absorption spectrum from the system
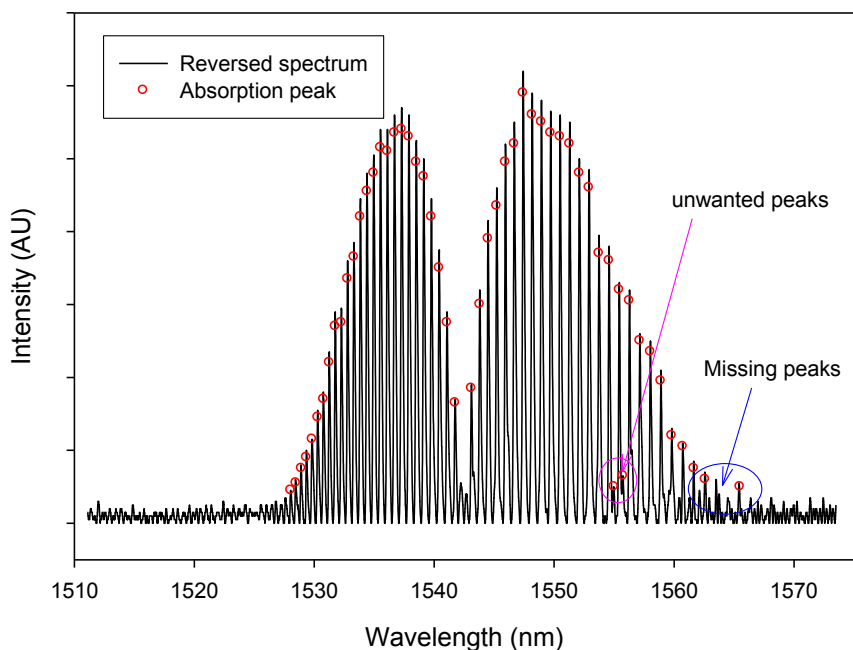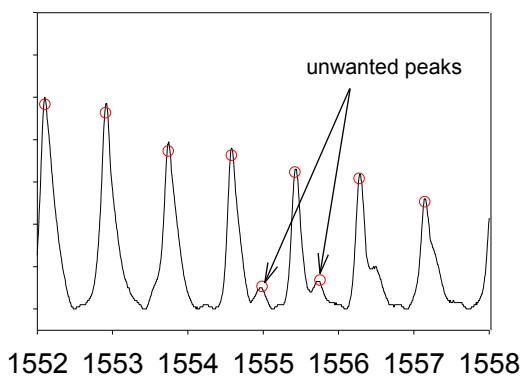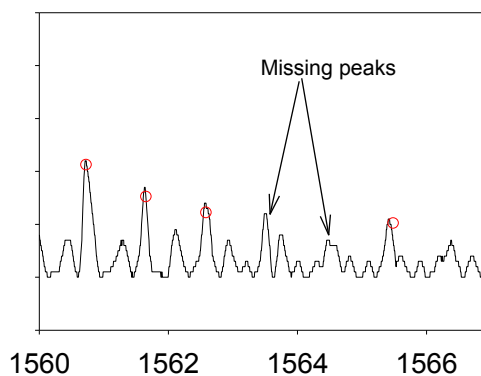
Figure 5.17: Optimization of the gas cell absorption for wavelength calibration through three steps: (a) reversed gas cell absorption spectrum to detect initial peaks; (b) remove unwanted peaked; (c) recover missing peaks

After the above optimization procedure, the wavelength calibration for the system can be undertaken based on the optimized data set ($\lambda_{Abs}^{i}, V_{F-P}^{i}$) (($i$= 1...51) using 2nd order polynomial fitting as mentioned above.   Figure 5.18 shows the results obtained from a typical calibration process, which enables the wavelengths of the FBG sensors to be calculated using the parameters obtained.
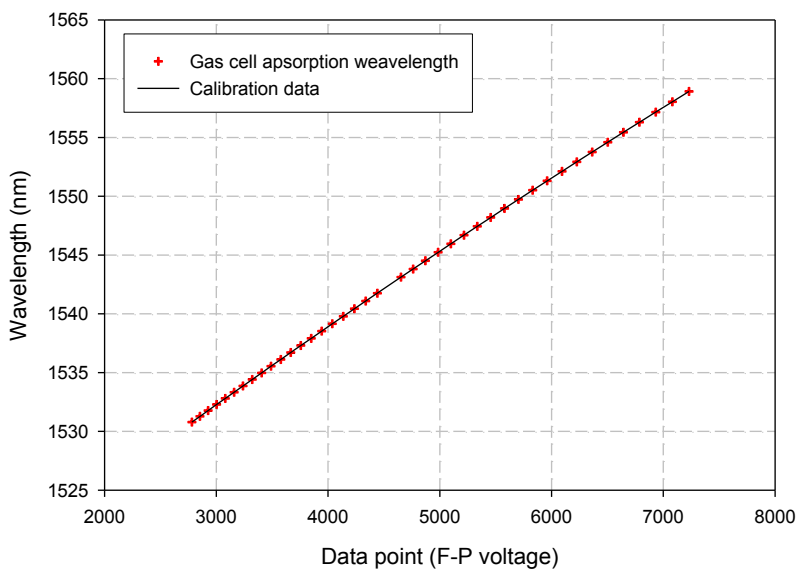
Figure 5.18: Wavelength calibration of the gas cell absorption reference

● **Measurement stability and accuracy**

It has been demonstrated that FBG wavelength interrogation system with a gas cell reference had a very good stability and wavelength accuracy. Figure 5.19 shows the temperature measurement in 2 hour using such a system, compared to that of the system using 2-FBG reference. It is clearly shown that the gas cell based system had
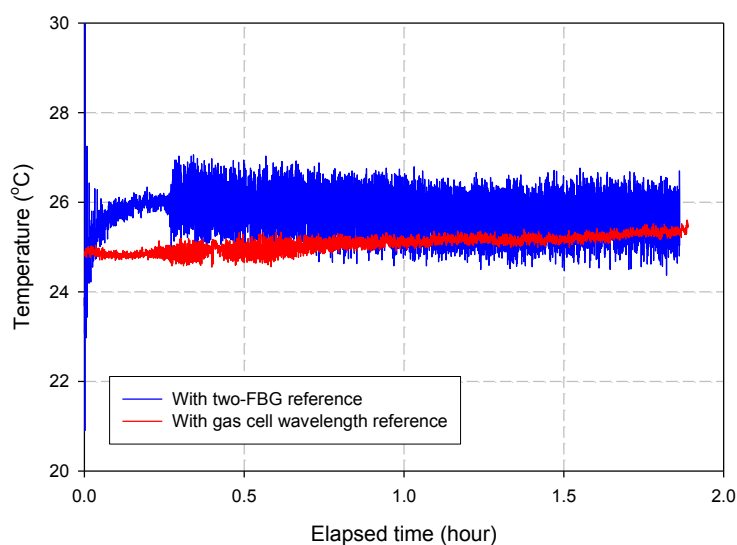
Figure 5.19: Cross-comparison of a FBG sensor system with gas cell reference and with two grating reference

much better stability and accuracy of about ±0.1°C, while the accuracy of a 2-FBG reference system was some ±1°C. Further evaluations of the system and results obtained are presented in section 5.2.4.

5.2.2   Optoelectronic hardware of the system

The hardware setup of the system is shown in Figure 5.20.   To make the prototype a step closer to the commercial market, the system was designed in a modular format. The system comprises four modules, and they are power supply module, light source module, photo-detection and F-P control module, and DSP card. These modules are interchangeable between different sensor units, thus making the system easier to be debugged and/or repaired.
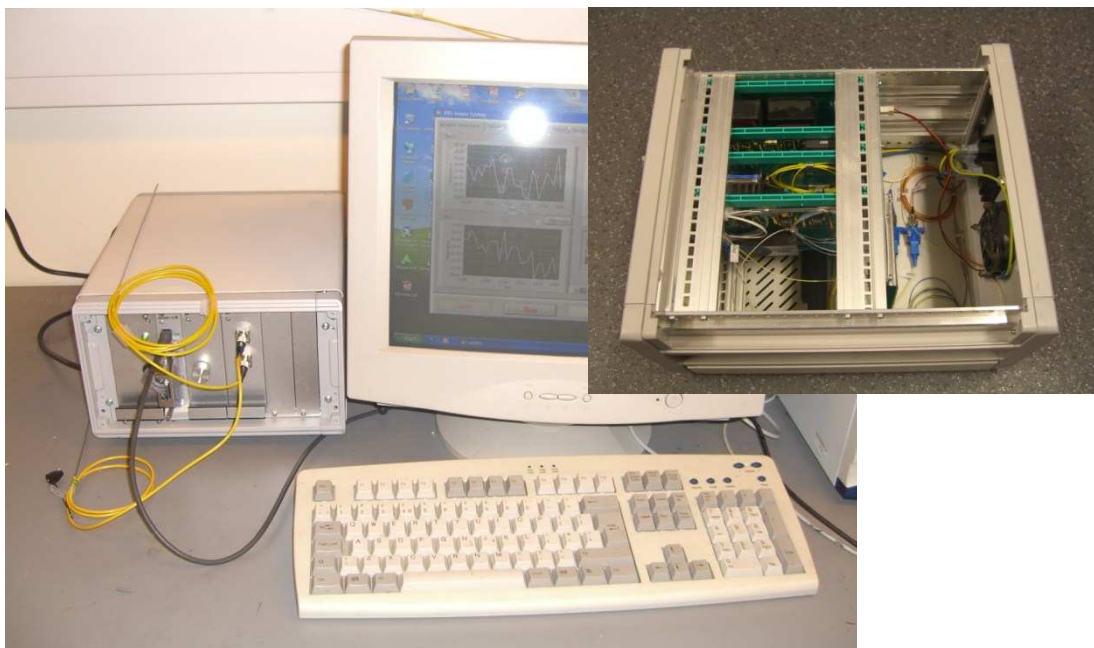
Figure 5.20: Photo of the FBG based sensor system
(inset: the modular-based sensor interrogation unit)

● Power supply module

Two AC-DC modules, together with two DC-DC converter TMS 15512 and TMS 15124 from Traco Power Ltd, are used to provide quad outputs, +5 V, +24 V, and ±12 V. The 5V output is used for the DSP card and the SLED light source module. 24 V output is used for a bias voltage to enable the control of the F-P filter. The ±12 V outputs are used for the photo detection system.

- Light source module

  A thermally-cooled SLED, CS3705, from Denselight, Singapore, driven by a LD current control module LD2332, from Wavelength Electronics, USA, is used to provide a 3 mW broadband light with a 60nm 3dB bandwidth and a central wavelength of 1555nm for the system. The operation temperature of the SLED is controlled by a TEC for intensity stabilization.

- Photo detection and F-P control module

  Two channels of a 3-stage PIN photo-detector and amplifier are used to convert the optical signals from FBGs and the gas cell when they are illuminated by a broadband light into electrical signals.   A signal conditioning circuit is also included in this module to buffer the scanning signal from DSP card to control the F-P filter.

- DSP card module

  An ADwin-light-16-ERUO DSP card was specifically chosen and used in the system, as it offers a cost-effective solution requiring only a limited number of inputs and outputs.   One analogue output is used for F-P filter scanning, and two analogue inputs are used for FBG wavelength and gas cell absorption signal sampling.   The card has 8 analogue inputs, offering capacity for the upgrade to create a multi-channel FBG sensor system.

5.2.3   Interface and control software

Interface software for the FBG based system has been programmed in LabView 7.1 platform. Figure 5.21 shows one screen printout of the main interface user panel.
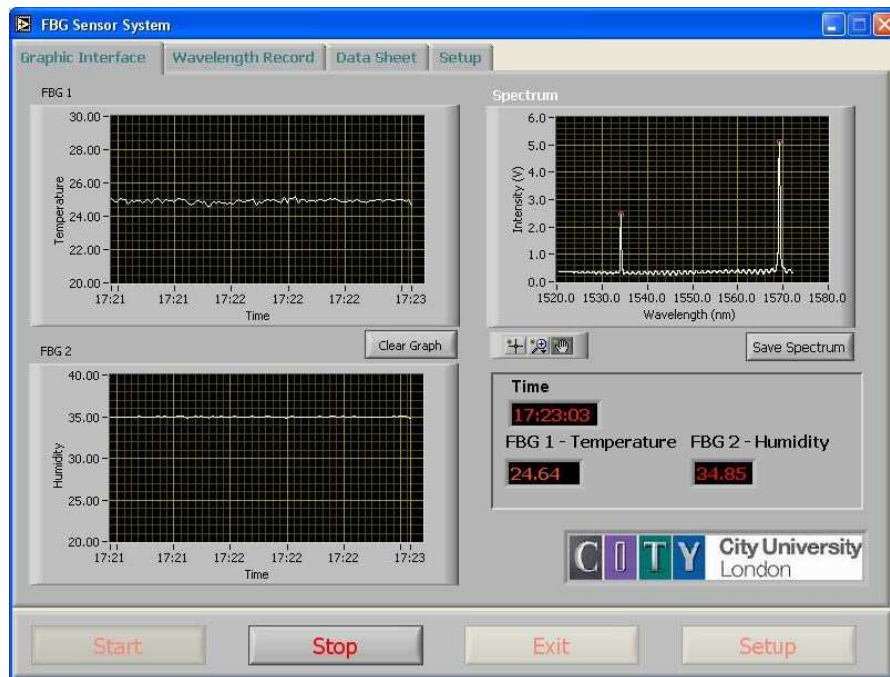
Figure 5.21: Screen printout of the interface designed for FBG sensors

The main functions incorporated in the interface design have included:

- F-P filter controlling

- Data acquisition via the DSP card

- Signal processing

- Wavelength calibration

- Temperature calibration

- Data management

5.3   Test and evaluation of the FBG-based sensor system

5.3.1   Temperature calibration and resolution

Based on the specifications of the components used in the system, such as the pass bandwidth of the F-P filter and the bandwidth of the FBG probe, the sensor system should, theoretically, have an overall wavelength resolution of 1 pm, and a temperature resolution of 0.1 ^{o}C.   In this work, the system performance and the actual resolution of the measurement was evaluated through a simple experiment set up for that purpose. In order to verify the temperature resolution of the system, a standard setup which can provide temperatures with a small step change (e.g. 0.1^{o}C) should be used. However,

there is some difficulty in realizing this requirement experimentally, thus in this work, the temperature step change was achieved by a slowly cooling water bath from 30°C to room temperature. The temperature change of the water with time is shown in Figure 5.22.
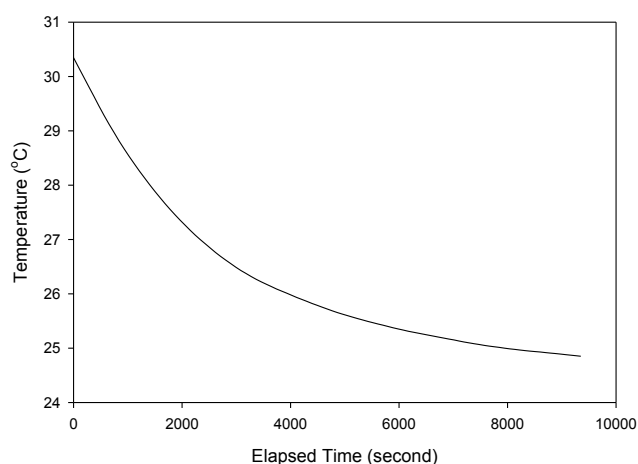
Figure 5.22: Temperature change with time when the water in a water bath is cooling down from 30°C to room temperature

As shown in Figure 5.22, it took around 1 hour for the water in the water bath to cool down from 26 ^{o}C to 25 ^{o}C at a rate of around 0.1^{o}C per 5 minutes.   Therefore the temperature data obtained from the temperature sensor during each period were used and analysed for evaluating the temperature resolution of the system.   In doing so the wavelength and temperature readings obtained within the first 30 seconds of every 5 minutes were extracted and averaged and plotted as in Figure 5.23.   It is reasonable to assume that the temperature variation is negligible within each 30 second period and the temperature difference is around 0.1 ^{o}C between each 5 minutes gap.   As illustrated in Figure 5.23, both wavelength and temperature recorded have shown clear differences of 1~1.2 pm and 0.08-0.1 ^{o}C respectively, between each 5 minutes span. The results clearly implied that the FBG-based sensor system had a wavelength resolution of around 1 pm and a temperature resolution better than 0.1 ^{o}C.
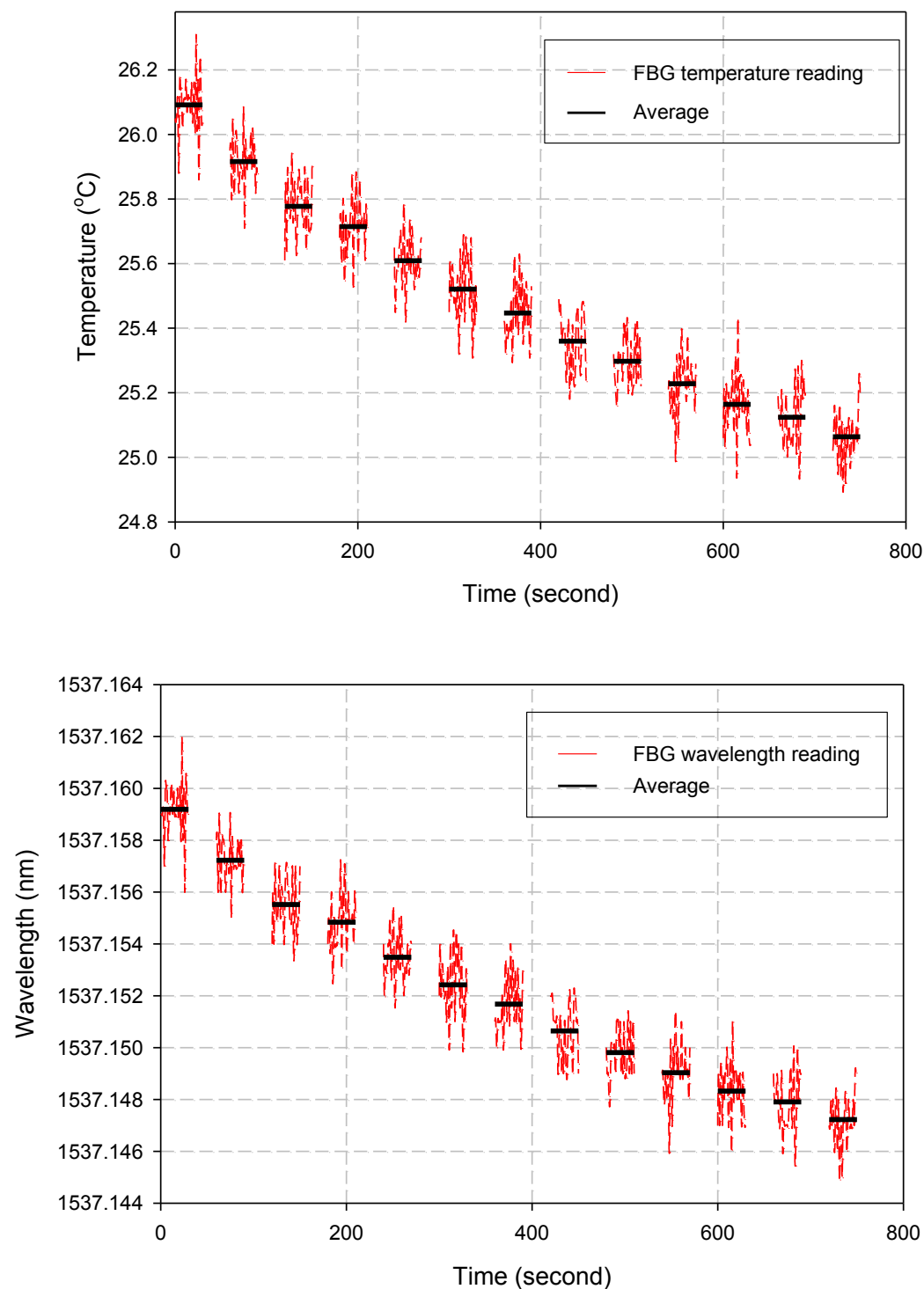
Figure 5.23: Temperature and wavelength resolution of the FBG sensor system

5.3.2 Response time

The response time of system is determined by both the response time of the FBG probe to temperature change and the scanning time of the wavelength interrogation

system. The wavelength scanning time is mainly dependent on the scanning rate of the F-P filter, which is up to 100Hz for the filter used. The actual scanning rate of the system used was set at 10 Hz.   The scanning rate could be increased but with a decreased accuracy.   Based on the experimental results obtained, the overall response time of the sensor system was largely determined by the response time of the FBG to temperature variation.

To investigate the response time of the FBG-based temperature sensor system, a series of evaluation tests was carried out simply by dipping the probe into hot water at temperatures of 90°C and 60°C respectively. The FBG probe was intimately attached to a K-type thermocouple for cross comparison. Both temperature probes were exposed to heated water baths at these temperatures for periods of 1 second, or 5 to 6 seconds. The results of the tests are illustrated in Figure 5.24, which shows that the FBG system can quickly respond to the temperature changes, both under the rising and falling conditions. The thermocouple has also shown a rapid response to the temperature
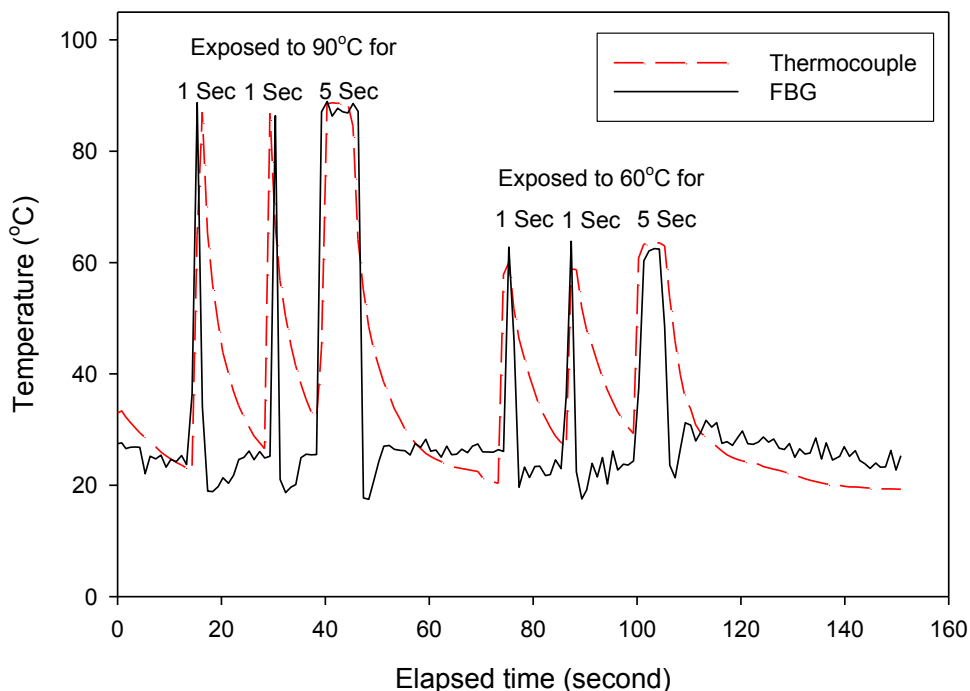
Figure 5.24: Temperature change while the FBG probe being dipped into and taking out form hot water tank.

rising but could not reach the actual value within 1 second. It also had a slower response to decreasing temperatures compared to that of the FBG probe. The results clearly show that the FBG system has a faster response than that of the thermocouple.

Another experiment for evaluating the response time of the system was carried out by testing the response of the FBG sensor to a temperature 'spike', rapid temperature change. These 'spikes' were simulated by submerging the probe to the $90^{o}C$ water bath before and after being placed in a $60^{o}C$ water bath. The FBG probe (together with thermocouple), was dipped into the $90^{o}C$ water bath (from room temperature) for around 1 second, then was quickly removed from it within 1 second, before being exposed to the $60^{o}C$ water bath. Some sharp temperature changes (spikes) were generated during this period. This procedure was repeated several times. The temperature readings of the FBG system and the thermocouple were recorded, and as shown in Figure 5.25 the temperature spikes were observed. The inset picture shows the response of the temperature sensors to the first temperature 'spike' created. The rapid temperature change was picked up by both the FBG probe and thermocouple, however the fast temperature drop during the very short period (less than 1 second) by moving the probes from $90^{o}C$ water to air before being placed into the $60^{o}C$ bath was only detected by the FBG probe. This test showed that the FBG system could capture a temperature spike when there was a rapid temperature change, and again, the response time, which is less than 1 second, is quicker than that of the thermocouple.
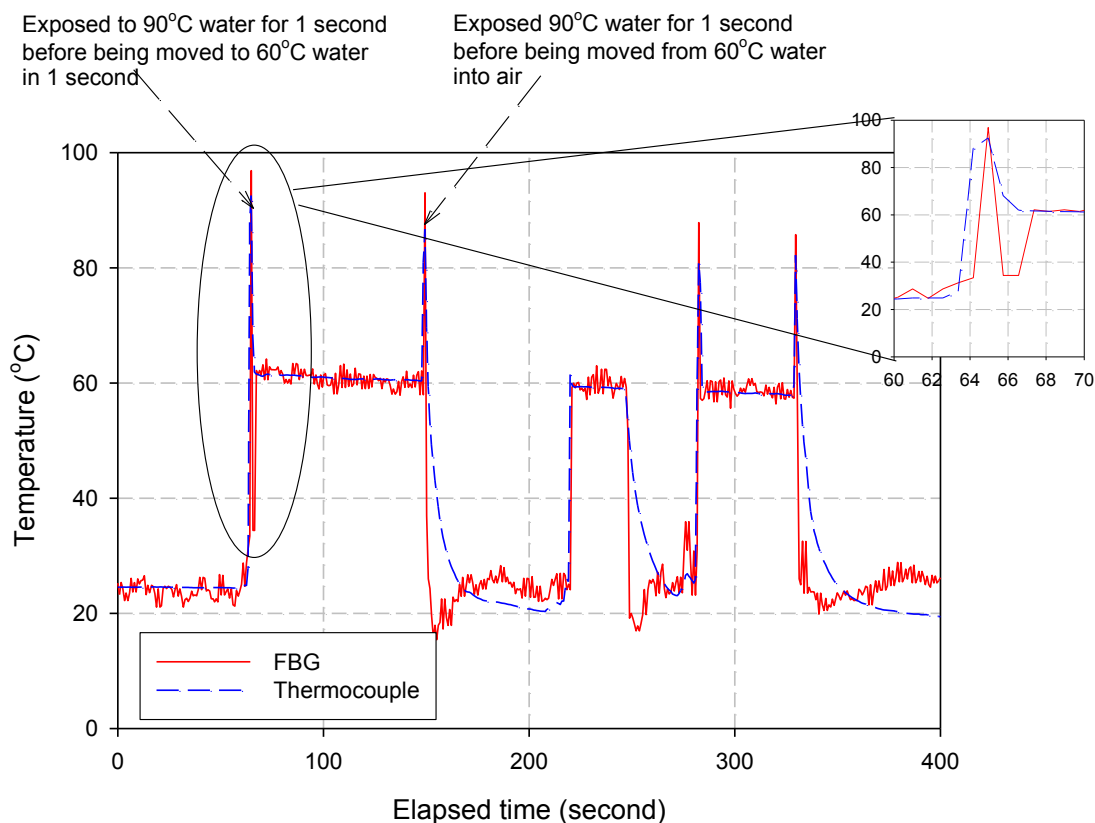
Figure 5.25: Simulated temperature spike picked up by the FBG temperature sensor

5.3.3   Long term stability

The FBG-based system established was kept running continually for over 10 days for long term stability test. The FBG probe, together with a K-type thermocouple, was placed inside a tube oven for temperature monitoring. The oven was set at different temperatures for testing the system stability at various temperatures. The results obtained are shown in Figure 5.26, where a good long term stability of the FBG temperature sensor system has been demonstrated during the test of 280 hours, showing a comparable performance with that of the thermocouple. The slight temperature discrepancy between the two sensors was attributed to the initial calibration differences and their offset of locations .
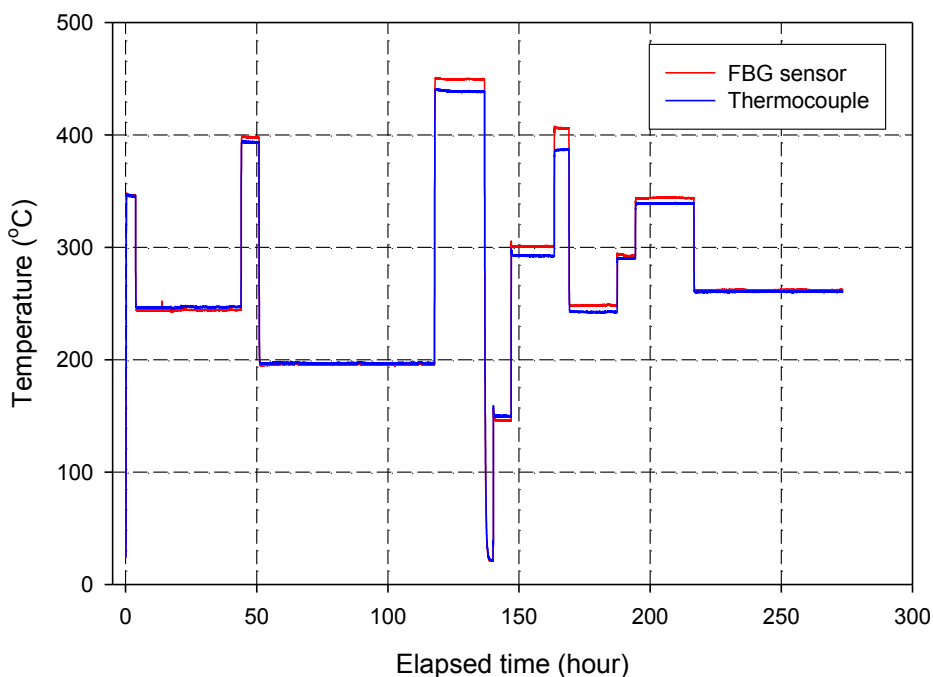
Figure 5.26: Long term stability of the FBG-base sensor system, together with a
thermocouple, over 10 days

5.3.4   Absolute wavelength accuracy

As discussed above, both the wavelength resolution and relative wavelength
accuracy are important parameters for a FBG-based temperature sensor system, as the
wavelength shift is utilized for measurements. *Absolute wavelength accuracy* is
another important parameter for a sensor product.

In order to verify the absolute wavelength accuracy of the sensor system developed,
the absorption wavelengths of the traceable gas cell were measured by the FBG sensor
system (after some modifications of the software, as the original software was designed
specifically to detect FBG reflection peaks).   Three HP18460 series OSAs were also
used in the laboratory for absorption peak search and identification. The wavelength
measurement deviations from the standards arising from the FBG system and OSAs
are shown in Figure 5.27. The results clearly indicate that the FBG system developed
has a higher absolute wavelength accuracy of around 10pm, compared to that of 150pm
for the OSAs.
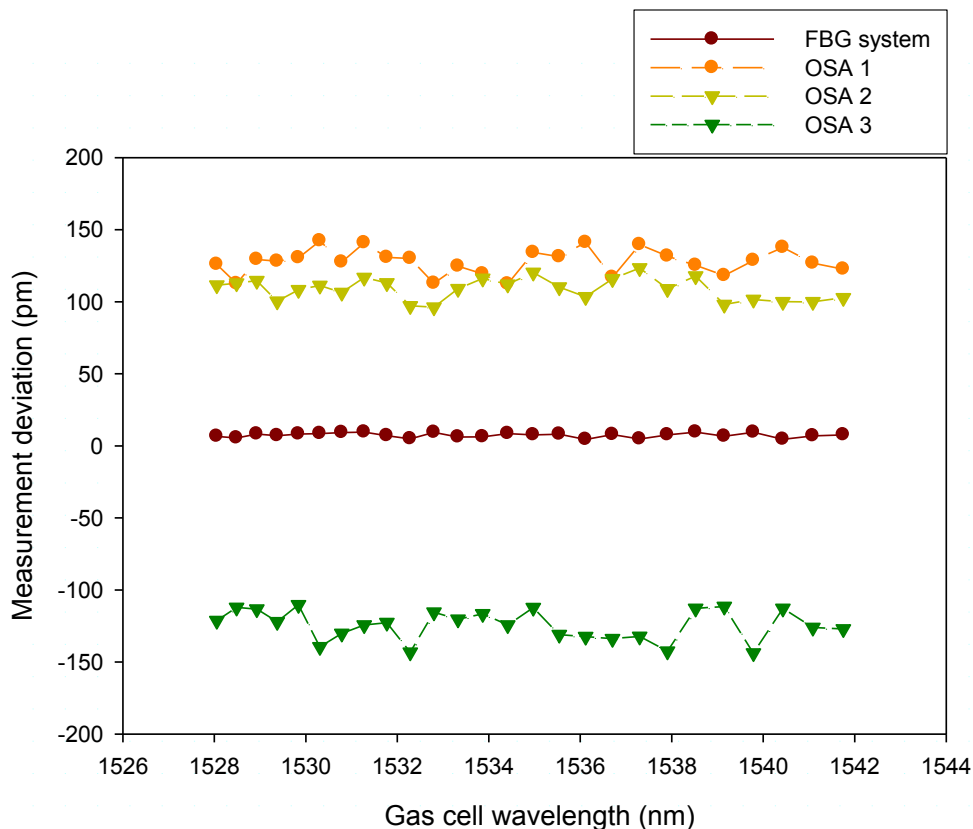
Figure 5.27: Gas cell absorption wavelength (R Branch) measurement deviations arising from the FBG system and OSAs

5.3.5   System performance specifications

Based on the extensive evaluation and calibration undertaken above, the system specifications of the FBG based sensor system developed can be summarized in Table 5.3

Table 5-3: System specifications of the FBG based sensor system

Wavelength Accuracy (absolute)	Better than 10 pm
Wavelength resolution	1 pm
Temperature resolution	0.1°C
Response time	~1 second

5.4 *Field tests of the FBG-based temperature sensor - Temperature monitoring of automotive emissions*

5.4.1 Background of the application

Exhaust emissions from cars, trucks and other road vehicles produce a major source of air pollution [1]. The increasing traffic volume produces a high level of gas species, such as CO, NO_x, HC and SO_x, in the urban environment, which affects the health of human beings and animals. It has become vital to keep pollutant emissions to a minimum. Using emission control technology is a practical way to do this, involving reliable, robust and cost effective means of monitoring the pollutant and containment levels in the exhaust systems.

The main pollutants, CO, NO_x, HC and SO_x, can be monitored through the measurement of spectroscopic absorptions by specific pollutant gases in the vehicle exhaust system. It is also important to measure the temperature of the exhaust gases, as the optical absorption of the various species is temperature dependent, and for control of the engine operational conditions.

Vehicle emissions can be hostile, with hot corrosive gases being present. In addition, electromagnetic interference (EMI) in vehicles is a growing problem in sensor design for the range of measurements required. For example, the use of a new microwave powered catalytic converter, under development, may result in the presence of an intense localised electromagnetic field in the vehicle engine [4]. Therefore an optical fibre temperature sensor offers an effective solution to the problems highlighted. As identified by industrial partners, the major requirements for exhaust gas temperature monitoring are as follows:

- High temperature operation range: The temperature of the exhaust gas could reach up to 600°C

- Insensitivity to mechanical vibration: The exhaust systems in road vehicles encounter considerable vibration and bumping therefore the performance of the

sensor mounted on the exhaust system is required to be free from these environmental perturbations.

- Insensitivity to chemical corrosion: The combined heat and water contents of exhaust emissions result in a highly corrosive mixture, which would result in damage to many conventional sensors.   The sensor used for this application is required to be resistant to these chemical attacks.

- Immunity to EMI. The intense electric fields present in the vehicle, may interfere with the operation of conventional electronic sensors.   Therefore an optical fibre sensor has shown advantages.

In response to the above, the FBG-based temperature sensor systems developed has been used for monitoring the dynamic temperature changes of the exhaust gases from a vehicle engine, experiencing vibration conditions in use. The work has been an integral part of a EU Framework 6 research project, which was aimed to monitor vehicle emissions under operational conditions using advanced optical techniques.

The optical temperature sensor system developed in this work can readily be integrated with other optical sensors to form an intelligent emission monitoring system for vehicles.   Figure 5.28 shows the schematic set-up of an integrated vehicle exhaust gas monitoring system developed, jointly with the EU project partners [44].   Such an optical system offers a high level of flexibility, which can be located at any point along the exhaust system, e.g. immediately down stream of the catalytic converter, where
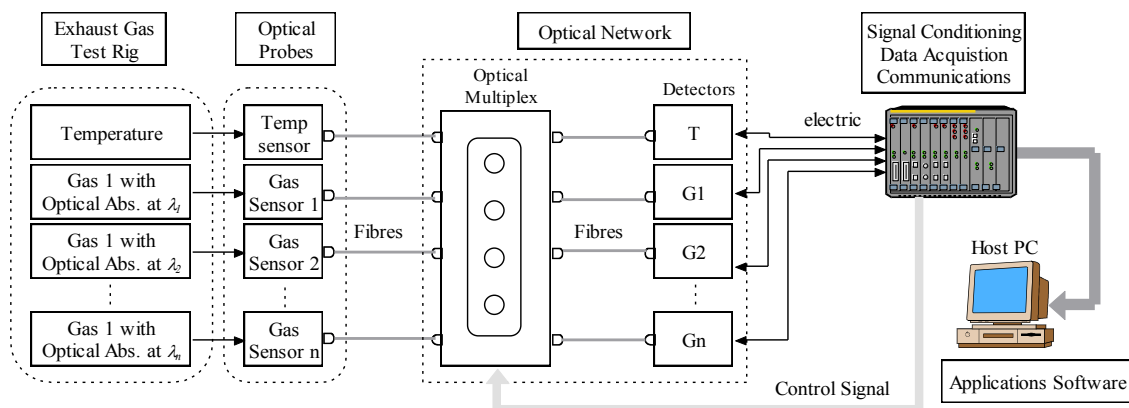
Figure 5.28: Configuration of an optical sensor network for vehicle exhaust gases measurement

such measurements are particularly important.

5.4.2   Experimental results

- **Test at the University of Liverpool**

The first set of tests of the FBG-based temperature sensor for monitoring the temperatures of the exhaust gases of a vehicle engine was undertaken at the University of Liverpool, one of the EU project partners.   For ease of cross-comparison, both a fluorescence-based temperature sensor and a thermocouple were placed in intimate contact with the FBG probe to enable a comparison with the readings from the optical sensors to be made.   As shown in Figure 5.29, all the sensor probes were fixed within the exhaust pipe of the engine to allow simultaneous measurements to be made and cross-compared.

(a)

(b)
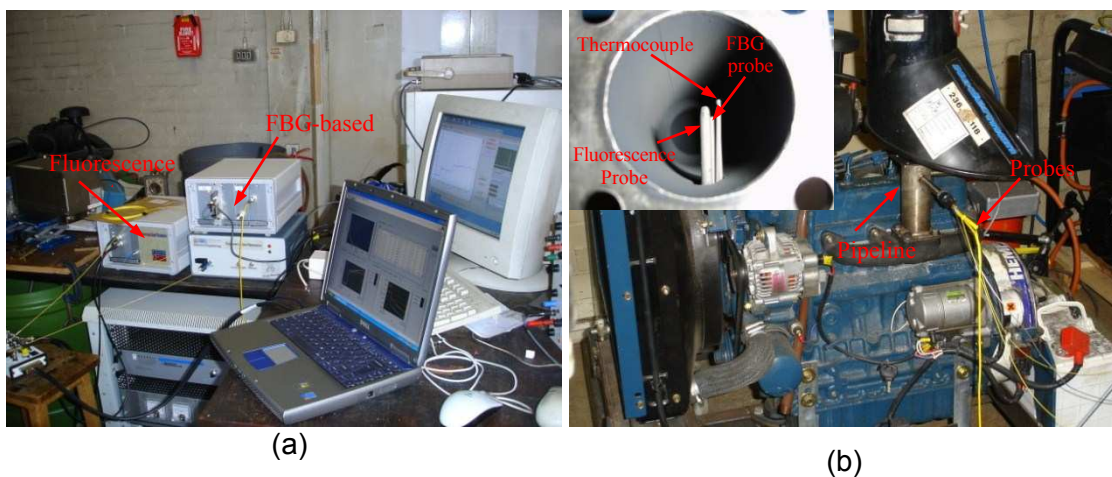
Figure 5.29: Experiment setup for temperature monitoring of vehicle engine exhaust under vibration conditions
(a) optical sensor systems involved (b) probes mounted on the engine exhaust pipeline (inset: locations of the probes)

A series of tests was carried out under different vibration conditions, through the control of engine running speed. Figure 5.30 shows the results obtained while the vibration was being changed randomly by changing the operation speed of the engine for 20 minutes. The temperature differing readings among the probes were believed to be due to the different positions they were located

The results show that the measurement accuracy of the fluorescence-based sensor

under vibration conditions for a 'spot' measurement was dramatically decreased to ±15°C, from ±2°C when there was no vibration. The main reason for this performance degradation is that the intensity of the optical signal was affected by the vibration applied on the probe structure and the resultant change in the optical intensity received, thereby affected the performance of the phase-locked detection scheme for fluorescence-based temperature sensors. This limitation could be overcome through appropriate design of the sensor probe to allow the impact from mechanical perturbations to be minimized.

(a)

(b)
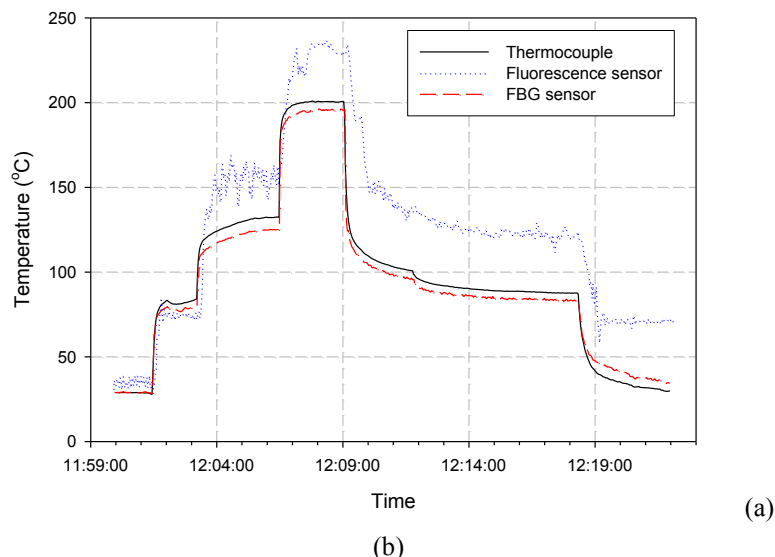
Figure 5.30: Temperature monitoring when the vibration condition was being changed randomly for 20 minutes

By contrast, the results obtained from the FBG-based temperature sensor system, show that the sensor performance was not degraded by vibration, showing a similar measurement precision of about ±1°C under different vibration condition or without vibration. This is due to the fact that the FBG sensor system is based on wavelength modulation rather than intensity modulation. In addition, the FBG is an in-fibre sensor, and is thus less sensitive to environmental mechanical disturbances when the probe is well designed.

- **Field test at CRF, Fiat, Italy**

Further to the preliminary tests carried out at the University of Liverpool, which proved that the FBG-based temperature sensor was well suited for the application of car engine exhaust temperature monitoring, a series of subsequent tests was undertaken at the laboratories of Centro Research Fiat (CRF), FIAT in Italy and Figure 5.31 shows one of the experimental setups.
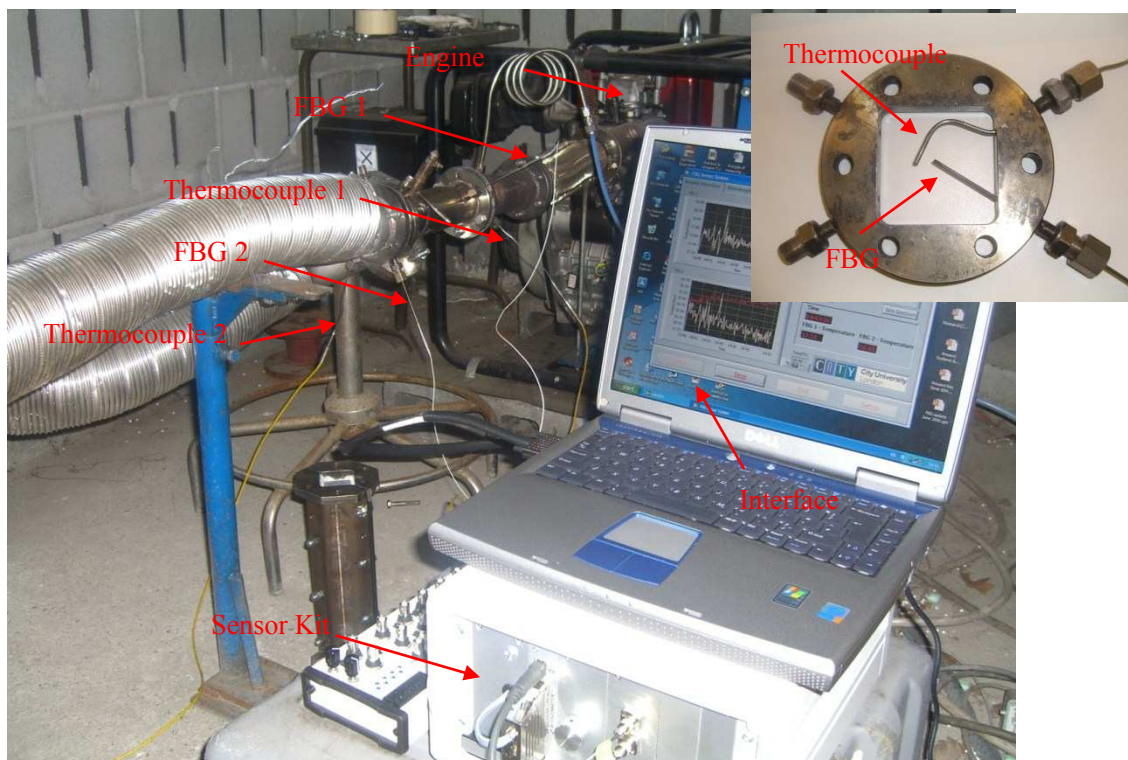
Figure 5.31: Experiment setup of car engine exhaust temperature monitoring at CRF, Fiat, Italy

In the experiment, four temperature probes (two FBG probes and two thermocouples) were used for the temperature monitoring of the engine exhaust. The positions of the sensors were:

FBG1 &Thermocouple1: located close to each other at the engine side of the pipe

FBG2 & thermocouple2: located close to each other and at the end side of exhaust pipe

Various experimental conditions were thus created, e.g. by changing the engine

speed, to facilitate the evaluation of the sensor performance and thus judge the suitability of the FBG based temperature sensor for such applications. One of the test results is illustrated in Figure 5.32. During this test, the engine running speed was firstly gradually increased step by step to the maximum speed, which yields a temperature of over 600 ^{o}C at the exhaust pipe. Then the engine was turn off and on for a few cycles. A good agreement has been seen between the FBG and thermocouple, apart from the last cycle, where there were considerable differences between the temperature sensors. The differences were caused by the annealing effect on the FBG sensor, which had been annealed at a relative low temperature of around 400 ^{o}C before being employed in the test.   This difference in reading could be easily eliminated by annealing the FBG probe at an elevated temperature.
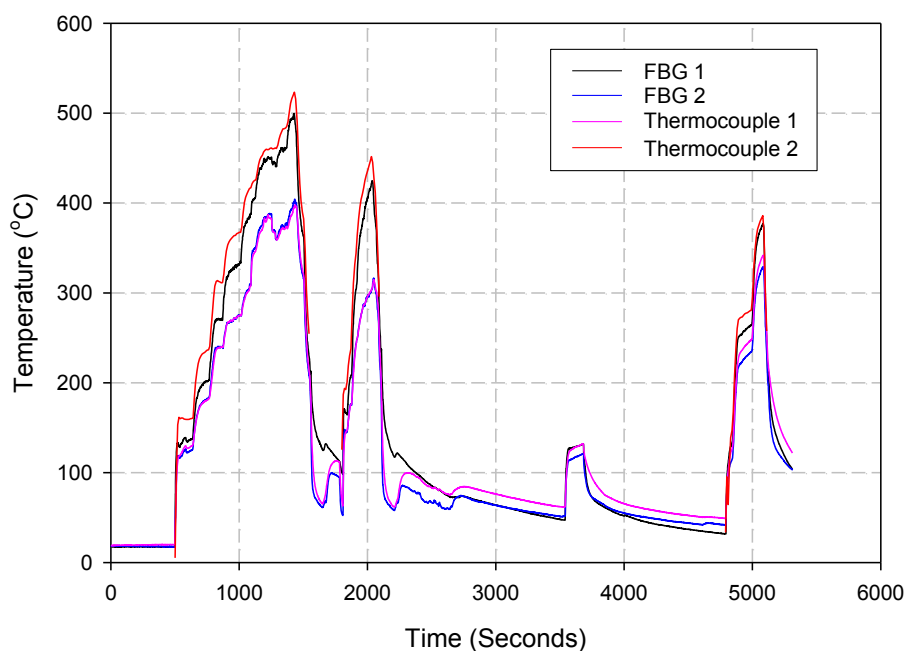
Figure 5.32: Car engine exhausting temperatures measured by FBG sensor and thermocouple

5.5   Summary

In this chapter, following a review of a number of Bragg wavelength interrogation schemes, a compact and reliable FBG sensor system using a tunable Fabry-Perot filter has been successfully developed.   To achieve better performance with higher accuracy for wavelength measurement, some wavelength reference methods have been

incorporated successfully into the system design and as a result the system has shown

a good wavelength resolution of 1 pm (equivalent to a temperature resolution of 0.1 $^{\circ}$C),

with an absolute wavelength accuracy of better than 10 pm.   Prior to the field tests, the

FBG sensor system was calibrated and cross-compared with the other types of optical

and electrical sensor systems when they were subjected to various environmental

conditions.   The FBG system has shown advantageous characteristics for some

specific industrial applications and this has been confirmed by the positive results

obtained from various field tests.

Reference

[1].   A. Othonos and K. Kalli, "*Fiber Bragg Gratings: Fundamnetals and Applications in Telecommunication and sensing*", Artech House, 1999

[2].   S. M. Melle, K. Liu and R. M. Measures, "*A passive wavelength demodulation system for guided-wave Bragg grating sensors*", IEEE Photonics Technology Letters, Vol. 4, 1992, pp. 516-518

[3].   M. A. Davis and A. D. Kersey, "*All-fibre Bragg grating strain sensor demodulation technique using a wavelength division coupler*", Electronics Letters, Vol. 30, 1994, pp. 75-77

[4].   A. D Kersey, T. A. Berkoff, and W. W. Morey, "*Multiplexed fiber Bragg grating strain sensor system with a fiber Fabry-Perot wavelength filter*", Optics Letters, Vol. 18, 1993, pp. 1370-1372

[5].   M. G. Xu, H. Geiger, J.L. Archambault, L. Reekie, J.P. Dakin, "*Novel interrogation system for fibre Bragg grating sensors using an acousto-optic tunable filter*", Electronics Letters, Vol. 29, 1993, 99.1510-1511

[6].   D. A. Jackson, D. A. Jackson, A. B. Lobo Ribeiro, L. Reekie, and J. L. Archambault, "*Simple multiplexing scheme for fier optic grating sensor network*", Optics Letters, Vol. 18, 1993, pp. 1192-1194

[7].   Fabry C. and Perot A., "*Sur les franges des lames minces argentées et leur application á la mesure de petites épaisseur d'air*", Annales de Chimie et de Physique, vol. 12, 1897, pp. 459 -501

[8].   H. Y. Tam, S. Y. Liu, et al., "Fiber Bragg Grating Sensors for Structural and Railway Applications", In Engineering Structures, International Society for Optical Engineering (SPIE), Beijing, PR China, 2004, pp. 85-97.

[9].   S C Tjin, Y Wang, et al., "*Application of quasi-distributed fibre Bragg grating sensors in reinforced concrete structures*", Measurement Science and Technology, vol. 13, 2002, pp. 583

[10]. M.A. Davis, D.G. Bellemore, M.A. Putnam, A.D. Kersey, "*Interogation of 60 fibre bragg gratin sensors with microstrain resolution captivity*", Electronics letters Vol 32, 1996, pp 1393-1394

[11]. S. E. Harris, R.W. Wallace, "*Acousto-optic tunable filter*", Journal of Optics. Society

American, vol. 59, 1969, pp.744

[12]. M.S. Gottlieb, "*Acousto-optic tunable filter, Design and Fabrication of Acousto-Optic Devices*", Marcel Dekker, New York, 1994.

[13]. C. Boulet, , D.J. Webb, et al., "*Simultaneous interrogation of fiber Bragg grating sensors using anacoustooptic tunable filter*", Photonics Technology Letters, IEEE, Vol 13, 2001, pp1215-1217

[14]. D. C. C. Norman and D J Webb, "*Fibre Bragg grating sensor interrogation using an acousto-optic tunable filter and low-coherence interferometry*", Measurement Sciences and Technology, Vol. 18, 2007, pp. 2967-2971

[15]. S. Tanaka, K. Yamada, H. Kobayashii, and M. Kadota "*Application of Acoustooptic Tunable Filter to Strain- or Vibration-Sensing System*", Japan Journal of Applied Physics, Vol. 46, 2007, pp. 4633-4635

[16]. C, Antonio, "*AOTF interrogation scheme for FBG*", Proc. SPIE Vol. 2722, Smart Structures and Materials, 1996, pp.107-110

[17]. H. Gieger, M. G. Xu, J. P. Dakin, N. C. Eaton, and P. J. Chivers,., "*Progress on grating interrogation schemes using a tunable filter*", Proceedings of the Optical Fiber Sensor Conference (OFS11), Sapporo, Japan, 1996, pp. 576-379

[18]. M. G. Xu, H. Geiber and J. P. Dakin, "*Electronic tracking system for multiplexed fibre grating sensors*", Electronics Letters, Vol. 31, 1995, 1228-1229

[19]. J. R. Dunphy, G.A. Ball, F.X. D'Amato, P. Ferraro, S. Inserra, A. Vanucci and M. Varasi, "*Instrumentation development in support of fiber grating sensor array*", Society of Photo-optical Instrumentation Engineers, Distributed and Multiplexed Fiber sensors III, Soston, 1993, Vol. 32071, pp. 2-11

[20]. G. P. Brady, et al., "*Demultiplexing of fibre Bragg grating sensor with microstrain resolution capability*", Optics Communications Vol. 11, 1994, pp. 51-54

[21]. M. A. Davis, Kersey, A.D "*Matched-filter interrogation technique for fibre Bragg grating arrays*", Electronics letters, Vol. 31, 1995, pp. 822-823

[22]. C. M. Tay, K.M. Tan, S.C. Tjin, C.C. Chan, "*A high-resolution tunable fiber Bragg grating filter*", Microwave and Optical Technology Letters, Vol. 42, 2004, pp. 89 - 92,

[23]. N. Mohammad, W. Szyszkowski, W. J. Zhang, E. I. Haddad, J. Zou, W. Jamroz, and R. Kruzelecky, "*Analysis and development of a tunable fiber Bragg grating filter based on axial tension/compression*", Journal of Lightwave Technology, Vol. 22, 2004, pp. 2001-2013

[24]. T. Coroy, M. N. Measures, "*Active wavelength measurement system using an InGaAs-InP quantum-well electroabsorption filtering detector*", IEEE Photonics Technology Letters, Vol. 8, 1996, pp. 1686 - 1688

[25]. T. Coroy, Measures M. N, "*Demodulation system for Bragg grating fiber optic sensors using a quantum well electro-absorption filtering detector*", Smart Materials Structure, Vol. 7, 1998, pp. 265-271

[26]. G. A. Ball, "*Fibre Laser Source analyzer for Bragg grating sensor array interrogation*", IEEE Journal of Lightwave Technology, Vol. 12, 1994, pp.700-703

[27]. M. A. Putman, M.L. Dennis, J.U. Kang, TE Tsai., "*Sensor Grating demodulation using a passively mode locked fibre laser*", Technical Digest Optical Fiber communications Conference, Optical Society of America, Vol. 6, 1997, p.156.

[28]. M. L. Dennis, M. A. Putnam, J. U. Kang, T.E. Tsai, I.N. Duling III, and E.J. Friebele., "*Grating sensor array demodulation by use of a passively mode-locked fibre laser*", Optics letters, Vol. 22, 1997, pp. 138-140

[29]. X. Wan, H.F. Taylor, "*Multiplexing of FBG sensors using mode locked wavelength-swept fibre laser*", Electronics Letters, Vol. 39, 2003, pp.1512 – 1514

[30]. S. H. Yun, D.J. Richardson and B.Y. Kim,, "*Interrogation of fibre Bragg arrays with a wavelength swept fibre laser*", Optics Letters, Vol. 23, 1998, pp. 138-140.

[31]. Y. F. Takushima, F. Futami, K. Kikuchi,, "*Generation of over 140 nm wide super continuum from a normal dispersion fibre by using a mode-locked semiconductor laser*", IEEE Photonics Technology Letters, Vol. 10, 1998, pp.1560-1562

[32]. S. J. Gong, G.H. LV, X.S. Li, X. Jiang, S.H. Shang, et. al., "*A novel design of CCD spectral detection circuit for FBG sensor interrogation*", Proceedings of SPIE, Vol. 6595(2), 2007, pp. 65953F.1-65953F.7

[33]. G. Y. Li, H. Zhang, B. Liu, J. Zhang, S.Z. Yuan, G.Y, Kai, X.Y. Dong, "*The interrogation system for FBG sensing based on the InGaAs linear image sensor*", Microwave and Optical Technology Letters, Vol. 50, 2008, pp.1101 – 110

[34]. Uwe C. Mueller, Thomas Zeh, et Al., "*Fiber optic Bragg grating sensors for high-precision structural deformation control in optical systems*", Proceedings of SPIE Vol. 6167, 2006, pp. 61670A.1-61670A.

[35]. C. G. Athkins, M. A. Putnam, and E. J. Friebele, "*Instrumentation for interrogating many-element fiber Bragg grating arrays embedded in fiber resin composites*", Society of Photo-optical Instrumentation Engineers, Smarting Sensing Processing and Instrumentation, 1995, Vol. 2444, pp. 257-266

[36]. A. D. Kersey, T. A. Berkoff, and W. W. Morey., "*Interrogation and multiplexing techniques for fibre Bragg grating strain sensors*", Society of Photo-Optical Instrumentation Engineers, Distributed and Multiplexed Fiber Optic Sensors III, Boston, Vol. 2071, 1993, pp. 30-48

[37]. A. D. Kersey. T.A. Berkoff, W.W. Morey, "*High-resolution fibre grating based strain sensor with interferometric wavelength-shift detection*", Electronics Letters, Vol. 18, 1992, pp. 1081-1083

[38]. W.R. Stephen, B.L.Bachim,, "*Source-noise-induced resolution limits of interferometric fibre Bragg grating sensor demodulation systems*", Measurement Science Technology Vol. 12, 2001, pp.782-785

[39]. M. A. Davis and A. D. Kersey, "*Fiber Fourier transform spectrometer for decoding Bragg grating sensors*", Proceedings of the Optical Fibre Sensors Conference (OFS10), Glasgow, UK, 1994, pp. 167-170

[40]. A. D. Kersey, T. A. Berkoff, and W. W. Morey ,"*Fiber-optic Bragg grating strain sensor with drift-compensated high-resolution interferometric wavelength-shift detection*", Optics Letters, Vol. 18, 1993, pp72-74.

[41]. M. A. Davis and A. D. Kersey. "*Application of a fiber Fourier transform spectrometer to the detection of wavelength encoded signals from Bragg grating sensors*", IEEE Journal of lightwave Technology, Vol. 13, 1995, pp. 1289-1295

[42]. G. Gagliardi, M Salza, P Ferraro and P De Natale, "*Interrogation of FBG-based strain sensors by means of laser radio-frequency modulation techniques*", Journal of optics.

A, Pure and applied optics, Vol. 8, 2006, pp. 507-513

[43]. Hydrogen Cyanide Gas Cell Datasheet, www. wavelengthreferences.com

[44]. W. Z. Zhao, T. Sun, K. T. V. Grattan, J. Lucas and A. I. Al-Shamma'a, "*Temperature monitoring of vehicle engine exhaust gases using optical fibre temperature sensor systems*", Proc. SPIE 5855, 2005, pp.832

Chapter 6. Fibre Bragg grating based fire alarm system

6.1   Fluorescence-based and FBG-based fire alarm systems

In Chapter 3, a fluorescence-based temperature sensor system has been specifically designed and evaluated for early fire detection, showing promise to be a practical alternative to the conventional fire alarm system used in aero industries. However the fluorescence-based system has some limitations, such as being sensitive to light source fluctuation and to the locations of the temperature excursions, etc.   The FBG-based temperature sensor system, discussed extensively in Chapter 5, has shown better performance for temperature measurement with higher accuracies, longer term stability and insensitivity to environmental changes etc.   Thus this Chapter describes the extensive work undertaken to explore the potential and suitability of using a FBG-based temperature sensor system for early fire detection.

As discussed in Chapter 4, FBGs written into conventional telecommunications fibres cannot sustain elevated high temperatures and this has limited their applications for high temperature measurements, such as for early fire detection in the aerospace industry.   However, as described in Chapter 4, when the gratings are written into some specialist fibres, strong FBGs with high temperature sustainability (up to $900^{o}C$) can be created and used for high temperature measurements. In particular, the recent development by the research group at City University London of the novel Bi/Ge co-doped fibres [1-3] has enabled strong FBGs to be written into, showing potential to establish a FBG-based fire alarm system in order to better meet the requirements highlighted in section 3.1.1.

6.1.1   FBG-based fire alarm system

The FBG-based fire alarm system is designed to measure the temperature of a hot spot and the background temperature simultaneously, using a series of gratings written into a single fibre, or a few fibres if more measurement channels are required. The operational principle of the fire alarm system is similar to the FBG temperature sensor

system developed in Chapter 4 and system setup is illustrated in Figure 6.1. The probe contains a series of FBGs written at the same wavelength, and when exposed to a uniform background temperature, either being constant or varying, the spectral profile of the reflected light from all the FBGs within the probe would have a single peak, as shown in Figure 6.1(b). This single reflective Bragg wavelength, λ_b, represents the background temperature. When a hot spot, which has a different temperature (normally higher) than that of the background, is present at any location along the probe, a second reflective peak occurs, showing a different wavelength, λ_h, corresponding to the temperature of the hot spot as shown in Figure 6.1(c). Therefore, the temperatures of the hot spot and the background can be derived from the wavelengths of these two peaks based on equation (6.1).

$$T_h = f(\lambda_h), \ \ T_b = f(\lambda_b) \hspace{3cm} (6.1)$$

where T_h, and T_b are the temperature of the hot spot and the background respectively. Thus the background temperature and the temperature of hot spot can be measured simultaneously, even when the background temperature varies. The temperature of the hot spot has to be a certain degree higher than that of the background to be detectable. This minimum detectable temperature difference between the hot spot and the background is mainly determined by the overall bandwidth of the FBG series and the resolution of the wavelength interrogation system. In this specific fire alarm system developed, the minimum detectable temperature difference is about 30-40 ^{o}C, which is sufficient for the particular application of aero engine temperature monitoring. The sensor is placed inside a stainless tube to ensure the robustness of the probe for both laboratory and field tests.
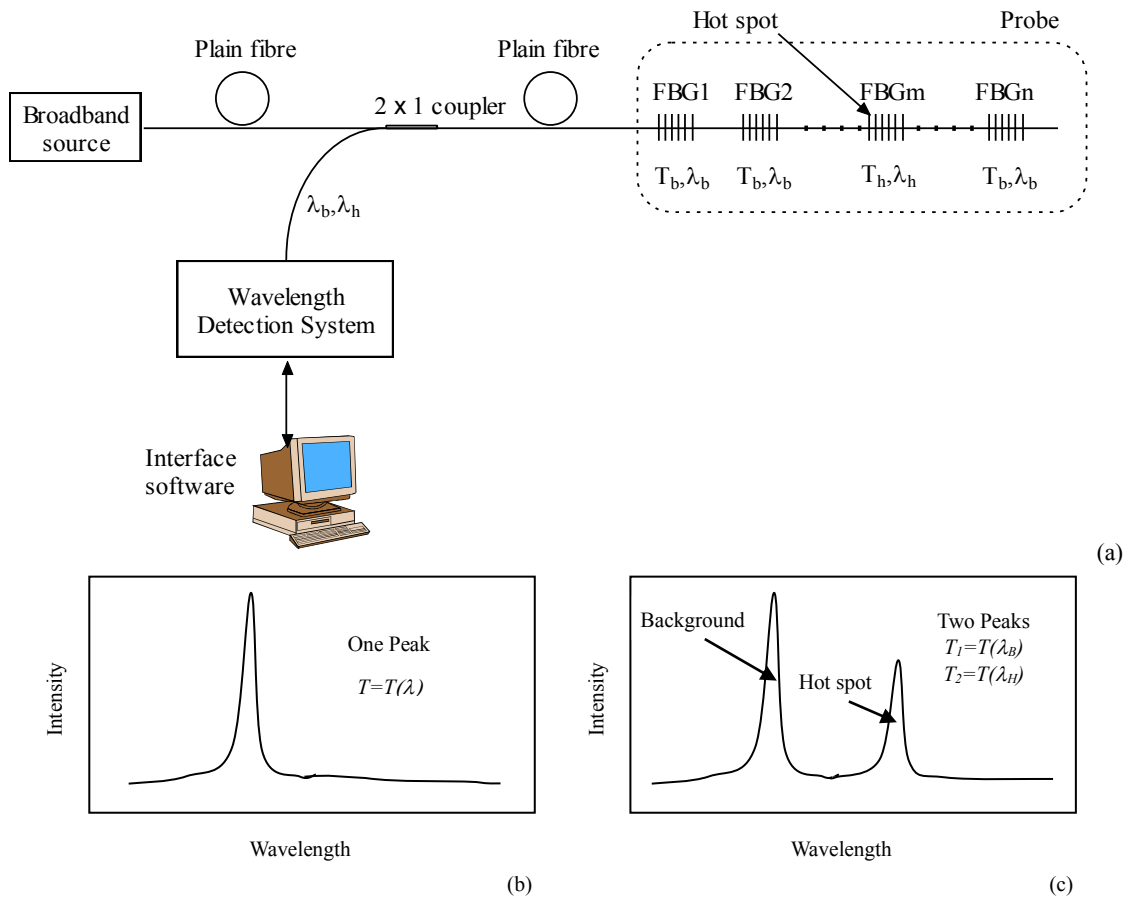
Figure 6.1: Experimental setup of the FBG-based fire alarm system
(a) Hardware setup. (b) Spectrum when FBGs are exposed to a uniform background
temperature. (c) Spectrum when a hot spot is present

6.1.2   System setup

Based upon the FBG-based temperature sensor system discussed in Chapter 5, a prototype FBG-based fire alarm system was established and evaluated. As shown schematically in Figure 6.2 and photographically in Figure 6.3, the system primarily consists of:

● Wavelength interrogation system

The hardware used for the FBG-based temperature sensor for wavelength interrogation was also used in the fire alarm system without any major modifications. This shows the flexibility of using an F-P filter scheme for wavelength interrogation
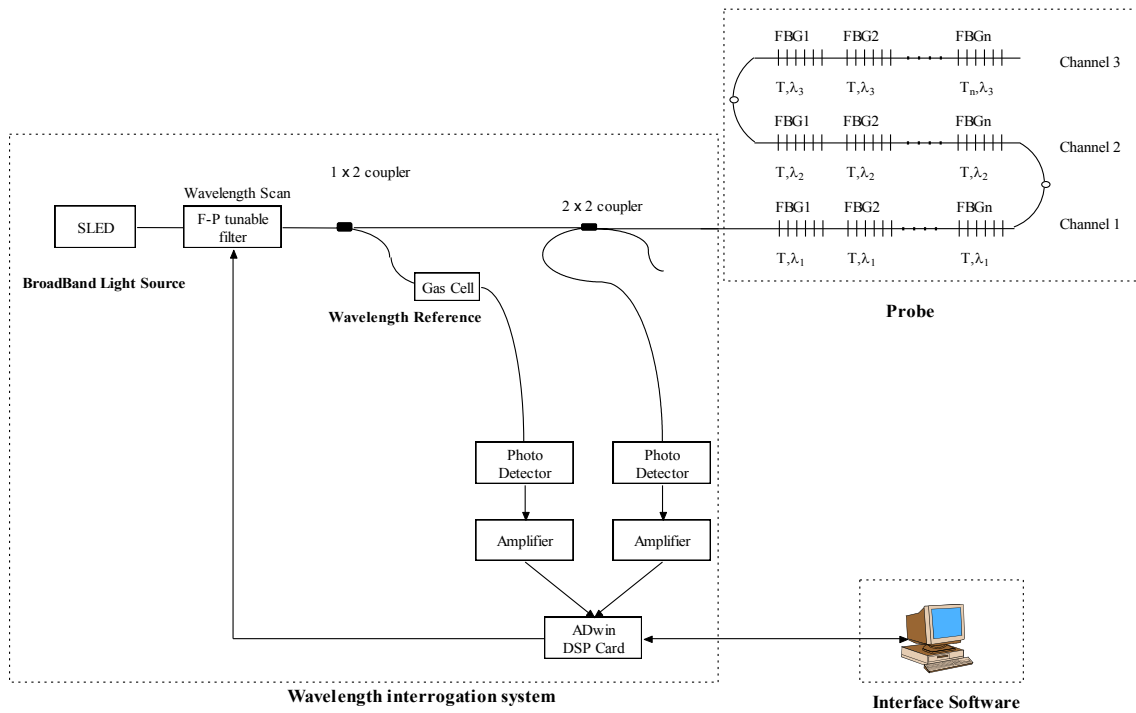
Figure 6.2: Schematic of the FBG-Based fire alarm system
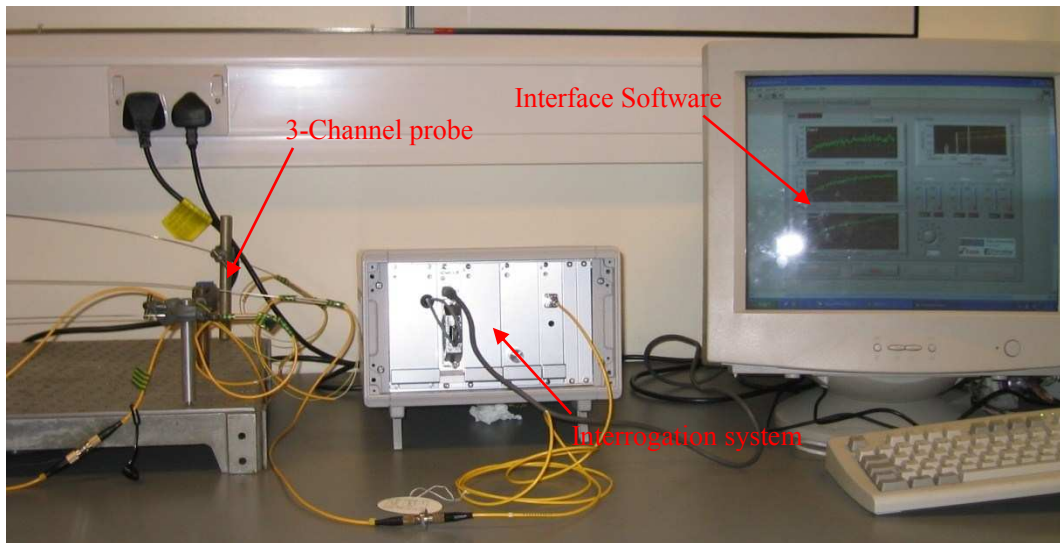
Figure 6.3: Experimental setup of the FBG-based fire alarm system

● Probe

The sensor probe has included three channels of FBG arrays, with each channel containing 22~25 FBGs at a same wavelength in a single fibre of 1 meter length. The difference between the channels is represented by their respective reflected wavelengths, indicating which zone the hot spot is located.

● Interface Software

With some minor modifications, the interface software developed for the FBG temperature sensor system can be used for the fire alarm system.

6.1.3 Probe fabrication

A probe comprising 3 FBG array channels was used for the preliminary test and evaluation as a FBG-based fire alarm system. As illustrated above, each channel of the probe contains an array of around 25 FBGs, uniformly spaced on a 4 cm interval in a one-meter fibre. The 25 FBGs in the same array have the same back-reflected Bragg wavelength, but have different wavelengths in different channels. Therefore in this work the spectrum of the probe shows three different wavelengths representing three different channels, when the probe is exposed to a uniform background temperature. After the series of gratings being written into the fibre and subsequently being annealed at a temperature of 250°C for over 24 hours, the sensing probe was then protected by inserting into a single 1.2-meter steel tubing to ensure the robustness of the sensor for further tests.

To ensure the fabrication of a series of gratings with the same Bragg wavelength for each channel, it was essential to maintain the grating writing conditions, such as laser energy and frequency, fibre tension, etc. This has been successfully achieved to ensure that all the FBGs within the same channel have the same Bragg wavelength within a fractional tolerance, thus enabling the overall bandwidth of all the FBGs in the same channel to be kept within a certain defined range. This overall bandwidth is correlated to the minimum detectable temperature difference between the hot spot and the background. As illustrated in Figure 6.4, a -3dB bandwidth of each FBG array has been achieved to be around 400pm, compared to ~200pm of a single FBG. This is due to small overlaps of the spectra of the gratings. With such a bandwidth, the minimum detectable temperature difference was calculted to be around 30°C, which satisfies the industrial requirements for a fire alarm system as summarized in section 3.1.1.
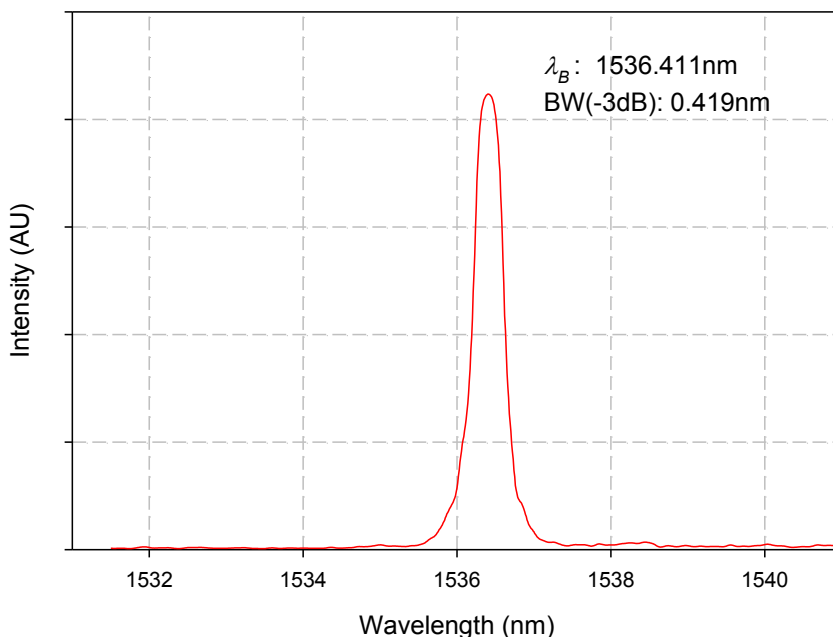
Figure 6.4: Spectrum of a FBG array for the fire alarm probe

6.1.4 Interface software

Similar to the interface designed for the FBG-based temperature sensor system discussed in Chapter 5, the interface software of the fire alarm system has built-in functions for F-P filter controlling, wavelength data retrieving, analyzing and displaying, thus providing a user-friendly interface. Some screen shots of the modified interface software are shown in Figure 6.5. Figure 6.5 displays the temperatures of both the hot spot, if present, and the background of three different channels monitored. A visual alarm will be triggered whenever the measured temperature of the hot spot, in any channel, is shown above the threshold (such as $50^{o}C$) above the temperature of the background.
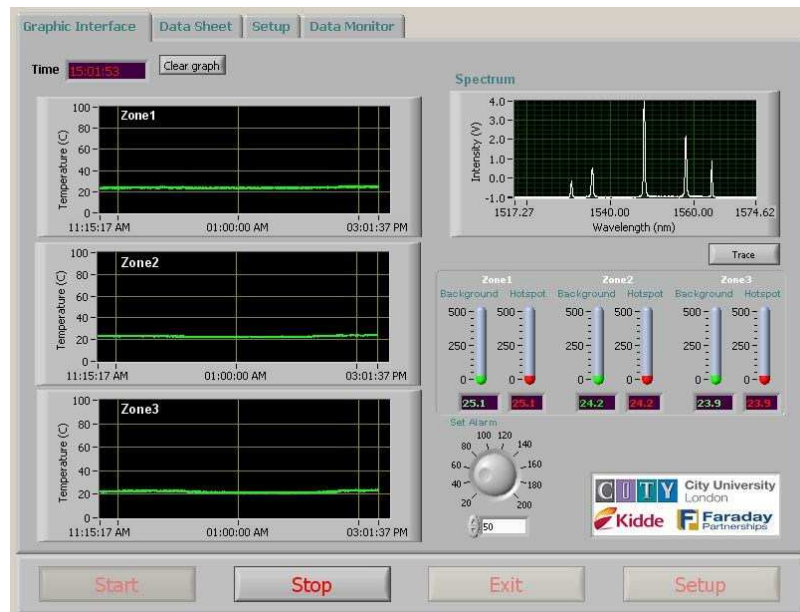
Figure 6.5: Screen print out of the interface software for FBG fire alarm system
(Showing the graphic presentation of the temperatures of the hot spot and the background of
three channels)

6.2   Experimental tests and evaluation of the FBG-based fire alarm system

The prototype of the FBG-based fire alarm system developed at City University London was subjected to a series of tests to evaluate its performance, in term of spatial resolution, temperature resolution, response time and stability, etc, both in the laboratory and in the industrial test environment.

6.2.1   Spatial resolution of the FBG-based fire alarm system

The spatial resolution termed here is not referring to the spatial resolution of the hotspot location, which is distinguishable between different zones (channels) in a range of 1 meter, but to a minimum detectable hot spot size.   As discussed above, the spacing between gratings within each channel is 4 cm therefore the minimum detectable size should be 4cm to enable the temperature excursion to be detected by at least one FBG.   To verify this, the fire alarm system was used to record the temperatures of the hot spot when the probe was exposed to various simulated hot spots with different size and temperature profile at different locations.   The simulated hot spots were provided by two small heat sink blocks, one was 5 cm in length and the

other 2 cm. These heat sinks provided roughly uniform hot spots along their lengths when heated by a heating element. The hot spot temperature readings were recorded while the heat sinks were being moved along the fibre sensing length, while the background temperature was kept at room temperature. The results are shown in Figure 6.6. The readings with the 2 cm length heat sink fluctuated dramatically with positions, while that with the 5 cm one was of relative small fluctuation. Such an experiment was not carried out under the best test condition due to the limitation of facility, however, it was clearly indicated that the minimum detectable hot spot size is approximately equivalent to the spatial gap between the adjacent FBGs.

(a)

(b)
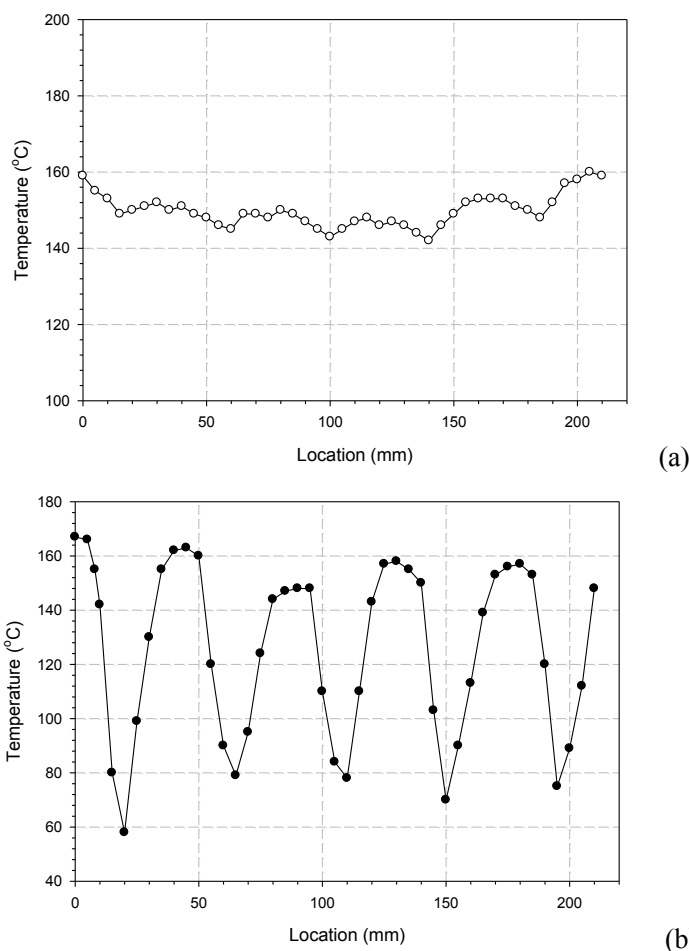
Figure 6.6: Spatial resolution of the FBG based fire alarm system under different stimulated hotspots. (a) 5 cm heat sink (b) 2 cm heat sink

6.2.2 Temperature resolution of the FBG-based fire alarm system

Similar to the fluorescence-based fire alarm system developed and discussed in

chapter 3, the minimum detectable temperature difference between the temperature of the hot spot and that of the ambient background temperature is an important specification for a FBG-based fire alarm system. As mentioned above, the minimum detectable temperature difference of the system is mainly determined by the bandwidth of the overall spectrum of the FBG array and the wavelength resolution of the interrogation system. A simple experiment was carried out to verify this and to determinate the minimum temperature difference which can be discerned by the system. In this experiment, one sensing channel of the 3-channel system was kept at a room temperature (~25°C) while one section (~5cm) of it was exposed to a heating element simulating a hot spot. The spectra of the FBG array of the channel, as shown in Figure 6.7, were retrieved and recorded by the interrogation unit, while the temperature of the heating element varied at room temperature, 50°C, 55°C and 100°C respectively. The
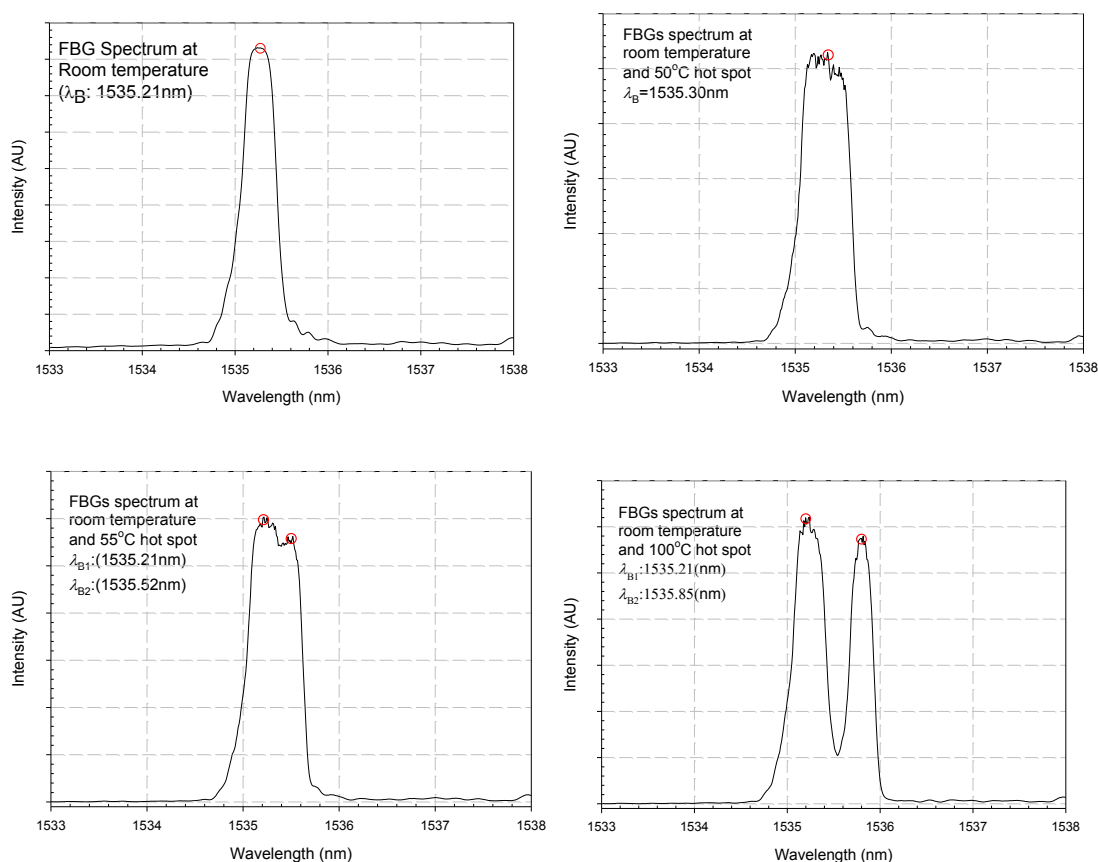
Figure 6.7: Spectrum of an FBG array of 24 FBGs, being placed at room temperature as background and a section of 5cm exposed to a hot spot with a varying temperature of: (a) no hot spot, (b) 50°C, (c) 55°C, (d) 100°C)

results clearly indicated that the system could identify a hot spot of 55°C but not that of 50°C, which showed the minimum detectable temperature difference of the FBG based fire alarm system was of 30°C, which is sufficient to meet the requirement of the application for fire alarm detection of aircraft engine as detailed in the project.

6.2.3   Response time test of the FBG-based fire alarm system

The response time of the FBG-based fire alarm system was tested under a room temperature background. A heat-gun was used to provide a hot spot over a spatial region of < 10cm, with the maximum temperature achieved to be about 300°C. A typical set of results obtained is shown in Figure 6.8, which is a printout from the interface software.   Figure 6.9 shows the results obtained from both the FBG-based fire alarm system and from the K-type thermocouple (corresponding to the data circled in Figure 6.8).   The results show the FBG-based fire alarm system had a response time of less than one minute, which is much faster than that of the K-type thermocouple unit used for comparison.   It is also shown in Figure 6.9 that there is a sudden temperature drop to the background temperature whenever the hot spot temperature is lower than 55°C, 30°C above the background temperature - this again confirms the minimum detectable temperature difference between the hot spot and the background as observed in the previous experiment.   The system cannot identify the difference between the hot spot and the background when their temperature difference is smaller than the minimum detectable temperature difference.
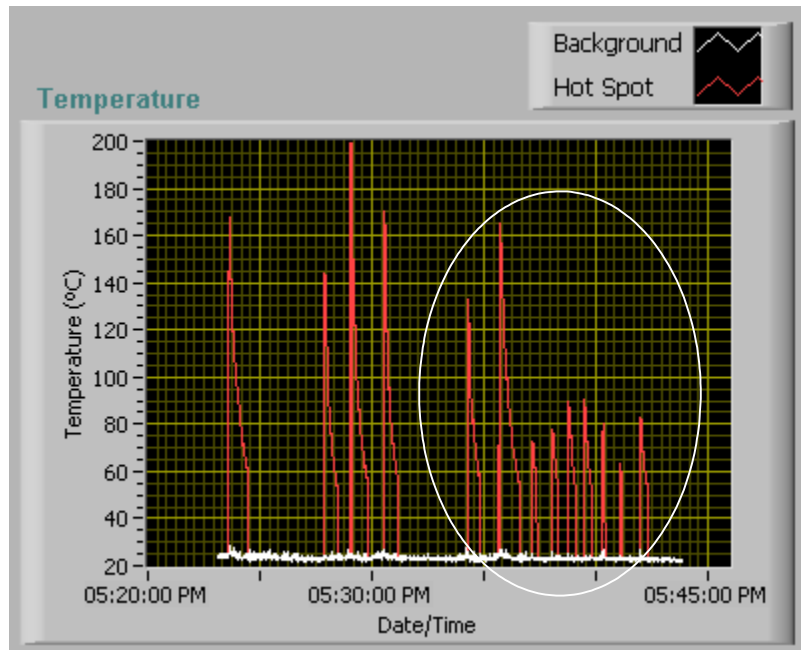
Figure 6.8: Response of the FBG-based fire alarm system to hot spot temperature variations
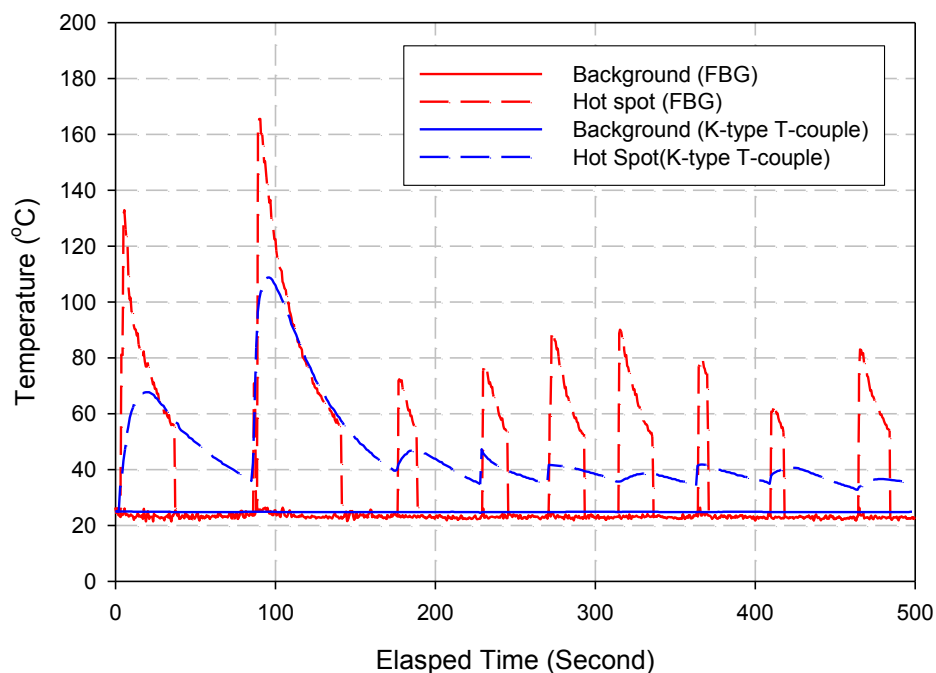
Figure 6.9: Response of FBG-based fire alarm system to hot spot compared to that of the K-type thermocouple

6.2.4   Stability test

The long term stability of the system is important for being used in aerospace industries.   The FBG based fire alarm system developed has been tested for its long term stability. During the test, all three sensing channels of the system were placed at a

room temperature environment while a small section of each channel was kept at a temperature of 180°C using a small aluminium block with heating element, for around 45 hours. Then the heated sections were cooled naturally to the room temperature. The results, together with readings from two thermocouples (with one for background temperature measurement and the other for hot spot), are presented in Figure 6.10. It is shown that the FBG based fire alarm system had a very stable reading during the

(a)

(b)

(c)
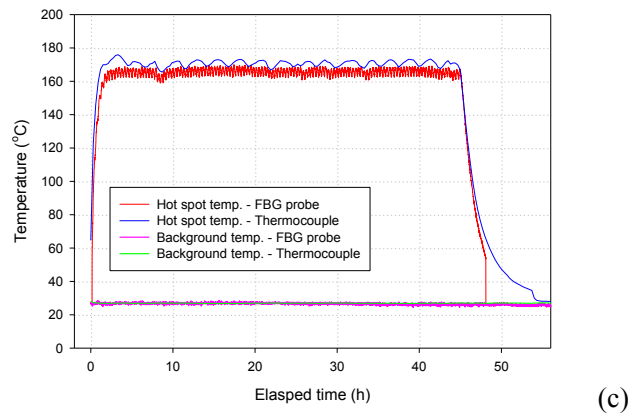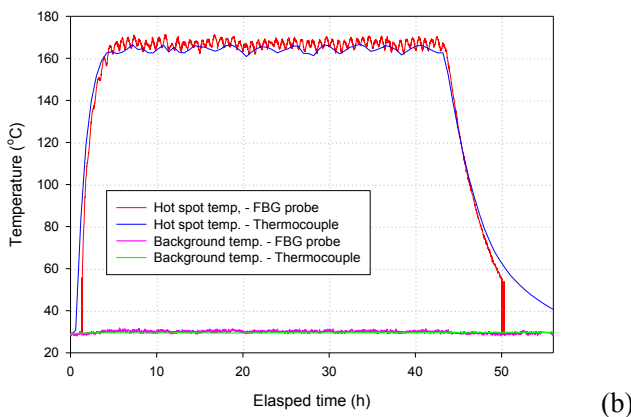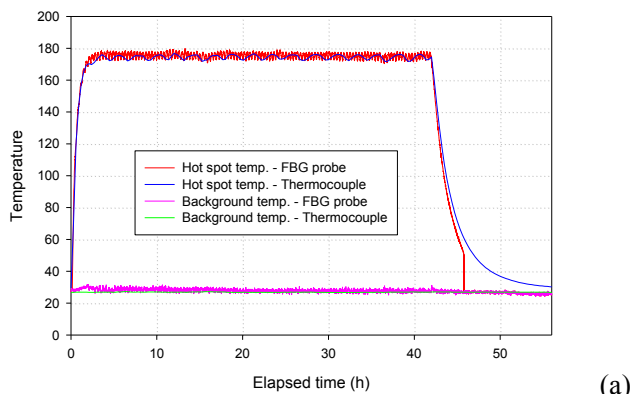
Figure 6.10: Long term stability test of the FBG based system
(a) Channel 1, (b) Channel 2, and (c) Channel 3

testing period, with a standard deviation of less than 1.5^{o}C over 45 hours, where the actual temperature fluctuation was not excluded. The actual standard deviation of the system should be much less than that, if the actual temperature fluctuation, which is around 4°C and limited by the heating element and its temperature control unit, were addressed. This test has therefore demonstrated the stability of the system, which was met well with the requirement proposed by the industrial partner.

6.2.5   Industrial test of the FBG-based fire alarm system

Because of the limitation of the test facility in the University lab, the above tests were all carried out using room temperature as background temperature.   More extensive tests under varying background temperatures were undertaken on the site of Kidde Plc, UK, an industrial partner of the project.   The experimental setup is illustrated in Figure 6.11. One sensing channel of the system was put in a chamber oven, which could provide any temperature between -40°C to 400°C, and a section of this channel was heated by a heating block to create a simulated hot spot.   In such a case, the

Figure 6.11: Experimental setup of the FBG based fire alarm system in Kidde PLC, UK

temperature of the hot spot can be changed under a varied background temperature.

A series of tests was undertaken using the FBG based fire alarm system. The first was to verify the system performance under varied ambient background temperature. The ambient temperature, which is the temperature of the chamber oven, was set at different values from -25°C to 100°C. The temperature of the hot spot was increased from the background temperature to up to 200°C, which is simulated by the heating block. Both the temperatures of the hot spot and of the background were recorded by the FBG based fire system, and by thermocouples for calibration and cross-comparison. A set of the typical results obtained is illustrated in Figure 6.12. The results showed that the hot spot temperature readings of the FBG based system agreed well with those of the thermocouple under different background temperature, except when the background was set at -25°C. This discrepancy was believed to result from the use of a temperature sensitivity of FBGs calibrated at temperatures above the room temperature rather than that of lower temperatures. This deviation could be easily eliminated by calibrating the sensor at lower temperatures, such as at -25°C in this
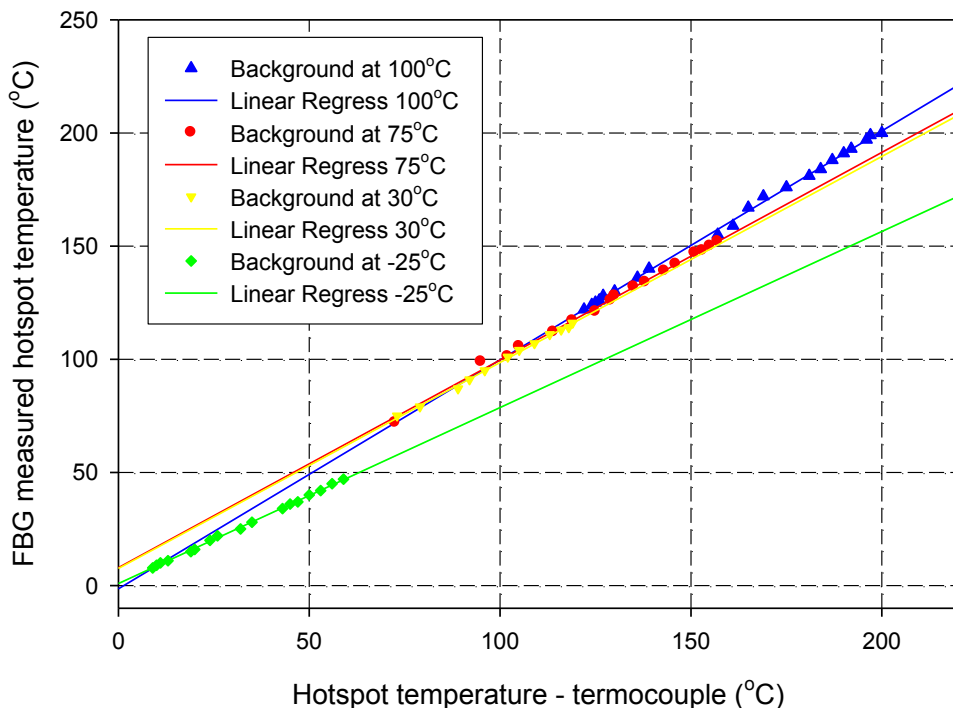
Figure 6.12: The hot spot temperatures measured by the FBG-based fire alarm system as a function of those by a thermocouple under different background temperatures

case.

Another experiment was carried out to evaluate the minimum detectable temperature difference under different ambient background temperatures. The result, illustrated in Figure 6.13, showed the minimum detectable temperature difference decreased with increasing of ambient temperature. This meant a higher sensitivity at a higher background temperature, which is desirable as the fire alarm system is mainly designed to be used at elevated ambient temperatures, although this may result in a more complicated calibration process to cover the wide range of the operating temperature.
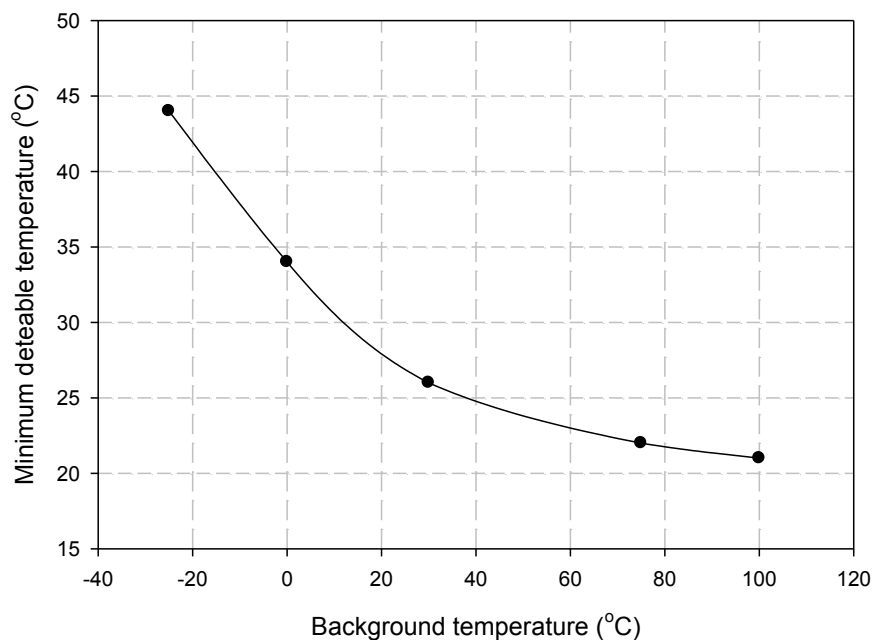
Figure 6.13: Minimum detectable temperature difference under different background temperatures

6.2.6   Advantages over the fluorescence-based system

Compared to the fluorescence-based fire alarm system discussed in Chapter 3, FBG-based sensor system has shown some advantages and these are highlighted below.

● Faster response time.

Due to the use of a complex signal processing algorithm to identify the very weak fluorescence signal from the hot spot, the response time of fluorescence-based fire

alarm system is limited to be around 2 seconds for the signal integration and data processing. The response time of the FBG-based fire alarm system developed is around 1 second, which is similar to that of a FBG temperature sensor system discussed in Chapter 5. This can be further improved by using a smaller packaging tubing to enable quick thermal transfer and a faster F-P scanning frequency.

- Higher accuracy

Compared to the fluorescence-based fire alarm system, the FBG-based system has demonstrated a much higher accuracy for both the hot spot and the background temperature measurements see Table 6.1 and Table 3.1.

- Higher temperature resolution

The FBG-based fire alarm system has higher temperature resolution than the fluorescence-based fire alarm system, especially for the hot spot temperature measurement, also see Table 6.1 and Table 3.1.

- Higher spatial resolution

The fluorescence based fire alarm system needs a certain section of fibre being exposed to a hotspot to generate a detectable fluorescence signal and this limits its spatial resolution to be a few centimetres. The special resolution of the FBG fire alarm system is mainly limited by the distance between consequent FBGs, which is about 4 cm in this case.

- Insensitivity to light source fluctuation

The FBG-based fire alarm system is wavelength encoded, therefore intensity-independent.

- Insensitivity to hotspot location

The fluorescence-based fire alarm system is sensitive to the hot spot location as its corresponding fluorescence signal varies with its location. The FBG-based

system, however, is not sensitive to the hot spot location, but only its temperature.

● Longer sensing fibre

The sensing fibre length of the fluorescence-based system is limited by the light source intensity and the absorption losses when the fibre is pumped by light from a laser diode to emit fluorescence.   As shown in Figure 3.3, the fluorescence signal generated from the middle section of the fibre would be very weak when the fibre is of several meters and pumped from both ends.   The FBG-based sensor system, however, has demonstrated flexibility in writing required FBGs within any defined sensing length, although there is a compromise between the sensing length and spatial resolution of the system.

● Ease of multiplexing

The sensing principle of the FBG-based fire alarm system is based upon the multiplexing capability of FBGs, therefore the system is not limited only to detect one hot-spot, but multiple ones.   With the presence of several hot spots, the fluorescence-based system would have some difficulty in deconvolving the combined signals.

6.3   Summary

In this chapter, an FBG based fire alarm system was designed to offer an enhanced and better performance over the fluorescence-based optical fibre fire alarm system discussed in Chapter 3, taking the advantages of fibre Bragg gratings, such as faster response, higher accuracy, higher spatial resolution, easy to be multiplexed, etc.

A prototype system of the FBG-based fire alarm system, together with a three channel FBG array probe, was successfully built, tested and evaluated extensively, both in the lab and in industry. The results have confirmed that the FBG based fire alarm system has a better performance than that of the fluorescence based fire alarm system.

In summary, the system specifications achieved are listed in table 6.1.   As discussed in this chapter, the performance of the sensor system can be further

improved to meet the demands from aerospace applications.

Table 6-1: Specifications of the FBG-based fire alarm system

Spot measurement precision	Background	$\pm 2\,^{o}C$
	Hotspot	$\pm 5\,^{o}C$
	Relative difference	$\pm 4\,^{o}C$
Minimum detectable temperature difference between the hot spot and background		$\sim 35\,^{o}C$
Probe length (22~25 FBGs in each channel)		3 x 1.5m (1m sensing area)
Fibre material		Ge-doped fibre (or B-Ge co-doped fibre)
Operation temperature range		0~650 (^{o}C)
Long term stability (^{o}C, 24 hours)		$\sim \pm 2\,^{o}C$
Response time (second)		0.5~1
Light source output power (dBm / mW)		3 / 2

References

[1]. Y. Shen, T. Sun, K.T.V. Grattan and M. Sun, "*Highly photosensitive Sb/Er/Ge codoped silica fibre for fibre Bragg grating (FBG) writing with strong high-temperature sustainability*", Optics Letters, Vol.28, 2003, pp.2025-2027

[2]. Y. Shen, J. He, T. Sun, K.T.V. Grattan, "*High temperature sustainability of strong FBGs written into Sb/Ge co-doped photosensitive fibre - decay mechanisms involved during annealing*", Optics Letters, Vol.29, 2004, pp.554-556

[3]. Y. Shen, J. Xia, T. Sun and K.T.V. Grattan, "*Photosensitive Indium doped germano-silica fibre for strong FBGs with high temperature sustainability*", IEEE Photonic Techology Letters, vol. 16, 2004, pp. 1319-1321

Chapter 7. Remote monitoring of FBG sensor system using GSM short message

7.1   Application background

7.1.1   The need for a remote monitoring system

As discussed in previous chapters, FBG sensor systems have demonstrated advantages over conventional techniques in many applications. In Chapters 5 and 6, the FBG-based sensor systems developed at City University London have been used in civil engineering, automotive industries, and aerospace. In addition to these applications, FBG sensors can be and have been widely used for applications in wind energy, offshore engineering, maritime, pipeline, power transformers. Most of in-situ applications are carried out in the field where regular personnel on-site monitoring and maintenance are not very convenient and sometimes very costly, but essential.   For such applications, a sensor system, which can somehow send the monitoring data and operational conditions to a control centre, will be preferable and could be more efficient. In this chapter, a remote monitoring system of FBG sensor using GSM short message is presented. This remote sensor system can extend its application to many field applications, and reduce the operation cost.

7.1.2   Wireless communication technologies

Wireless networks are becoming more pervasive, accelerated by new wireless communication technologies and inexpensive wireless equipment. These networks are transforming the way people use computers and other personal electronics devices at work and home and when travelling. The wireless networks can also be used for remote monitoring and controlling, and data communication of measurement instruments, such as the case arises here for remote monitoring of FBG sensor system.

There are many wireless communication technologies, which can be differentiated by the frequency, bandwidth, range, and applications. These technologies are generally

classified into four categories, depicted in Figure 7.1, in terms of coverage range [1]. The categories range from wireless personal area network (WPAN), which covers less than 10 meters, to wireless wide area network (WWAN), which covers the widest global area.
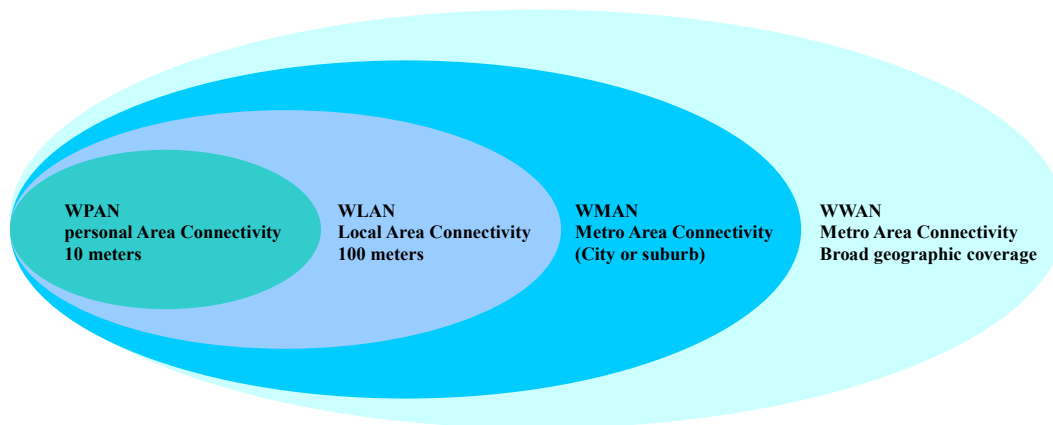
Figure 7.1: Wireless technologies categorized by range

- **Wireless Personal Area Network (WPAN) [1]**

A Wireless Personal Area Network WPAN is a very small computer network used for communications among computer devices (including telephones and personal digital assistants) close to one person, which typically extend to 10 meters or less. Because of their limited range, WPANs are used mainly as cable replacement technologies for data synchronization and connectivity for device that are close to each other. Whilst USB and FireWire are the commonly used cable technologies for personal area networks, the wireless technologies of personal area networks are Bluetooth, IrDA (Infrared Data Association), and High-bandwidth UWB (Ultrawideband).

- **Wireless Local Area Networks (WLAN) [1]**

A Wireless Local Area Network (WLAN) is a wireless local area network, which is the linking of two or more computers without using wires. In contrast to WPANs, WLANs provide robust wireless network connectivity over a local area of approximately 100 meters between the access point and associated clients. Today's WLANs are mainly based on the IEEE 802.11 standard and are referred as Wi-Fi networks. 802.11b was

the first commercially successful WLAN technology. It operates in the 2.4 GHz frequency band at 11 Mbps. By implementing a different data transmission method, data transfer rate was increased to 54 Mbps with 802.11g in the 2.4 GHz band.

- **Wireless Metro Area Network (WMAN) [1]**

A Wireless Metro Area Network (WMAN) is a wireless communication network that covers a large geographic area, such as a city or suburb. It provides WLAN-like service, primarily Internet access to an entire city. The best-known of these technologies of the air interface for WMAN is IEEE 802.16d or "WiMax", which operates in the 2-11 GHz frequency range. The maximum data transfer rate under ideal conditions is 70 Mbps over 50 kilometers.

- **Wireless Wide Area Network (WWAN) [1]**

A Wireless Wide Area Networks (WWAN) is digital cellular networks for mobile and data transmission, operated by network carries, such as Vodafone. WWAN covers a much more extensive area than WLANs. They provided connectivity over a wide geographical area. WWANs allow users to have access to the Internet, e-mail, and corporate applications and information even being away from their office. But, until recently, data rates of up to 115 Kbps have been relatively low compared to other more localized wireless technologies. Two WWAN technologies, Global System for Mobile Communication (GSM) and Code Division Multiple Access (CDMA), dominate the WWAN deployments worldwide.

Europe standardized early on GSM technology. Nowadays, GSM and its associated wireless data capability, General Packet Radio Service (GPRS) and the next generation Enhanced Data GSM Evolution (EDGE), have about two-thirds of the world wide market. The technologies have been widely deployed in North America, Europe, and Asia. CDMA technology has seen strong deployments in North America, Japan, Korea and China.

7.1.3   System setup of remote monitoring using GSM network

These wireless technologies summarized above can be potentially used for wireless remote sensing. The selection of the technology is mainly based on the requirement of the sensor system, such as the coverage range, data transfer rate, and maintenance cost etc. As far as the remote sensing system of FBG sensor is concerned, GSM WWAN technology is the most promising technique to be used, as GSM networks cover almost every corner worldwide, while the FBG sensor is proposed to be deployed in long term monitoring of some off-shore and in-field applications, such as remote bridge and tunnel condition monitoring.   In this Chapter, a remote monitoring FBG sensor system is to be established. Figure 7.2 illustrates the system layout for remote monitoring based on GSM (GPRS) network for data communication using GSM short message via GSM/GPRS modems.
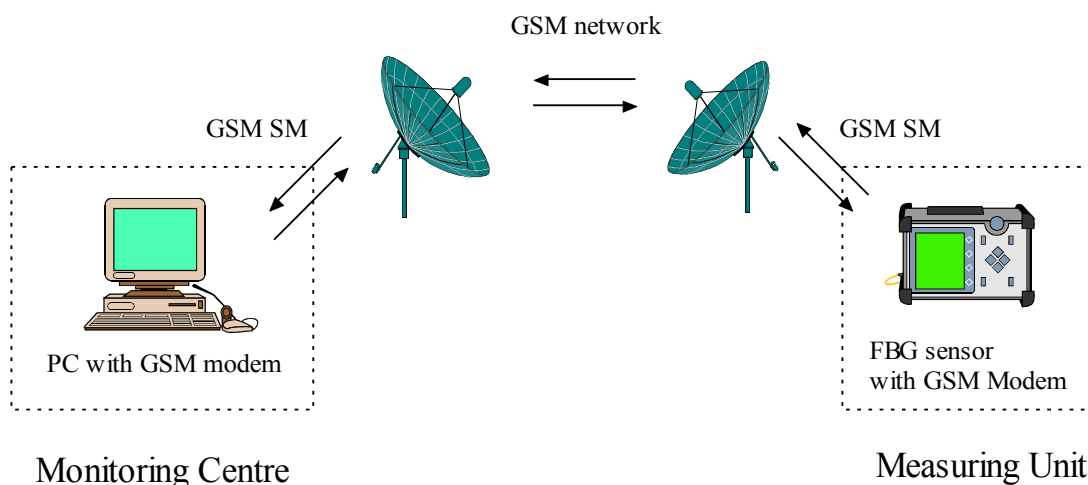
Figure 7.2: Configuration of the remote monitoring FBG sensor system

As shown in Figure 7.2, the monitoring centre and the measuring unit can send and receive short messages containing the information of command or measurement data to and from each other, and demodulate the information of the message received. The main functions of these units are described below

Monitoring Centre

The monitoring centre consists of a PC connected with a GSM modem, and

interface software for monitoring and recording.

Its main functions are to

- send command to control the measuring unit via GSM short message

- receive data from the measuring site sent by the sensor system via short message

- request data to be sent anytime under the command of user

Measuring Unit

The measuring unit consists of an integrated FBG sensor interrogation system (Mini industrial PC + interrogation box) with GSM modem, similar software as currently used with GSM short message (or GPRS in the future if required for high volume data transfer) add-on.

Its main functions are to

- receive measurement data from the FBG sensor

- send measurement data regularly to the monitoring centre by GSM short message

- respond to the command sent from monitoring centre via short message

- send alarm signal to monitoring centre when the measured data exceed the preset threshold

7.2   *Stand-alone FBG sensor system with GSM Modem*

A remote FBG sensor system can be implemented by connecting the GSM modem to the PC, which is linked with the FBG sensor system, as illustrated in Figure 7.3. But it

GSM modem   **PC with interface**   **FBG probe**

Interrogation unit
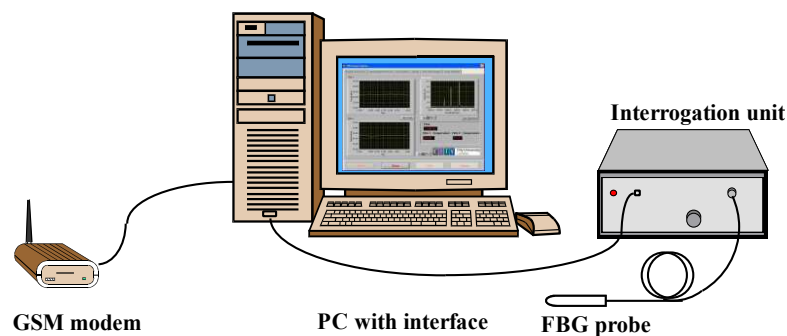
Figure 7.3: Remote sensor system with separated units

will be much more convenient to integrate all the units into one compact box for remote sensing in applications, e.g. for remote bridge monitoring.

In this project, a stand-alone sensor kit was created through the integration of the FBG interrogation unit, a micro-industrial standard main-board together with a GSM modem. The system built is shown in Figure 7.4. The main-board used was VIA VB6002 mini-ITX main-board, which is fully compatible with Microsoft® Windows® 2000/XP, CE

(a)
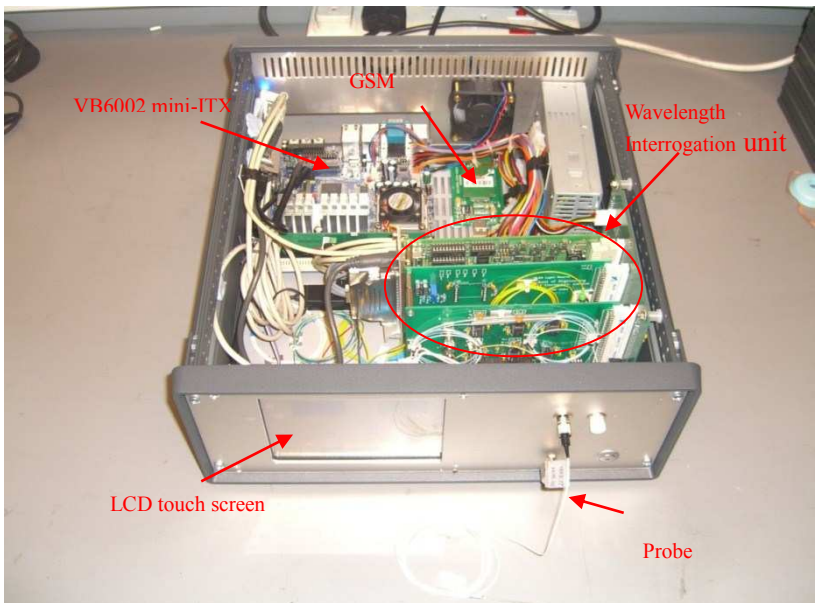
(b)

Figure 7.4: Integrated stand-alone remote FBG sensor system
(a) overview, (b) internal view

and XP, and Linux operating systems, from VIA Technologies Inc, Taiwan. A 6.5" TFT LCD with touch screen was used for display and user interface for data input.   With the interface software being developed (discussed in the following sections), the kit has been effectively used for stand-alone remote sensing applications.

7.3   *Remote monitoring of FBG system using GSM short message technique*

The measurement data of the FBG sensor system and the control information form the monitoring centre are communicated using GSM short message through the GSM modem. In the following sections, the methods of sending and receiving short messages using a PC via the GSM modem are discussed.

7.3.1   Introduction of GSM AT command

Most of the GSM modems (and mobile phones) can support the AT command set by GSM 07.05, which is published by European Telecommunications Standards Institute (ETSI) [2]. It includes the control of the Short Message Service (SMS). The main AT commands related to SMS and used in this project are listed in Table 7.1. A PC thus can control the GSM modem (or mobile) by sending AT commands to it via COM port.

Table 7-1: Main SMS AT commands

AT+CMGR	Read SMS message
AT+CMGS	Send SMS message
AT+CMGC	Send an SMS command
AT+CMGD	Delete SMS message
AT+CMGF	Select SMS message format
AT+CMGL	List SMS message from preferred store
AT+CMGW	Write SMS message to memory
AT+CMSS	Send SMS message from storage
AT+CNMI	New SMS message indications
AT+CPMS	Preferred SMS message storage
AT+CSCA	SMS service centre address

AT+CSMP	Set SMS text mode parameters
AT+CSMS	Select Message Service

7.3.2   Sending and receiving message using a PC via GSM modem in Protocol Data Unit (PDU) mode

7.3.2.1 Short message modes

There are three interface protocols, termed as SMS block mode, SMS text mode and SMS PDU (Protocol Data Unit) mode, of a GSM Modem or mobile phone[4]. The mode that a GSM/GPRS modem or mobile phone is operating determines the syntax of some SMS AT commands and the format of the responses returned after execution.

Text mode is simpler to implement but has some limitations, conversely, PDU mode is more difficult to implement but more flexible. In this project, the PDU Mode was used for sending and receiving the short messages.

7.3.2.2 Receiving a message in the PDU mode

When a new message arrives, the following AT command is used to read it form MT.

AT+CMGR = *Index* (index is the index number of the ME storage where the message is saved)

The MT responds to the following messages to the TE, which include the PDU string.

The PDU string contains not only the message, but also a meta-information about the sender, SMS Centre, the time stamp etc. It is all in the form of hex-decimal octets or decimal semi-octets. The construction of the PDU string is detailed in Table 7.2 [2].

Table 7-2: Structure of the PDU string of a received message

Octet(s)	Description
07	Length of the SMSC information (in this case 7 octets)
91	Type-of-address of the SMSC. (91 means international format of the phone number)
72 38 01 00 10 F5	Service centre number (in decimal semi-octets). The length of the phone number is odd (11), so a trailing F has been added to form proper octets. The phone number of this service centre is "+27831000015".
04	First octet of this SMS-DELIVER message.
0B	Address-Length. Length of the sender number (0B hex = 11 dec)
C8	Type-of-address of the sender number
72 38 88 09 00 F1	Sender number (decimal semi-octets), with a trailing F
00	TP-PID. Protocol identifier.
00	TP-DCS Data coding scheme
99 30 92 51 61 95 80	TP-SCTS. Time stamp (semi-octets)
0A	TP-UDL User data length, length of message. The TP-DCS field indicated 7-bit data, so the length here is the number of septets (10). If the TP-DCS field were set to indicate 8-bit data or Unicode, the length would be the number of octets (9).
C8329BFD0E01	TP-UD. Message "Hello!", 8-bit octets representing 7-bit data.

All the octets above are hex-decimal 8-bit octets, except the Service Centre number, the sender number and the timestamp; they are decimal semi-octets. The message part in the end of the PDU string consists of hex-decimal 8-bit octets, but these octets represent 7-bit data, PDU encoded (discussed later).

7.3.2.3 Sending a message in the PDU mode

The following example shows how to send the message "hello!" in the PDU mode

   AT+CMGF=0   //Set PDU mode

   AT+CMGS=23   //Send message, 23 octets (excluding the two initial zeros)

MT responses: **>**

TE sends: *0011000B916407281553F80000AA0AE8329BFD4697D9EC37*

There are 23 octets in this message (46 'characters'). The first octet ("00") doesn't count, it is only an indicator of the length of the SMSC information supplied (0). The PDU string consists of the following information:

Table 7-3: Structure of the PDU string of a sent message

Octet(s)	Description
00	Length of SMSC information. Here the length is 0, which means that the SMSC stored in the phone should be used.
11	First octet of the SMS-SUBMIT message.
00	TP-Message-Reference. The "00" value here lets the phone set the message reference number itself.
0B	Address-Length. Length of phone number (11)
91	Type-of-Address. (91 indicates international format of the phone number).
6407281553F8	The phone number in semi octets (46708251358). The length of the phone number is odd (11), therefore a trailing F has been added, as if the phone number were "46708251358F". Using the unknown format (i.e. the Type-of-Address 81 instead of 91) would yield the phone number octet sequence 7080523185 (0708251358). Note that this has the length 10 (A), which is even.
00	TP-PID. Protocol identifier
00	TP-DCS. Data coding scheme. This message is coded according to the 7bit default alphabet. Having "02" instead of "00" here, would indicate that the TP-User-Data field of this message should be interpreted as 8bit rather than 7bit (used in e.g. smart messaging, OTA provisioning etc).
AA	TP-Validity-Period. "AA" means 4 days. Note: This octet is optional, see bits 4 and 3 of the first octet
0A	TP-User-Data-Length. Length of message. The TP-DCS field indicated 7-bit data, so the length here is the number of septets (10). If the TP-DCS field were set to 8-bit data or Unicode, the length would be the number of octets.
C8329BFD0E01	TP-User-Data. These octets represent the message "Hello!". How to do the transformation from 7bit septets into octets is shown here

7.3.2.4 PDU encode

For sending a short message in PDU mode, the user's message is required to be transformed into PDU string, namely PDU encoded. However the whole message to be sent includes some other information as mentioned above. This transformation is described in detail in GSM 03.38. The following shows how the message "Hello!" is transformed into PDU string, as an example.

The message "hello!" consists of 6 characters, called septets when represented by

7 bits each. These septets need to be transformed into octets for the SMS transfer. This transforming process is shown in Table 7.4. The transformation is based on the 7 bit default alphabet, but an application built on the PDU mode can use any character encoding.

Table 7-4: process of encoding message into PDU string

Original String	H	e	l	L	O	!
Original Hex	0x48	0x65	0x6C	0x6C	0x6F	0x21
Original binary	01001000	01100101	01101100	01101100	01101111	00100001
Original septet	1001000	110010 1	11011 00	1101 100	110 1111	01 00001
Coding process						
Object Octet	1 1001000	00 110010	100 11011	1111 1101	00001 110	000000 01
Object Hex	0xC8	0x32	0x9B	0xFD	0x0E	0x01
Object String	C8329BFD0E01					

The first septet 1001000 ("H") is turned into an octet by adding the most right bit of the second septet. This bit is inserted to the left which yields 1 + 1001000 = 11001000 ("C8"). The most right bit of the second septet 1100101 of the second character ("e") is then consumed, so it needs two bits of the third septet to make an 8 bit octet. This process carries on until the last character. Leading 0s are added if the last octet has less than 8 bits. The octets are then turned into hex, and hence the original message "Hello!" is transformed into the 8-bit octets PDU string "C8329BFD0E01".

7.3.2.5 PDU decode

While receiving a message sent in PDU mode, the message is PDU encoded and is needed to be transformed into normal string, thus to interpret 8-bit octets as 7-bit messages. The following shows how 8-bit octets PDU string "C8329BFD0E01" is decoded to 7-bit message "Hello!".

Table 7-5: process of decoding PDU string into message string

Original String	C8329BFD0E01					
PDU Hex	0xC8	0x32	0x9B	0xFD	0x0E	0x01
PDU binary	1 1001000	00 110010	100 11011	1111 1101	00001 110	000000 01
Coding process						
Object septet	1001000	110010 1	11011 00	1101 100	110 1111	01 00001
Object Oct	0100100	01100101	01101100	01101100	01101111	00100001
Object Hex	0x48	0x65	0x6C	0x6C	0x6F	0x21
Object String	H	E	l	L	O	!

The first octet 11001000 (0xC8) is turned into a septet by moving the most significant bit (MSB) 1, resulting in 1001000 (0x48). The removed MSB is then added to the right of the second octet while removing the most left 2 bits into the next septet to yield 110010 + 1 = 1100101 (0x65). This process carries on until the last character. Leading 0s of the last octet are removed. The septets are then turned into hexes and their ASCII letter accordingly. Therefore the 8-bit octets PDU string "C8329BFD0E01" is transformed into message "Hello!".

7.3.2.6 Instant message reading

As discussed in the previous sections, the TE (a PC) can send and receive short messages from GSM modem by controlling it with AT commands. Among these AT commands, the PC sends an initiative enquiry command to receive/read message form the GSM modem. For example, TE sends "AT+CMGL" command, MT then replies with the received and saves message(s); TE sends "AT+CMGR=<index>", and MT replies with the message saved at <index>. This kind of enquiring and retrieving method is the operational principle of AT commands. However, these are some limitations in real applications.

● When receiving a message, MT saves it, and sends it to TE when requested, there will be a delay between them, which depends on the enquiry frequency.

● When TE sends the requesting AT command "AT+CMGL", TE will receive the final "OK" signal from MT, no matter whether the MT has the message or how many messages it has. This results in a long period of waiting, normally of 5-10

seconds.

For many applications, this type of delay is undesirable as frequent enquiries occupy lots of CPU resource. Therefore, a technique of "instant" receiving/reading message was introduced. When MT receiving a message, it will inform TE or send it to TE automatically. It works like an interrupt rather than the enquiry mechanism discussed above.

Most of GSM modems support a AT command "AT+CNMI", to select the procedure of how to receive new messages from the network and TE is informed of this when TE is active, e.g. through sending indication to TE or forwarding message to TE directly.

There are different modes of using command "AT+CNMI", Please refer GSM 07.05 standard for details [4]. In this project, the mode of "AT+CNMI=2, 1" is used. In this mode, when TE receive the indication "+CMTI" of new message from MT, it sends "AT+CMGR" command to read the message context form MT.

7.4   Interface Software

Based on the technique for sending and receiving SMS discussed above, the interface software for both the monitoring centre and the FBG sensor kit with GSM function add-on was developed using Labview platform.

7.4.1   GSM add-on software module for the sensor kit

As the main FBG wavelength interrogation unit in the stand-alone system stems from the FBG-sensor system developed and discussed in Chapter 4, the interface software for the FBG-based sensor system can be easily modified to be used in the stand-alone sensor kit.   However, an add-on module requires the interface software to be developed for data transfer using GSM short message to enable the remote sensor system to be created.

As shown in Figure 7.7, the GSM add-on module provides the following main functions:

- Configures for GSM modem communication
- Encodes the measurement result into PDU string

- Decodes the control message (in PDU string) sent by the monitoring centre

- Automatically sends data to the monitoring centre or any other predefined user at a desired period. This function can also be turn on and off by the monitoring centre, remotely.

- Sends alarm data when the value exceeds the threshold. This function can also be turn on and off by the monitoring centre.

- Actively sends measurement data as a short message to a receiver, e.g. monitoring centre or a mobile phone.

- Responds to a data acquisition request.

In addition to these features, other functions, such as remote control and set the sensor kit operation, remote system diagnose, etc., can be easily added on, to provide full functional remote controlling and monitoring.
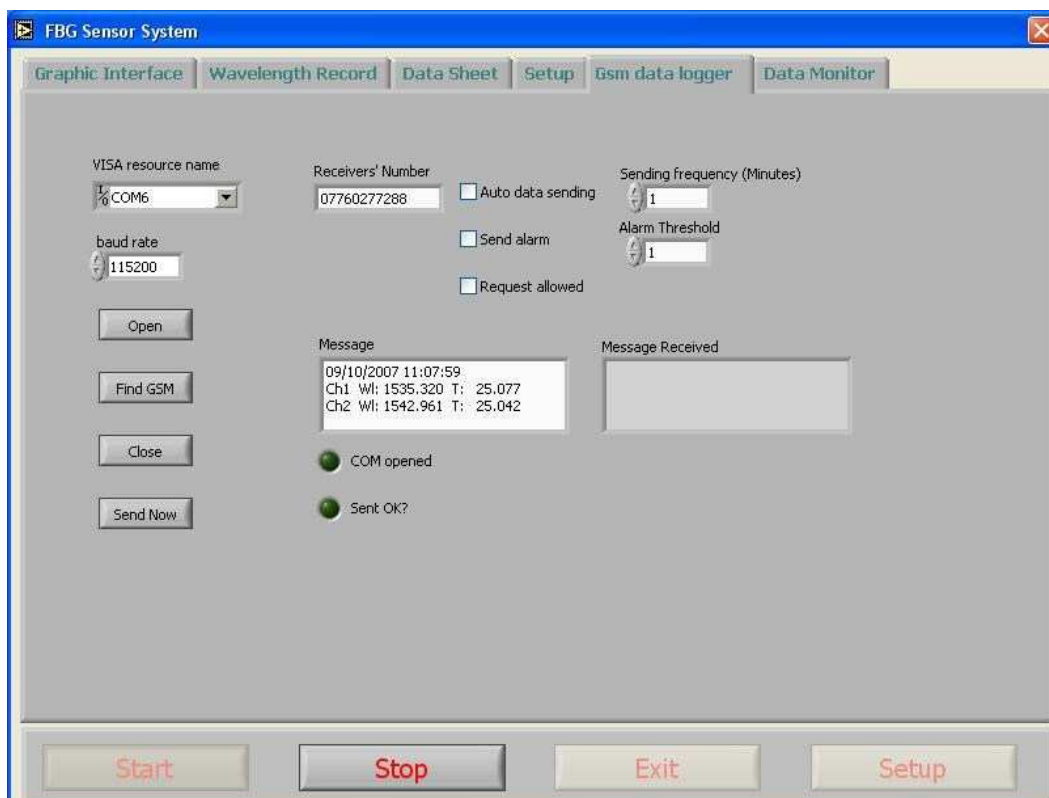
Figure 7.5: Screen printout of the GSM add-on module of the stand alone FBG sensor kit

7.4.2 User interface software for remote monitoring centre

The remote sensor kit with GSM add-on module can simply be controlled and monitored by a mobile phone through short message communications. However, a

dedicated monitoring centre with appropriate program is able to provide the following desirable functions.

- Encodes and sends command, such as switch on and off, set data sending frequency, alarm threshold hold, to control the measuring kit via GSM short message.

- Gets and decodes data from the measuring site sent by the sensor system via short message.

- Requests data to be sent anytime under the command of user.

- Presents and manages the measurement data as a real-time system.

The initial user interface software was programmed using Labview platform, with the front panels being shown in Figure 7.8.
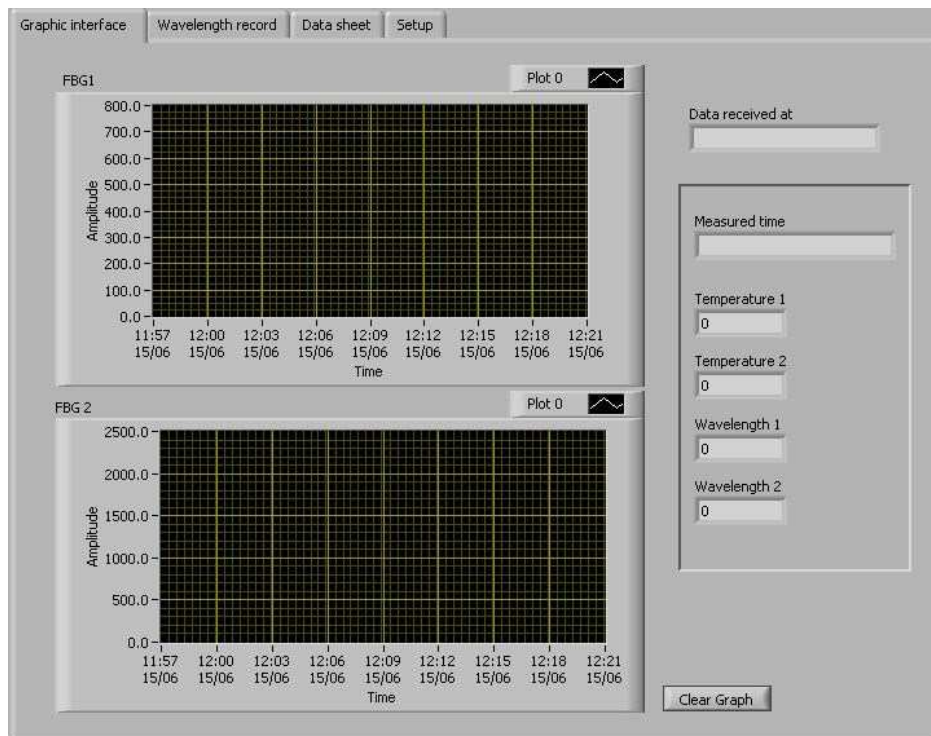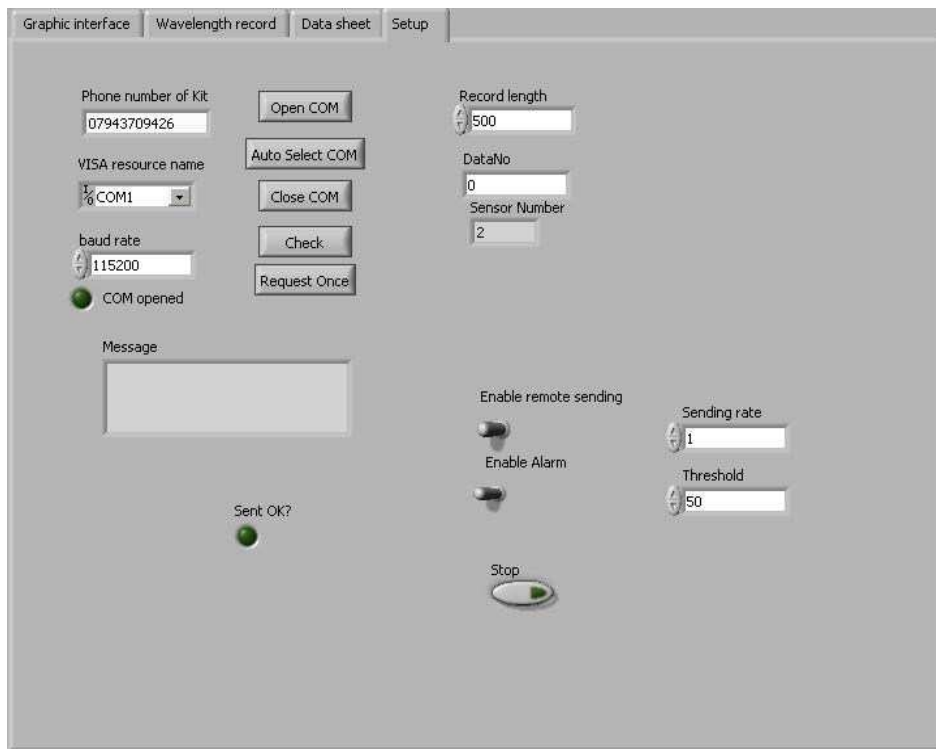
Figure 7.6: Front panel of monitoring centre interface software

7.5   Summary

Driven by the motivation of potential applications for remote field measurement and monitoring of the FBG based system, the GSM short message technology was explored in this work to facilitate the wireless sensing and monitoring with FBG sensor system. The technique of using PC to send and receive short messages is briefly discussed and implemented with the software developed on the Labview platform.

Subsequently a stand-alone FBG sensor kit was developed with the intention of field applications in remote areas, such as off-shore applications and remote bridge monitoring applications. User interface software for a monitoring centre has also been developed in association with the remote measurement system.

This method of utilising GSM short message technology used in this work for remote sensing is generic and can be easily adapted for other wireless sensing applications, which do no require huge amount of data transfer but require wide range coverage.

Reference

[1]. Liam Quinn, Pratik Mehta, Alan Sicher "*Wireless communications technology landscape*", white paper, Feb 2005, Dell.

[2]. GSM_07.05_Specification, European Telecommunication Standard, ETS 300 585, April 1997

Chapter 8. Conclusions and future work

8.1   Summary of the major achievements

The main work of this thesis focused on the development of two major optical fibre sensor systems: novel fibre temperature sensor system based on the fluorescence decay lifetime thermometry and FBG sensor system based on strong FBGs written into novel photosensitive fibres.   Based on the fundamental theoretical analysis, much of the emphasis and effort was on the realization of the sensor systems through experimental practices, i.e. by building and evaluating an optical fibre sensor system for practical industrial applications.   As a result, several sensor systems have been successfully designed, created, tested and evaluated with an aim to meet the specifications identified by industrial partners.   Thus the major achievements and innovations of this work are summarized and listed below.

1. A robust fluorescence lifetime-based optical fibre sensor system has been successfully developed, with the implementation of phase-locked detection (PLD) signal processing scheme and microchip unit for period measurement. In this work, the Tm doped YAG crystal was selected as a sensing material to construct the fluorescence-based thermometer. Its strong signal and long fluorescence lifetime over the temperature range from room temperature to above 1000°C enabled the thermometer to cover a wide temperature sensing range with a relatively high resolution, showing good repeatability and long term stability [1,2].

2. An optical fire alarm system, based on double exponential fluorescence lifetime measurement using data fitting method, was developed and evaluated. It has demonstrated the potential of their applications in aero industry [3]. However, the system showed certain level of limitations for practical applications.

3. A novel photosensitive fibre, Bi/Ge co-doped fibre, has been designed and

fabricated specifically for the creation of strong FBGs for high temperature applications. The photosensitivity and thermal characteristics of fibre Bragg grating inscribed into this novel fibre have been tested and evaluated. The results show that the strong gratings written into the Bi/Ge fibre can retain high reflectivity after being annealed at elevated temperatures over 900 ^{o}C, therefore are well suited for high temperature applications [4].

4. A compact and reliable FBG sensor system based on a tunable Fabry-Perot filter was built. The system has shown a good wavelength resolution of 1 pm (equivalent to a temperature resolution of 0.1 ^{o}C), with an absolute wavelength accuracy of better than 10 pm. Following successfully testing in several field applications, the system has been verified to be well suited for in-situ monitoring [5].

5. A prototype system of the FBG-based fire alarm system together with a three channel FBG array probe, were built and evaluated, both in the lab and in industry. The results have indicated that the FBG based fire alarm system has shown a better performance, in terms of faster response, higher accuracy, higher spatial resolution, easier to be multiplexed, than that of the fluorescence based fire alarm system. The FBG based fire alarm system has shown promise and several key advantageous features for aerospace applications.

6. Driven by the motivation of potential application in the remote field measurement and monitoring of the FBG based system, the GSM short message technology was explored to enable the wireless sensing and monitoring with FBG sensor system. The technique of using PC to send and receive short messages is briefly discussed and implemented with the interface software being developed on the Labview platform.

7. A stand-alone FBG sensor kit integrated with GSM short message technology for wireless sensing and monitoring was developed with the intention of field applications in remote areas, such as off-shore and remote bridge monitoring. User interface software for a monitoring centre has also been developed in

association with the remote measurement system.

In summary, with reference to the aims and objectives set out in Chapter 1, all of the following were achieved and delivered.

- A fluorescence based optical thermometer, with its user interface software, was built and evaluated

- A fluorescence based optical fibre alarm system was developed and tested

- A novel photosensitive fibre was fabricated, and characteristics of the strong FBGs written into this were studied.

- A compact and reliable FBG sensor interrogation system was developed and applied in several applications.

- A FBG based fire alarm system was built and test both in laboratory and industries.

- Remote sensing system utilizing the GSM technology was studied. A stand-alone FBG sensor kit developed.

- Results obtained have been reported in the peer reviewed literatures and at international conferences.

8.2   *Suggestions for the future work*

This thesis covers the details of the development of a wide range of optical fibre sensor systems and their key technologies being used. The work has been mainly focused on the practical aspects of the sensor system, further work could be on the theoretical research and simulation, which may provide good guidance for the sensor system performance improvement and optimization.

As an example, in the field of fluorescence lifetime based thermometry, a detailed investigation of the concentration of Tm dopant in the YAG crystal would be valuable in obtaining a better knowledge of the concentration dependence of the fluorescence lifetime and the fluorescence intensity, and thus providing an effective means of optimizing the probe through the selection of a sensor material with an appropriate dopant concentration.

For the FBG based optical fibre systems, further work should be focused on two aspects: novel photosensitive fibres and the wavelength interrogation system. Through some theoretical modelling, more thermal-sustainable photosensitive fibres, such as the Bi doped fibres discussed in the thesis, with optimized compositions may be realized.   It is also important to increases the resolution and accuracy of the sensor system through the improvement on the wavelength interrogation algorithms.

Finally, the GSM technique employed for the FBG-based remote sensing system can and should be further incorporated into some other sensor systems to create more remote sensing systems due to its generic nature.

Reference

[1]. Y. H. Shen, W. Z. Zhao, J. L. He, et al., *"Fluorescence decay characteristic of Tm-doped YAG crystal fibre for sensor applications, investigated from room temperature to 1400°C"*, IEEE Sensors Journal, vol. 3, 2003, pp. 507-512

[2]. Y. H. Shen, W. Z. Zhao, et al., "Characterization of an optical fibre thermometer using Tm3+:YAG crystal, based on the fluorescence lifetime approach", Sensors and Actuators, A: Physical, vol. 109, 2003, pp. 53-59

[3]. Y. H. Shen, J. I. He, W. Z. Zhao, et al., "Thermal decay characteristics of strong fiber Bragg gratings showing high-temperature sustainability," J. Opt. Soc. Am. B Vol. 24, 2007, pp.430-438

[4]. W. Zhao, Y. Shen, T. Sun, and K. T. V. Grattan, " FBGs in Bi-Ge Co-doped Photosensitive Fibre for High Temperature Measurement up to 1000ºC," in Optical Fiber Sensors, OSA Technical Digest (CD) (Optical Society of America, 2006), paper TuE86.

[5]. W. Z. Zhao, T. Sun, and K. T. V. Grattan, et al., *"Nd-doped fluorescent fibre fire alarm system based on signal regression approaches"*, OFS(16), 2003, TuP-30

[6]. W. Z. Zhao, T. Sun, et al., "Temperature monitoring of vehicle engine exhaust gases under vibration condition using optical fibre temperature sensor systems" ,Journal of Physics: Conference Series, Vol. 45, 2006, pp.215

Appendix: Relevant publications by the author

A. Papers published in journals

[1]. Y. H. Shen, **W. Z. Zhao**, et al., "*Fluorescence decay characteristic of Tm-doped YAG crystal fibre for sensor applications, investigated from room temperature to 1400°C*", IEEE Sensors Journal, Vol. 3, 2003, pp. 507-512

[2]. Y. H. Shen, S. Y. Chen; **W. Z. Zhao**, et al., *Growth characteristics and potential applications in optical sensors of composite Cr^{4+}:yttrium-aluminum-garnet (YAG)-Nd^{3+}:YAG crystal fibre*", Review of Scientific Instruments, Vol. 74, 2003, pp.1187-1191

[3]. Y. H. Shen, **W. Z. Zhao**, T. Sun, K. T. V. Grattan, "*Characterization of an optical fibre thermometer using Tm^{3+}:YAG crystal, based on the fluorescence lifetime approach*", Sensors and Actuators, A: Physical, Vol. 109, 2003, pp. 53-59

[4]. Y. H. Shen; J. L. He; **W. Z. Zhao,** et al. "*Fibre-optic sensor system for heat-flux measurement", Review of Scientific Instruments*, Vol. 75, 2004, pp.1006-1012

[5]. Y. H. Shen, J. l. He, **W. Z. Zhao**, et al., "Thermal decay characteristics of strong fiber Bragg gratings showing high-temperature sustainability," J. Opt. Soc. Am. B Vol. 24, 2007, pp.430-438

[6]. Y. H. Shen, Y. Q Qiu, **W. Z. Zhao**, et al., "*Short cavity single frequency fiber laser for in-situ sensing applications over a wide temperature range*," Optical Express Vol. 15, 2007, 363-370

[7]. S. Y. Chen, T. L. Yeo, **W. Z. Zhao**, et al., "*Development of multi-wavelength microsphere fibre laser system for potential sensor applications*", Optics Communications, Vol. 282(3), 2009, pp. 401-405

[8]. E Lewis, G Dooly, E Hawe, C Fitzpatrick, P Chambers, J Clifford, **W.Z Zhao**, T Sun, K.T.V Grattan and J Lucas, et al. "Overview of the OPTO-EMI-SENSE Project: Optical Fibre Sensor Network for Automotive Emission Monitoring", Sensors, Vol. 21(II), 2008, pp. 179-196

[9]. H Dong, **W. Z. Zhao**, T Sun, et al. Vibration-insensitive temperature sensing

system based on fluorescence decay and using a digital processing approach, Measurement Science and Technology, Vol. 17, 2006, pp. 2010

B. Papers presented in conferences

[1]. Y. H. Shen, W. Z. Zhao, J. L. He, T. Sun, K.T.V. Grattan，*"Fibre thermometer based on the cross detection of the fluorescent decay of Tm:YAG crystal fibre and background radiation"*, SPIE Proceedings, Vol. 4920, 2002, pp.16-24

[2]. Y. H. Shen, S. Y. Chen, **W. Z. Zhao**, J. Chen. *"Composite Cr^{4+}:YAG- Nd^{3+}:YAG crystal fibre: growth characteristics and passively Q-switched laser operation"*, Proceedings of SPIE, Vol. 4918, 2002, pp.20-9

[3]. L. H. Ye, Y. F. Zhang, **W. Z. Zhao**, Y. H. Shen. *"Sapphire fibre thermometer based on fluorescence lifetime measurement"*, Proceedings of SPIE, Vol.4920, 2002, pp.25-30

[4]. Y. H. Shen, **W. Z. Zhao**, Jinglei He, et al., *"Fibre thermometer based on the cross detection of the fluorescence decay of Tm:YAG crystal fibre and background radiation"*, Proceedings of SPIE, Vol.4920, 2002, pp.16-24

[5]. **W. Z. Zhao**, Y. H. Shen, et al., *"Precision free electron laser materials adhesion monitoring using an optical fibre temperature sensor system"*, OFS(16) 2003, Tu4-4.

[6]. **W. Z. Zhao**, T. Sun, and K. T. V. Grattan, et al**.,** *"Nd-doped fluorescent fibre fire alarm system based on signal regression approaches"*, OFS(16), 2003, TuP-30

[7]. **W. Z. Zhao**, T. Sun, et al., *"Temperature monitoring of vehicle engine exhaust gases using optical fibre temperature sensor systems"*, Proc. SPIE 5855, 2005, pp.832

[8]. J. Mulrooney, J. Clifford, C. Fitzpatrick, E. Lewis, **W. Z. Zhao**, T. Sun, K. T. V. Grattan, et al., *"Optical fibre sensors for the monitoring of harmful emissions from land transport vehicles"*, Proc. SPIE 5826, 2005, pp. 586

[9]. **W. Z. Zhao**, T. Sun, et al., *"Temperature monitoring of vehicle engine exhaust gases under vibration condition using optical fibre temperature sensor*

systems" ,Journal of Physics: Conference Series, Vol. 45, 2006, pp.215

[10]. M. O'Farrell, C. Sheridan, E. Lewis, **W. Z. Zhao**, T. Sun and K. T. V. Grattan, "*An integrated probe design for measuring food quality in a microwave environment*", Proc. SPIE 6619, 2007, p. 66190N

[11]. **W. Z. Zhao**, Y. H. Shen, T. Sun, and K. T. V. Grattan, "*FBGs in Bi-Ge Co-doped Photosensitive Fibre for High Temperature Measurement up to 1000°C,*" in Optical Fiber Sensors, OSA Technical Digest (CD) (Optical Society of America, 2006), paper TuE86.

[12]. S K T Grattan, P A M Basheer, S E Taylor, **W. Z. Zhao**, et al., "*Corrosion induced strain monitoring through fibre optic sensors*", Journal of Physics: Conference Series, Vol. 85, 2007, 012017

C. Patents

[1]. K.T.V Grattan, T. Sun, **W. Z. Zhao**, "Fibre bragg grating sensors", United States Patent, No. US 7418171 B2, August 2008